

**“SYNTHESIS, CHARACTERIZATION AND GLUCOSE  
SENSING OF ELECTRODEPOSITED LANTHANUM  
OXIDE THIN FILMS DOPED WITH SILVER AND  
MANGANESE”**

**A THESIS SUBMITTED TO  
D. Y. PATIL EDUCATION SOCIETY (DEEMED TO BE  
UNIVERSITY), KOLHAPUR**



**FOR THE DEGREE OF  
DOCTOR OF PHILOSOPHY  
IN  
PHYSICS  
UNDER THE FACULTY OF  
INTERDISCIPLINARY STUDIES**

**BY  
Mr. SATISH BAJIRAO JADHAV**

**M.Sc., B.Ed.**

**UNDER THE SUPERVISION OF  
Dr. PADAMAJA N. PAWASKAR**

**M.Sc., Ph.D.**

**ASSISTANT PROFESSOR, (MEDICAL PHYSICS),  
CENTRE FOR INTERDISCIPLINARY RESEARCH,  
D. Y. PATIL EDUCATION SOCIETY (DEEMED TO BE UNIVERSITY),  
KOLHAPUR- 416 006, MAHARASHTRA, (INDIA)**

**2022**

## **DECLARATION**

I hereby declare that the thesis entitled ***"SYNTHESIS, CHARACTERIZATION AND GLUCOSE SENSING OF ELECTRODEPOSITED LANTHANUM OXIDE THIN FILMS DOPED WITH SILVER AND MANGANESE"*** submitted for the degree of Doctor of Philosophy (Ph.D.) in the Centre for Interdisciplinary Research faculty of the D. Y. Patil Education Society (Institution Deemed to be University), Kolhapur is completed and written by me, has not before made the basis for the award of any degree/diploma/other related heading of this or any other university in india/any other country/examining body to the best of my knowledge. Further, I assert that, I have not dishonored any of the requirements under copyright and piracy/cyber/IPR act amended by UGC from time to time.

**Place: Kolhapur**

**Date: 06 / 01 / 2022**



**Mr. Satish B. Jadhav**

**(Research Student)**

**D. Y. Patil Education Society (Deemed to be University), Kolhapur**

**Centre for Interdisciplinary Research**




**Certificate**


This is to certify that the thesis entitled "**SYNTHESIS, CHARACTERIZATION AND GLUCOSE SENSING OF ELECTRODEPOSITED LANTHANUM OXIDE THIN FILMS DOPED WITH SILVER AND MANGANESE**" which is being submitted herewith for the award of the Degree of **Doctor of Philosophy (Ph.D.)** in **Physics** of **D. Y. Patil Education Society (Institution Deemed to be University), Kolhapur**, is the result of the original research work completed by **Mr. Satish Bajirao Jadhav** under my supervision and guidance and to the best of my knowledge and belief the work embodied in this thesis has not formed earlier the basis for the award of any Degree or similar title of this or any other University or examining body.

Place: **Kolhapur**

Date: **06/01/2022**

Research Guide

  
**Dr. Padamaja N. Pawaskar**  
Assistant Professor  
(Medical Physics)

  
Forwarded through,  
**Prof. C. D. Lokhande**  
Head and Research Director,  
Centre for Interdisciplinary Research

D. Y. Patil Education Society  
(Institution Deemed to be University)  
869, 'E', Kasaba Bawada  
KOLHAPUR- 416006

# ACKNOWLEDGEMENT

*A journey is easier when you travel together. Interdependence is certainly more valuable than independence. This thesis is the result of work where I have been accompanied and supported by many peoples.*

*At the completion of my Ph.D. thesis, I would like to express my sincere gratitude towards my advisor, **Dr. P. N. Pawaskar** Assistant Professor (Medical Physics), Centre for Interdisciplinary Research (CIR), D. Y. Patil Education Society (Deemed to be University), Kolhapur for the continuous support during my Ph.D. study and related research, for his motivation, and immense knowledge. I thank her not only for the guidance she rendered in the field of research but also for enlightening the path of my life with a deep love for science. With his support, I could overcome my personal and scientific problems on writing scientific papers including this Ph.D. thesis and this work could not have been completed without his inspiring guidance and constant encouragement during the course of research tenure.*

*I sincerely acknowledge the whole hearted help, valuable discussions, guidelines and suggestions focused by **Prof. C. D. Lokhande**, Dean and Research Director, Centre for Interdisciplinary Research (CIR). He provided a very fruitful discussion and helpful guidance for time management regarding my Ph.D. progress.*

*I would like to express my sincere thanks to Vice-Chancellor **Prof. R. K. Mudgal**, Pro-Vice Chancellor **Dr. Shimpa Sharma** and Registrar **Dr. V. V. Bhosale** for the inspiration and support. I thank **Dr. U. M. Patil**, **Dr. J. L. Gunjekar**, and **Dr. Vishwajeet Khot** who helped me to analyze the results with all their empathy and cooperative mind. I also thank **Dr. A. C. Lokhande**, **Dr. R. N. Bulakhe** and **Dr. S. B. Kale** for providing me very important sample characterization data, during entire research work.*

*I am also thankful to **Dr. S. R. Sabale**, Assistant professor, Department of chemistry, and Coordinator of DST-FIST lab, Jaysingpur College Jaysingpur, for insightful guidelines, providing basic characterizations, scientific discussions and valuable suggestions on the present work. Good scientific research could not blossom in an alienated desert; it is a result of fruitful discussions and co-operative exercises of many analytical minds. I am also thankful (**Mr. Ramdas sir and Miss. Namarata***

*Mam) and non-teaching staff of the CIR Department for their kind co-operation during my research work.*

*In addition, I acknowledge the funding support from **Chhatrapati Shahu Maharaj Research Training and Human Development Institute (SARTHI), Pune** of the **Government of Maharashtra State** for **Chhatrapati Shahu Maharaj National Research Fellowship (CSMNRF)** sanctioned to me. And I also thankful to **D. Y. Patil Education Society, Kolhapur-416006 (India)**, for financial support through research project sanction No. **DYPES/DU/R&D/3099**.*

*I own a word of thanks to all my friends and research colleague from CIR department viz. **Sachin, Dhanaji, Vikas, Yogesh, Shivaji, Navnath, Rohini, Shrikant, Suraj, Priti, Vikas, Shirin,***

*I hereby express my deepest appreciation and regards to my beloved parents (**Aai and Baba**), brother (**Sunil, and Sachin**), all of family members who in spite of their hard times and sufferings, continuously supported and encouraged me to complete my research.*

*I would like to confess that even though I try my best, it is not possible for me to acknowledge and thank all those known and unknown faces individually for their direct and indirect contribution for the successful completion of this work. I am grateful to all of you for your kind cooperation.*

**Place-** Kolhapur

**-Satish Jadhav**

**Date:**     /     /2022

## SUMMARY OF RESEARCH WORK

### A) Papers Published/Submitted at International Journals:

- 1) **S. B. Jadhav**, D. B. Malavekar, R. N. Bulakhe, U. M. Patil, Insik In, C. D. Lokhande, P. N. Pawaskar. Dual-Functional Electrodeposited Vertically Grown Ag-La<sub>2</sub>O<sub>3</sub> Nanoflakes for Non-Enzymatic Glucose Sensing and Energy Storage Application, Surface and Interfaces. 23, (2021), 101018. **(I.F. - 4.83)**.
- 2) **S. B. Jadhav**, U. M. Patil, R. N. Bulakhe, Insik In, C. D. Lokhande, P. N. Pawaskar. Vertically Aligned Nanosheets of an Electrodeposited Lanthanum Oxide Electrode for Non-Enzymatic Glucose Sensing Application, journal of electronic materials., 50, (2021), 675-685. **(I.F. - 1.93)**.
- 3) **S. B. Jadhav**, D. B. Malavekar, S. B. Kale, S. R. Sabale, U. M. Patil, C. D. Lokhande, P. N. Pawaskar, Reliable Glucose Sensing Properties of Electrodeposited Vertically Aligned Manganese Oxide Thin Film Electrode'' Applied Physics A, 127, (2021), 391. **(I.F.- 2.58)**.
- 4) Yogesh Chitare, **satish jadhav**, Padmaja Pawaskar, Vikas Magdum, Jayavant Gunjekar, Chandrakant Lokhande, Metal Oxide Based Composites in Non-Enzymatic Electrochemical Glucose Sensors, Industrial & Engineering Chemistry Research, **(I.F.- 3.5)**
- 5) Madhuri Anuje, Padmaja N. Pawaskar, Vishwajeet Khot, Ajay Sivan, **Satish Jadhav**, Jagruti Meshram, Balu Thombare, Synthesis, Characterization, and Cytotoxicity Evaluation of Polyethylene Glycol Coated Iron Oxide Nanoparticles for Radiotherapy Application, Journal of medical physics.
- 6) **S. B. Jadhav**, P. N. Pawaskar, D. B. Malavekar, S. B. Kale, S. R. Sabale, U. M. Patil, C. D. Lokhande, Electrochemical Fabrication of Mn-doped La<sub>2</sub>O<sub>3</sub> Nano-Flakes Based Electrode for Efficient Non-Enzymatic Glucose Sensing Applications, Materials Science in Semiconductor Processing. ([Status: Under review](#))
- 7) D. B. Malavekar, **S. B. Jadhav**, S. B. Kale, S. A. Khalate, U. M. Patil, C. D. Lokhande, Facile One Pot Synthesis of 3D-hexagon-like Copper Selenide for Electrochemical Non-enzymatic Glucose Sensing, Journal of Materials Science: Materials in Electronics. ([Status: Under review](#)).

**B) Submitted (Indian) Patents:**

- 1) Padmaja N. Pawaskar, Madhuri Anuje, **Satish Jadhav**, Chandrakant D. Lokhande, Vishwanath V. Bhosale, Radiosensitizer based on iron oxide nanoparticles, (2021), Application No.- **202121017519**.

**C) Papers/Poster Presented at National/International Conferences:**

- 1) **Satish B. Jadhav**, Non-enzymatic electrochemical glucose sensing lanthanum oxide thin film electrode, West Zone Inter-University Student Research Convention, (Anveshan 2019-2020), Association of Indian University, New Delhi.
- 2) **Satish B. Jadhav**, Chandrakant D. Lokhande, Padamaja N. Pawaskar, Synthesis and characterization of lanthanum oxide thin film for non-enzymatic glucose sensing application, AMSCA-2018, Savitribai Phule Pune University, Pune.
- 3) **Satish B. Jadhav**, Chandrakant D. Lokhande, Padamaja N. Pawaskar, Synthesis and characterization of lanthanum hydroxide thin film by electrodeposition method, MAS-2019, K. N. Bhise Arts, Commerce and Vinayakrao Patil Science College, Bhosare (Kurduwadi), Solapur.
- 4) **Satish B. Jadhav**, Chandrakant D. Lokhande, Padamaja N. Pawaskar, Synthesis of lanthanum oxide thin films using facile electrodeposition method for glucose sensing application, 4<sup>th</sup> ICPM-MDF-2019, Shivaji University, Kolhapur.
- 5) **Satish B. Jadhav**, Chandrakant D. Lokhande, Padamaja N. Pawaskar, Non-enzymatic electrochemical glucose sensing by fibrous porous structured lanthanum oxide electrode, ICSMN-2020, SKN Sinhgad College of Engineering, Pandharpur-413304, Maharashtra.

**D) Workshops Attended:**

- 1) Participated in “Biodiversity conservation and biodiversity act 2002” held at D. Y. Patil Education Society (Institution Deemed to be University), Kolhapur at **15<sup>th</sup> February 2019** organized by Department of Stem Cell and Regenerative Medicine, Centre for Interdisciplinary Research.
- 2) Participated in “Entrepreneurship and innovation as carrier opportunity” held at D. Y. Patil Education Society (Institution Deemed to be University), Kolhapur during **19<sup>th</sup> December 2019** organized by Institution Innovation Council (IIC).

# CONTENTS

Chapter No.	Title	Page No.
1	General introduction and literature survey	1-36
2	Theoretical background of electrodeposition method and thin film characterization techniques	37-70
3	Synthesis and characterization of lanthanum oxide thin film electrodes for glucose sensing application.	71-94
4	Synthesis and characterization of silver doped lanthanum oxide thin film electrodes for glucose sensing application.	95-116
5	Synthesis, characterization of manganese doped lanthanum oxide thin film electrodes for glucose sensing application.	117-140
6	Ag-La <sub>2</sub> O <sub>3</sub> and Mn-La <sub>2</sub> O <sub>3</sub> thin film used for real blood sample analysis	141-148
7	Summary and conclusions	149-156
8	80-Recommendations	157-162

## *List of Figures*

<b>Chapter 1</b>	<b>Introduction to Biosensor and literature review</b>	
<b>Figure 1.1</b>	Numbers of adults with diabetes by year	01
<b>Figure 1.2</b>	Shows the 1 <sup>st</sup> half reaction of glucose is oxidized by the GOx enzyme to gluconolactone	04
<b>Figure 1.3</b>	The mechanism of first, second and third generation of enzymatic glucose oxidation	07
<b>Figure 1.4</b>	The scheme of activated chemisorptions model	13
<b>Figure 1.5</b>	The scheme of IHOAM model proposed by L. D. Burke	14
<b>Chapter 2</b>	<b>Experimental and characterization techniques</b>	
<b>Figure 2.1</b>	Three electrode electrochemical cell system	41
<b>Figure 2.2</b>	Schematic diagram of saturated calomel electrode (SCE)	51
<b>Figure 2.3</b>	CHI660E electrochemical work station	52
<b>Figure 2.4</b>	Voltage sweep CV study	53
<b>Figure 2.5</b>	The anodic and cathodic peak presented in CV curve	54
<b>Figure 2.6</b>	Block diagram of SEM instrument	58
<b>Figure 2.7</b>	The ray diagram of emission X-ray spectrum in EDS	59
<b>Figure 2.8</b>	Schematic of X-ray diffractometer	61
<b>Figure 2.9</b>	The block diagram of TEM	63
<b>Figure 2.10</b>	XPS instrument analysis	65
<b>Figure 2.11</b>	Schematic diagram of BET isotherm	68
<b>Chapter 3</b>	<b>Synthesis and characterization of lanthanum oxide thin film electrode for non-enzymatic glucose sensing application</b>	
<b>Figure 3.1</b>	The schematic presentation of lanthanum oxide thin film by ED method	74
<b>Figure 3.2</b>	Deposition potential curve of La <sub>2</sub> O <sub>3</sub> on SS substrate at -1 V/SCE	75
<b>Figure 3.3</b>	Non-enzymatic electrochemical glucose sensing experimental setup	77
<b>Figure 3.4</b>	The XRD pattern of La <sub>2</sub> O <sub>3</sub> thin film	78
<b>Figure 3.5</b>	(a) Full range XPS spectrum for La <sub>2</sub> O <sub>3</sub> sample, high resolution spectrum for (b) La3d and (c) O1s	80
<b>Figure 3.6</b>	The FE-SEM images of La <sub>2</sub> O <sub>3</sub> film at (a) 1000X and (b) 15000X magnifications	81
<b>Figure 3.7</b>	EDS spectrum of La <sub>2</sub> O <sub>3</sub> film electrode	81
<b>Figure 3.8</b>	TEM images at magnification of (a) 80000X and (b) 200000X and (c) crystallite size of La <sub>2</sub> O <sub>3</sub> sample	83
<b>Figure 3.9</b>	(a, b) The N <sub>2</sub> sorption isotherms of mesoporous La <sub>2</sub> O <sub>3</sub> sample	84
<b>Figure 3.10</b>	(a) The CV curves at various scan rates of 10 to 100 mV s <sup>-1</sup> and (b) displays peak current as a function of square root of different scan rate (V <sup>1/2</sup> )	85
<b>Figure 3.11</b>	Plots of anodic and cathodic peak voltages vs. square root of the different scan rates	86
<b>Figure 3.12</b>	The CV curves in absence and presence of different glucose concentrations in 1 M KOH solution at 20 mV s <sup>-1</sup>	87
<b>Figure 3.13</b>	(a) Response time obtained with increasing glucose concentration in steps of 1.25 mM at La <sub>2</sub> O <sub>3</sub> electrode and (b) detection time (less than 1 second)	88
<b>Figure 3.14</b>	Current response vs. the glucose concentration at La <sub>2</sub> O <sub>3</sub> electrode with two different slopes	89
<b>Figure 3.15</b>	Plot of the La <sub>2</sub> O <sub>3</sub> film electrode for successfully addition of glucose and interferences in aqueous 1 M KOH solution at +0.43 V/SCE	90
<b>Figure 3.16</b>	(a) Bar graph of reproducibility and (b) stability graph in the presence of 1 mM glucose concentration of La <sub>2</sub> O <sub>3</sub> film electrode	91

<b>Chapter 4</b>	<b>Synthesis and characterization of silver doped lanthanum oxide thin film electrode for non-enzymatic glucose sensing application</b>	
<b>Figure 4.1</b>	LSV curves for precursor solution of lanthanum nitrate (black curve) and silver lanthanum nitrate (red curve) at $20 \text{ mV s}^{-1}$ .....	98
<b>Figure 4.2</b>	Schematic presentation of ED method of $\text{La}_2\text{O}_3$ and Ag- $\text{La}_2\text{O}_3$ thin films.....	99
<b>Figure 4.3</b>	XRD patterns of $\text{La}_2\text{O}_3$ and Ag- $\text{La}_2\text{O}_3$ thin films.....	102
<b>Figure 4.4</b>	FE-SEM images of (a) $\text{La}_2\text{O}_3$ at 15 KX, (b) Ag- $\text{La}_2\text{O}_3$ at 10 KX magnification, (c) EDX spectrum of $\text{La}_2\text{O}_3$ , (d) EDX spectrum of Ag- $\text{La}_2\text{O}_3$ thin film electrode .....	103
<b>Figure 4.5</b>	Elemental mapping image show the distribution of oxygen, lanthanum and silver.....	104
<b>Figure 4.6</b>	BET surface area analysis of (a) $\text{La}_2\text{O}_3$ , (b) Ag- $\text{La}_2\text{O}_3$ samples, the BJH pore size distribution plots of (c) $\text{La}_2\text{O}_3$ , (d) Ag- $\text{La}_2\text{O}_3$ samples.....	105
<b>Figure 4.7</b>	CV curves of (a) $\text{La}_2\text{O}_3$ , (b) 1%Ag- $\text{La}_2\text{O}_3$ , (c) 3%Ag- $\text{La}_2\text{O}_3$ , and (d) 5%Ag- $\text{La}_2\text{O}_3$ film electrode at various scan rates from 10 to $100 \text{ mV s}^{-1}$ in 0.1M NaOH electrolyte.....	106
<b>Figure 4.8</b>	The CV curves of $\text{La}_2\text{O}_3$ and Ag- $\text{La}_2\text{O}_3$ at $50 \text{ mV s}^{-1}$ in 0.1 M NaOH electrolyte.....	107
<b>Figure 4.9</b>	CV curves of $\text{La}_2\text{O}_3$ electrode at different scan rates (5 to $100 \text{ mV s}^{-1}$ ) in 0.1 M NaOH solution.....	108
<b>Figure 4.10</b>	The CV curves of Ag- $\text{La}_2\text{O}_3$ at (a) different scan rates ( $10\text{-}100 \text{ mV s}^{-1}$ ) and (b) different glucose concentration at fixed scan rate of $50 \text{ mV s}^{-1}$ .....	109
<b>Figure 4.11</b>	(a) Current verses time measurement at +0.43 V vs. SCE with successive addition of $100 \mu\text{M}$ of glucose in 60 s time intervals, (b) calibration graph of dependence on current with respect to glucose concentration .....	110
<b>Figure 4.12</b>	(a) i-t amperometric response of Ag- $\text{La}_2\text{O}_3$ electrode for successive addition of glucose and interferences in 0.1 M NaOH at +0.43 V vs. SCE, (b) stability graph in presence of $500 \mu\text{M}$ glucose concentrations in 0.1 M NaOH solution, and (c) reproducibility of Ag- $\text{La}_2\text{O}_3$ electrodes in $100 \mu\text{M}$ glucose concentration.....	112
<b>Chapter 5</b>	<b>Synthesis and characterization of manganese doped lanthanum oxide thin film electrode for non-enzymatic glucose sensing application</b>	
<b>Figure 5.1</b>	Deposition curve of 1% Mn doped $\text{La}_2\text{O}_3$ film electrode on SS substrate.....	121
<b>Figure 5.2</b>	The XRD patterns of (a) $\text{La}_2\text{O}_3$ , b) 1% Mn- $\text{La}_2\text{O}_3$ , c) 3% Mn- $\text{La}_2\text{O}_3$ , and d) 5% Mn- $\text{La}_2\text{O}_3$ thin films on SS substrate .....	123
<b>Figure 5.3</b>	The FE-SEM images of (a, b) $\text{La}_2\text{O}_3$ , (c, d) 1% Mn- $\text{La}_2\text{O}_3$ and (e, f) 3% Mn- $\text{La}_2\text{O}_3$ and (g, h) 5% Mn- $\text{La}_2\text{O}_3$ at different magnifications.....	125
<b>Figure 5.4</b>	The EDX spectra of (a) $\text{La}_2\text{O}_3$ , (b) 1, (c) 3 and (d) 5% Mn- $\text{La}_2\text{O}_3$ thin film electrodes .....	126
<b>Figure 5.5</b>	The XPS spectrum of 1% Mn- $\text{La}_2\text{O}_3$ electrode, XPS spectrum of b) $\text{La}3\text{d}$ , c) Mn, and d) O .....	127
<b>Figure 5.6</b>	CVs studies of a) $\text{La}_2\text{O}_3$ , b) 1% Mn- $\text{La}_2\text{O}_3$ , c) 3% Mn- $\text{La}_2\text{O}_3$ , d) 5% Mn- $\text{La}_2\text{O}_3$ film electrode at various scan rates ( $5$ to $150 \text{ mV s}^{-1}$ ) in 0.1 M NaOH solution.....	128
<b>Figure 5.7</b>	The CV curves of $\text{La}_2\text{O}_3$ , 1, 3, and 5% Mn- $\text{La}_2\text{O}_3$ electrodes at the scan rate of $50 \text{ mV s}^{-1}$ .....	129
<b>Figure 5.8</b>	a) The CV curves of 1% Mn- $\text{La}_2\text{O}_3$ at various scan rates ( $5$ to $150 \text{ mV s}^{-1}$ ), b) $\log I_{\text{pa}}$ vs. $\log v$ (c) the CV curves in absence and presence of glucose at the fix scan rate of $50 \text{ mV s}^{-1}$ , d) current vs. time measurement at potential +0.41 V/SCE with successive addition of $50 \mu\text{M}$ of glucose in 60 s time intervals, e) calibration curve, and f) response time curve of 1% Mn- $\text{La}_2\text{O}_3$ film electrode	

	in 0.1 M NaOH electrolyte.....	131
<b>Figure 5.9</b>	a) <i>i-t</i> amperometric curve obtained at 1% Mn-La <sub>2</sub> O <sub>3</sub> film electrode in the presence of 0, 0.5, 1.0, 1.5, and 2.0 mM glucose concentrations, (b) $I_{cat}/I_L$ vs. $t^{1/2}$ plot obtained from <i>i-t</i> amperometric data for 0.5, 1.0, 1.5, and 2.0 mM glucose concentrations, and (c) catalytic rate constant vs. concentration of glucose.....	133
<b>Figure 5.10</b>	a) <i>i-t</i> amperometric response of 1% Mn-La <sub>2</sub> O <sub>3</sub> film electrode for successive addition of glucose and interferences, b) long term stability graph of during 36 days by adding 100 $\mu$ M glucose concentration, and c) current response at 5 different electrodes.....	135
<b>Chapter 6</b>	<b>Ag-La<sub>2</sub>O<sub>3</sub> and Mn-La<sub>2</sub>O<sub>3</sub> film electrodes for direct monitoring of glucose from human blood samples</b>	
<b>Figure 6.1</b>	<i>i-t</i> amperometry plots of with and without blood samples. A, B, C, D, E, and F are the different human blood samples tested in 0.1 M NaOH electrolyte.....	147

## *List of Tables and Charts*

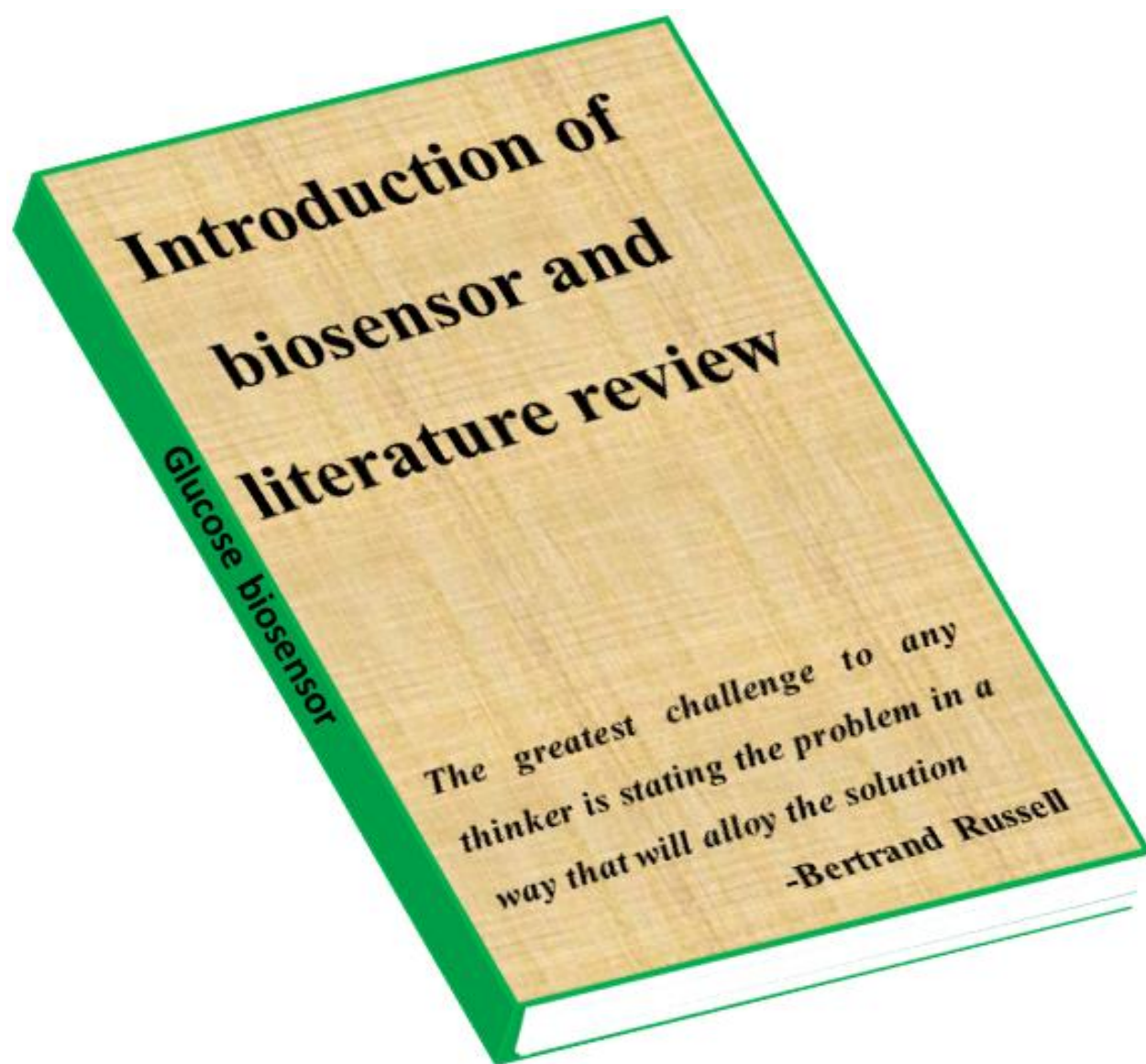
---

<b>Table 1.1</b>	Table 1: Various mediators classified in three groups .....	08
<b>Table 1.2</b>	Literature survey of transition metal oxides with their composites materials.....	23
<b>Table 2.1</b>	The common laboratory analytical grade chemicals were used in the present work.....	37
<b>Chart 2.1</b>	Categorization of thin film deposition methods.....	39
<b>Table 6.1</b>	The statistical data of successive addition of pure glucose and human samples.....	148
<b>Table 7.1</b>	Metal oxide based electrodes for non-enzymatic glucose sensing application .....	156

## *Abbreviation*

<b>AA</b>	<i>Ascorbic Acid</i>	<b>Lac</b>	<i>Lactose</i>
<b>CC</b>	<i>Carbon Cloth</i>	<b>LSV</b>	<i>Linear Sweep Voltammetry</i>
<b>CFP</b>	<i>Carbon Fiber Paper</i>	<b>NF</b>	<i>Nickel Foam</i>
<b>CNT</b>	<i>Carbon Nanotube</i>	<b>NPs</b>	<i>Nanoparticles</i>
<b>CV</b>	<i>Cyclic Voltammetry</i>	<b>NRs</b>	<i>Nano rods</i>
<b>CVD</b>	<i>Chemical Vapor Deposition</i>	<b>NW</b>	<i>Nano Wire</i>
<b>DDW</b>	<i>Double Distilled Water</i>	<b>OHads</b>	<i>Adsorption of hydroxyl radicals</i>
<b>ED</b>	<i>Electrodeposition</i>	<b>PD</b>	<i>Polymer Dot</i>
<b>FAD</b>	<i>Flavin Adenine Dinucleotide</i>	<b>rGO</b>	<i>Reduced Graphene Oxide</i>
<b>Fru</b>	<i>Fructose</i>	<b>SAED</b>	<i>Selected Area Diffraction</i>
<b>IDF</b>	<i>International Diabetes Federation</i>	<b>SCE</b>	<i>Saturated Calomel Electrode</i>
<b>GDH</b>	<i>Glucose Dehydrogenase</i>	<b>SS</b>	<i>Stainless Steel</i>
<b>GO</b>	<i>Graphene Oxide</i>	<b>WHO</b>	<i>World Health Organization</i>
<b>GOx</b>	<i>glucose oxidase</i>	<b>XPS</b>	<i>X-ray Photoelectron Spectroscopy</i>
<b>KOH</b>	<i>Potassium Hydroxide</i>	<b>XRD</b>	<i>X-ray Diffraction</i>
<b>LCVD</b>	<i>Laser Chemical Vapor Deposition</i>	<b>μA</b>	<i>Micro Ampere</i>
<b>LOD</b>	<i>Limit of Detection</i>	<b>μM</b>	<i>Micro Molar</i>
<b>IHMO</b>	<i>Incipient Hydrous Oxide Adatom Mediator</i>		
<b>EDX</b>	<i>Energy-Dispersive X-Ray Spectroscopy</i>		
<b>EIS</b>	<i>Electrochemical Impedance Spectroscopy</i>		
<b>FE-SEM</b>	<i>Field Emission Scanning Electron Microscopy</i>		
<b>HR-TEM</b>	<i>High-Resolution Transmission Electron Microscopy</i>		
<b>MOCVD</b>	<i>Metal-Organic Chemical Vapor Deposition</i>		
<b>SILAR</b>	<i>Successive Ionic Layer Adsorption and Reaction</i>		
<b>MWCNT</b>	<i>Multiwalled Carbon Nanotube</i>		

# CHAPTER I



## Index

Sr. No.	Details	Page No.
1.1	Glucose biosensors	1
1.2.	Enzymatic glucose biosensors	3
	1.2.1. <i>Glucose oxidase</i>	3
	1.2.2. <i>1<sup>st</sup> generation glucose biosensors</i>	5
	1.2.3 <i>Major drawbacks of 1<sup>st</sup> generation glucose biosensor</i>	6
	1.2.4. <i>2<sup>nd</sup> generation glucose biosensor</i>	6
	1.2.5 <i>Mediators</i>	7
	1.2.6 <i>Major drawbacks of 2<sup>nd</sup> generation glucose biosensor</i>	10
	1.2.7. <i>3<sup>rd</sup> generation glucose biosensors</i>	10
1.3	Non-enzymatic electrochemical glucose biosensor	11
1.4	Mechanism of glucose oxidation on electrode surface	12
	1.4.1. <i>Activated chemisorption model</i>	12
	1.4.2 <i>Incipient hydrous oxide adatom mediator model</i>	13
1.5	Metal oxide based non-enzymatic glucose sensor	15
	1.5.1 <i>Literature survey on transition metal oxides with their composites</i>	15
1.6	Orientation and purpose of the thesis	26
1.7	References	29

## 1.1 Glucose biosensors:

Biosensors have widely used for different applications with main goal to improve the quality of human life. Generally, an application covers their use for disease detection, food safety, drug discovery, environmental monitoring, and many more. Apart from that, the main application of biosensors is the detection of biomolecules from human blood. In that context, glucose detection has an important role in the area of clinical diagnosis and monitoring of diabetes. Nowadays 9.5 % of the people are suffering from diabetes all over the world and they are facing various health problems such as eye diseases, strokes, and heart diseases, failure of kidney, gum and dental diseases [1]. International Diabetes Federation (IDF) was searched and reported statistical data that owing to diabetes 5 million people deaths in 2015 [2]. According to IDF, statistics of diabetes patients there are 1 in 11 adults in the range between 20-79 years have diabetes (463 million people), 1 in 5 adults (above 65 years) have diabetes (136 million people), 1 in 6 live births have affected by hyperglycemia in pregnancy (20 million) 2 in 3 lives in urban areas (out of the 84 %) have gestational diabetes. A decade ago, in 2010, the global projection for diabetes in 2025 has been estimated 438 million. Still, four years to go, and the prediction is already crossed. According to IDF, there will be 578 million adults with diabetes by 2030 and 700 million by 2045. **Fig. 1.1** indicates the expected and approximation number of adults suffering with diabetes. According to World Health Organization (WHO), these people will become seventh leading cause of death upto 2030. Lacking of insulin in the human body (i.e. type 1 diabetes) and in other side by the disability of insulin (i.e. type 2 diabetes) can be treated efficiently by providing necessary insulin to the human body. [3].

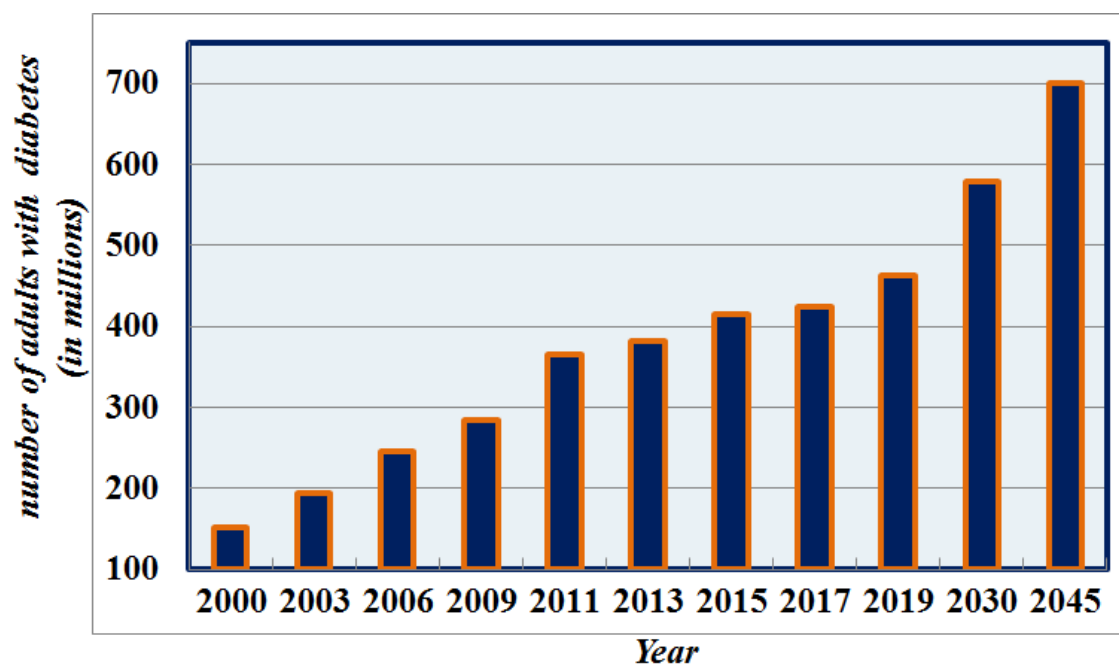


**Figure 1.1** Numbers of adults with diabetes by the year

It is imperative to regularly check the blood sugar level in the human blood sample to see if the treatment works effectively [4]. Due to the various applications in the arena of medicine, pharmaceutical, food, environmental industry, biotechnology, etc., quantitative and qualitative analysis of glucose has attracted attention. To overcome the challenges posed specially by diabetes, a very quick and reliable diagnosis of the glucose level in blood sample helps in proper treatment and strict control of diabetes. Thus, for the clinical diagnostics, to make the highly sensitive, accurate, fast, and rapid sensing devices that check the sugar level in blood sample is a serious challenge in the present situation [1, 5]. Thus, the glucose biosensor market is growing fast; there is a lot of interest to develop new biosensors for glucose monitoring. So, many scientists, researchers, and industries are jointly working together to overcome some the drawbacks of present biosensor. Various methods including colorimetry, conductometry, electrochemical, optical, fluorescent spectroscopy have been employed for glucose sensing. Out of theses, from last 4

decades, the glucose sensing domain was dominated by electrochemical glucose sensor owing to their fast response, simple instrumentation, sensitivity, excellent stability, inexpensive, high specificity, and low detection limit.

Generally, two types of glucose sensors (enzymatic and non-enzymatic) available for the measurement of glucose levels. The different types of enzymatic techniques are available for glucose sensing which followed in two routes:

- ❖ One is the oxidation of glucose by dehydrogenation with subsequent determinations of the cofactor.
- ❖ The second one is based on the monitoring of glucose by the formation of hydrogen peroxide; the hydrogen peroxide is the consumption of oxygen or direct generation of the active center of the enzyme.

## **1.2 Enzymatic glucose biosensors:**

### **1.2.1 Glucose oxidase:**

The most of the enzymes used by the researchers for direct oxidation are glucose oxidase (GOx) take out from *Aspergillus niger* acid (i.e. E.C.1.1.3.4) and glucose dehydrogenase (GDH) take out from *Acinetobacter calcoaceticus* acid (i.e. E.C.1.1.1.47) [6]. The group of glucose oxidase belong to flavoproteins, consists of flavin adenine dinucleotide (FAD) as a cofactor. FAD is does not bound covalently to enzyme and it's also crucial for the oxidation of glucose. GOx is a function of oxido-reductase of glucose molecule which acts as a catalyst leading to transfer of electrons from the electron donor, glucose. **Fig. 1.2** displays 1<sup>st</sup> half reaction of glucose is oxidized by the GOx to gluconolactone, after that gluconolactone is hydrolyzed spontaneously to convert into gluconic acid. In the 2<sup>nd</sup> half reaction, FAD mediator acts as an electron acceptor and at that time reduced, that is oxidized by molecular

oxygen ( $O_2$ ). The end point electro-active reaction is by reduction of oxygen to hydrogen peroxide [6]. The above explanation presented in the form of reaction in figure below:

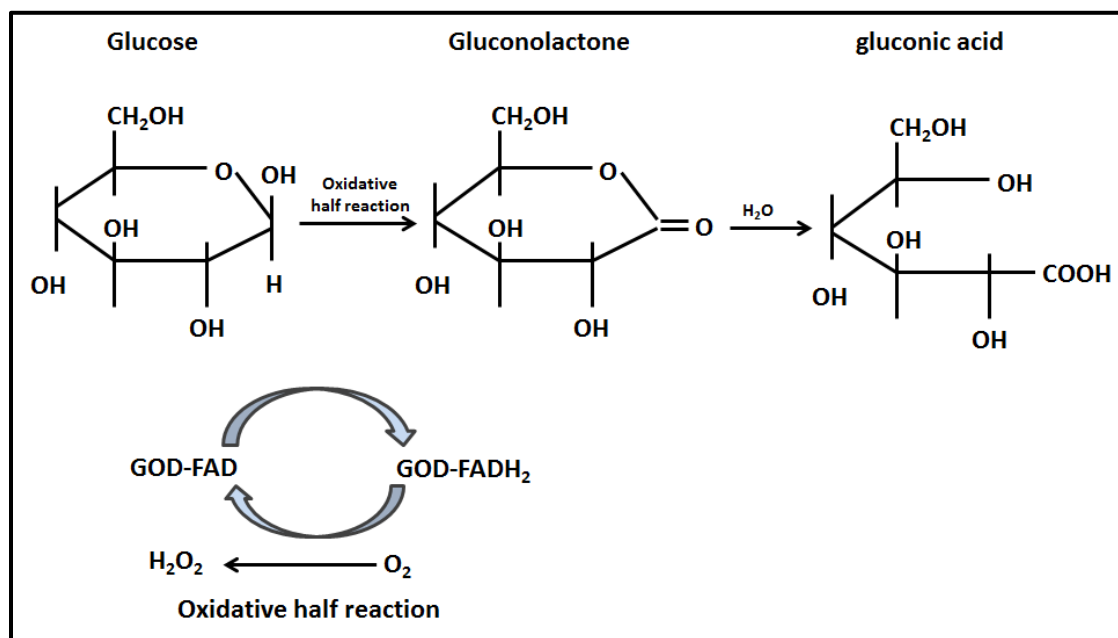


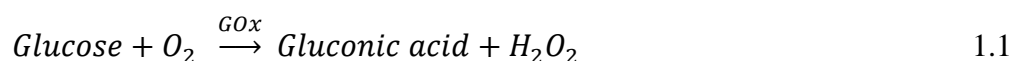
**Figure 1. 2** Shows the 1<sup>st</sup> half reaction of glucose is oxidized by the GOx enzyme to glucanolactone

The first glucose sensor (enzymatic) was developed by Clark and Lyons in 1962 [7], the oxygen consumption was monitored during the catalytic oxidation of glucose. However, complications varying the amount of oxygen led to the development of new oxygen sensor by Updike and Hicks [8] with background corrected oxygen levels. The first amperometric glucose sensors (enzymatic) was developed in 1973 [9], the production of hydrogen peroxide was studied alternatively by the oxygen reduction current. Since, this innovative work on the enzymatic glucose sensors progressed rapidly due to the advanced electrochemical and nanotechnology. The two main types of enzyme such as glucose oxidase (GOx) and glucose dehydrogenase are mostly used in this technology, while, GOx is highly stable and

selective towards glucose molecules than other enzymes. Potential response electrode is quickly losses the both activity above pH 8 or below pH 2 and also it is easily affected by sodium dodecyl sulfate, surfactants at a low pH and hexadocyl trimethyl ammonium bromide at higher than 10 pH. Also, it is relatively showing low activity due to the dependence of oxygen concentration by surrounding atmosphere. This is marked in the review by Wilson and Turner [10] in 1992, by ideal enzyme for glucose oxidation

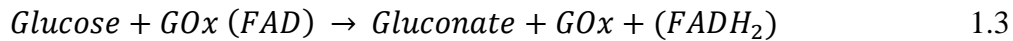
### 1.2.2 First generation glucose biosensor:

The first amperometric biosensor for glucose analysis based on oxygen consumption in the presence of enzyme, reported by Lenard C. Clark [7] represents the first generation of biosensors. The first generation glucose sensors estimated the glucose concentration by means of the amount of hydrogen peroxide produced by the GOx in the presence of dissolved oxygen. As discussed above, glucose oxidation involves charge transfer from the active center of GOD flavin adenine di-nucleotide (FAD) cofactors that are tightly bound and deeply buried in the protein shell of the GOD [6-10]. In GOD catalyzed glucose oxidation, FAD acts as initial electron acceptor and is reduced to FADH<sub>2</sub>. FADH<sub>2</sub> is then oxidized by the final electron acceptor, O<sub>2</sub> because it has a higher reduction potential and O<sub>2</sub> is then reduced to hydrogen peroxide (H<sub>2</sub>O<sub>2</sub>). These are represented by the following equations 1.1-1.5.



A negative voltage is applied to the any working electrode for oxygen consumption as





The again formation of the cofactor of enzyme GOx is occurred in the presence of oxygen molecule, revealing the formation of hydrogen peroxide ( $\text{H}_2\text{O}_2$ ) as,



In that regard, we assume that the rate of reduction of oxygen is directly propositional to the glucose concentration that is measuring reduction of oxygen as well as measuring the concentration of hydrogen peroxide.

### 1.2.3 Major drawbacks of first generation glucose sensor:

- The selectivity of electrode is poor due to the presence of hydrolyzing and reducing agents like ascorbic acid, uric acid, dopamine, fructose, and other constituents of blood.
- Diminishing linear range of the biosensor because lack of oxygen.

The main two approaches reduce the first generation glucose biosensor quality.

In the first method, the oxygen soluble fluorocarbon pasting liquid is used for GOx. And second method utilized two dimensional electrodes to avoid the diffusion of glucose in one way, while oxygen is ready to diffuse from both directions at the immobilized enzyme. Hence, the results of sensors are very poor. These results are due to very low charge transfer ability of GOD. Thereof redox active centers are covered within the enzyme and protected by protein layer. The developed mediators to carry out easily electron transfer between the electrode and enzyme and enhance reaction rates.

### 1.2.4 Second generation glucose biosensor:

Second generation glucose sensor have been introduced in 1980 which are based on artificial mediators. Artificial electron mediators are to enhance the charge transfer rate and to remove the oxygen dependency in the second generation biosensor. The lower redox potential mediators are required for glucose oxidation reaction. The second generation is classified as shown in **Fig 1.3**.

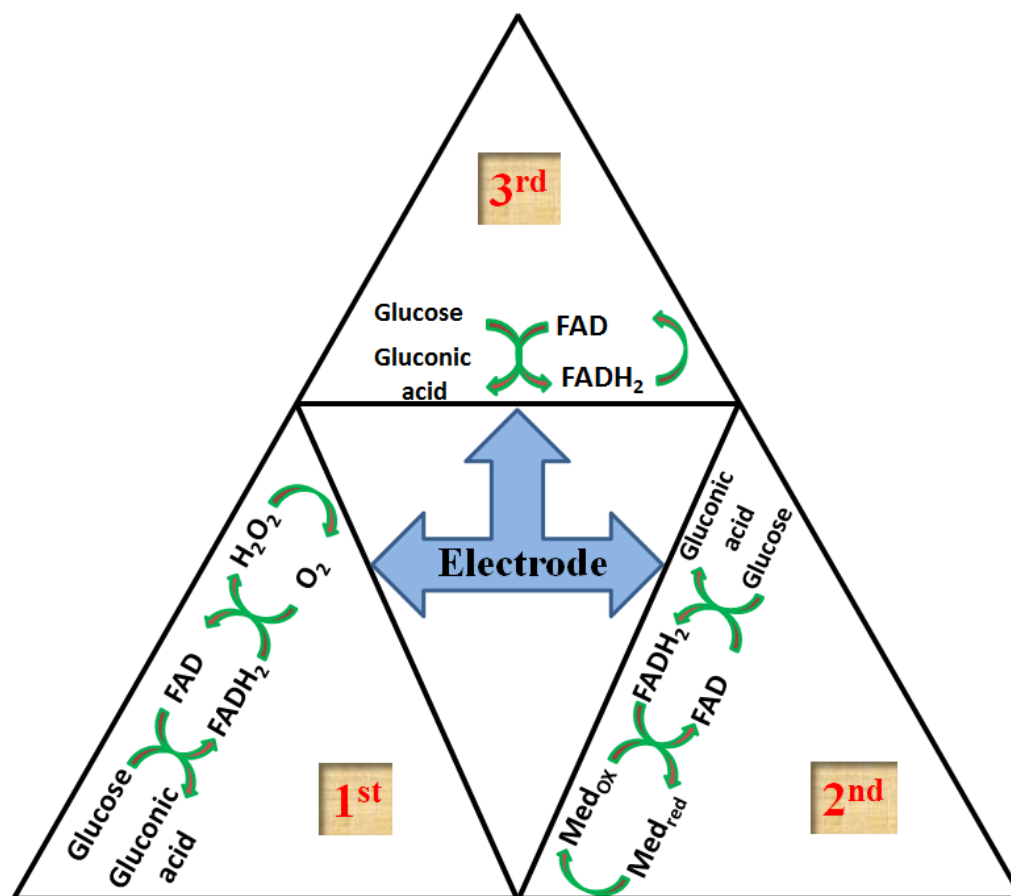


**Figure 1. 3** The mechanism of first, second and third generation of enzymatic glucose oxidation

### 1.2.5 Mediators:

The mediators are key role agents in the second generation glucose biosensor. These mediators are given up new horizons in the glucose biosensor. Many mediators require lower redox potential for glucose oxidation. The glucose reaction with reduced

form of enzyme formed by the glucose oxidation and to diffuse on the electrode surface. The main two advantages of mediators are given bellow.

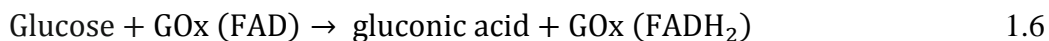
1. The dissolved oxygen concentration is not affected by the GOD ( which acts as an catalyst)
2. And lower oxidation potential is required for hydrogen peroxide or glucose monitoring. Moreover, the mediators are independent of temperature or pH, and do not react with involved oxygen, highly reactive and of low toxicity.

The mediators are classified in the three groups, namely organic, inorganic, and organo-metallic. These are listed in the following **Table 1**.

**Table 1:** Various mediators classified in three groups

Organic	Inorganic	Metal-Organic
Quinines	Hydrogen peroxide (H <sub>2</sub> O <sub>2</sub> )	Osmium complexes
Quinine and its derivatives	Oxygen	Ferrocene derivatives
Quinoid dyes	Hexacyano-complexes of	Ruthenium complexes
Oxidized viologens	ruthenium, iron, and cobalt	Chromium derivatives
Conducting salts		
Heterocyclic		
dihydropolyazines		
Tetracyanoquinodimethane		
Tetrathiafulvaline		

The mechanism of second generation biosensor is explained in following reaction.



While, all the organic mediators worked as catalysis in the enzymatic reaction [11], the quinines, and their derivatives are manifest to react with other proteins [12]. As well, these organic mediators are mostly sensitive to acidic and basic solution, and their stability is dubious [13]. In that context, many researchers have decided to overcome these problems; the Tetrathiafulvalene and its products are generally used for the electron transfer process, mainly for flavoenzymes used [14-16]. Lower oxidation potential between 0.1-0.3 V/SCE of this compound stops the interference from the undesired species [11, 17]. Hydrogen peroxide and oxygen are natural intermediaries for GOx, despite that, they should high oxidation potential (0.7 V/SCE) for peroxide. Then, hexacyano-complexes like  $[\text{Co}(\text{CN})_6]^{3-/4-}$ ,  $[\text{Ru}(\text{CN})_6]^{3-/4-}$ , and  $[\text{Fe}(\text{CN})_6]^{3-/4-}$  [18], which are proposed for transfer of electron very fast in biosensors basically in enzymatic glucose sensor [19, 20]. Because of their low molecular weight, (small size) they easily diffuse into the enzyme redox center and facilitate the charge transfer mechanism and develop strip-based glucose sensor strips based on screen-printed carbon.

Organo-metallic mediators such as ferrocene and osmium complexes are also exhibited to possess excellent durability and quick transfer of electron rate in between enzyme and electrode. These advantages promote the expansion of strip-based glucometers for society use by company ExacTech from Medisense [21] which are compared with conventional carbon pest. Recently, many researchers have used carbon nanotubes (CNT) that can enhance the electron transfer rate [22]. The increased charge transport path way in CNT is due to the acceptable changes of the GOx exposing the kinetic path way of GOx for more rapidly electron transfer [23]. Other than carbon nano materials, platinum [24], gold [25], silicon particles [26],

---

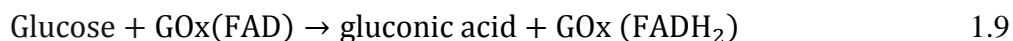
silver [27], and laponite silicon materials with polycrystalline sub-nanometer are increases the electron transfer rate [28, 29]. However, these nanoparticles are reported that drastically increase the enzyme performance.

### 1.2.6 The major drawbacks of mediators in second generation glucose sensor:

- The competition of dissolved oxygen, synthetic mediators, and GOx is high and also that accumulates of the hydrogen peroxide near the potential electrode surface.
- Interference that oxidizes with mediators at lower applied potential that will do not providing accuracy and enhances reaction of mediators with interfering species.
- Highly diffusive nature and small sizes of mediators poses difficulties and restriction their applications.

### 1.2.7 Third generation glucose biosensor:

The many more complication of using synthetic mediators in second generation is avoided by new developing third generation glucose biosensors. Researchers have developed 3<sup>rd</sup> generation glucose sensor that allows electrons to be transferred directly to the electrode surface and to active redox sites of enzyme, increase the sensitivity and reproducibility. This generation glucose biosensor is appropriate for monitoring blood sugar due to its stability and biocompatibility. The mechanism of third generation biosensor explained is in following reactions.



Third generation biosensor could be operated at a low potential which results to diminished interferential electro-active species. But still this generation biosensor

suffered from relatively smaller linear range compared to first and second generation glucose sensors and also restriction emerged from humidity, temperature etc. [30, 31].

### **1.3 Non-Enzymatic electrochemical glucose sensor:**

Hence, due to intrinsic disadvantages of GOx based enzymatic sensor like complicated and multi-step immobilization procedures, humidity, thermal stability, chemically instable, pH, high cost etc. researchers across the globe devoted more effort towards the non-enzymatic glucose sensor which could become alternative for enzymatic glucose sensor [32]. Non-enzymatic glucose sensors due to their easy preparation procedure, ultra-high sensitivity, rapid measurements, very less amount of analyte/samples required for calibration, long term durability, extraordinary selectivity, low detection limit, reproducibility, low cost, high stability, flexible operating system were considered as a 4<sup>th</sup> generation glucose biosensor [33, 34].

There are various methods have been developed for glucose sensing including colorimetry, electrochemical method, conductometry, optical method and fluorescent spectroscopy. Out of theses, electrochemical glucose sensor attracted more attention over the last 40 years because of their fast response, simple instrumentation, sensitivity, excellent stability, inexpensive, high specificity and low detection limit. Among the electrochemical detection approaches, two specific methods, named potentiometric and amperometric are used mostly in monitoring glucose concentration. In potentiometric mode, the potential difference between the reference electrode and indicator (working) electrode is measured at zero applied current. It is commonly used to measure glucose concentration in the order of few  $\mu\text{M}$ . As concentration of glucose changes, the potential of working electrode also changes [35, 36]. In an amperometric mode, constant bias potential is applied and resulting current

is measured. When glucose undergoes chemical reaction, current starts to flow as electrons are produced. The resulting current is proportional to the concentration of glucose [37]. An amperometric biosensor consists of two or three electrodes. The use of a two-electrode system is limited because controlling the potential at a high current is difficult. Therefore, three electrodes system (reference electrode, counter (auxiliary) electrode, and working electrode) is commonly introduced. The potential changes of the working electrode are measured independent of changes that may occur at the counter electrode.

### **1.4 Mechanism of glucose oxidation on electrode surface:**

For conventional enzymatic sensors, the enzymes e.g. GOx or glucose dehydrogenase (GDH) are used as an electrocatalyst on the electrode. In the case of a non-enzymatic glucose sensor, GOx and GDH are not used as electrocatalyst instead electrode surfaces are modified with the large number of active nanomaterials themselves act as electrocatalyst for oxidation of glucose. Generally, two major mechanisms have been proposed to explain the electrocatalytic processes in non-enzymatic glucose sensors.

#### **1.4.1 Activated chemisorption model:**

The activated chemisorption model was first proposed by D. Pletcher in 1984. This model assumes that the oxidation process initiated with adsorption of glucose molecule on the surface of electrode via the unpaired d-electrons of unfilled d-orbital's of transition metal atoms, which are readily available to generate the bond with adsorbates [38]. Pletcher suggested that the process of hydrogen abstraction and adsorption of organic species occurs simultaneously, leading to the electrocatalysis of glucose oxidation. In most of the glucose electro-oxidation experiments, the

abstraction of hydrogen (removal of the hemiacetalic hydrogen atom) is considered the rate-determining step, and chemisorptions of glucose were generally considered to occur simultaneously. Therefore, the nearby active metal center is occupied by single adsorbate, implying that well-spaced adsorption sites on electrocatalysts surface enhance the glucose oxidation process. The activated chemisorptions model is explained in the following **Fig 1.4**. The activated chemisorptions model fails to explain the role of hydroxyl radicals generated in alkaline medium [39, 40].

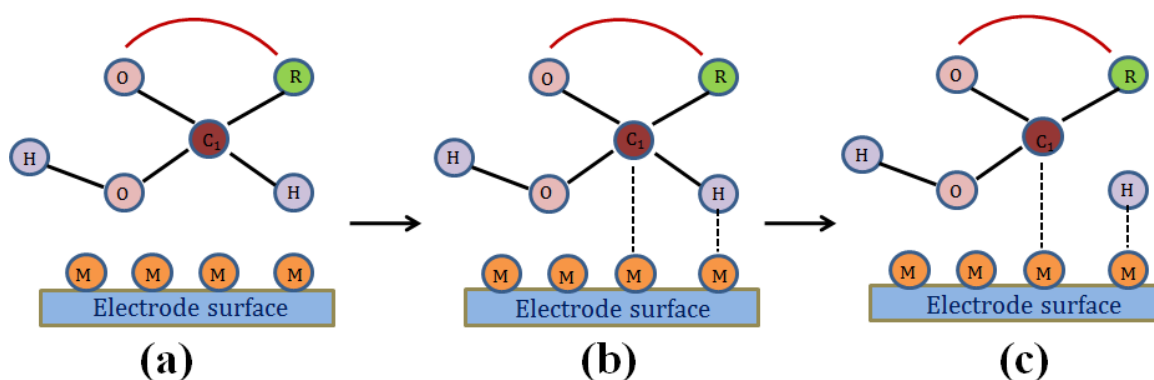


**Figure 1.4** The scheme of activated chemisorptions model

In the scheme of activated chemisorptions model M is metal atom, C is hemiacetalic carbon atom and R is other components of the glucose molecule.

#### 1.4.2 “Incipient hydrous oxide adatom mediator” model:

The activated chemisorption model explains only the process of adsorption at the interface of electrode but fails to explain role of hydroxyl radicals generated in a medium. It is evident in numerous publication that electro-oxidation of glucose can occur via adsorption of hydroxyl radicals ( $\text{OH}_{\text{ads}}$ ) [41, 42]. The “Incipient hydrous oxide adatom mediator” model (IHOAM) has been discussed by L. D. Burke [43]. This model was based on the observation that active surface metal atoms undergo a pre-monolayer oxidation step that formed an incipient hydrous oxide layer of reactive

hydroxyl radicals ( $\text{OH}_{\text{ads}}$ ). The generated  $\text{OH}_{\text{ads}}$  layer work for mediating oxidation and inhibiting reduction of kinetically slow electrode reaction. Following fig illustrate this proposed model which shows oxidative and reductive processes at metal surface [44].

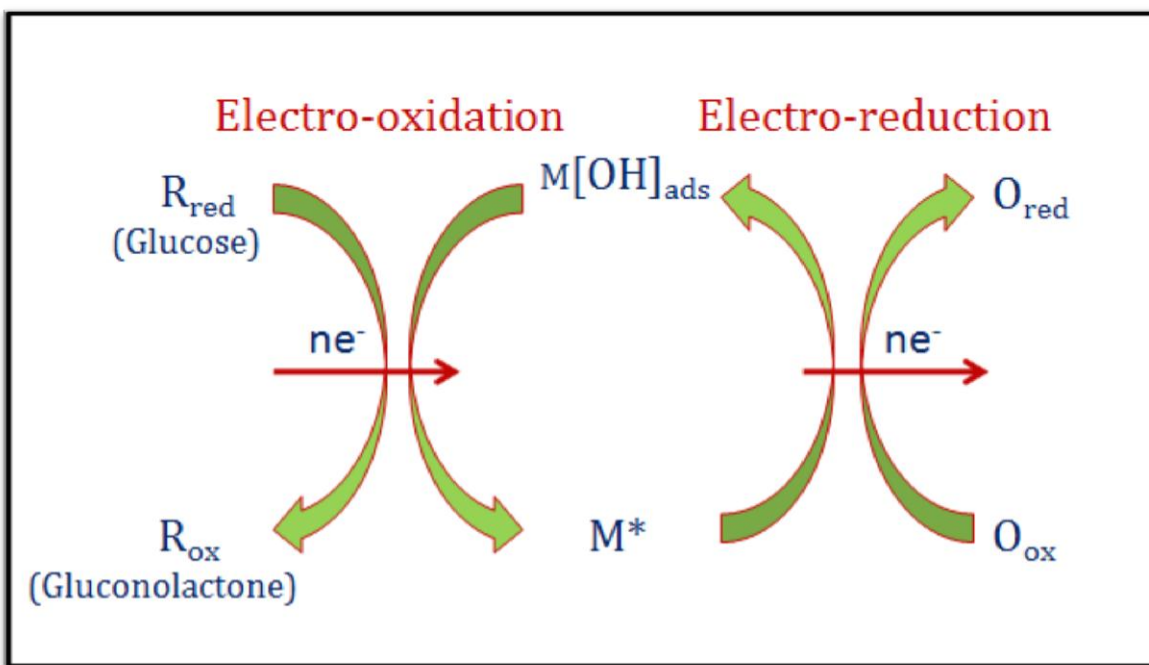


**Figure 1. 5** The scheme of IHOAM model proposed by L. D. Burke [43]

The active hydroxide anion produced by the dissociation of water electro-oxidation of glucose and many other organic molecules is well known. The chemisorptions of hydroxide anions on the reductive metal adsorption sites lead to formation of  $\text{MOH}_{\text{ads}}$  which is catalytic component of electrocatalysts for glucose.



As seen in the above equation, it is believed that increase in the  $\text{OH}^-$  concentration surely increases the formation of  $\text{MOH}_{\text{ads}}$ . So non-enzymatic glucose sensing is pH dependant reaction. Therefore, for formation of  $\text{MOH}_{\text{ads}}$  species alkaline environment

is suitable i.e. at higher pH value environment a higher sensitivity is generally observed in alkaline medium for non-enzymatic glucose sensor [45]. The scheme of IHOAM model proposed by L. D. Burke is shown in **Fig. 1.5**. In the IHOAM model,  $M[OH]_{ads}$  is the oxidative adsorbed hydroxide radical, and  $M^*$  is the reductive metal adsorption site.

### **1.5 Metal oxide based non-enzymatic glucose sensor:**

Non-precious transition metals and metal based oxides, hydroxides, phosphides, sulfides, and their complexes have been greatly employed to fabricate non-enzymatic competent glucose sensors. It is well known that the properties of the nanoscale metal oxide materials are very much different from their bulk materials. Because of its small size, well order crystalline structure, large surface to volume ratio, and dimensions comparable to Debye length, nanoscale metal oxides could appreciably enhance their glucose sensing activity [46]. Noble metal like gold, platinum, and palladium have been used as a catalyst for enzyme less glucose sensor thereof costing of material as well their device fabrication is high [47, 48]. Transition metals have the potential to adopt several oxidation states also can absorb on the surfaces of other species to form intermediates and channelize them in the reaction process [49]. Elements coming in the third line of the periodic table are comparatively inexpensive and can provide quick and sensitive responses towards glucose molecules [50].

#### **1.5.1 Literature survey on transition metal oxides with their composites:**

Several researchers have explored numerous metal oxides for the glucose sensing purpose employing various synthesis strategies in order to achieve different morphologies which results in enhanced performance in terms of sensitivity, linear

range, and limit of detection (LOD) and response time. As long as results are concerned, synthesis method, annealing temperature, morphology, surface area and precursors used play an important role. Table 1 briefly summarizes the effect of above mentioned parameters on the sensing properties of metal oxides and their composites. Many researchers have synthesized nanomaterials by varying various parameters and obtained different morphologies including thorn, nanoplates and nanosheets. Kannan et al. [51] reported thorn and nanowire like morphology of  $\text{Co}_3\text{O}_4$  after reversing the molar ratio of precursor used. In which he found that the thorn like morphology possesses high surface area ( $86.2 \text{ m}^2 \text{ g}^{-1}$ ) than the nanowire ( $67.5 \text{ m}^2 \text{ g}^{-1}$ ). The enhancement in sensitivity was observed due to high surface area, providing direct connection with glucose molecule and  $3\text{D}/\text{Co}_3\text{O}_4$  directly grown on the carbon fiber paper (CFP) substrate [55]. On the other hand, L-lysine played unique role in preparation of porous  $\text{Co}(\text{OH})_2$  nanoplates. The L-lysine controls the redissolution-recrystallization and dehydration condensation reaction of  $\text{Co}(\text{OH})_2$ . After thermal decomposition,  $\text{Co}(\text{OH})_2$  gets converted into  $\text{Co}_3\text{O}_4$  [52]. Also, Liu et al. [53] studied glucose sensing performance using  $\text{Co}_3\text{O}_4$  nanosheets grown uniformly on CC which provides more active sites for ion transformation process and facilitates electrocatalytic reaction. Therefore, nanosheets structured  $\text{Co}_3\text{O}_4$  electrodes exhibited ultrahigh sensitivity of  $8506 \mu\text{AmM}^{-1}\text{cm}^{-2}$ . Both  $\text{Co}_3\text{O}_4$  nanosheets and highly conducting carbon cloth (CC) enhanced glucose sensing performance as compared to  $\text{Co}_3\text{O}_4$  having other morphologies. In order to enhance the glucose sensing performance, hybridization strategy is also found to be very useful. Hybrid structure of  $\text{Co}_3\text{O}_4$  with graphene oxide and graphene oxide hydrogels (GOH) fabricated on GCE by Yang et al. [54] and Hoa et al. [55] respectively. Microsphere like morphology of

$\text{Co}_3\text{O}_4@\text{G}$  showed highest sensitivity because well-ordered porous structure with remarkable electrical conductivity and more active sites. A microsphere with average diameter of 8.2  $\mu\text{m}$  was assembled by large number of nanosheets. Therefore, strong mutual interaction between the  $\text{Co}_3\text{O}_4$  and graphene sheets triggered hierarchical co-assembly of microspherical structure in order to minimize surface energy. The surface area of  $\text{Co}_3\text{O}_4/\text{GOH}$  deposited for 12 h was found to be  $291.86 \text{ m}^2 \text{ g}^{-1}$  that was 3.8 and 1.4 time greater than that of pure  $\text{Co}_3\text{O}_4$  and GOH, respectively but could not achieve sensitivity greater than  $\text{Co}_3\text{O}_4@\text{G}$ . The porous structure of  $\text{Co}_3\text{O}_4$  and graphene sheets offers large number of active sites and continuous pathway for transfer of electron through interconnected network of  $\text{Co}_3\text{O}_4$  and graphene.

Different transition metals such as Zn, Cu and Ni with  $\text{Co}_2\text{O}_4$  electrode showed micro-rice, nanosheets and nanowires like morphology after annealing, respectively. Zhang et al. [56] reported  $\text{ZnCo}_2\text{O}_4$  that showed micro rice morphology obtained after annealing at 400  $^\circ\text{C}$  for 2 h. The obtained sensitivity of porous  $\text{ZnCo}_2\text{O}_4$  was  $436.1 \mu\text{A mM}^{-1} \text{ cm}^{-2}$ . In a study reported by Liu et al. [57] flower-like  $\text{CuCo}_2\text{O}_4$  nanosheets were directly deposited on graphite paper and subsequently annealed at 350  $^\circ\text{C}$  for 3 h. For the comparison purpose,  $\text{Co}_3\text{O}_4$  was grown on graphite paper by same method without using Cu precursor which revealed formation of nanoflakes. The performance of sensor was evaluated at 0.6 V in alkaline solution. The synthesized electrode showed excellent sensitivity of  $3625 \mu\text{A mM}^{-1} \text{ cm}^{-2}$ . The enhancement in sensitivity was attributed to the 2D nanosheet which again provides more active sites as described earlier. Porous  $\text{NiCo}_2\text{O}_4$  nanowire arrays were directly grown on CC having area (2.5 cm  $\times$  2 cm) reported by Luo et al. [58]. The bath was prepared in the molar ratio of 1:2:3 for  $\text{NiCl}_2:\text{CoCl}_2:\text{urea}$ . The reaction was carried out at 120  $^\circ\text{C}$  for 6 h and the

resultant product was annealed at 350 °C for 3 h in air atmosphere. From SEM image it was observed that entire surface of CC was covered by nanowire arrays and BET measurement revealed surface area of NiCo<sub>2</sub>O<sub>4</sub> NWs was 35.8 m<sup>2</sup> g<sup>-1</sup>. For the comparison, bare NiO and Co<sub>2</sub>O<sub>4</sub> were also synthesized. But electrochemical behavior showed larger current response for NiCo<sub>2</sub>O<sub>4</sub> than that of bare NiO and NiCo<sub>2</sub>O<sub>4</sub> towards 0.5 mM glucose in alkaline solution. Amperometric technique was used to further investigate performance of NiCo<sub>2</sub>O<sub>4</sub> electrode at an optimized potential of 0.5 V. The prepared electrode showed extraordinary sensitivity of 4120 μAmM<sup>-1</sup>cm<sup>-2</sup>, LOD of 0.5 μM, quick response within 5 s and linear response in the range between 1 μM to 0.63 mM. This higher performance was obtained because a nanowire of NiCo<sub>2</sub>O<sub>4</sub> favors more active sites, superior electrical conductivity because of binary metal oxide component and binder free construction of electrode. Further enhancement was achieved by Saraf et al. [59] on NiCo<sub>2</sub>O<sub>4</sub> by obtaining nanorod like morphology onto GCE. The combined effect of nanorod like morphology and GCE favored for the greater sensitivity of 4710 μAmM<sup>-1</sup>cm<sup>-2</sup> than previously reported nanowires. In addition, the extraordinary performance was obtained due to suitable pore size which can accelerate the electron transfer rate by minimizing ion diffusion path. Several researchers used NF as a platform to synthesize various composites of NiCo<sub>2</sub>O<sub>4</sub>. Different morphologies were obtained with suitable bath parameters. In a report prepared by Duan et al. [60] formation of nanowire took place on NF. In other cases, sheet, urchin and nanoneedles were obtained on the NF. Again the morphology dependent nature of sensitivity was highlighted by obtaining 3059, 956 and 806.17 μAmM<sup>-1</sup>cm<sup>-2</sup> for nanowires, sheets/ urchin and nanoneedles respectively. Sequential method was applied to fabricate multi component composite of NiCo<sub>2</sub>O<sub>4</sub>@polypyrrole

(NiCo<sub>2</sub>O<sub>4</sub>@Ppy) nanowires. At first, hydrothermal method was used followed by calcination to synthesis NiCo<sub>2</sub>O<sub>4</sub> on NF substrate and then polymerization of pyrrole on NiCo<sub>2</sub>O<sub>4</sub>@Ppy was carried out. Amperometric measurement of NiCo<sub>2</sub>O<sub>4</sub>@ppy electrode showed excellent sensitivity. NiCo<sub>2</sub>O<sub>4</sub> composite with Mn<sub>2</sub>O<sub>3</sub> showed sheets and urchin like morphology reported by Mary et al. [61] In addition, Jo et al. [62] developed polymer dot (PD) bridged NiCo<sub>2</sub>O<sub>4</sub> which showed nanoneedle like morphology. The NiCo<sub>2</sub>O<sub>4</sub>@ppy showed maximum sensitivity due to multi component synergy contribution to construct suitable path for electron transfer and shortening the distance of electron transportation. Yu et al. [63] prepared core-shell structure of NiCo<sub>2</sub>O<sub>4</sub>@PANI, modified on GC electrode used as the working electrode which showed ultrahigh sensitivity. Upon comparison of NiCo<sub>2</sub>O<sub>4</sub>@PANI with previously mentioned NiCo<sub>2</sub>O<sub>4</sub> composite, it can be seen that NiCo<sub>2</sub>O<sub>4</sub>@PANI exhibit highest sensitivity of them all with the sensitivity being 4550  $\mu\text{AmM}^{-1}\text{cm}^{-2}$ . The NiCo<sub>2</sub>O<sub>4</sub>@PANI composite had maximum sensitivity of reported NiCo<sub>2</sub>O<sub>4</sub> with Ppy, Mn<sub>2</sub>O<sub>3</sub> and PD mainly due to large active sites and higher conductivity of NiCo<sub>2</sub>O<sub>4</sub>@PANI composite. Additionally, core-shell structure provides large number of channels for electron transportation as well as shortening the pathway for electron transportation. Heidari et al. [64] synthesized CoO nanoparticles grown on rGO pasted electrode (r-GOPE) via CV process in the potential window (P.W.) between 0.2 to 1.0 V vs. SCE at a scan rate 25 mV/s. The deposition was carried out in 0.1 M acetate solution at pH 7.5 containing 20 mM Co(NO<sub>3</sub>)<sub>2</sub>. The prepared sensor showed sensitivity of 1210  $\mu\text{AmM}^{-1}\text{cm}^{-2}$ . Electrodeposited NiCo<sub>2</sub>O<sub>4</sub> electrode fabricated by Li et al. [65] and Au- NiCo<sub>2</sub>O<sub>4</sub> by Naik et al. [66] sensor revealed nanowalls and nanosheets like morphologies, respectively. Naik et al. [66] reported fascinating

performance of the noble metal nanoparticles of Au and Ag hybridized with  $\text{NiCo}_2\text{O}_4$  deposited on highly conducting NF that showed superior performance as non-enzymatic glucose sensor. The prepared biosensor Au- $\text{NiCo}_2\text{O}_4$  demonstrated higher activity than that of Ag- $\text{NiCo}_2\text{O}_4$  and bare  $\text{NiCo}_2\text{O}_4$ . The sensitivity for pristine  $\text{NiCo}_2\text{O}_4$  was found to be  $20800 \mu\text{AmM}^{-1}\text{cm}^{-2}$  that is less in comparison with Ag- $\text{NiCo}_2\text{O}_4$  and Au- $\text{NiCo}_2\text{O}_4$ . The sensitivity exhibited by Ag- $\text{NiCo}_2\text{O}_4$  was  $29860 \mu\text{AmM}^{-1}\text{cm}^{-2}$  and for Au- $\text{NiCo}_2\text{O}_4$  it was  $44860 \mu\text{AmM}^{-1}\text{cm}^{-2}$  in the same linear range of 5-45  $\mu\text{M}$  with response time 8-15 s. The performance of hybrid Au- $\text{NiCo}_2\text{O}_4$  nanosheets was ultrahigh because it contains number of electrocatalytic and biocatalytic active sites and its surface to volume ratio was higher than that of pure  $\text{NiCo}_2\text{O}_4$ . Also, the noble metals Ag and Au acts as a catalyst which enhances the rate of oxidation and electrochemical reactions involved towards glucose molecules. The rate of charge transportation and diffusion of electrons/ions towards electrode increase leading to increases in electro-bio catalysis performance of the materials. Mondal et al. [67] presented, for the first time, various shapes like spherical nanoparticles (NP), porous nanorods (NR) and nanoflower of cobalt oxide by wet chemical method. After studying the electrochemical properties of different structures, it was observed that nanoflower shape of cobalt oxide was best candidate for glucose detection. The developed CoO nanoflower showed excellent sensitivities for two different linear ranges having LOD 0.04  $\mu\text{M}$  and 0.14  $\mu\text{M}$ . A stepwise process including magnetic sputtering, anodic oxidation and CBD at 85  $^\circ\text{C}$  for 1 h followed by annealing at 350  $^\circ\text{C}$  for 2 h was employed to fabricate  $\text{Co}_3\text{O}_4/\text{CuO}$  nanorod array on CC reported by Cheng et al. [68]. The fabricated electrode showed excellent sensitivity of  $5405 \mu\text{AmM}^{-1}\text{cm}^{-2}$  with linear response up to 500  $\mu\text{M}$ , LOD of 0.38  $\mu\text{M}$  and response time

1.9 s. The excellent performance was mainly achieved due to stable matrix of  $\text{Co}_3\text{O}_4$  shell that connects core CuO nanorods as well as core shell structure found to be well supported on CC without binder. Harry et al. [69] used chemical solution method to develop elemental Cu doped  $\text{Co}_3\text{O}_4$  electrode on FTO substrate. Initially,  $\text{CoCl}_2$  and sodium oleate precursor were used to synthesize cobalt oleate and then Cu solution was added to the cobalt oleate solution at various volume percentages (98: 2 V/V, 90:10 V/V, 85: 15 V/V, and 80: 20 V/V). After preparation of electrode on FTO, the electrodes were annealed at 350 °C for 4 h. electrochemical behavior of developed electrode showed highest activity for 90:10 volume percentages in comparison with other ratios. In this study, thickness of film on FTO played key role in sensing glucose. Hydrothermal method was employed for synthesis of  $\text{Co}_3\text{O}_4$  acicular nanotube arrays which was further used as a platform to grow  $\text{TiO}_2$  by spin coating technique by Gao et al. [70]. At first, acicular nanowire arrays were grown on FTO and then converted into acicular nanotube arrays through alkaline treatment.  $\text{TiO}_2$  nanoparticles decorated on its surface by spin coating method showed excellent performance than that of pristine  $\text{Co}_3\text{O}_4$  electrode. CoO/Au nanostructured electrode was developed by Su et al. [71] by electrodeposition (ED) and galvanic replacement reaction. FTO substrates were used to fabricate CoO/Au nanocomposite electrode. A very small amount of Au loaded on surface of nanosheets of CoO improved the transportation of electron which enhanced sensitivity of electrode. Such electrode showed sensitivity of  $6000 \mu\text{A}\text{mM}^{-1}\text{cm}^{-2}$  with linear response from 0.2  $\mu\text{M}$  to 20 mM with LOD of 0.1  $\mu\text{M}$ . Tang et al. [72] composited  $\text{NiCoO}_2$  material on CNT coated with sulfonated polystyrene. The obtained product was heated at 400 °C for 2 h under nitrogen atmosphere. CNT was capable to adsorb metal ions and induce the growth of

---

metal oxides. Finally, fabricated NiCoO<sub>2</sub>@CNT showed significant response in the concentration range from 0.01-1.55 mM, high sensitivity of 1424.41  $\mu\text{AmM}^{-1}\text{cm}^{-2}$  and LOD 1.14  $\mu\text{M}$  at an optimized potential of 0.5 V. Among these materials, nano-structured oxides have been widely used for application in glucose biosensors.

**Table No. 1:** Literature survey of transition metal oxides with their composites materials.

Sr. No	Electrode material	Morphology	Sensitivity ( $\mu\text{AmM}^{-1}\text{cm}^{-2}$ )	Linear range (mM)	LOD ( $\mu\text{M}$ )	Response time (s)	Working potential (V)	Electrolyte	Selectivity	Ref.
1	$\text{Co}_3\text{O}_4$	Nanowires	180	0.001 - 1	0.046	-	0.55	0.1 M NaOH	AA, UA, DA, Fru, Lac, Gal, cysteine, serotonin	[51]
2	$\text{Co}_3\text{O}_4$	Nanoplates	212.92	0.05 - 3.2	2.7	5	0.38	0.1 M NaOH	UA, AA, NaCl, KCl, $\text{NaNO}_3$ , D-gal, Fru	[52]
3	$\text{Co}_3\text{O}_4$	Nanosheets	8506	0.01 to 2.0	1	< 6	0.55	1 M NaOH	Fru, Lac, Mal, AA, UA	[53]
4	$\text{Co}_3\text{O}_4@\text{G}$	Hierarchical porous microsphere	628	0.02 - 8	0.038	4	0.55	0.1 M NaOH	AA, UA, DA	[54]
5	$\text{Co}_3\text{O}_4/\text{GOH}$	Nanoflowers	492.8	0.25 - 10	-	8	0.62	0.1 M NaOH	AA, UA, DA	[55]
6	$\text{ZnCo}_2\text{O}_4$	Micro-rice	436.1	0.01 -0.55	5	< 3	0.55	0.1 M NaOH	AA, UA, DA	[56]
7	$\text{CuCo}_2\text{O}_4$	Nanosheets	3625	up to 0.32	5	6	0.6	0.1 M NaOH	AA, UA, DA	[57]
8	$\text{NiCo}_2\text{O}_4$	Nanowires	4120	0.001 - 0.63	0.5	5	0.5	0.1 M NaOH	AA, UA, DA	[58]
9	$\text{NiCo}_2\text{O}_4$	Nanorods	4710	0.001 -0.88	0.063	3	0.4	0.1 M NaOH	AA, DA, UA, Fru, Gal, Mal, creatinine,	[59]

									acetaminophen	
10	NiCo <sub>2</sub> O <sub>4</sub> @Ppy	Nanowires	3059	0.001 -0.1	0.22	-	0.5	0.1 M NaOH	AA, DA, Suc, Lac, Fru, NaCl	[60]
11	Mn <sub>2</sub> O <sub>3</sub> /NiCo <sub>2</sub> O <sub>4</sub>	Sheet and urchin	956	0.01 -0.15	35	-	0.7	0.1 M NaOH	AA, UA, DA	[61]
12	PDs-NiCo <sub>2</sub> O <sub>4</sub>	Nanoneedles	806.17	0.005 - 0.25	2.75	-	0.5	0.1 M KOH	AA, DA, Lac, urea, NaCl	[62]
13	NiCo <sub>2</sub> O <sub>4</sub> @PANI	Core-shell	4550	upto 4.73	0.38	-	0.5	0.1 M NaOH	DA, AA, UA, NaCl	[63]
14	CoO/r-GOPE	Nanosheets	1210	0.040 - 4	1.4	-	0.45	0.1M NaOH	Saccharose, Fru, L-histidine, L-phenylalanine, L-methionine	[64]
15	NiCo <sub>2</sub> O <sub>4</sub>	Nanowalls	387.1	0.01 - 21	1	1	0.45	0.1 M NaOH	Urea, AA, DA, UA, AP, NaCl, Fru, Lac, Mal, Suc, Man	[65]
16	Au-NiCo <sub>2</sub> O <sub>4</sub>	Nanosheets	44860	0.005 - 0.045	2.64	8-15	0.4	0.1 M NaOH	AA, UA, DA, LA, Mal	[66]
17	CoO	Nanoflowers	693.02	0.005 - 0.060	0.04	3	0.60	0.01 M NaOH	AA, UA, DA	[67]
18	Co <sub>3</sub> O <sub>4</sub> /CuO	Nanorod	5405	0.001 -0.5	0.38	1.9	0.55	0.1 M	AA, UA,	[68]

		array						NaOH	DA, Suc, Fru	
19	Cu:Co <sub>3</sub> O <sub>4</sub>	-	1850	up to 7.6	0.153	10	0.6	0.1 M NaOH	AA, AC ,DA, Suc, Fru, NaCl, KCL	[69]
20	TiO <sub>2</sub> /Co <sub>3</sub> O <sub>4</sub>	Nanotube arrays	2008.82	0.01~3.0	0.339	5	0.5	1 M NaOH	AA, UA	[70]
21	CoO/Au	Flowers	6000	0.0002 - 20	0.1	-	0.60	0.1 M NaOH	AA, UA, DA	[71]
22	NiCoO <sub>2</sub> @ CNT	Nanoflakes	1424.41	0.01 - 1.55	1.14	-	0.5	0.1M NaOH	AA, UA, DA	[72]

### **1.6 Orientation and purpose of the thesis:**

All researchers, scientists, and industries are working together on improvement of non-enzymatic electrochemical glucose sensing application by means to enhance sensitivity, long term stability as well as cost effective synthesis process. The non-enzymatic glucose biosensor and its devices with outstanding electrochemical performance as well low cost fabrication process may raise its demand over the world. The working electrode material and electrolyte are the key factors and influence glucose sensing performance. However, the sensitivity of the glucose sensor are still low, to overcome this challenging aspect in the field of glucose biosensors, demands to prepare efficient working electrode with high sensitivity, wide linear range, long term stability and reproducibility. Previously prepared non-enzymatic glucose sensors of transition metal oxide based biosensors and their composites have tried to overcome these factors. Recently, transition metal oxides with doping of other elements are attracting more attention among the working electrodes for non-enzymatic glucose sensing application.

In the literature survey, we have observed that the transition metal oxide and their composites materials were effective with excellent non-enzymatic glucose sensing performance, but they have some drawbacks such as poor long term stability, reproducibility and reputability. In addition, the fabrication is complex and environment factors such as humidity, toxic chemicals, pH, and temperature damage the enzyme activity. These problems can be easily overcome by finding easy preparation method to improve surface texture leading to increases the surface area. So, sequentially doping and addition of metal ions can changes physical and chemical activities of the materials. Binary transition metal oxides noble solution used to rectify the drawbacks of single transition metal material where debility of one material

increases by another. So, the prime aim of this research is to explore the usefulness of  $\text{La}_2\text{O}_3$  and doping with silver (Ag) and manganese (Mn) for glucose sensing application. Some transition metals have multiple oxidation states such as Ag and Mn which reduce resistance of the electrode and participate in reaction mechanism.

The basic requirements for non-enzymatic glucose sensing electrode includes high conductivity, more surface area, chemical and mechanical stability which leading to enhance sensitivity, long term stability, wide linear range, reproducibility and reputability. Binder free electrochemical deposition is used for thin film preparations which enhance electrical conductivity of the working electrode. Binder free directly grown nanostructures of the materials on conducting substrate have better structural and mechanical stability. Hence many researches choice binder free thin film electrodes for non-enzymatic glucose sensing application.

For the preparation of binder free and without additives lanthanum oxide ( $\text{La}_2\text{O}_3$ ), silver doped lanthanum oxide ( $\text{Ag-La}_2\text{O}_3$ ) and manganese doped lanthanum oxide ( $\text{Mn-La}_2\text{O}_3$ ) thin film electrodes employed for non-enzymatic glucose sensing application. Simple, cost effective chemical method (ED) is selected for thin film preparation. This method is easy to handle, and useful to large area deposition. Preparative parameters such as deposition potential, pH of solution, deposition temperature, deposition time, and varies concentration bath can be easily controlled in this chemical method. This method offers gives materials properties such surface morphology, crystal structure and control the thickness of the film. The prepared thin films are characterized by physical and chemical methods such as X-ray diffraction (XRD), field emission scanning electrode microscopy (FE-SEM), energy dispersive spectroscopy (EDX), X-ray photoelectron spectroscopy (XPS), transmission electron microscopy (TEM), Brunauer-Emmitt-Teller (BET) techniques. The non-enzymatic

glucose sensing properties of prepared film electrodes by ED method is investigated by cyclic voltammetry, *i-t* amperometric techniques. Three electrode system is used for electrochemical study. The prepared film electrode used as working electrode, platinum sheet used as counter electrode and saturated calomel electrode used as reference electrode. Furthermore, the electrochemical performance of film electrode is evaluated in terms of sensitivity and long term stability.

Our main three important and challenging aspects of this works are to detect glucose concentration from human serum sample, enhance long term stability and selectivity leading to the improve quality devices which are helpful for the society. Hence, the prepared  $\text{La}_2\text{O}_3$ ,  $\text{Ag-La}_2\text{O}_3$  and  $\text{Mn-La}_2\text{O}_3$  thin film electrodes for glucose and different analyte detection such as ascorbic acid (AA), dopamine (DA), fructose (Fru) and lactose (Lac) which are commonly presents in the human blood. They are strong oxidizing agents similar to the glucose. as per aforementioned, the conclusions are evaluated on the basis of the electrochemical non-enzymatic glucose sensing performance of  $\text{La}_2\text{O}_3$ ,  $\text{Ag-La}_2\text{O}_3$  and  $\text{Mn-La}_2\text{O}_3$  thin film electrodes.

---

## 1.7 References:

1. H. Cao, A. Yang, H. Lia, L. Wang, S. Lib, J. Konga, X. Bao, R. Yang, A non-enzymatic glucose sensing based on hollow cuprous oxidenanospheres in a Nafion matrix. *Sens. Actuator B-Chem*, 214, 2015, 169-173, DOI: 10.1016/j.snb.2015.03.026.
2. M. Baghayeria, H. Veisi, M. G. Motlagh, Amperometric glucose biosensor based on immobilization of glucoseoxidase on a magnetic glassy carbon electrode modified with a novelmagnetic nanocomposite, *Sens. Actuator B-Chem*, 249, 2017, 321-330, DOI: 10.1016/j.snb.2017.04.100.
3. K. Tian, M. Prestgard, A. Tiwari, A review of recent advances in nonenzymatic glucose sensors, *Mater. Sci. Eng. C*, 41, 2014, 100-118, DOI: 10.1016/j.msec.2014.04.013.
4. T. Alizadeh, S. Mirzagholidpur, A Nafion-free nonenzymatic amperometric glucose sensor based on copper oxide, *Sens. Actuator B-Chem*, 198, 2014, 1-44, DOI: 10.1016/j.snb.2014.03.049.
5. Q. Balouch, Z. H. Ibupoto, G. Q. Khaskheli, R. A. Soomro, Sirajuddin, M. K. Samoon, V. K. Deewani, Cobalt oxide nanoflowers for electrochemical determination of glucose, *Journal of Electrochromic Materials*, 44, 2015, 3724-3732, DOI: 10.1007/s11664-015-3860-z.
6. J. Raba, H. A. Mottola, Glucose Oxidase as an Analytical Reagent, *Crit. Rev. Anal. Chem*, 25, 1995, 1-42, DOI: 10.1080/10408349508050556.
7. L. C. Clark, Jr. C. Lyons, electrode systems for continuous monitoring in cardiovascular surgery, *Ann. N. Y. Acad. Sci.*, 102, 1962, 29-45, DOI: 10.1111/j.1749-6632.1962.tb13623.x.
8. S. J. Updike, and G. P. Hicks, The Enzyme Electrode, *Nature*, 214, 1967, 986-988, DOI: 10.1038/214986a0.
9. G. G. Guilbault, G. J. Lubrano. An enzyme electrode for the amperometric determination of glucose. *Anal. Chim. Acta*, 64, 1973, 439-455. DOI: 10.1016/S0003-2670(01)82476-4.
10. R. Wilson, A. P. F. Turner. Glucose oxidase: an ideal enzyme. *Biosens. Bioelectron.*, 7, 1992, 165-185, DOI: 10.1016/0956-5663(92)87013-F.

11. H. Adam, B. Feldman. Electrochemical glucose sensors and their applications in diabetes management. *Chemical reviews*, 108, 2008, 2482-2505. DOI: 10.1021/cr068069y.
12. T. A. McDonald, S. Waidyanatha, S. M. Rappaport. Production of benzoquinone adducts with hemoglobin and bone-marrow proteins following administration of [13C6] benzene to rats. *Carcinogenesis*, 14, 1993, 1921-1925. DOI: 10.1093/carcin/14.9.1921.
13. M. Gerard, A. Chaubey, B. D. Malhotra. Application of conducting polymers to biosensors. *Biosens. Bioelectron.*, 17, 2002, 345-359. DOI: 10.1016/S0956-5663(01)00312-8.
14. Turner, Anthony, I. Karube, George S. Wilson. *Biosensors: fundamentals and applications*. Oxford university press, 1987.
15. J. Kulys, T. B. Rasmussen, K. Bechgaard, J. Marcinkeviciene, H. E. Hansen, Glucose oxidase electrode based on graphite and methylthio tetrathiafulvalene as mediator. *Anal. Lett.*, 26, 1993, 2535-2542. DOI: 10.1080/00032719308017971.
16. G. Palleschi, A. PF Turner. Amperometric tetrathiafulvalene-mediated lactate electrode using lactate oxidase absorbed on carbon foil, *Anal. Chim. Acta*, 234, 1990, 459-463. DOI: 10.1016/S0003-2670(00)83591-6.
17. J. Kulys, V. Simkeviciene, I. J. Higgins. Concerning the toxicity of two compounds used as mediators in biosensor devices: 7, 7, 8, 8-tetracyanoquinodimethane (TCNQ) and tetrathiafulvalene (TTF), *Biosens. Bioelectron.*, 7, 1992, 495-501. DOI: 10.1016/0956-5663(92)80006-W.
18. S. M. Zakeeruddin, D. M. Fraser, M. K. Nazeeruddin, M. Gratzel, Towards mediator design: characterization of tris-(4, 4'-substituted-2, 2'-bipyridine) complexes of iron (II), ruthenium (II) and osmium (II) as mediators for glucose oxidase of *Aspergillus niger* and other redox proteins. *J. Electroanal. Chem.*, 337, 1992, 253-283. DOI: 10.1016/0022-0728(92)80542-C.
19. S. H. Lee, H. Y. Fang, W. C. Chen, H. M. Lin, C. Allen Chang, Electrochemical study on screen-printed carbon electrodes with modification by iron nanoparticles in Fe (CN) 6 4-/3- redox system, *Anal. Bioanal. Chem.* 383, 2005, 532-538. DOI: 10.1007/s00216-005-0034-5.
20. S. A. Jaffari, and A. PF. Turner, Novel hexacyanoferrate (III) modified graphite disc electrodes and their application in enzyme electrodes-Part I. *Biosens. Bioelectron.*, 12, 1997, 1-9, DOI: 10.1016/0956-5663(96)89084-1.

- 
21. S. Rao, Exactech blood glucose meter, *Diabetic medicine: a journal of the British Diabetic Association*, 12, 1995, 450-451, DOI: 10.1111/j.1464-5491.1994.tb00315.x.
  22. C. Chenxin, and J. Chen, Direct electron transfer of glucose oxidase promoted by carbon nanotubes. *Anal. Biochem.*, 332, 2004, 75-83. DOI: 10.1016/j.ab.2004.05.057.
  23. H. Z. Zhao, J. J. Sun, J. Song, Q. Z. Yang, Direct electron transfer and conformational change of glucose oxidase on carbon nanotube-based electrodes. *Carbon*, 48, 2010, 1508-1514. DOI: 10.1016/j.carbon.2009.12.046.
  24. L. Bahshi, M. Frasconi, R. T. Vered, O. Yehezkeli, I. Willner, Following the biocatalytic activities of glucose oxidase by electrochemically cross-linked enzyme Pt nanoparticles composite electrodes. *Anal. Chem.*, 80, 2008, 8253-8259. DOI: 10.1021/ac801398m.
  25. S. Zhao, K. Zhang, Y. Bai, W. Yang, C. Sun, Glucose oxidase/colloidal gold nanoparticles immobilized in Nafion film on glassy carbon electrode: direct electron transfer and electrocatalysis. *Bioelectrochemistry*, 69, 2006, 158-163. DOI: 10.1016/j.bioelechem.2006.01.001.
  26. Y. Zou, C. Xiang, L. X. Sun, F. Xu, Glucose biosensor based on electrodeposition of platinum nanoparticles onto carbon nanotubes and immobilizing enzyme with chitosan-SiO<sub>2</sub> sol-gel. *Biosens. Bioelectron.*, 23, 2008, 1010-1016. DOI: 10.1016/j.bios.2007.10.009.
  27. S. Ma, W. Lu, J. Mu, F. Liu, L. Jiang, Inhibition and enhancement of glucose oxidase activity in a chitosan-based electrode filled with silver nanoparticles. *Colloids Surf. A Physicochem. Eng. Asp. COLLOID SURFACE A*, 324, 2008, 9-13. DOI: 10.1016/j.colsurfa.2008.03.029.
  28. D. Shan, J. Zhang, H. G. Xue, S. N. Ding, S. Cosnier, Colloidal laponite nanoparticles: extended application in direct electrochemistry of glucose oxidase and reagent less glucose biosensing. *Biosens. Bioelectron.*, 25, 2010, 1427-1433. DOI: 10.1016/j.bios.2009.10.046.
  29. N. German, A. Ramanaviciene, J. Voronovic, A. Ramanavicius, Glucose biosensor based on graphite electrodes modified with glucose oxidase and colloidal gold nanoparticles. *Microchim. Acta*, 168, 2010, 221-229. DOI: 10.1007/s00604-009-0270-z.
-

30. S. Park, H. Booa, T. D. Chung, Electrochemical non-enzymatic glucose sensors, *Anal. Chim. Acta*, 556, 2006, 46-57, DOI: 10.1016/j.aca.2005.05.080.
31. P. Si, Y. Huang, T. Wang, J. Ma, Nanomaterials for electrochemical non-enzymatic glucose biosensors, *RSC Advances*, 3, 2012, 3487, DOI: 10.1039/c2ra22360k.
32. S. Liu, J. Tian, L. Wang, X. Qin, Y. Zhang, Y. Luo, A. M. Asiri, A. O. Al-Youbi, X. Sun, A simple route for preparation of highly stable CuO nanoparticles for nonenzymatic glucose detection, *Catal. Sci. Technol.*, 2, 2012, 813-817, DOI: 10.1039/c2cy00453d.
33. K. Li, G. Fan, L. Yang, F. Li, Novel ultrasensitive non-enzymatic glucose sensors based on controlled flower-like CuO hierarchical films, *Sens. Actuator B-Chem*, 199, 2014, 175-182, DOI: [10.1016/j.snb.2014.03.095](https://doi.org/10.1016/j.snb.2014.03.095).
34. S. S. Pujari, S. A. Kadam, Y. R. Ma, S. A. Khalate, P. K. Katkar, S. J. Marje, U. M. Patil, Highly sensitive hydrothermally prepared nickel phosphate electrocatalyst as non-enzymatic glucose sensing electrode, *J. Porous Mater*, 48, 2020, DOI: 10.1007/s10934-020-01000-0.
35. K. Dhara, and D. R. Mahapatra, Recent advances in electrochemical nonenzymatic hydrogen peroxide sensors based on nanomaterials: a review, *J Mater Sci.*, 54, 2019, 12319-12357, DOI: 10.1007/s10853-019-03750-y.
36. Md. Mahbubur Rahman, A. J. Saleh Ahammad, J. Hyung Jin, S. Jung Ahn, J. Joon Lee, A comprehensive review of glucose biosensors based on nanostructured metal-oxides, *Sensors*, 10, 2010, 4855-4886, DOI: 10.3390/s100504855.
37. S. Y. Tee, C. P. Teng, E. Ye, Metal nanostructures for non-enzymatic glucose sensing, *Mater. Sci. Eng. C*, 70, 2017, 1018-1030, DOI: 10.1016/j.msec.2016.04.009.
38. D. Pletcher, Electrocatalysis: present and future, *J. Appl. Electrochem*, 14, 1984, 403-415, DOI: <https://doi.org/10.1007/BF00610805>.
39. H. Zhu, L. Lic, W. Zhou, Z. Shao, X. Chen, Advances in non-enzymatic glucose sensors based on metal oxides, *J. Mater. Chem. B*, 4, 2016, 7333-7349, DOI: 10.1039/C6TB02037B.
40. G. G. kumar, G. Amala, S. M. Gowtham, Recent advancements, key challenges and solutions in non-enzymatic electrochemical glucose sensors based on graphene platforms, *RSC Adv.*, 7, 2017, 36949-36976, DOI: 10.1039/c7ra02845h.

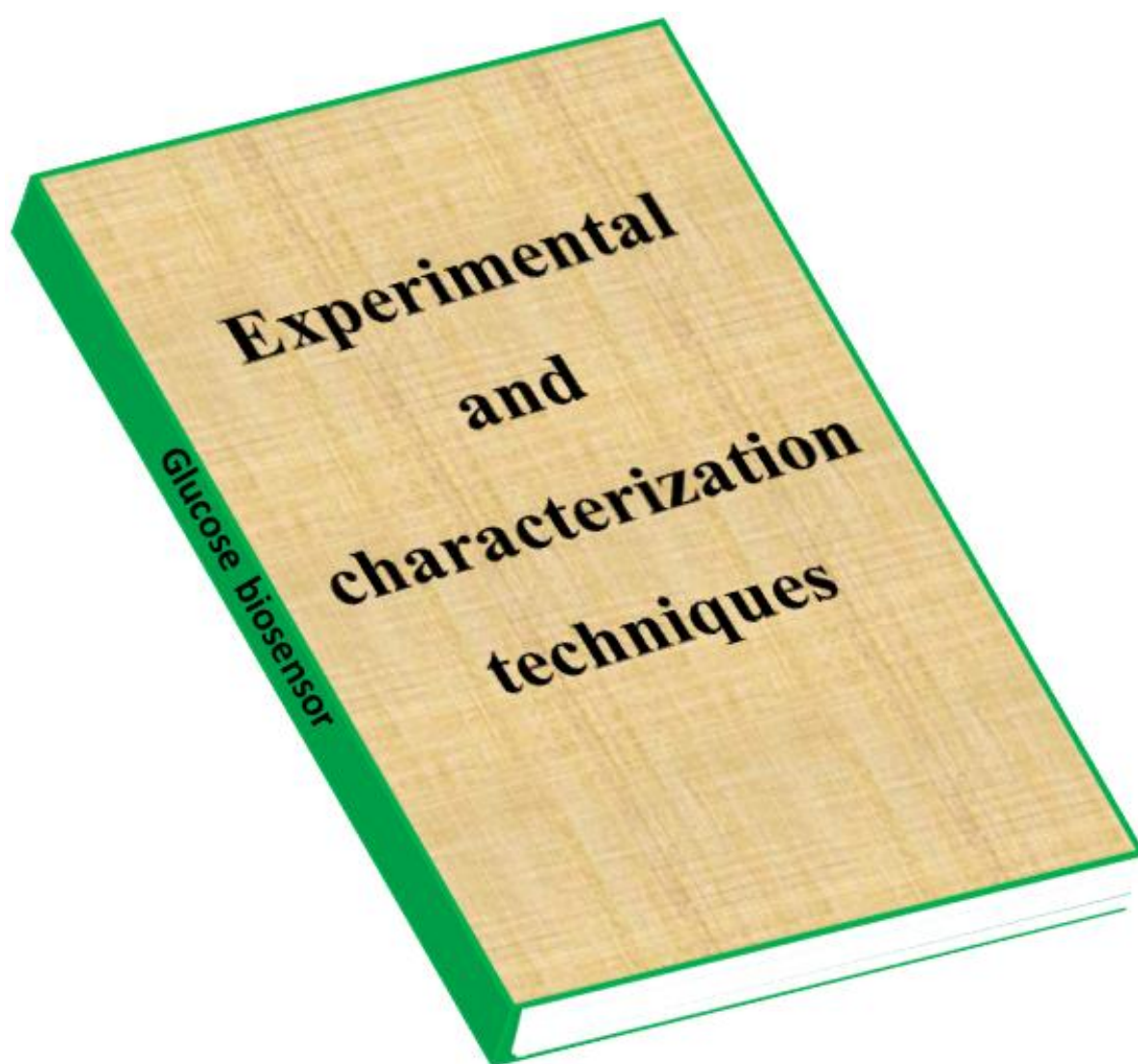
41. M. W. Hsiao, R. R. Adzic, E. B. Yeoger, Electrochemical oxidation of glucose on single crystal and polycrystalline gold surfaces in phosphate buffer, *J. Electrochem. Soc.*, 143, 1996, 759-767, DOI: 10.1149/1.1836536.
42. L. A. Larew and D. C. Johnson, Transient generation of diffusion layer alkalinity for the pulsed amperometric detection of glucose in low capacity buffers having neutral and acidic pH values, *J. Electroanal. Chem.*, 264, 1989, 131-147, DOI: 10.1016/0022-0728(89)80152-4.
43. L. D. Burke, Premonolayer oxidation and its role in electrocatalysis, *Electrochimica Acta*, 39, 1994, 1841-1848, DOI: 10.1016/0013-4686(94)85173-5.
44. G. Wang, X. He, L. Wang, A. Gu, Y. Huang, B. Fang, B. Geng, X. Zhang, Non-enzymatic electrochemical sensing of glucose, *Microchim Acta*, 180, 2013, 161-186, DOI: 10.1007/s00604-012-0923-1.
45. C. Chen, Q. Xie, D. Yang, H. Xiao, Y. Fu, Y. Tan S. Yao, Recent advances in electrochemical glucose biosensors: a review, *RSC Adv*, 3, 2013, 4473-4491, DOI: 10.1039/c2ra22351a.
46. Y. Ding, Y. Liu, J. Parisi, L. Zhang, Y. Lei, A novel NiO–Au hybrid nanobelts based sensor for sensitive and selective glucose detection, *Biosens. Bioelectron*, 28, 2011, 393-398, DOI: 10.1016/j.bios.2011.07.054.
47. N. A. Choudhry, D. K. Kampouris, R. O. Kadara, N. Jenkinson C. E. Banks, Next generation screen printed electrochemical platforms: Non-enzymatic sensing of carbohydrates using copper (II) oxide screen printed electrodes, *Anal. Methods*, 1, 2009, 183-187, DOI: 10.1039/b9ay00095j.
48. L. Ju, G. Wu, B. Lu, X. Li, H. Wu, A. Liu, Non-enzymatic amperometric glucose sensor based on copper nanowires decorated reduced graphene oxide, *Electroanalysis*, 28, 2016, 2543-2551, DOI: 10.1002/elan.201600100.
49. X. Liu, W. Yang, L. Chen, J. Jia, Synthesis of copper nanorods for non-enzymatic amperometric sensing of glucose, *Microchim Acta*, 183, 2016, 2369-2375, DOI: 10.1007/s00604-016-1878-4.
50. X. Niu, X. Li, J. Pan, Y. He, F. Qiu, Y. Yan, Recent advances in non-enzymatic electrochemical glucose sensors based on nonprecious transition metal materials: opportunities and challenges, *RSC Adv.*, 6, 2016, 84893-84905, DOI: 10.1039/c6ra12506a.
51. P. Kannan, T. Maiyalagan, E. Marsili, S. Ghosh, L. Guo, Y. Huang, J. A. Rather, D. Thirupathi, J. N. Jönsson, M. J. Niedziolka, Highly active 3-dimensional

- cobalt oxide nanostructures on the flexible carbon substrates for enzymeless glucose sensing, *The Analyst*, 142, 2017, 4299-4307, DOI: 10.1039/c7an01084b.
52. M. Kang, H. Zhou, N. Zhao, B. Lv, Porous  $\text{Co}_3\text{O}_4$  nanoplates as an efficient electromaterial for non-enzymatic glucose sensing, *CrystEngComm*, 2020, 22, 35-43, DOI: 10.1039/c9ce01396b.
53. F. Liu, P. Wang, Q. Zhang, Z. Wang, Y. Liu, Z. Zheng, X. Qin, X. Zhang, Y. Dai, L. Li, B. Huang, Porous  $\text{Co}_3\text{O}_4$  nanosheets as a high-performance non-enzymatic sensor for glucose detection, *Anal. Bioanal. Chem*, 410, 2018, 7663-7670, DOI: 10.1007/s00216-018-1380-4.
54. M. Yang, J. Jeong, K. G. Lee, D. H. Kim, S. J. Lee, B. G. Choi, Hierarchical porous microspheres of the  $\text{Co}_3\text{O}_4$ @graphene with enhanced electrocatalytic performance for electrochemical biosensors, *Biosens. Bioelectron*, 89, 2017, 612-619, DOI: 10.1016/j.bios.2016.01.075.
55. L. T. Hoa, J. S. Chung, S. H. Hur, A highly sensitive enzyme-free glucose sensor based on  $\text{Co}_3\text{O}_4$  nanoflowers and 3D graphene oxide hydrogel fabricated via hydrothermal synthesis, *Sens. Actuator B-Chem*, 223, 2016, 76-82, DOI: 10.1016/j.snb.2015.09.009.
56. D. Zhang, Z. Wang, J. Li, C. Hu, X. Zhang, B. Jiang, Z. Cao, J. Zhang, R. Zhang, MOF-derived  $\text{ZnCo}_2\text{O}_4$  porous micro-rice with enhanced electro-catalytic activity for the oxygen evolution reaction and glucose oxidation, *RSC Adv.*, 10, 2020, 9063-9069, DOI: 10.1039/c9ra08723k.
57. S. Liu, K. S. Oscar Hui, K. N. Hui, Flower-like copper cobaltite nanosheets on graphite paper as high performance supercapacitor electrodes and enzymeless glucose sensors, *ACS Appl. Mater. Interfaces*, 8, 2016, 3258-3267, DOI: 10.1021/acsami.5b11001.
58. X. Luo, M. Huang, D. He, M. Wang, Y. Zhang, P. Jiang, Porous  $\text{NiCo}_2\text{O}_4$  nanoarrays integrating binder-free 3D open electrode offers a highly efficient sensing platform for enzyme-free glucose detection, *The Analyst*, 143, 2018, 2546-2554, DOI: 10.1039/C8AN00668G.
59. M. Saraf, K. Natarajan, M. M. M. Shaikh, Multifunctional porous  $\text{NiCo}_2\text{O}_4$  nanorods: sensitive enzymeless glucose detection and supercapacitor properties with impedance spectroscopic investigations, *New J. Chem.*, 41, 2017, 9299-9313, DOI: 10.1039/C7NJ01519D

- 
60. X. Duan, K. Liu, Y. Xu, M. Yuan, T. Gao, J. Wang, Nonenzymatic electrochemical glucose biosensor constructed by  $\text{NiCo}_2\text{O}_4$ @Ppy nanowires on nickel foam substrate, *Sens. Actuator B-Chem*, 292, 2019, 121-128, DOI: 10.1016/j.snb.2019.04.107.
61. A. J. C. Mary, S. S. Shalini, R. Balamurugan, M. P. Harikrishnan, A. C. Bose, Supercapacitor and non-enzymatic biosensor application of the  $\text{Mn}_2\text{O}_3/\text{NiCo}_2\text{O}_4$  composite material, *New J. Chem.*, 2020, 1-20, DOI:10.1039/D0NJ01942A.
62. H. J. Jo, A. Shit, H. S. Jhon, S. Y. Park, Highly sensitive non-enzymatic wireless glucose sensor based on Ni-Co oxide nanoneedle-anchored polymer dots, *Journal of Industrial and Engineering Chemistry*, 89, 2020, 485-493, DOI: 10.1016/j.jiec.2020.06.028.
63. Z. Yu, H. Li, X. Zhang, N. Liu, W. Tan, X. Zhang, L. Zhang, Facile synthesis of  $\text{NiCo}_2\text{O}_4$ @Polyaniline core-shell nanocomposite for sensitive determination of glucose, *Biosens. Bioelectron*, 75, 2016, 161-165, DOI: 10.1016/j.bios.2015.08.024.
64. H. Heidari, and E. Habibi, Amperometric enzyme-free glucose sensor based on the use of a reduced graphene oxide paste electrode modified with electrodeposited cobalt oxide nanoparticles, *Microchim Acta*, 183, 2016, 2259-2266, DOI: 10.1007/s00604-016-1862-z.
65. W. Li, H. Qi, B. Wang, Q. Wang, S. Wei, X. Zhang, Y. Wang, L. Zhang X. Cui, Ultrathin  $\text{NiCo}_2\text{O}_4$  nanowalls supported on a 3D nanoporous gold coated needle for non-enzymatic amperometric sensing of glucose, *Microchimica Acta*, 185, 2018, 1-9, DOI: 10.1007/s00604-017-2663-8.
66. K. K. Naik, A. Gangan, B. Chakraborty, C. S. Rout, Superior non-enzymatic glucose sensing properties of Ag-/Au- $\text{NiCo}_2\text{O}_4$  nanosheets with insight from electronic structure simulations, *The Analyst*, 143, 2018, 571-579, DOI: 10.1039/C7AN01354J.
67. S. Mondal, R. Madhuri, P. K. Sharma, Probing the shape-specific electrochemical properties of cobalt oxide nanostructures for its application as selective and sensitive non-enzymatic glucose sensor, *J. Mater. Chem. C*, 5, 2017, 6497-6505, DOI: 10.1039/C7TC01411B.
68. S. Cheng, S. D. Cruz, C. Chen, Z. Tang, T. Shi, C. Carraro, R. Maboudian, Hierarchical  $\text{Co}_3\text{O}_4/\text{CuO}$  nanorod array supported on carbon cloth for highly
-

- sensitive non-enzymatic glucose biosensing, *Sens. Actuator B-Chem*, 298, 2019, 126860, DOI: 10.1016/j.snb.2019.126860.
69. M. Harry, M. Chowdhury, F. Cummings, C. J. Arendse, Elemental Cu doped  $\text{Co}_3\text{O}_4$  thin film for highly sensitive non-enzymatic glucose detection, *Sensing and Bio-Sensing Research*, 23, 2019, 100262, DOI: 10.1016/j.sbsr.2019.100262.
70. Z. Gao, L. Zhang, C. Ma, Q. Zhou, Y. Tang, Z. Tu, W. Yang, L. Cui, Y. Li,  $\text{TiO}_2$  decorated  $\text{Co}_3\text{O}_4$  a circular nanotube arrays and its application as a non-enzymatic glucose sensor, *Biosens. Bioelectron*, 80, 2016, 511-518, DOI: 10.1016/j.bios.2016.02.004.
71. Y. Su, B. Luo, J. Z. Zhang, A controllable Cobalt Oxide/Au hierarchically nanostructured electrode for non-enzymatic glucose sensing, *Anal. Chem*, 88, 2016, 1617-1624, DOI: 10.1021/acs.analchem.5b03396.
72. X. Tang, B. Zhang, C. Xiao, H. Zhou, X. Wang, Dalin He, Carbon nanotube template synthesis of hierarchical  $\text{NiCoO}_2$  composite for non-enzyme glucose detection, *Sens. Actuator B-Chem*, 222, 2016, 232-239, DOI: 10.1016/j.snb.2015.08.077.

# CHAPTER II



## Chapter II Experimental and Instrumentation Techniques

Sr. No.	Details	Page No.
2.1	Reagents used	37
2.2	Introduction	37
2.3	Electrodeposition method	40
	2.3.1. <i>Electrodes</i>	40
	2.3.2. <i>Fundamentals of electrodeposition</i>	41
	2.3.3. Faradays law of electrolysis	42
2.4	Various modes of electrodeposition method	43
	2.4.1 <i>Potentiostatic mode</i>	43
	2.4.2 <i>Galvanostatic mode</i>	44
	2.4.3 <i>Cyclic voltammetry mode</i>	44
2.5	Effect of parameters	45
	2.5.1 <i>Substrate</i>	45
	2.5.2 <i>Bath temperature</i>	46
	2.5.3 <i>Current density/Over potential</i>	47
	2.5.4 <i>Complexing agents</i>	47
	2.5.5 <i>pH of solution</i>	47
	2.5.6 <i>Advantages of electrodeposition</i>	47
2.6	Electrochemical cell	48
	2.6.1 <i>Working electrode</i>	48
	2.6.2 <i>Selection of working electrode</i>	49
	2.6.3 <i>Counter (auxiliary) electrode</i>	40
	2.6.4 <i>Reference electrode</i>	50
	2.6.5 <i>Supporting electrolyte</i>	51
2.7	Electrochemical technique	52
	2.7.1 <i>Cyclic voltammetry</i>	52
	2.7.2 <i>i-t amperometry</i>	55
2.8	Characterization techniques	56
	2.8.1 <i>Field emission -scanning electron microscopy (FE-SEM)</i>	56
	2.8.2 <i>Energy dispersive X-ray spectroscopy (EDX)</i>	58
	2.8.3 <i>X-ray diffraction (XRD)</i>	59
	2.8.4 <i>Transmission electron microscopy (TEM)</i>	62
	2.8.5 <i>X-ray photo electron spectroscopy (XPS)</i>	63
	2.8.6 <i>Brunauer-Emmett-Teller (BET)</i>	65
2.9	References	68



In this chapter, different chemicals, synthesis method, various characterization techniques and detail sensor fabrication process are briefly discussed.

## 2.1 Reagents used:

**Table 2.1:** The common laboratory analytical grade chemicals were used in the present work

Sr. No	Company name	Company and country of purchases
1	Lanthanum nitrate ( $\text{La}(\text{NO}_3)_3 \cdot 6\text{H}_2\text{O}$ )	SRL (INDIA)
2	Manganese nitrate ( $\text{Mn}(\text{NO}_3)_2 \cdot 4\text{H}_2\text{O}$ )	Sigma Aldrich (USA)
3	Silver nitrate ( $\text{AgNO}_3$ )	Thomas Baker (INDIA)
4	NaOH	Thomas Baker (INDIA)
5	KOH	Thomas Baker (INDIA)
6	KCL	Thomas Baker (INDIA)
7	Glucose	Thomas Baker (INDIA)
8	Fructose	Thomas Baker (INDIA)
9	Lactose	Thomas Baker (INDIA)
10	Ascorbic acid	Thomas Baker (INDIA)
11	Dopamine	Thomas Baker (INDIA)
12	Human blood	DYP Blood bank Kolhapur, INDIA

All the solutions/electrolytes were prepared in double distilled (DD) water for synthesis and non-enzymatic electrochemical glucose sensing experiments.

## 2.2 Introduction:

Interest in the study of science and technology of thin films enhances due to its applicability, technical values, properties, and curiosity in two-dimensional solids. Thin films have been developed to study the change in physical properties and their connection with the structure of solids. Also, thin films are used in many devices such as optical instruments, electrical circuits, sensor, magnetic information storage devices, etc [1]. In the formation of thin films, the various materials are deposited on the surface of a clean substrate up to a certain thickness. Changes in physico-chemical properties are observed

due to alteration of structure (bulk to thin film) of material, which is dependent on the order and periodicity of the material.

The system of thin film possesses at most two-dimensional order or periodicity, that highly influences the physico-chemical properties and also responsible for change in properties than bulk material. Many of these applications require nano-crystalline form of material for enhancement in the properties. Materials in nanometer scale offer several advantages such as large surface area, improved diffusivity, high electrical resistivity and high mechanical properties than their bulk counterpart [2]. Nanomaterials can be prepared by two ways; first way is top-down approach, where nanomaterials are prepared by breaking of bulk material into nanoscale pieces via chemical or mechanical processes. Another way is bottom-up approach, in which material allows to grow from atomic or molecular species. Most of the research has been devoted towards developing the capability to control shape, size and structure of material. Nanocrystalline form of materials has been prepared via numerous chemical synthesis methods and also some novel methods are also developed.

Thin film properties depend on deposition methods and preparative conditions, and by selecting the proper method desired properties can be achieved. Basically, thin film deposition methods divided into the class of physical and chemical methods [3, 4]. In physical method, there are two branches, one is vacuum evaporation and other is sputtering [5], where materials are required to transfer in gaseous state for evaporation method and impact processes for sputtering deposition. In chemical method, there are also two branches. One branch is gas phase chemical process and it contains different deposition methods such as, conventional chemical vapor deposition (CVD), laser CVD, photo CVD, metal organo-chemical vapor deposition (MOCVD) and plasma enhanced CVD. Another branch is liquid phase chemical methods which include electrodeposition

(ED), CBD, successive ionic layer adsorption and reaction (SILAR), spray pyrolysis, liquid phase epitaxy, sol gel process, reflux method, spin coating, dip coating, etc. In chemical methods, growth of material is obtained through chemical solutions [6]. Physical methods have many drawbacks such as high working temperature, small area deposition, requires sophisticated instruments, costly system, material wastage, high vacuum, etc. In comparison with physical methods, chemical methods are simple, economic, and suitable for large area deposition over any kind of substrate [3, 5, 6]. Also, preparative parameters are easy to control like concentration of solution, pH of solution, temperature, complexing agent, etc. Various chemical methods operate at low temperature that eliminates issue of corrosion and oxidation of metallic substrate. Also, these deposition methods are capable to deposit uniform and pinhole free thin films. So, the chemical processes are advantageous in the preparation of various materials in thin film form. The categorization of thin film deposition methods is summarized in **chart 2.1**.

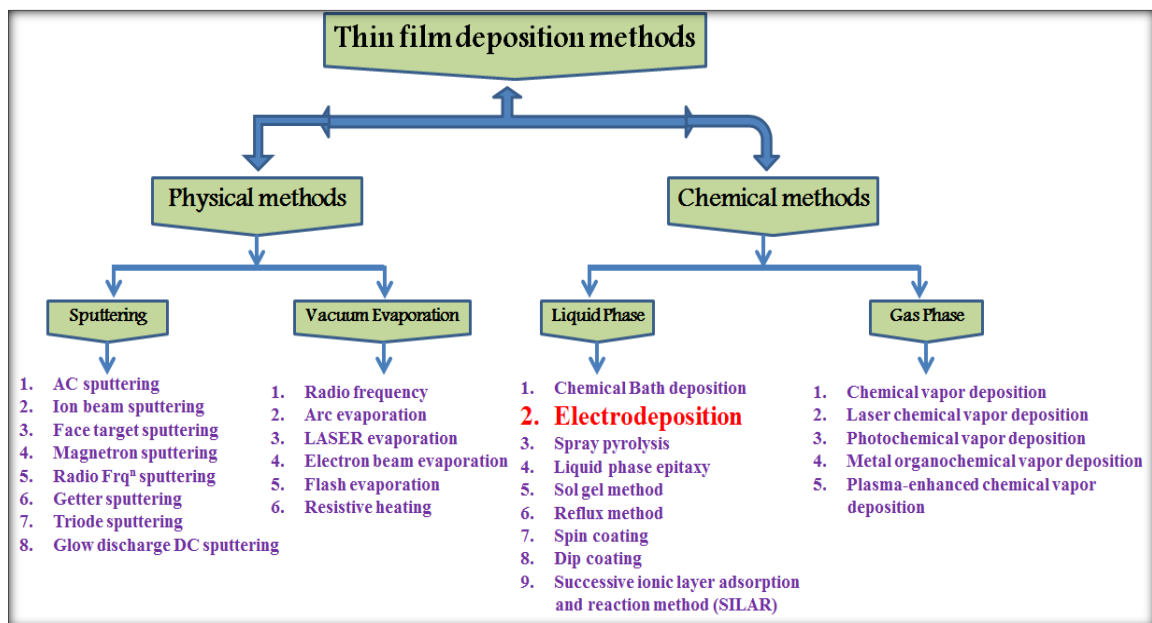


**Chart 2.1:** Categorization of thin film deposition methods.

This chapter contains three major parts: first part deals with theoretical background of ED, second part deals with different deposition modes as well as

importance of electrodes and third part deals with study of basic principle and importance of technique for thin films characterization.

### **2.3 Electrodeposition method:**

In the ED process, a layer of one or more metals is simply coated on conducting materials by exchanging electrons with ions (oxidation-reduction reaction) in the electrolyte. Easy and economic process for fabrication of metallic coating makes it famous in the field of coating (galvanization/electroplating). Also, it is used to prepare numerous nanostructured materials in thin film form. This method is widely used for soft and hard coatings for decorative and protective purposes, so it is explored in the electronic industry for new emerging applications [7].

ED is easy for handling, attractive, and well-known technique in comparison with the other physical and chemical methods due to several advantages. By this method, many properties can be controlled easily with accuracy like conductivity of semiconductor (n- or p-type), variation in the bandgap, control over stoichiometry and doping, etc. Up to now, several materials in the thin film form have been deposited using the ED method such as semiconductors [8], ceramics [9], metals [10], superconductors [11], hydroxides [12], oxides [13], etc., for different applications. There is an incredible difference in the ED compared with other chemical reaction based methods, where ED produces a chemical substance in a controlled manner.

#### **2.3.1 Electrodes:**

The conventional three-electrode system was employed for the deposition of thin films and electrocatalytic glucose detection experiments. 0.5 mm diameter platinum (Pt) sheet ( $1 \times 5 \text{ cm}^2$ ) and 2 mm diameter graphite sheet ( $1 \times 5 \text{ cm}^2$ ) were used as a counter electrode, saturated calomel electrode (SCE) and stainless steel (SS) substrate ( $1 \times 5$

cm<sup>2</sup>) was used as reference electrode and working electrode respectively for deposition of thin film and glucose sensing experiment.

### 2.3.2 Fundamentals of Electrodeposition:

An exchange of ions or atoms among the electrolyte and electrode occurs in electrochemical deposition processes [14]. In ED process, generally direct current is delivered through a metal ion-containing solution for the deposition of metal atoms on a conducting substrate. The schematic of ED system is shown in **Fig. 2.1**. The main components in the typical ED setup are discussed below.

As shown in **Fig. 2.1**, cathode, anode, and reference electrode are dipped in the metal ions containing electrolyte, when direct current is passed through anode and cathode then positively charged metal ions attracts towards the cathode, gets deposited on cathode and becomes electrically neutral [15].

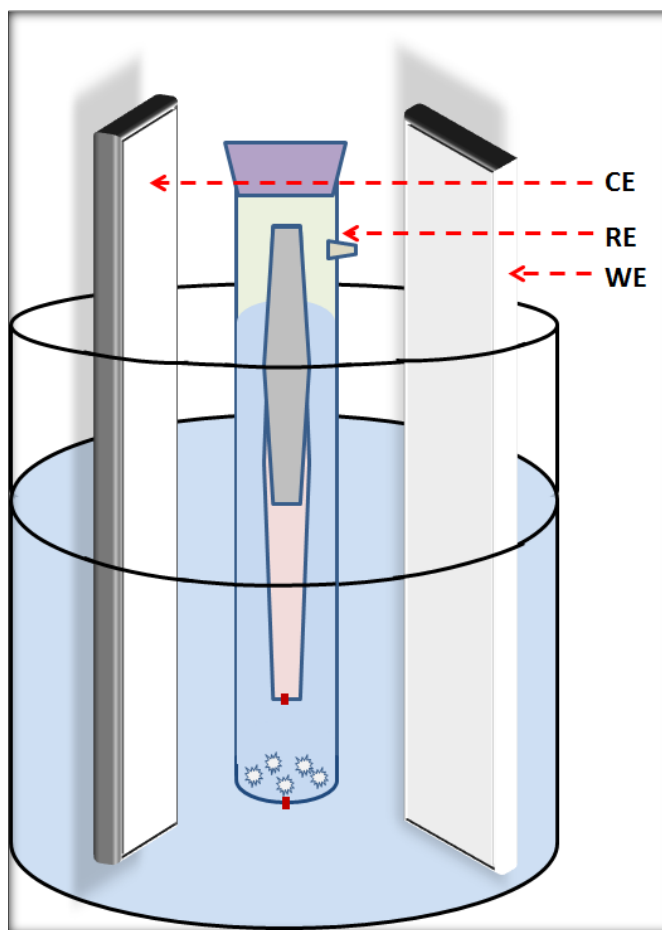
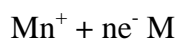


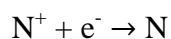
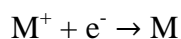
**Figure 2.1** Three electrode electrochemical cell system

By controlling charge amount and charge rate passing through electrolyte, the process of deposition can be controlled. Thus, chemical changes can be observed over the substrate or in electrolytes due to electrical energy. The deposition of metal on the cathode from the electrolyte containing metal ions takes place as per following reaction [16].



where  $\text{Mn}^+$  = metal ions,  $e^-$  = electron and  $n$  = number of charges.

On the other hand, electrolyte-containing more than one cationic species, cations get deposited on cathode simultaneously. For two different cationic species, the reaction in the ED process can be written as below,



where  $\text{N}^+$  is the another metal ion. The amount of deposition can be determined according to Faraday's law.

### 2.3.3 Faraday's laws of electrolysis

In 1834, Michael Faraday established a relationship between the chemical changes in electrolyte solution and electricity passed through it for deposition or liberation of material at electrode.

#### ❖ Faraday's first law

“The amount of substance deposited or liberated on the electrode surface is proportional to the quantity of charges passed” and this expression mathematically written as,

$$W \propto Q$$

where ‘W’ amount of substance liberated (g), and ‘Q’ the quantity of charge passed through electrolyte (Coulomb). If current (I) transfer with respect to time (t) then the quantity of charges is written in equation form.

---

Quantity of charge = Current (I) x time (t)

$$Q = I \times t$$

$$W \propto I t \text{ or } W = z I t$$

Here, 'z' the proportionality constant, known as 'Electrochemical equivalent'. It can be defined as, "The amount of substance liberated (g) on the electrode surface on passing a current of 1 A for 1 sec or passing 1 coulomb of electricity" [17].

#### ❖ Faraday's second law

"If the same amount of electricity is passed through different electrolytes, then the amount of substance liberated on the respective electrodes will be having in the ratio of their equivalent weights". An important overtone of Faraday's second law is that the ratio of the mass of electrodeposition to its equivalent weight (g) is a constant equivalent to 1 Faraday or 96,500 Coulombs (C) or 26.3 Ah [18].

### 2.4 Various modes of Electrodeposition

In ED method, three different modes can be used for the deposition of material as,

1. Potentiostatic mode (At constant potential)
2. Galvanostatic mode (At constant current)
3. Cyclic voltammetry (Potential and current varies with time)

#### 2.4.1 *Potentiostatic mode (At constant potential)*

In potentiostatic mode, the deposition of substance is carried out at constant DC voltage. The different charge transfer reactions are carried at constant interfacial overpotential in steady-state condition and current density is varied. The selection of deposition potential depends on various preparative parameters such as substrate nature (working electrode), the composition of bath, and reversible potential of deposited species. Appropriate potential is required for electrodepositing particular species and discovered with the guidance of standard electrode potential (reference electrode). Nevertheless, the actual potential for the deposition of substance influences by several factors like the interaction between substrate and depositant, overpotential of

hydrogen/oxygen evolution, the bath polarization characteristics, and also interaction between the various compounds in the case of compound ED. The deposition of species is done in pure activation, diffusion, or mixed depending on the selection of deposition potential. In potentiostatic deposition following features are important,

- 1) In this mode working electrode potential is controlled with respect to reference electrode.
- 2) To develop required potential across the working electrode, the potential is driven through counter electrode.
- 3) The cell current behavior varies with respect to time (t) as the output waveform.

### **2.4.2 Galvanostatic mode (*At constant current*)**

In galvanostatic mode, the deposition of substance is carried out at constant direct current (DC). In this mode, during the deposition process current between working and counter electrodes is kept constant and this is very important for uniform and adherent deposition of substance. The rate of deposition is proportional to the current densities. Following characteristics are important in the galvanostatic deposition,

1. The applied current between the counter and working electrode should free to drive electrolyte ions.
2. Desired cell current is generated by the proper potential applied through the counter electrode.
3. Current is not controlled by the reference electrode; it's only used for potential measurement in the electrochemical cell.
4. The cell potential varies concerning time as the output waveform.

### **2.4.3 Cyclic voltammetry (CV) technique (*potentiodynamic method*)**

CV is generally called a potentiodynamic method. The current of electrolysis is measured as a function of applied potential. In potentiodynamic mode, CV and linear

sweep voltammetry can be used. The CV technique is used to study electrochemical behaviors of material that take place through electrolysis like, electrode kinetics, charge transfer, etc. Further, it provides qualitative information on electrochemical reactions. Redox potential analysis of electroactive species present in the solution can be determined using a CV. In this method, the redox reaction of electroactive species can confirm new material on the substrate. In a single step, all metal oxides can be easily deposited by this method. A thin film can be formed on the conducting metal substrate by the reduction of metal ions (at reduction potential) subsequently oxidation (at oxidation potential) of metal ions. The thickness of the material on the film can be controlled by some repeated deposition cycles. Important characteristics of the potentiodynamic method for deposition are as follows,

- 1) Measurement of the anodic and cathodic current during the triangular potential sweep and both responses can be observed.
- 2) Detail mechanism about electroactivity of electrolyte species and electrode/substrate provides by output waveform which has forward and reverses peaks.

ED of ionic species from the electrolyte/solution occurs in following successive steps.

- 1) Ionic transport
- 2) Discharge
- 3) Breaking of ion-ligand bond (if the bath is complexed)
- 4) Incorporation of adatoms on to the substrate followed by nucleation and growth.

## **2.5 Effect of preparative parameters**

Many properties of the material (morphological, structural, and optical etc.) directly depend on the various parameters of the deposition process. Uniform, smooth, adherent and stoichiometric films can be obtained by controlling proper parameters like nature of substrate, applied current or voltage, complexing agents, temperature, and pH of

the bath, etc., [19, 20]. Some preparative parameters are discussed in brief as given below.

### **2.5.1 Substrate**

In the ED method, the conducting substrate plays a significant role and acts as a backbone with mechanical support for the ED process which leads to influence the morphology of the growing material. Further, the optical and electronic properties of the material can be investigated. Following the points of reference of the substrate are important for uniform ED [21].

1. Substrate should be highly conducting.
2. Thermal expansion measurements of the substrate should match with deposition.
3. The mechanical strength should be good.
4. Substrate should be stable in acidic and basic solution.
5. Substrate should clean with acetone or ethanol then washed with DDW.

Generally, highly conducting metal substrates are widely employed for ED of material due to their low cost, easy availability as well as handling.

### **2.5.2 Bath temperature**

The diffusion rate and ionic mobility enhance with increasing the temperature of the bath. The higher temperature of the bath raises current density along with increased nucleation rate, hence smooth, adherent and fine-grained particle size can be formed on thin film. Again, at a higher temperature, gas evolution potential and precipitation of salts could be decreased. Thus, maintaining the proper temperature of the bath is more difficult for deposition on thin film and they could be optimized by performing the experiments.

### **2.5.3 Current density/Over potential**

The deposition rate also depends upon the applied current density/potential. At lower current density/potential, slow-moving of ions occurs that reduces the growth of

rate and forms a closely packed structure of the material. On the other hand, maximum current density/potential the rate of nuclei formation increases correspondingly resulting in fine grain and favors in the deposition of material. Although, at a very high current density/overpotential rate of hydrogen separation or evolution from the electrolyte is very fast that affect the growth of material, and porous and spongy material can be formed on the substrate. Further, it is responsible for salt precipitation. So, the applied current density/over potential can control the thickness and structure of deposited material

#### **2.5.4 *Complexing agent***

The positively charged complex ions are formed by a chemical combination of unstable metal ions with neutral molecules. The complex compounds offers two advantages such as the continuous supply of ions for the deposition process and maintain a high concentration of metal complex but low metal ion concentration. The complex formation responsible for the growth of small grain and also decreases the precipitate formation.

#### **2.5.5 *pH of solution***

The pH of the bath is needed to control the high efficiency and required properties of the material. High pH values may lead to form hydroxide ions near the cathode surface that resulted in precipitation of basic salt. Thus, it alters the properties of ED. Hence, a higher current density with high efficiency is required for the deposition at a low pH bath.

#### **2.5.6 *Advantages of Electrodeposition method***

There are several mesmerizing advantages of the ED method for thin films as follows,

1. Quite a few structures, alloys, and compounds with prepared compositions can be deposited, which is difficult to prepare by other deposition methods.
2. By using potential and charge (current) like electrochemical parameters, the morphology and thickness of the thin film can be easily controlled.
3. Uniform deposition of material on a complex shape substrate is possible.

4. Precursors like toxic gases are not required (like gas-phase methods).
5. Required types of equipment's are inexpensive.
6. Compared to other gas-phase methods, a reaction in the deposition process arises closer to equilibrium so it is easy to control with accuracy.

### **2.6 Electrochemical cell:**

The three-electrode electrochemical cell is used for non-enzymatic electrochemical sensor studies as shown in **Fig. 2.1**. The electrodes themselves play an important role in the electrochemical biosensors. The electrode material, its surface texture, or its size, length, and dimensions affect the detection capability of the electrochemical biosensor. There are three kinds of electrodes performed in the electrochemical cell:

- Working electrode
- Counter (auxiliary) electrode
- Reference electrode

#### **2.6.1 Working electrode**

The working electrode can be clarified as the electrode where the electrochemical reaction behavior of interest occurs. By choice, it should have low cost, highly conducting, a good signal-to-noise ratio, high electrical stability, and reproducible response, no interfering reactions over the potential of interest, low toxicity, and long-term stability. In the electrochemical system, the working electrode can be applied as either anodic or cathodic substrate depending on the reaction either oxidation or reduction.

#### **2.6.2 Selection of Working Electrode**

Finalize the working electrode material is very critical to achieve experimental success. Some important factors should be considered. Firstly, the electrode material

should manifest good redox behavior with the molecule, continuous electron transfer without electrode disturbance. Secondly, the electrode material performs in a given electrolyte should be as wide as possible to allow for the greatest degree of analyte properties. Due to the above constituents, the working electrode materials have been made from noble metals such as silver (Ag), platinum (Pt), gold (Au), mercury (Hg) and carbon (C) in the form of graphite or carbon paste as well as stainless steel (SS). SS electrodes have been widely used in electrochemical studies as working electrodes for a variety of reasons, such as low cost, stability, availability, and low chemical interference, ability to easily control the surface texture, high mechanical strength, and barrier during water electrolysis.

Generally, nickel foam (NF), carbon fiber (CF), Pt plate, graphite sheets, titanium foil, copper foil, and SS are used as the substrates. SS substrate has many desirable properties that contribute greatly to its widespread application in the making of parts and components across many industrial sectors. The favorable properties for researchers are its high strength and durability, its high sensitivity and low temperature resistance, and it is environmentally friendly as well as recyclable. Platinum plate and titanium foil have high electrical conductivities than SS substrate but the cost of these materials is higher compared to SS. This factor prevents these substrates from commercialization. Therefore, many researchers generally prefer SS substrate. In addition, the SS substrate has not involved in the oxidation-reduction process during the electrochemical study. Therefore, we have used an SS electrode in the present investigations.

### **2.6.3 Counter (auxiliary) electrode**

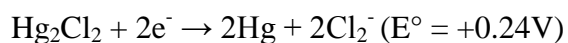
In the typical three-electrode system, the counter electrode has a function measuring of current passing through between the electrochemical cell and the electrolyte. The counter electrode works as a cathode or anode when one will operate as an opposite electrode and vice versa. The counter electrode does not measure potential

corresponding to the reference electrode but adjust the flow of current at the working electrode. This configuration allows the working electrode to be potentially measured against a known reference electrode. The counter electrode is generally fabricated from electrochemically inert or highly conducting materials such as Pt, Au, or graphite.

### 2.6.4 *Reference electrode*

The reference electrode is stable, conventional electrode potential and it is used as a reference in the electrochemical cell for potential control and measurement. The long-term stability of the reference electrode potential is generally reached by using a redox system with constant (saturated or buffered) concentrations of one and all participants of the redox reaction. Furthermore, the current flow along with the reference electrode is retained close to zero (ideally zero) which is achieved by using the CE to near the current circuit in the cell together with very high input impedance on the electrometer. The required condition for a reference electrode is to maintain constant potential in the electrolyte species, high or low temperature, and passage of current. A standard hydrogen electrode (SHE) is a commonly used reference electrode. Hydrogen is potentially explosive and highly flammable is not suitable using an electrode. Hence two mostly used and commercially available reference electrodes are Ag/AgCl and saturated-calomel electrode.

**Saturated Calomel Electrode:** Another name of Calomel is the mercurous chloride ( $\text{Hg}_2\text{Cl}_2$ ). Calomel electrode is consist of mercury, paste (mixture of potassium chloride and mercury (I) chloride powder) and saturated potassium chloride solution.



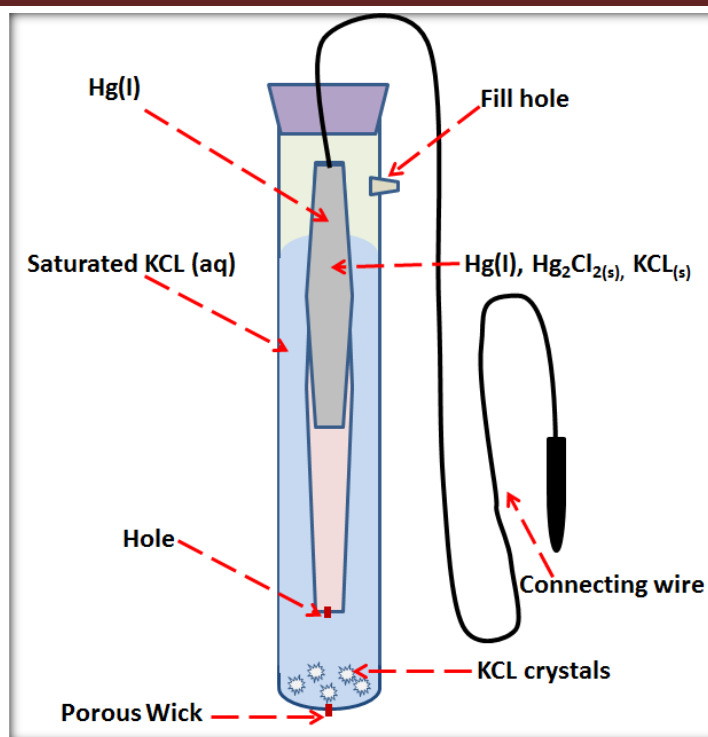


**Figure 2.2** Schematic diagram of saturated calomel electrode (SCE)

### 2.6.5 Supporting electrolyte

A supporting electrolyte is a chemical containing electrolyte species that are not electroactive (within the range of potential used) and which has an ionic strength and conductivity much larger than those electroactive species added to the electrolyte. The electrolyte is essential for the migration of charged reactants and products towards the respective electrodes. Water-ionizable molecules are generally chosen as electrolytes, which includes most soluble salts, acids and bases. Electrolytes can be categorized as strong or weak based upon their degree of ionization. An electrolyte can be considered as strong if it produces a high concentration of ions in solution. In contrast, a weak electrolyte produces only a small amount of ions on ionization.

The thermodynamic interaction between the solvent and solute molecules in solution is referred to as solvation which results in ionization of the solute. There are three functions of the supporting electrolyte. First, it carries most of the ionic current of the cells since its concentration is much larger than that of the other species in solution.

Thus, it serves to complete the circuit of the electrochemical cell and keep the cell resistance at a low value.

## 2.7 Electrochemical techniques:

Electrochemical techniques apropos to this work are described here, namely:

- Cyclic Voltammetry (CV):
- *i-t* amperometry:

*i-t* amperometric and CV techniques were carried out using CHI660E electrochemical workstation (CH instruments, USA)



**Figure 2.3** CHI660E electrochemical work station

### 2.7.1 Cyclic Voltammetry (CV)

CV technique is widely used for electrochemical studies. This technique provides detailed information about the thermodynamics and kinetics of redox reactions. It is a potentiodynamic technique, wherein potential is varied linearly and the resulting current is measured [22]. A typical voltage sweep in CV study is presented in **Fig. 2.4**.

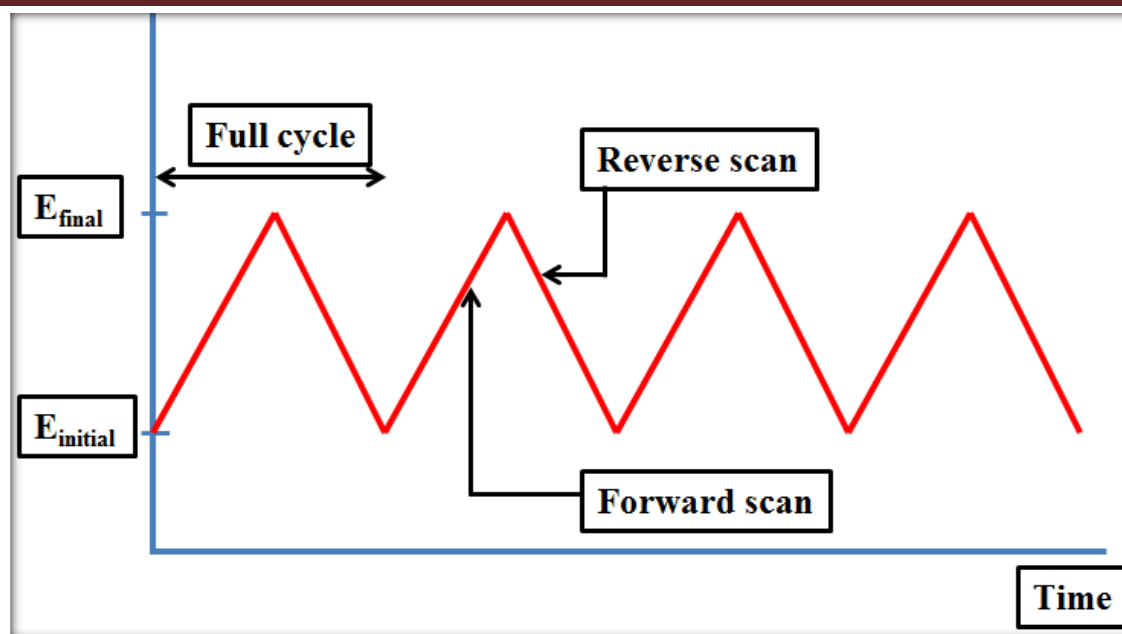


**Figure 2.4** Voltage sweep CV study

A full cycle potential triangular waveform consists of a forward scan and a reverse scan. The slope of the potential ramp is called scan rate ( $v$ ) and is expressed in  $V\ s^{-1}$ . The potential is applied between working and reference electrodes and the resulting current is measured flowing at the working to counter electrodes (such combination is called three electrode setup). To neglect the mass transport of molecules caused by convection and migration, CV is performed in unstirred solution with an excess of a supporting electrolyte. The results are presented as current versus potential plots called voltammograms (**Fig. 2.5**). The initial potential is generally chosen where no redox reactions occur. When the potential is shifted in forward direction a threshold potential towards the oxidation potential increases before the peak current  $I_p$  is reached. When the potential increases, the concentration of the reduced species on the electrode surface is depleted (redox process) which results in the change of concentration of the material and thus the increase of an anodic current. After that peak of oxidation current  $I_{OXI}$  has reached the potential that is shifted before the concentration of oxidized species is constant (i.e. constant current). At that point, the current is mass transport limited and not potential limited. During the reverse scan, the accumulated oxidized species are reduced

in the electrolyte which results in the decrease of cathodic current, after which the steady-state current is reached.

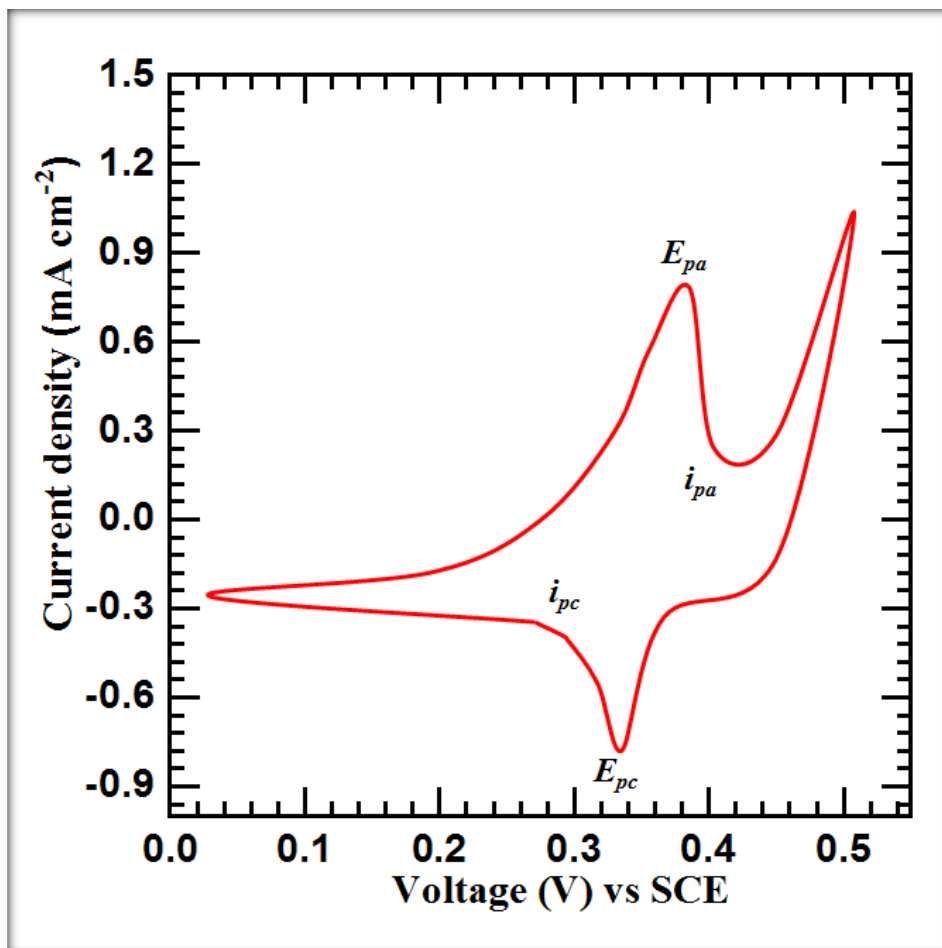


**Figure 2.5** The anodic and cathodic peak presented in CV curve

CV technique is explored to determine the kinetics of chemical reactions, especially whether the chemical reaction is thermodynamically reversible. For a reversible couple (at 25°C), the peak current ( $i_p$ ) is described by Randles Sevcik equation:

$$i_p = (2.69 \times 10^5) n^{\frac{3}{2}} A C D^{1/2} \gamma^{1/2} \quad (2.1)$$

where  $n$  is the number of electrons taking part in the reaction,  $A$  is the surface area of the electrode ( $\text{cm}^2$ ),  $C$  is the concentration of the reverse couple ( $\text{M cm}^3$ ),  $D$  is the diffusion coefficient ( $\text{cm}^2 \text{s}^{-1}$ ), and  $\gamma$  is the scan rate ( $\text{V s}^{-1}$ ). The above equation (2.1) can be used to measure the diffusion coefficient for an electro-active species from the graph of

current Vs. square root of the scan rate. Also, the study of different scan rates which gives the identical information to identify the various types of the reaction (reversible, quasi reversible, or irreversible) [23]. For an electrochemically reversible reaction system, the oxidation and reduction peak current ratio,  $I_{OXI}/I_{RED}$ , is unity and the separation between the peak potentials is followed as:

$$E_{OXI} - E_{RED} = 59mV/n \quad (2.2)$$

where  $E_{OXI}$  and  $E_{RED}$  are the oxidation and reduction potentials, respectively, and  $n$  is the number of electrons transferred.

Most electrochemical systems do not exhibit Nerstian behavior. Wherein, referred to as quasi-reversible process the electron transfer rate slower than that of voltage scan rate as the barrier to electron transfer needs to be overcome by the increased potential beyond  $E_{ox}$ . In turn, this separation of oxidation and reduction peaks observed on the CV, which may calculated from the below equation (at 25 °C):

$$E_{OXI} - E_{RED} = 48mV/\alpha n_a \quad (2.3)$$

Where  $\alpha$  is the transfer coefficient and  $n_a$  is the number of electrons commutation during the charge transfer step. Also, CV of a system which is irreversible exhibits a shift of  $E_p$  with the scan rate, or absence of the reverse peak.

### 2.7.2 *i-t* amperometric technique:

In the amperometric study, a constant potential is applied to a working electrode and the resulting current is measured with respect to time. The applied potential is usually chosen (based on the CV and LSV experiments) such that the resulting current is mass transport limited. Thus at a steady state, it represents a concentration of the electroactive species which are the analyte of interest or correlated to its concentration. This technique is explored to study the current response to a change of substrate concentration which leads to the observed kinetic chemical behavior. The current response determined by the sensor under the constant polarization immersed in the electrolyte as that period changing

the analyte concentration (gradually). The results are plotted as current Vs. time. The time between the changes of analyte concentration is determined by the properties of the sensor, namely by the time required for the current to reach an equilibrium state.

### **2.8 Surface characterization techniques:**

Surface characterizations are performed to understand the morphological, physical and chemical properties of the surfaces used in this work. It also helps us to understand the complex formation, which increases the sensitivity and stability. The surface studies used in this work are

- 1) Scanning electron Microscope (SEM)
- 2) Energy dispersive spectroscopy (EDS)
- 3) X-Ray Diffraction (XRD)
- 4) Transmission electron microscope (TEM)
- 5) X-ray photoelectron spectroscopy (XPS)
- 6) *Brunauer-Emmett-Teller* (BET)

#### **2.8.1 Scanning electron microscope (SEM):**

SEM images were obtained from Hitachi, PANalytical make (model S-3000H), Japan.

SEM is one of the most surprising aspects of which three-dimensional objects can be interpreted by any observer with no prior knowledge of the instrument. This is quite surprising because of the unusual way in which images are formed. This technique is somewhat different from normal humans experience with images, which is formed by light and viewed by the naked eye. The main components of a typical SEM instrument are electron column, scanning system, detector(s), display, vacuum system, and electronics controls (**Fig. 2.6**). The electron column of the SEM consists of an electron gun and two or more electromagnetic lenses operated in a vacuum. The electron gun generates free electrons and accelerates these electrons to energies in the range of 1-40

KeV in the SEM. The electron lenses create a small, focused electron beam on the sample. Most SEMs can generate an electron beam at the specimen surface with a spot size less than 10 nm in diameter while still carrying sufficient current to form an acceptable image. Typically the electron beam is defined by probe diameter ( $d$ ) in the range of 1 nm to 1  $\mu\text{m}$ , probe current ( $i_b$ ) pA to  $\mu\text{A}$ ; and probe convergence  $10^{-4}$  to  $10^{-2}$  radians. To produce a clear image, the electron beam is focused on a fine probe, which is scanned across the surface of the specimen with the help of scanning coils (**Fig. 2.6**). Each point on the specimen that is struck by the accelerated electrons emits a signal in the form of electromagnetic radiation. Selected portions of this radiation, usually secondary (SE) and/or backscattered electrons (BSE), are collected by a detector and the resulting signal is amplified and displayed on a TV screen or computer monitor. The resulting image is generally straightforward and very easy to interpret, at least for topographic imaging of objects at low magnifications.

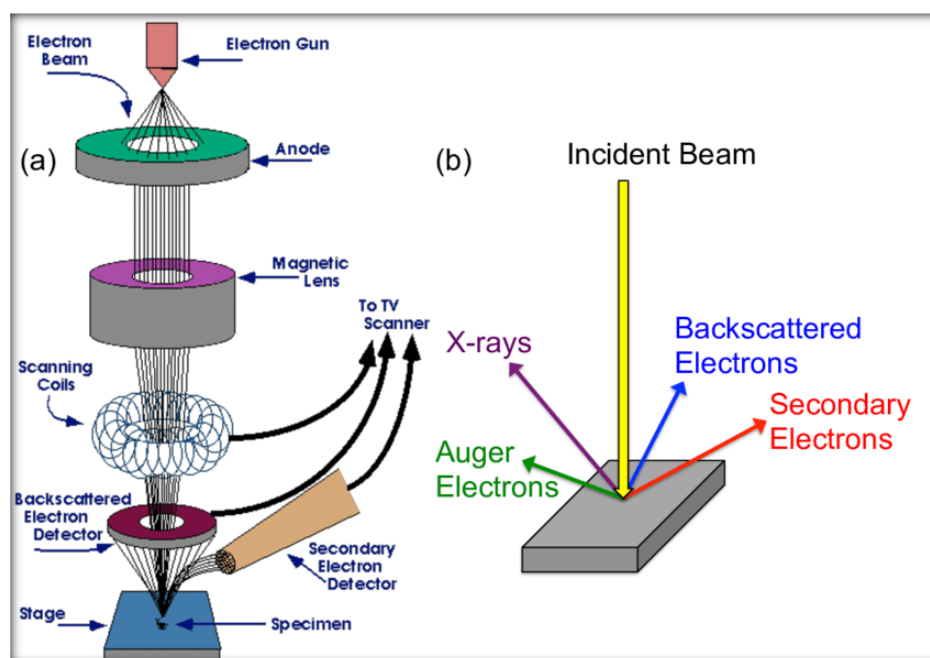


**Figure 2.6** Block diagram of SEM instrument [24]

The electron beam interacts with the specimen approximately to 1  $\mu\text{m}$  depth. Complex interactions of the electrons with the molecules present in the specimen produces radiation. The need for understanding the process of image formation is for

reliable interpretation of the images, which arises in special situations and mostly in the case of high-magnified images. In such cases knowledge of electron optics, beam-specimen interactions, detection, and visualization processes are necessary for successful utilization of the power of the SEM.

### **2.8.2 Energy Dispersive X-ray Spectroscopy (EDS):**

Energy-dispersive X-ray spectroscopy (EDS) is generally used for the elemental analysis or chemical characterization of samples and is also called energy dispersive X-ray analysis (EDAX) or energy dispersive X-ray microanalysis (EDXMA). The principle used in the EDS is that every element has a specific atomic structure and gives a unique set of peaks in the emission spectrum.

For the emission of characteristic X-rays from the sample, a charged particle beam or high-energy X-ray beam is focused on the specimen. Ground state electrons are present in the atom of the specimen at different energy levels. Electrons in the inner shell are excited or ejected after a beam incident on it and the hole is created after the ejection of an electron. Then, the electron from the higher shell occupies the vacant space, so the energy difference between the shells released in the form of an X-ray (shown ray diagram in **Fig. 2.7**). The energy dispersive spectrometer calculates energy and released a number of X-rays from the specimen. The energies of X-rays are characteristics of atomic structure and energy difference between two shells. Hence, the elemental composition of the specimen can be measured by EDS [25]. Following components are embedded in the EDS equipment;

1. The excitation source (X-ray beam or electron beam)
2. The X-ray detector
3. The pulse processor
4. The analyzer

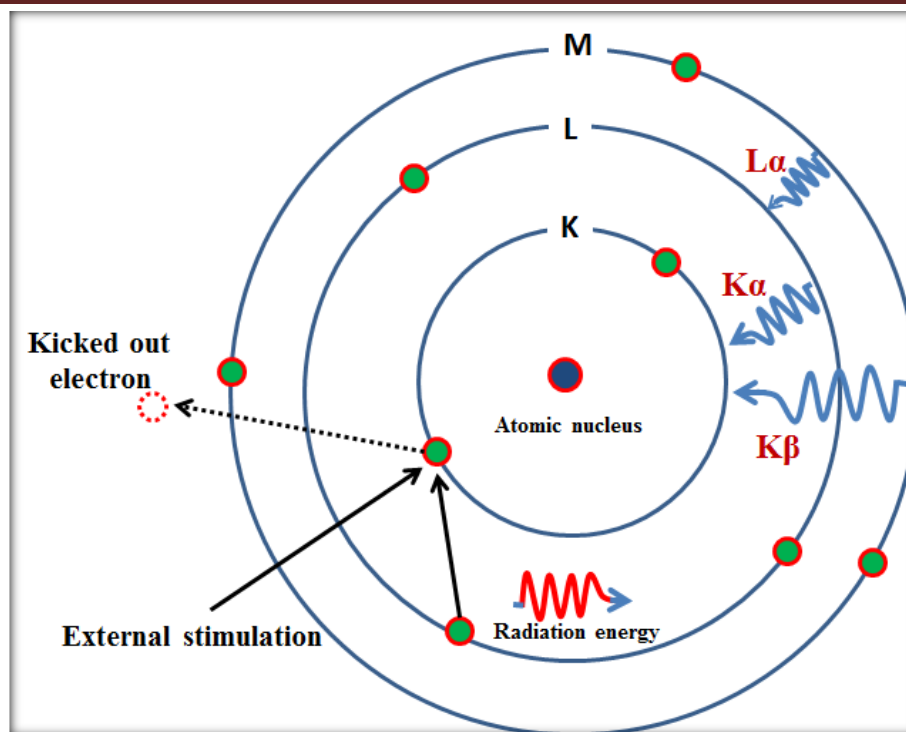


**Figure 2.7** The ray diagram of emission X-ray spectrum in EDS [25]

Emitted X-rays incident on the detector at that time charged pulses are formed. The detector converts that charged pulse into voltage signals with the help of amplifier. Charged pulse further deliver to a pulse processor, which measures signals and forward to the analyzer for data display. Elemental composition of the specimen is analyzed using spectrum from number of counts against the X-rays energy.

### 2.8.3 X-Ray diffraction (XRD):

X-ray diffractometer from Rigaku miniflex-600 (CuK $\alpha$ ,  $\lambda=1.5406\text{\AA}$  radiation) were used for acquiring XRD pattern. XRD technique is used to determine the crystal structure and phase confirmation of a subjected material. It is a non-destructive technique applied for the characterization of crystalline materials. It provides information about the structure, phase, preferred crystal orientation and structural parameters such as lattice parameter, crystallite size, strain and crystal defects. The diffraction of X-rays occurs only when the wavelength of the wave motion is of the same order of magnitude as the repeated distance between scattering centers. This diffraction condition is nothing but Bragg's law [26] and is given as:

$$2d\sin\theta = n\lambda \quad (2.4)$$

where  $d$  is the inter planer spacing,  $\theta$  is the diffraction angle,  $\lambda$  is the wavelength of X-ray and  $n$  is the order of diffraction.

In this technique, material to be examined is ground to a fine powder. The fine grains of sample are generally spread uniformly over a rectangular area of a glass slide. The sample usually adhered to glass either using binders like collodion grease or wax. Several types of sample holders namely glass slide, circular disc or thin capillary, etc. are used for the different designs of the instrument.

Various kinds of sources for X-rays are available, but in the most common laboratory diffractometers, sealed X-ray tube source is used. The X-rays are produced from the sealed X-ray tube. The basic construction of the tube is similar to that Coolidge tube. The X-rays are produced by bombarding high speed electrons on a metal target. When the X-ray beams incidents on the sample, it gets scattered from the sample. The scattered rays from the sample constructively interfere according to Bragg's law and produce a diffracted beam. The diffracted beams are scanned by sweeping the detector from one angle to another and count or count rates of X-ray photon are measured at different angles. The output is obtained as a plot of the intensity of diffracted X-rays (counts) vs. diffraction angle ( $2\theta$ ). A diffraction pattern appears which can be analyzed to determine various structural properties of the material. A schematic of X-ray diffractometer is shown in **Fig. 2.8**. When X-rays interact with a crystalline substance, gets a diffraction pattern. Each crystalline substance gives a pattern; the same substance always gives the same pattern; and in a mixture of substances, each phase produces its pattern independently. The XRD pattern of a particular substance is like a fingerprint of that substance.

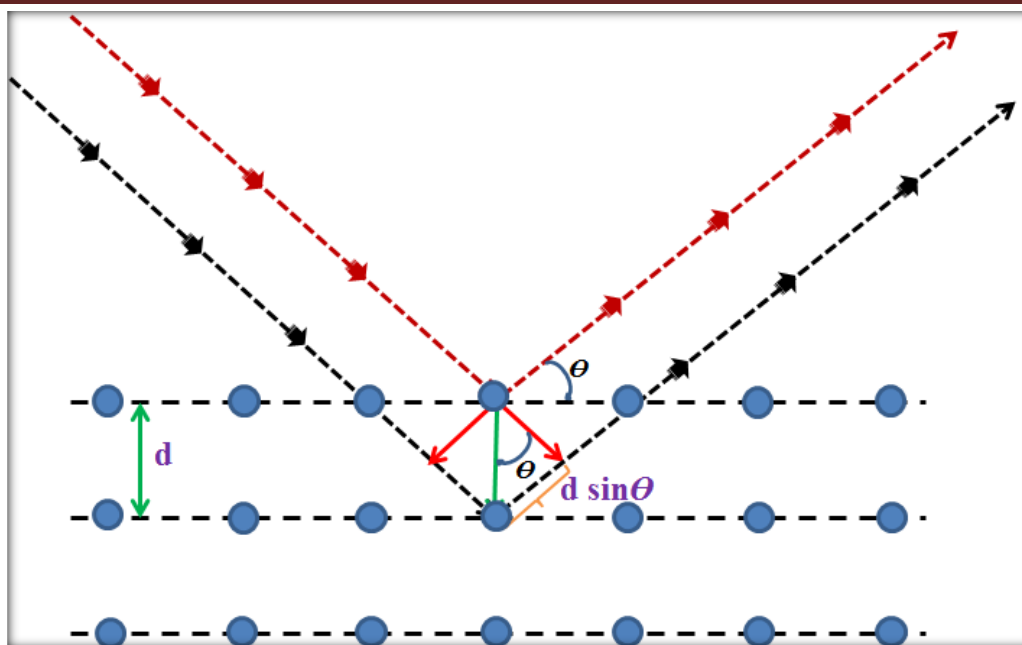


**Figure 2.8** Schematic of X-ray diffractometer [27]

The powder XRD method is useful in the qualitative phase analysis because every crystalline material has its own characteristic powder pattern. Hence, this method is also called the powder fingerprint method. Powder pattern depends on two main factors namely (a) the size and shape of unit cell and (b) the atomic number and position of various atoms in the cell. Thus, two materials may have the same crystal structure, but almost certainly they have quite distinct powder patterns. The powder pattern has two characteristic features, viz. d-spacing of the lines and their intensity. Out of these two, the d-spacing is very useful and capable of precise measurement. The d-spacing should be reproducible from sample to sample unless impurities are present to form a solid solution or the material is in some stress, disorder or meta-stable condition. While the intensities are more difficult to measure quantitatively and often vary from sample to sample. These can usually be measured only semi-quantitatively and may show variation.

PDF-2 2021 contains entries 316,800+ unique powder diffraction data sets have been collected from organic, organo-metallic, inorganic and mineral samples. These have been compiled into a database known as the JCPDS (joint committee on powder

diffraction standards). Identification of phase is made by matching the diffraction pattern with the standard JCPDS cards.

X-ray diffraction (XRD) is one of the most common and non-destructive characterization tool used to analyze all kinds of matters i.e. fluids, powders and crystals etc. It can be applied from research to production and engineering. XRD is also an indispensable method for structural materials characterization which uses the Debye-Scherrer method. This technique uses X-ray (neutral) diffraction on powder or microcrystalline samples, where ideally every possible crystalline orientation is represented equally. The resulting orientation averaging causes the three dimensional reciprocal space that is studied in single crystal diffraction to be projected onto a single dimension. This describes the three dimensional space with reciprocal axes i.e.  $x^*$ ,  $y^*$  and  $z^*$  or alternatively in spherical coordinates  $q$ ,  $\varphi^*$ ,  $\chi^*$ . The Debye-Scherrer method averages over  $\varphi^*$  and  $\chi^*$  and only  $q$  as an important measurable factors.

The diffracted intensity is shown as function either of the scattering angle  $2\theta$  or as a function of the scattering vector  $q$  which makes it independent of the used X-ray wavelength. The diffractogram is like a unique ‘fingerprint’ of materials. This material gives laboratories the ability to quickly analyze unknown materials and characterize them in such fields as metallurgy, mineralogy, forensic science, archeology and the biological and pharmaceutical sciences. Identification is performed by comparison of the diffractogram to known standards or to international databases.

### **2.8.4 Transmission electron microscope (TEM):**

TEM is the premier tool to acquire knowledge such as structure of materials at the nanometer level. It operates on the basic principle as the optical light microscope, but uses electron beam instead of light. The TEM image provides more depth information of morphology and in details of its size. Schematic of TEM is shown in **Fig. 2.9**.

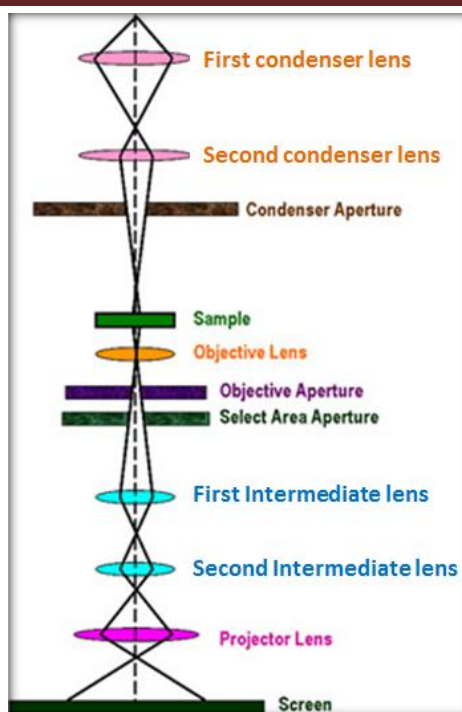


**Figure 2.9** The block diagram of TEM [28]

In TEM, an electron gun produces the bunch of monochromatic electrons. This bunch of electrons is focused to a thin, small, coherent beam by using coherent lenses 1 and 2. While electron beam strikes on the specimen, part of electron gets transmitted. This transmitted portion of electron is focused by the objective lens to form the image. It is essential requirement of sample for TEM analysis. It should thin sufficient beam to allow the electrons to be transmitted. The minimum thickness of the sample for TEM analysis is about  $0.5\ \mu\text{m}$ . The powder sample analysis is studied by dispersing in some dispersive media to form colloidal solution, and then small drop of solution is placed on a conducting grid (copper or silver) and dried. This grid acts as specimen for sample analysis using TEM. The square size of grid is near about  $1\ \mu\text{m}$ .

### 2.8.5 X-Ray Photoelectron Spectroscopy (XPS):

The surface properties of material or thin film can be identified by the X-ray photoelectron spectroscopy (XPS) technique and it also called as electron spectroscopy for chemical analysis (ESCA). This technique is based on photoelectric effect and X-rays are used as a source of photons. Electrons ejects from the material surface when the beam

of X-ray incident on the surface of material. The escaped electrons are called as photoelectrons and using the kinetic energies of photoelectrons elemental identification can be done directly. Also, the intensities of photoelectrons help to determine the relative composition of elements in the material. The ejected electrons kinetic energy can be calculated by the relation [29],

$$\text{K.E.} = h\nu - \text{B.E.} - \phi_s \quad (2.5)$$

where, K.E.,  $h\nu$ , B.E. and  $\phi_s$  are ejected photoelectrons kinetic energy, X-ray photons characteristic energy, binding energy of the atomic orbital from which the electrons originated and spectrometer work function, respectively.

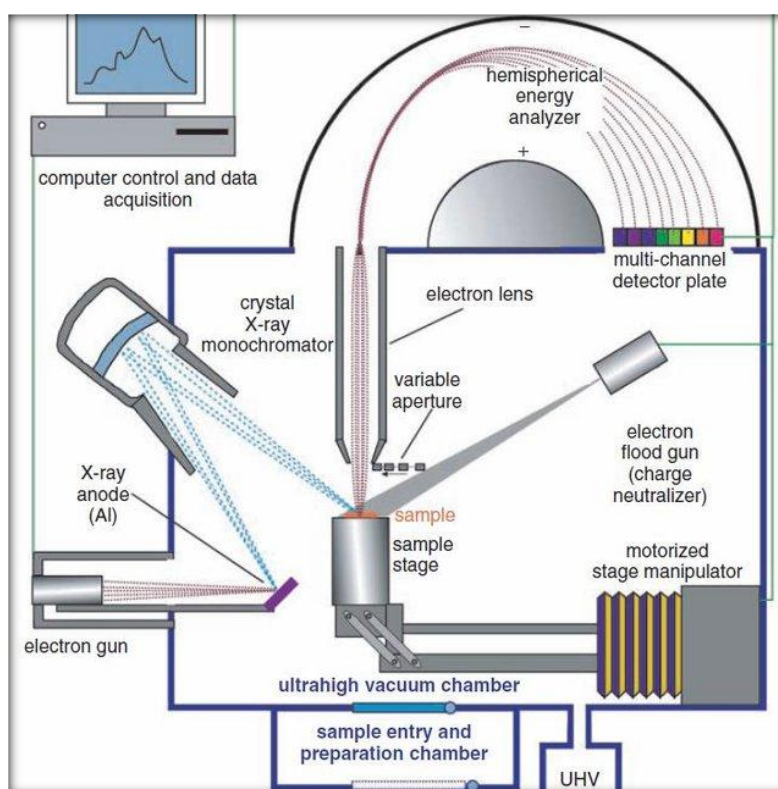


**Figure 2.10** XPS instrument analysis [30]

Ionization and emission of electrons in inner shell happen due to absorption of photons by the atom present in a molecule. Each element represents a characteristic peak in the spectrum of photoelectron due to each core level atomic orbital having characteristic binding energy. In XPS, very firstly the survey scan is done, in that all available energy measurements are carried out and confirm present elements in the

sample. In XPS study, energy spectrum is created by plotting binding/kinetic energies of emitted electrons and plot informs amount of elements present in the sample. The peaks at particular energies denote the presence of a specific element and these peaks are related to the electronic configuration of elements. This instrument is useful to identify oxidation state of elements. Ray diagram of XPS technique is shown in **Fig. 2.10**. XPS cannot provide a complete chemical analysis, since it is a surface phenomenon where signals used for analysis, originates generally from a few atomic layers of surface and very few from the deeper part of solids.

### 2.8.6 Brunauer-Emmett-Teller (BET):

The BET theory aims to measure the physisorption adsorption of the gas molecule on the solid surface of the materials and as an important analysis of technique for the measurements of specific surface area and pore volume. The specific surface area measurement is presented by Freundlich, Langmuir, and BET. There are three isotherms used for the measurement of specific surface area as explained in brief.

#### ❖ Freundlich adsorption isotherm:

In 1909, German scientist Freundlich provided an empirical relationship between the amount of gas adsorbed by unit mass of solid and pressure at particular temp. It is expressed using the following eq<sup>n</sup>.

$$\frac{x}{m} = k \cdot p^{\frac{1}{n}} \quad (n > 1) \quad (2.6)$$

Where x is the amount of adsorbate adsorbed, m is the amount of adsorbent, p is the pressure of the adsorbate, k & n are the constants.

#### Limitation of Freundlich isotherm:

Freundlich isotherm only approximately explains the behavior of the adsorption. The value of 1/n can be between 0 to 1. Therefore, the equation holds well only over the limited range of pressure.

1. When  $1/n = 0$ ,  $X/m$  is constant the adsorption is independent of pressure.
2. When  $1/n = 1$ ,  $X/m = k$ , p i.e  $X/m \propto p$

The experimental result supports both of the above condition. At high pressure, the experimental isotherms always seem to approach saturation. Freundlich isotherm does not explain this observation and therefore fails at high pressure.

The Freundlich isotherm was followed by two other isotherms-Langmuir adsorption and BET adsorption isotherms. The Langmuir isotherm assumed that adsorption is monolayer in nature whereas BET isotherm assumed that it is multilayer.

### **Langmuir isotherm:**

Langmuir proposed this model in 1916; this model is applicable for mono-layer of adsorption. It estimates adsorption capacity of the adsorbent as given bellow.

$$a = \frac{k_1 p}{k_2 p + 1} \quad (\text{a gives } x/m \text{ in Freundlich}) \quad (2.7)$$

Where  $a$  is the amount of adsorbate adsorbed per gram of adsorbent,  $p$  is the equilibrium pressure, and  $k_1$  &  $k_2$  are constant.

### **BET isotherm:**

This is proposed by BET in 1928. This isotherm is developed for measurement of multilayer adsorption of adsorbate per gram of adsorbent. The proposed isotherm is used for describing surface area and pore volume of solid materials by using BET formula.

$$\frac{1}{W((\frac{P}{P_0})-1)} = \frac{1}{W_m C} + \frac{C-1}{W_m C} \left(\frac{P}{P_0}\right) \quad (2.8)$$

where  $W$  is the weight of gas adsorbed,  $P/P_0$  is the relative pressure,  $W_m$  is the weight of adsorbate adsorbed as monolayer, and  $C$  is the BET constant.

The concept of BET isotherm is employed for multilayer adsorption with different hypothesis.

- a) Adsorbate is physically adsorb on solid surface
- b) No interaction occur between each adsorption isotherm

c) Also Langmuir theory is used for each layer

The number of active sites also depends on particle size, particle morphology, surface texture, and porosity. The ray diagram of BET isotherm is shown in **Fig. 2.11**.

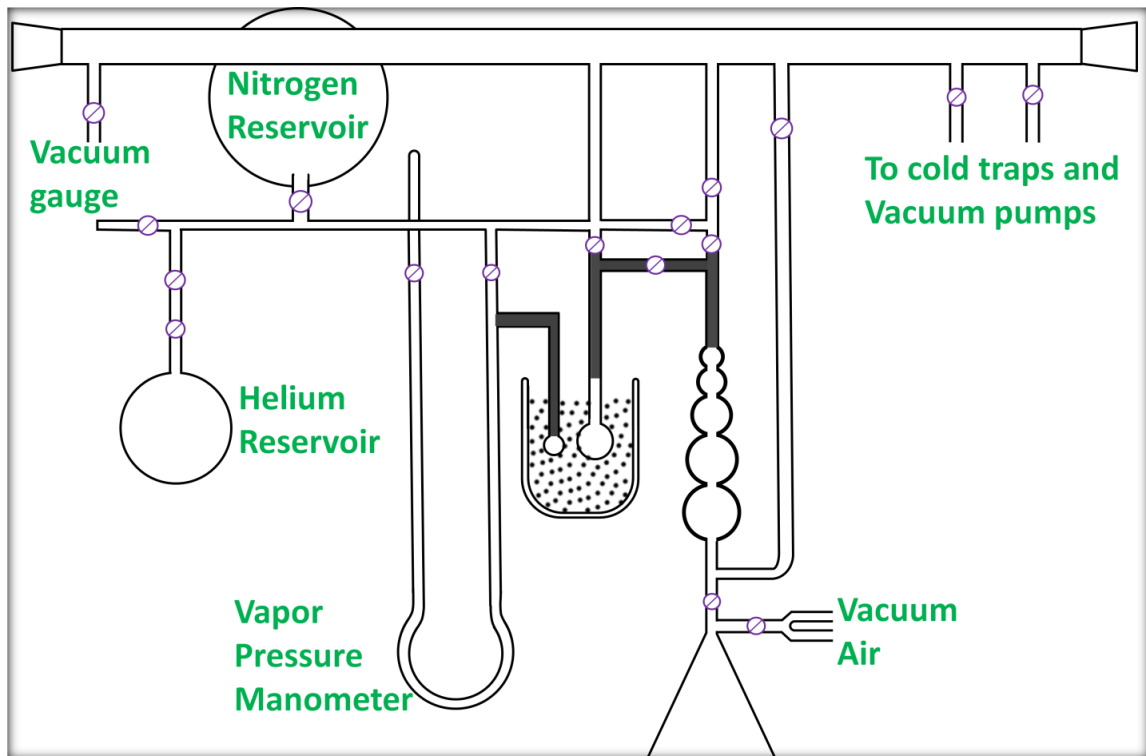


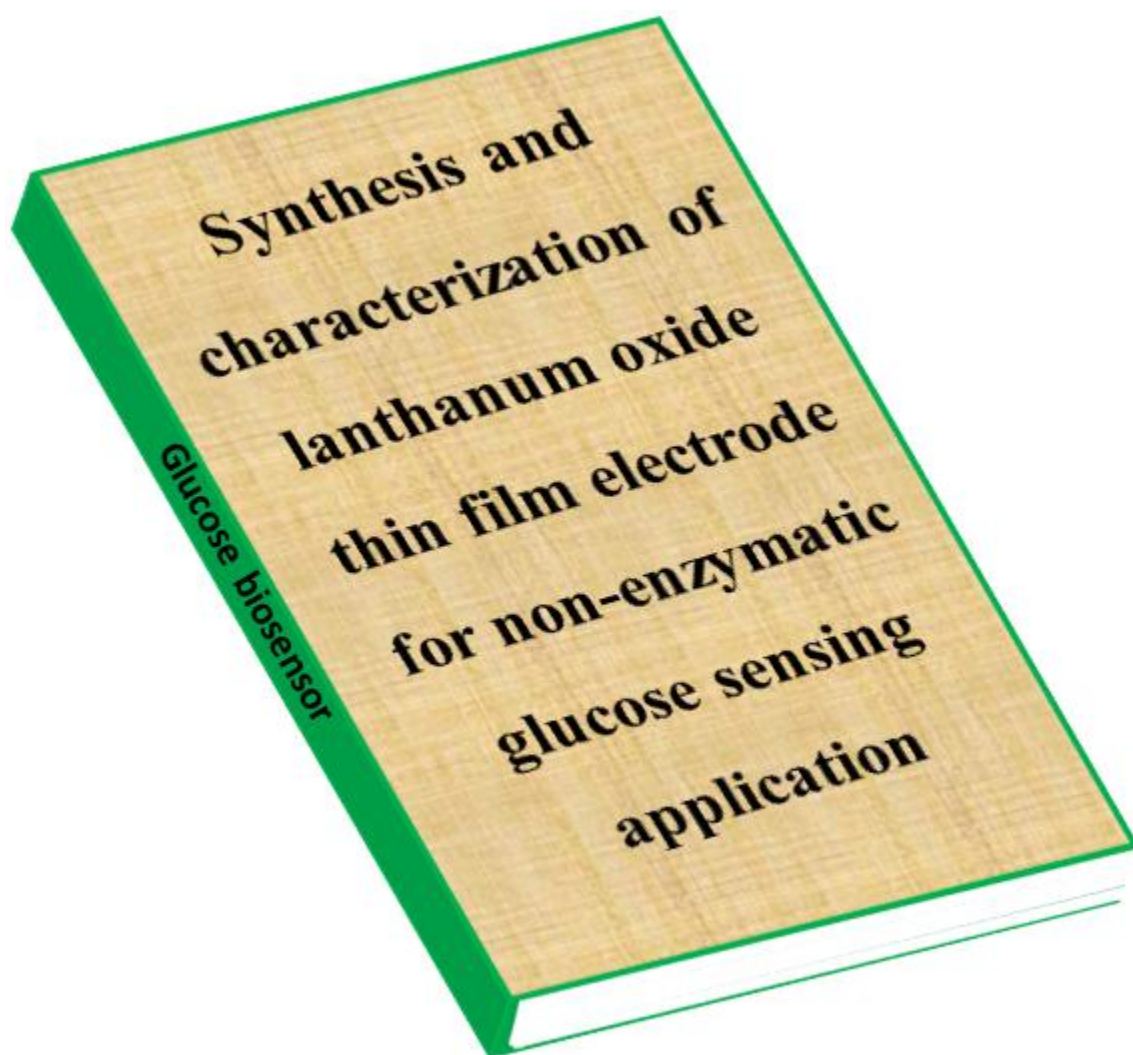
**Figure 2.11** Schematic diagram of BET isotherm [31]

**References:**

1. [https://en.wikipedia.org/wiki/Thin\\_film](https://en.wikipedia.org/wiki/Thin_film)
2. I. Gurrapp, L. Binder, *Sci. Technol. Adv. Mater.*, 9 (2008) 043001 (1-11).
3. J. George, "Preparation of Thin Films", Marcel Dekker, Inc., New York, (1992) 13-19.
4. K. Chopra, I. Kaur, "Thin film Device Application", Plenum Press, (1983) 101-102.
5. T. Niesen, M. De Guire, *Solid State Ion.*, 151 (2002) 61-68.
6. C. Lokhande, *Mater. Chem. Phys.*, 27 (1991) 1-43.
7. P. Andricacos, *Electrochem. Soc. Interface*, 8 (1999) 32-37.
8. G. Fulop, R. Taylor, *Ann. Rev. Mater. Sci.*, 15 (1985) 197-210.
9. I. Zhitomirsky, L. Gal-or, A. Kohn, *J. Mater. Sci.*, 30 (1995) 5307-5312.
10. M. Jeske, J. Schultze, M. Thonissen, H. Munder, *Thin Solid Films*, 255 (1995) 63-66.
11. G. Yi, W. Schwarzacher, *Appl. Phys. Lett.*, 74 (1999) 1746-1748.
12. C. Natarajan, H. Matsumoto, G. Nogami, *J. Electrochem. Soc.*, 144 (1997) 121-125.
13. S. Peulon, D. Lincot, *Adv. Mater.*, 8 (1996) 166-170.
14. A. Bard, L. Faulkner, "Electrochemical methods: fundamentals and applications", New York: Wiley, Second edition, (2000) 586-587.
15. A. Karatutlu, A. Barhoum, A. Sapelkin, "Emerging Applications of Nanoparticles and Architecture Nanostructures", Elsevier, (2018) 1-28.
16. R. Pandey, S. Sahu, S. Chandra, "Handbook of Semiconductor Electrodeposition", Marcel Dekker, Inc., (1996) 3-4.
17. Y. Gamburg, G. Zangari, "Theory and Practice of Metal Electrodeposition" Springer-Verlag New York, (2011) 2-3.
18. Jensen, W. B. Faraday's Laws or Faraday's Law? *J. Chem. Educ.*, 89, (2012), 1208–1209. doi:10.1021/ed101193q.
19. D. Sarkar, X. Zhou, A. Tannous, M. Louie, K. Leung, *Solid State Comm.*, 125 (2003) 365-368.
20. N. Gaikwad, V. Nikale, C. Bhosale, *J. Phys. Chem. Solids*, 64 (2003) 723-730.
21. J. Min, J. Wu, J. Cho, Q. Liu, J. Lee, Y. Ko, J. Chung, J. Lee, Y. Kim, *J. Magn. Mater.*, 304 (2006) e100-e102.

22. R. S. Nicholson, J. M. Wilson, M. L. Olmstead, *Anal. Chem.* 1966, 38, 4, 542–545. <https://doi.org/10.1021/ac60236a005>.
23. David C. Grahame, *Chem. Rev.* 1947, 41, 441–501, <https://doi.org/10.1021/cr60130a002>.
24. [https://icme.hpc.msstate.edu/mediawiki/index.php/Scanning\\_Electron\\_Microscopes.html](https://icme.hpc.msstate.edu/mediawiki/index.php/Scanning_Electron_Microscopes.html)
25. [http://www.wikiwand.com/en/Energy-dispersive\\_X-ray\\_spectroscopy](http://www.wikiwand.com/en/Energy-dispersive_X-ray_spectroscopy).
26. B. D. Cullity, *Elements of X-ray Diffraction*, Addison-Wesley Publishing Company Inc., Massachusetts 1956.
27. [http://chemwiki.ucdavis.edu/Analytical\\_Chemistry/Instrumental\\_Analysis/Diffraction/Powder\\_X-ray\\_Diffraction](http://chemwiki.ucdavis.edu/Analytical_Chemistry/Instrumental_Analysis/Diffraction/Powder_X-ray_Diffraction).
28. <https://www.mtm.kuleuven.be/equipment/TEM-CM-200/TEM-CM-200>.
29. S. Kerber, T. Barr, G. Mann, W. Brantley, E. Papazoglou, J. Mitchell, *J. Mater. Eng. Perform.* 7 (1998) 329-333.
30. <http://ywcmatsci.yale.edu/sites/default/files/resize/images/XPS-1-500x294.JPG>.
31. [http://www.pharmacopeia.cn/v29240/usp29nf24s0\\_c846.html](http://www.pharmacopeia.cn/v29240/usp29nf24s0_c846.html)

# CHAPTER III



## Index

Sr. No.	Details	Page No.
3.1	Introduction	71
3.2	Substrate cleaning	73
3.3	Experimental study	73
3.4	Structural and physical characterization	75
3.5	Electrochemical glucose sensing measurement	76
3.6	Results and discussion	77
	3.6.1 <i>Thin film growth mechanism</i>	77
	3.6.2 <i>X-ray diffraction</i>	78
	3.6.3 <i>X-ray photo electron spectroscopy</i>	79
	3.6.4 <i>Field emission scanning electron microscopy</i>	80
	3.6.5 <i>Transmission electron microscopy</i>	82
	3.6.6 <i>Brunauer-Emmett-Teller</i>	83
3.7	Enzymeless glucose detection	84
3.8	Selectivity, reproducibility and stability	89
3.9	Conclusions	91
3.10	References	92

### 3.1 Introduction:

Detection of biotic samples, mostly glucose molecule has huge significance regarding the various end treatment of the same in the fields of clinical, biological, chemical as well as in the food engineering [1]. Amperometric reagent based electrode on glucose oxidase was established for the first time in the 1962 [2]. The development of improper materials to be employed for the detection of glucose has seen a great traction. The persistent attention in the improvement of new improper materials required for reagent less electrochemical detection of biotic samples, like glucose detection further needs to improve the linear range, lower detection limits and selectivity. Glucose biosensors devices are divided into two types; enzymatic and non-enzymatic. The enzymatic glucose sensors have suffering with many drawbacks such as immobilization of enzyme depends upon the temperature, deficiency of long-term stability and maintain the pH of the solution and control the humidity [3]. Meanwhile, the reagent less glucose sensors exhibit high sensitivity, good stability, and quick response time. When, significant efforts have been prepared for the development of reagent less glucose sensors to improve their sensitivity, stability, linear range and reproducibility, up till now there exists crucial desire to develop new base material that can be working for electrochemical glucose detection to beat drawbacks of enzymatic and non-enzymatic sensors [4].

Literature survey tells that the electrodes with various microstructure show excellent performance in the field of supercapacitor, gas sensor and antibacterial applications [5-7]. Also, the porous microstructure of the thin film with the more specific surface area can increase the diffusion of glucose and assist to the useful ion exchange process during the glucose oxidation reaction time. Modified electrodes, electro-mediate and stimulate direct electron transfer during electrode and redox protein to assess the

redox potential of protein for the improvement in the non-enzymatic glucose sensor devices [8-10]. Therefore, it is crucial to make inoperative functional materials on electrode surface to hold the high activity of immobilized bio-molecule from electrochemically point of view. Various types of oxides [11-13], nano-materials [14-16], nano-composites [17, 18] and quantum dots [19, 20] have been examined to grow newly electrodes in order to achieve well performance.

Rare earth (RE) metal oxides are promising materials that can exhibit good supercapacitive performance, optical, magnetic, electrocatalytic, biosensing etc., applications due to the variation in the valence states, and high electrical conductivity. Yamada et al. [21] prepared first time lanthanum oxide ( $\text{La}_2\text{O}_3$ ) thin films on  $\text{SiO}_2$  substrate by using chemical vapor deposition method (CVD) and used for the gate insulator for MOSFETs. No et al. [22] fabricated  $\text{La}_2\text{O}_3$  materials using cyclic CVD method and investigated the crucial electrical properties. Nieminen et al. [23] synthesized  $\text{La}_2\text{O}_3$  thin film electrode by using atomic layer epitaxy on the soda-lime glass substrate and also deliberate its chemical stability in the surrounding temperature. Pointedly,  $\text{La}_2\text{O}_3$  is of great attention in the biomedicine fields, supercapacitor, high potential oxide ceramics, and hydrogen storage materials, etc. there is chemically stable, unsolvable in water and different crystal structures can be obtained [24-28].

This chapter describes a quick responsive reagent less biosensor for glucose detection.  $\text{La}_2\text{O}_3$  film electrodes were used for reagent less glucose detection.  $\text{La}_2\text{O}_3$  electrodes were fabricated by reasonable ED method and confirmed with various techniques like XRD, FE-SEM, XPS, EDX, TEM and BET. The electrochemical reagent less glucose sensing behavior of the  $\text{La}_2\text{O}_3$  film electrodes were studied using CV and *i-t* amperometric methods in 1 M KOH electrolyte.

### 3.2 Substrate cleaning (working electrode):

Ultraclean substrate is the most prime requirement during the thin film deposition process. Impurity having on the surface of the substrate is responsible for the unwanted growth of material and creation of non-uniform, non-resinous thin film. The basic requirement of sensing electrode is a highly conducting substrate, so low cost and easily available in marketplace conductive SS is used as a substrate. The typical cleaning procedure used for the SS substrate as follow,

1. The SS substrate was plane polished using zero grade polish paper
2. The substrate was cleaned and washed with acetone and double distilled water (DDW), respectively.
3. Then, it was ultrasonically cleaned for 15 minutes and naturally dried, and further used for the material deposition.

### 3.3 Experimental study:

All analytical grade chemicals such as lanthanum nitrate hexahydrate ( $\text{La}(\text{NO}_3)_3 \cdot 6\text{H}_2\text{O}$ ), potassium hydroxide (KOH), glucose ( $\text{C}_6\text{H}_{12}\text{O}_6$ ), ascorbic acid ( $\text{C}_6\text{H}_8\text{O}_6$ ), fructose ( $\text{C}_6\text{H}_{12}\text{O}_6$ ), and lactose ( $\text{C}_{12}\text{H}_{22}\text{O}_{11}$ ), were purchased from Thomas Baker (India) and used direct further purification. The  $\text{La}_2\text{O}_3$  film electrodes were deposited by potentiostatically and varied preparative parameters such as concentration of precursors, temperature, deposition potential and deposition time. The linear sweep voltammetry (LSV) technique was scanned in the potential range from 0 to -1.2 V vs SCE at scan rate of  $10 \text{ mV s}^{-1}$ . In this test, the negative potential increases up to -0.9V/SCE with no current observed. After that, reduction of the solution starts from -0.9 to -1.2 V/SCE as well as current suddenly increased due to reduction of lanthanum ion.

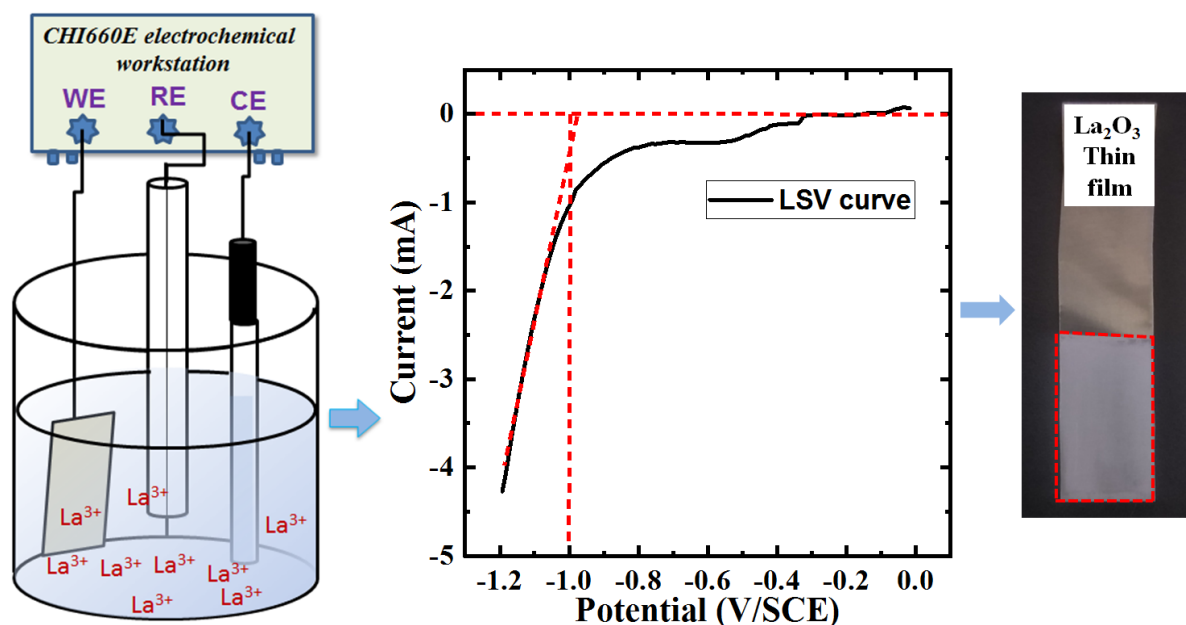


**Figure 3.1** The schematic presentation of lanthanum oxide thin film by ED method

The fresh electrolytic solution of 0.01M  $\text{La}(\text{NO}_3)_3 \cdot 6\text{H}_2\text{O}$  was prepared in the double distilled (DD) water. Three electrode system was designed using ultrasonically cleaned stainless steel (SS) substrate ( $50 \times 10 \times 0.5 \text{ mm}^3$ ), graphite plate, saturated calomel electrode (SCE) as a working, counter and reference electrode, respectively. The distance between the working and counter electrode was maintained as 10 mm and potentiostatic ED was carried out at -1.0 V/SCE. After deposition, whitish colored, well adherent, and uniform  $\text{La}_2\text{O}_3$  thin film was obtained at time of deposition of 1 hour. Deposited films were air dried and kept in closed box for further characterizations. The electrochemical setup, reduction of lanthanum ion within a potential window and deposited thin film is as displayed in **Fig. 3.1**. The potentiostatic curves of  $\text{La}_2\text{O}_3$  thin film formation on SS substrate at -1.0 V/SCE are shown in **Fig. 3.2**. Potentiostatic deposition curve is classified in to two regions, the first region exhibits nuclei formation and second region corresponds to film growth formation.

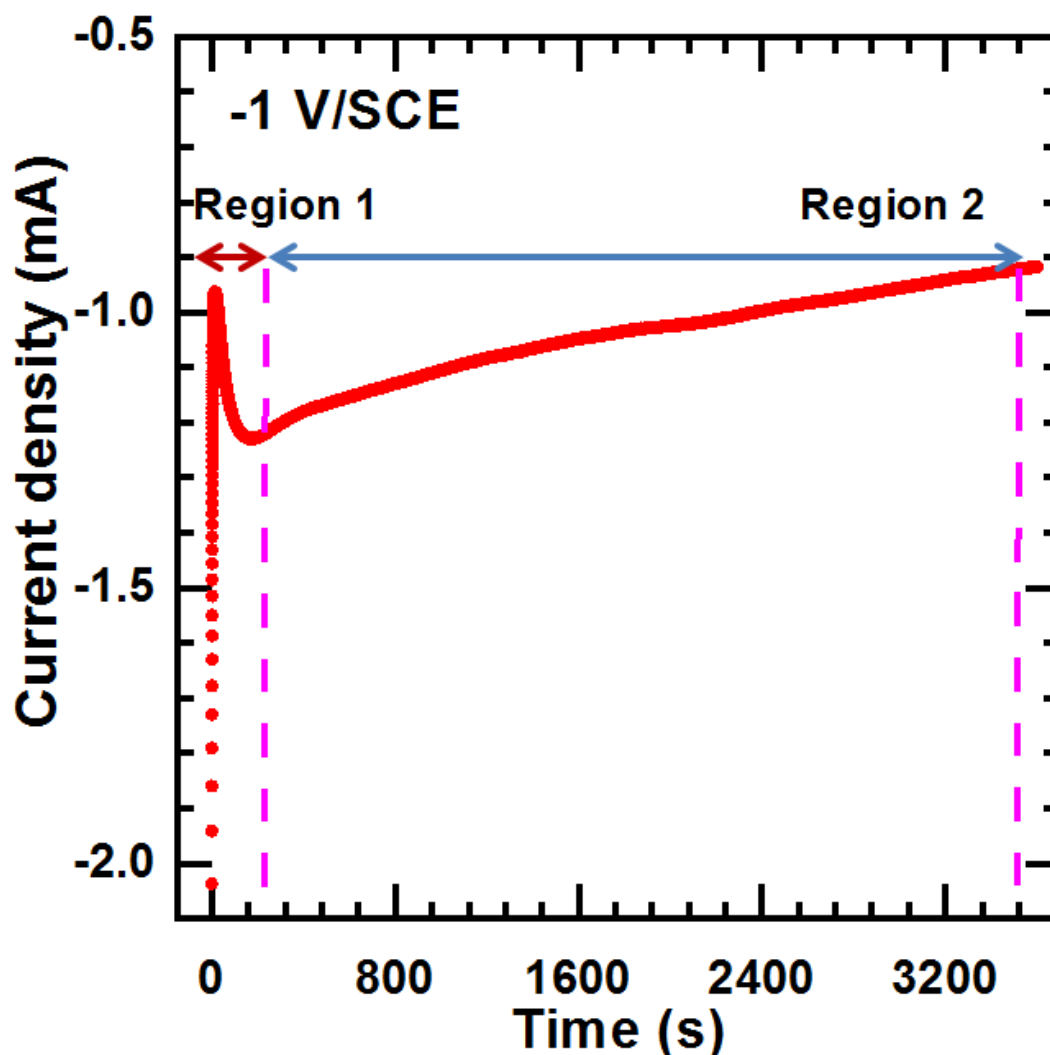


**Figure 3.2** Deposition potential curve of  $\text{La}_2\text{O}_3$  on SS substrate at -1.0 V/SCE

The observed initial flow of current response depends upon number of available cation at the interface of electrode which might be discharge immediately after the polarization of electrode (region-I). After the initial increment, the current decreases gradually due to cluster formation process continuously occurred such as adsorption and coalescence (region-II).

### 3.4 Structural and physical characterizations:

The  $\text{La}_2\text{O}_3$  film electrode was characterized via XRD. The XRD pattern was obtained by using Rigaku miniflex-600 ( $\text{CuK}\alpha$ ,  $\lambda=1.5406\text{\AA}$  radiation). The  $\text{La}_2\text{O}_3$  film

electrode material was used for detection of chemical states of elements and electronic configuration via XPS (Thermo VG scientific, United Kingdom), the surface texture was observed by using FE-SEM (ISM-7001F, and JEOL, Japan). The elemental analysis in the form of percentage was carried out using EDX (X-max, Oxford instruments). Crystallite size as well as particle size were estimated from TEM (Philips CM-30 unit, Point Resolution= 2.4Å) using an acceleration voltage (300 kV). Porosity and surface area of the film was studied by using BET (Belsorp II mini).

### 3.5 Electrochemical glucose sensing measurement:

The electrochemical performance of  $\text{La}_2\text{O}_3$  electrode was carried out using CV and *i-t* amperometry methods. Three electrode system was explained in the experimental study (section 3.3). The CV study was carried out within the potential window 0 to 0.5 V/SCE. For glucose sensing experiment, the  $\text{La}_2\text{O}_3$  film electrode was carried out in the potential window from 0 to 0.5 V/SCE, with and without glucose concentrations (5 to 25 mM) at a fixed scan rate of  $20 \text{ mV s}^{-1}$ . For *i-t* amperometry study, the *i-t* curve was obtained at fixed potential of +0.43 V/SCE after addition of different molar concentration of glucose. The interference study was executed by performing *i-t* experiment in the presence of different interfering species such as ascorbic acid, fructose, and lactose. The CV and *i-t* amperometry measurements were carried out in 1 M KOH solution and kept stirring constant speed 310 rpm. **Fig. 3.3** shows the schematic of glucose sensing experiment.

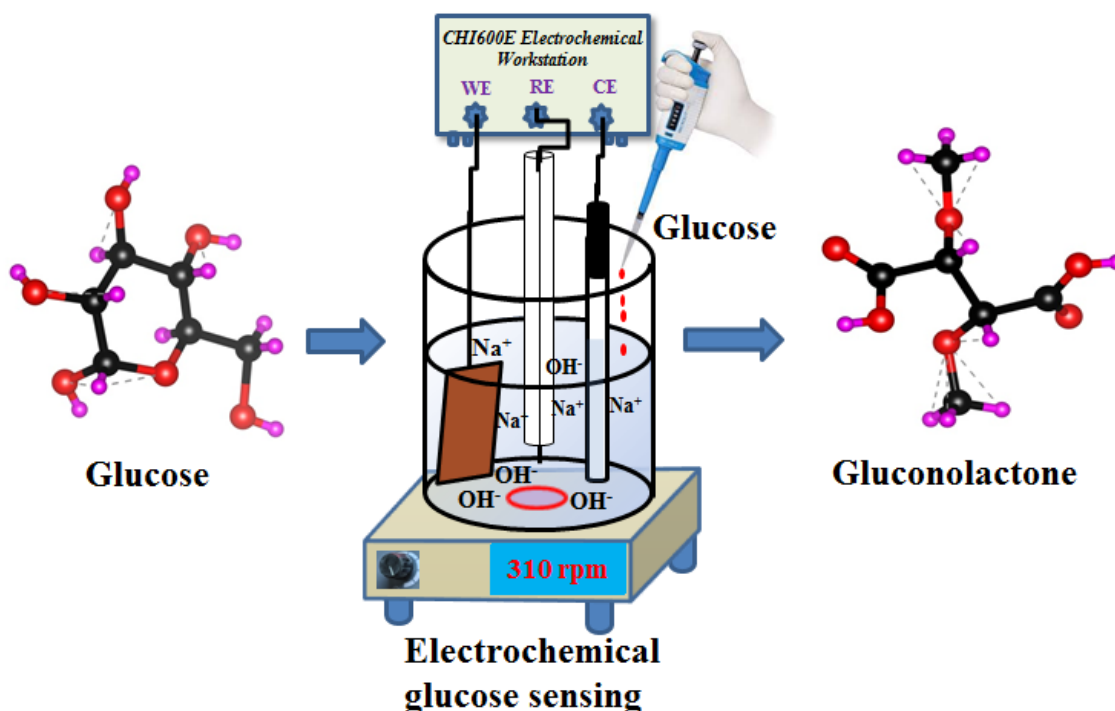


**Figure 3.3** Non-enzymatic electrochemical glucose sensing experimental setup

### 3.6 Results and discussion:

#### 3.6.1 Thin film growth mechanism:

Case: 1 the cathodic ED of  $\text{La}(\text{OH})_3$  was obtained at the cathode surface through the mechanism of base ( $\text{OH}^-$ ) electro-generation in the nitrate solution. These reactions include nitrate ions, dissolved oxygen and reduction of water. The reaction mechanism is given below.



The above reactions in an increase of  $\text{OH}^-$  ions due to pH of the solution increased near the electrode surface  $\text{La}(\text{OH})_3$  will form and deposit on the electrode surface.



Case 2: After deposition of  $\text{La}(\text{OH})_3$  that is an heated 773K in muffle furnace at 2h and naturally cooling down at room temperature due to the adsorbed hydroxyl contain easily removed.



### 3.6.2 X-ray diffraction (XRD) analysis:

**Fig. 3.4** shows XRD pattern of  $\text{La}_2\text{O}_3$  film electrode. The intense peaks observed in XRD pattern at  $2\theta$  correspond to (111), (401), (702), (611) and (703) planes of monoclinic  $\text{La}_2\text{O}_3$  crystal structure (JCPDS card no. 22-0641). A high intense XRD peak confirms well crystalline nature of the material.

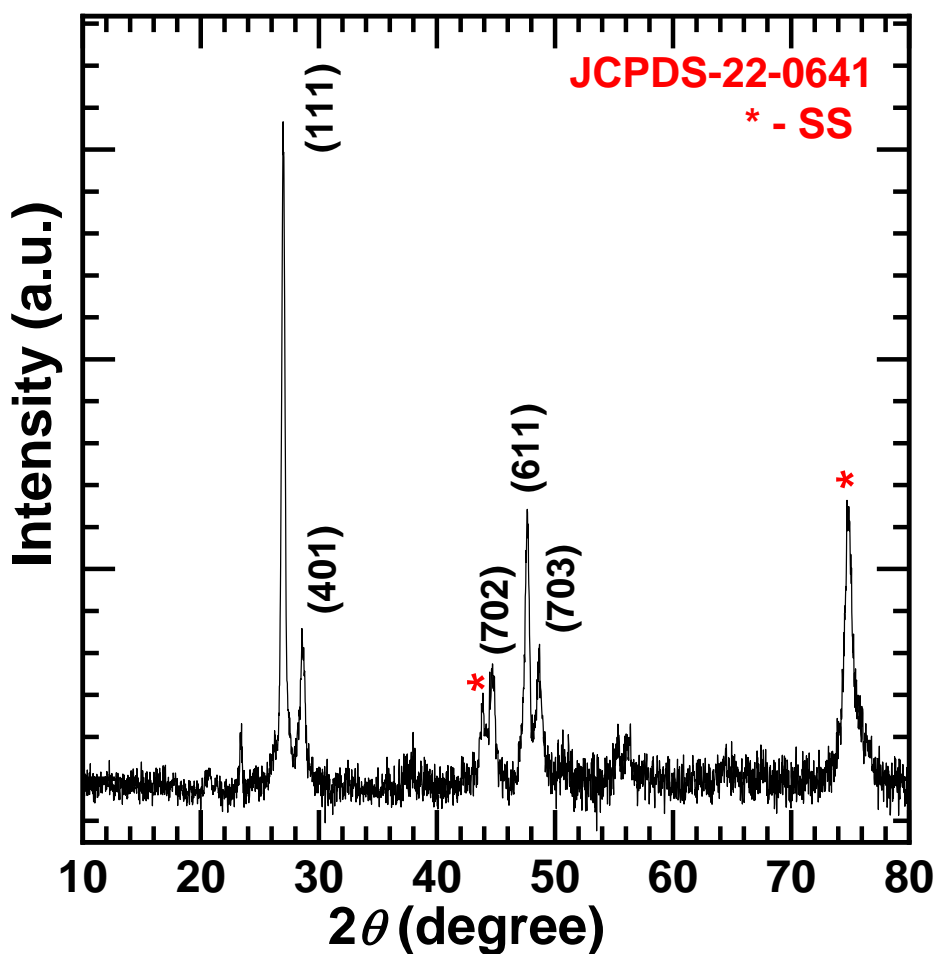


**Figure 3.4** The XRD pattern of  $\text{La}_2\text{O}_3$  thin film

The remaining peaks marked by (\*) in the XRD pattern correspond to SS substrate. The average crystallite size was calculated for high intense peak by using Scherrer's relation (3.7) as

$$D = \frac{K\lambda}{\beta \cos \theta} \quad (3.7)$$

where  $\beta$  stands for full width at half maxima,  $K$  stands for constant (0.91) and  $\lambda$  stands for wavelength of Cu-K $\alpha$  X-ray source (1.5406Å). The average crystallite size was calculated as 16.55 nm. Kolitsch et al. [29] prepared La<sub>2</sub>O<sub>3</sub> material by co-precipitation method and identified monoclinic phase.

### 3.6.3 X-ray photoelectron spectroscopy (XPS) analysis:

Using the XPS technique oxidation states of La and O were analyzed. **Fig. 3.5(a)** indicates the survey spectrum of La<sub>2</sub>O<sub>3</sub> thin film. **Fig. 3.5(b)** displays deconvoluted XPS spectrum of Lanthanum in La3d oxidation state which splits into two well separated main and satellite spin orbits by binding energy (BE) difference of 3.4 and 3.7 eVs, respectively. The two main peaks of La3d<sub>3/2</sub>, and La3d<sub>5/2</sub> at the BE 851.5 and 834.8 eVs, respectively designate the being oxidation state as La<sup>3+</sup> in the material. According to literature survey, La3d<sub>5/2</sub> (La<sup>3+</sup>) has BE in the range 834.4-834.9 eV [25]. The spin orbit splitting of La3d among La3d<sub>3/2</sub> and La3d<sub>5/2</sub> peaks through an energy gap of 16.7 eV is a characteristic of La<sup>3+</sup> oxidation state. In the oxygen spectrum, **Fig. 3.5(c)** displays O1s oxidation state of oxygen in the high resolution spectrum. The high intense peak at BE 531.24 eV indicates the presence of oxygen in O<sup>2-</sup> state. The XPS spectrum confirms the crucial formation of La<sub>2</sub>O<sub>3</sub> with suitable valence states.

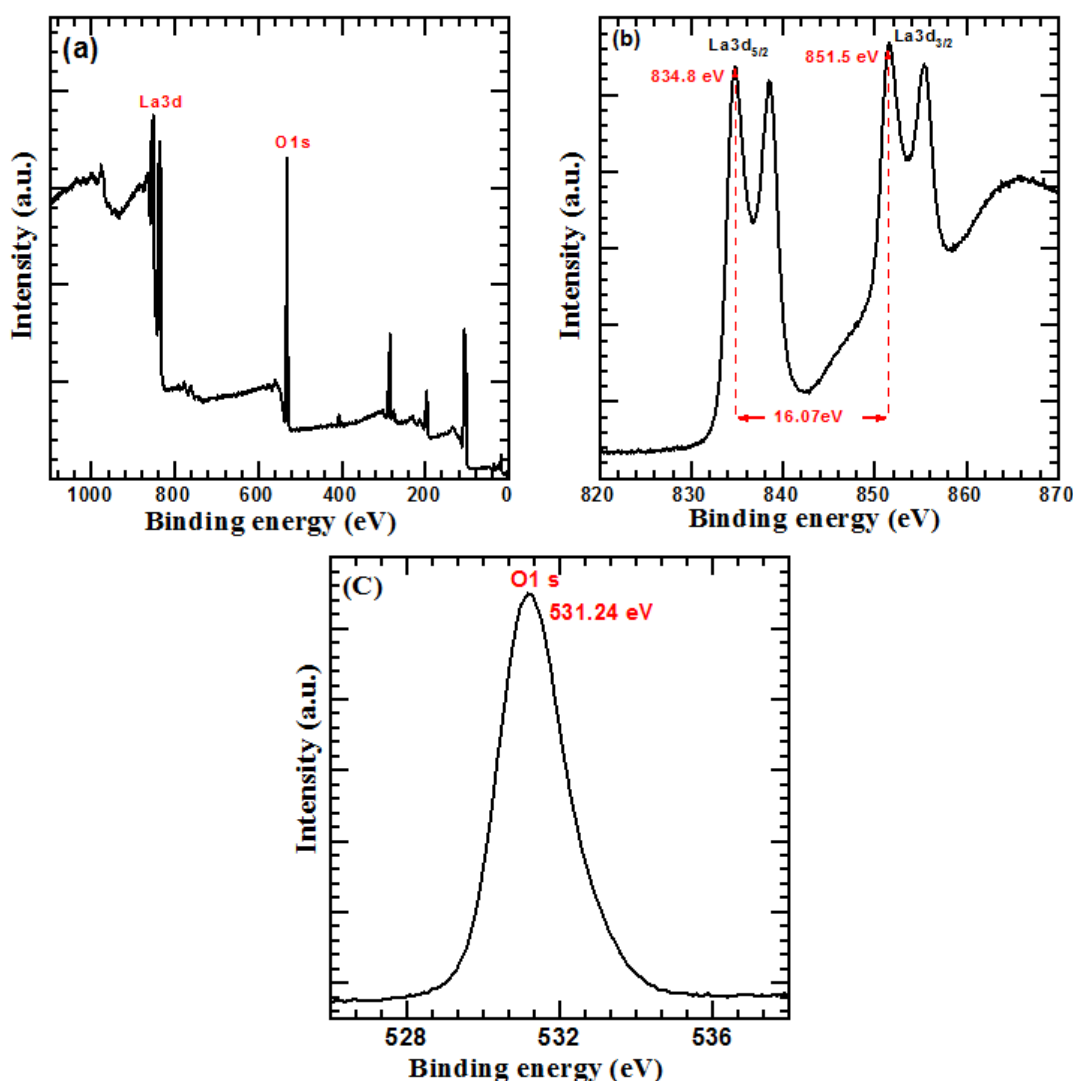


**Figure 3.5** (a) Full range XPS spectrum for La<sub>2</sub>O<sub>3</sub> sample, high resolution spectrum for (b) La 3d and (c) O 1s

### 3.6.4 Field emission-scanning electron microscopy (FE-SEM) analysis:

Surface texture study of La<sub>2</sub>O<sub>3</sub> film electrode was carried out using FE-SEM. FE-SEM surface micrographs of La<sub>2</sub>O<sub>3</sub> film electrode for two different magnifications (1000X and 15000X) are shown in **Fig. 3.6(a, b)**. From the FE-SEM analysis, vertically aligned asymmetrical nano sheets are deposited on conducting SS substrate. The intersected asymmetrical nano sheet grown all over the surface of the electrode is shown in **Fig 3.6a**. The average length of nano sheets is to be ~1.1  $\mu\text{m}$  as shown in **Fig. 3.6b**.

Vertically aligned nano sheets produce its identifiable path to electron transfer into pores and decrease its contact resistance of the electron. Also vertically aligned nano sheets lead to improvement of the  $\text{La}_2\text{O}_3$  electrode performance owing high surface area, additional desirable surface to volume ratio and exposer electro-catalytically dynamic site on  $\text{La}_2\text{O}_3$  film electrode.

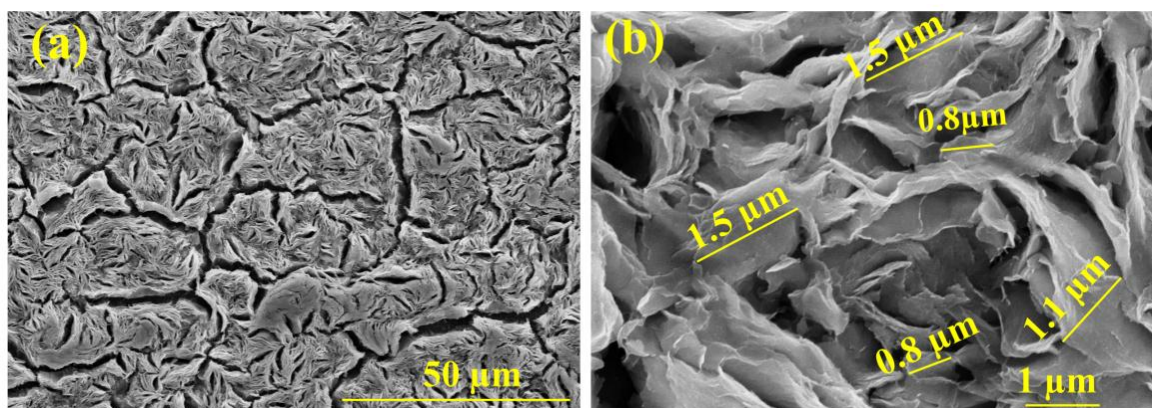


**Figure 3.6** The FE-SEM images of  $\text{La}_2\text{O}_3$  film at (a) 1000X and (b) 15000X magnifications

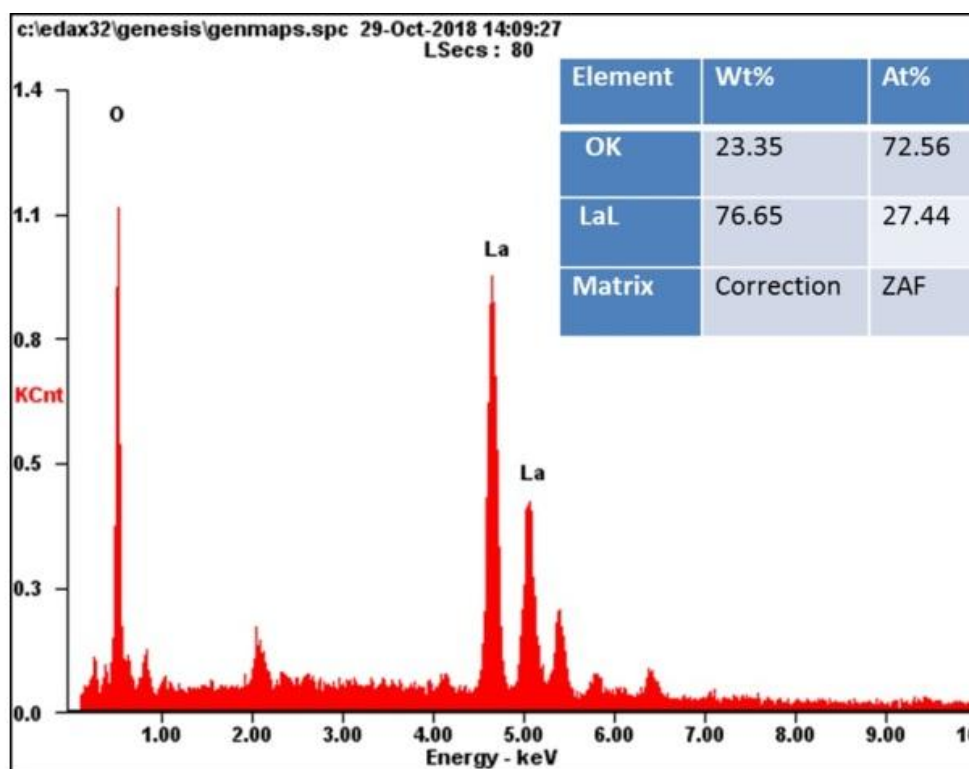


**Figure 3.7** EDS spectrum of  $\text{La}_2\text{O}_3$  film electrode

Several types of morphologies have been described for  $\text{La}_2\text{O}_3$  film electrodes synthesized from various methods. Yadav et al. [5] achieved porous honeycomb-like morphology by using sprayed  $\text{La}_2\text{O}_3$  film electrodes. Liu et al. [7] experimentally achieved polyhedron, spindle and sphere-like morphology for precipitated  $\text{La}_2\text{O}_3$  film electrode material. The percentage study of elemental arrangement in  $\text{La}_2\text{O}_3$  thin film has been studied by EDX method. **Fig. 3.7** displays the EDX spectrum and their percentage of lanthanum and oxygen elements in as deposited  $\text{La}_2\text{O}_3$  film electrode. The atomic percentage of lanthanum and oxygen within the  $\text{La}_2\text{O}_3$  is 38.18 and 61.82%, respectively that can nearly equal to ideal percentage value of 40:60%.

### 3.6.5 Transmission Electron Microscopy (TEM) analysis:

The crystal shape and construction of the layer by layer intercalated arrangement of  $\text{La}_2\text{O}_3$  nanoparticles were confirmed by TEM. TEM images of  $\text{La}_2\text{O}_3$  electrode material at different magnifications is as shown in **Fig. 3.8(a-c)**. The TEM image showed in **Fig. 3.8a** tells that, all the nanosheets are interrelated and agglomerated. The average particle size in the range of ~15 to 30 nm is observed. The TEM image examination show inter planer d-spacing of 0.326 nm calculated from the fringe spacing that corresponds to (111) (*hkl*) plane of  $\text{La}_2\text{O}_3$  material as displayed in **Fig. 3.8b**. The inter planer d-spacing of 0.326 nm is in the good agreement with crystallographic interatomic distance calculated from XRD analysis. The crystallite size is noticeably observed in **Fig. 3.8c**, the average crystallite size in the range of ~5 to 20 nm that is good agreement with XRD study. The above explanation suggest that  $\text{La}_2\text{O}_3$  nanoparticle is well crystalline in nature and the interconnected nano sheets leads to high surface area with better diffusion path provided a glucose sensing application.

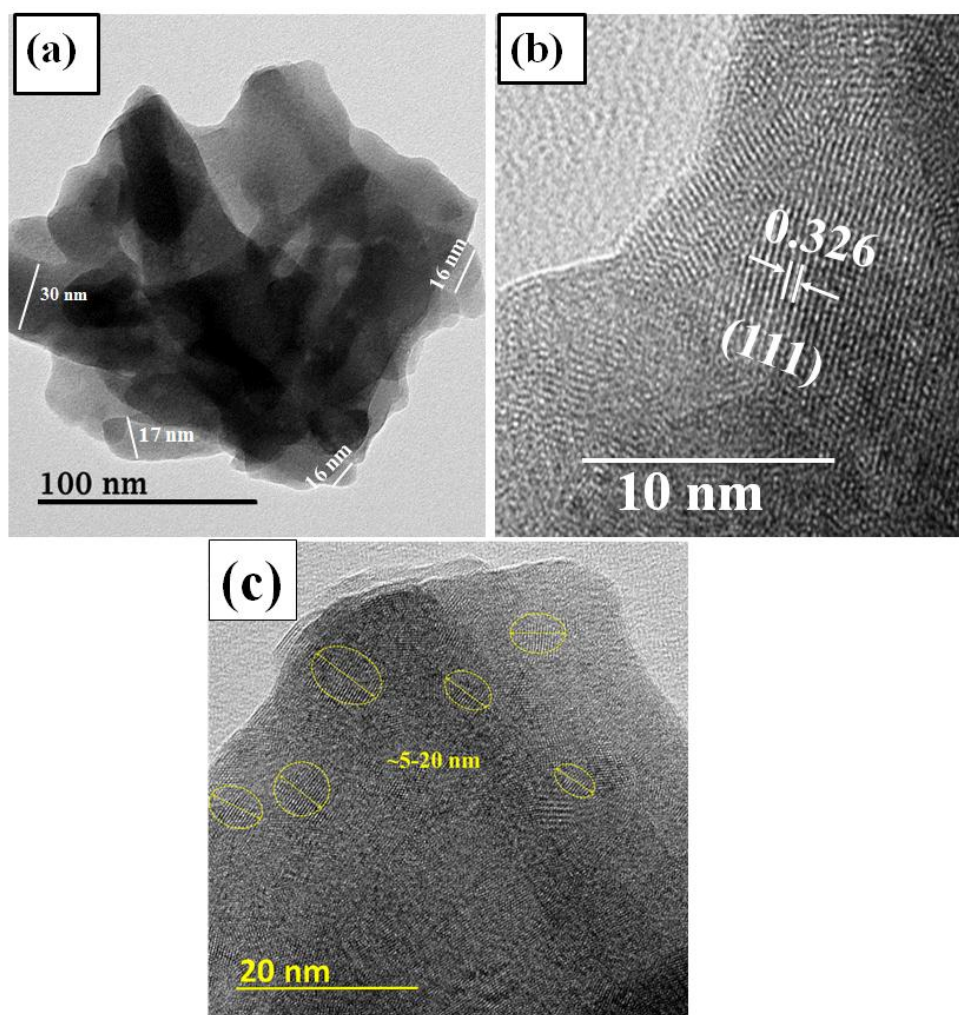


**Figure 3.8** TEM images at magnification of (a) 80000X and (b) 200000X and (c) crystallite size of  $\text{La}_2\text{O}_3$  sample

### 3.6.6 Brunauer Emmett Teller (BET) analysis:

The pore size distribution, specific surface area and porous texture of the scratched  $\text{La}_2\text{O}_3$  material were studied by physical sorption of  $\text{N}_2$  gas using BET method. **Fig. 3.9(a)** displays isotherm of  $\text{La}_2\text{O}_3$  materials, a small hysteresis loop represent between the higher to middle pressure range (1- 0.74 Pa) of isotherm that indicates  $\text{La}_2\text{O}_3$  material becomes a mesoporous structure. The specific surface area (BET) investigation of  $\text{La}_2\text{O}_3$  materials was carried out in the relative pressure ( $p/p_0$ ) range from 0.02-0.2 Pa and measured in the form of specific surface area was  $14.17 \text{ m}^2 \text{ g}^{-1}$ . The isotherm of

$\text{La}_2\text{O}_3$  material was exhibits type of IV(b) isotherm noticed that this materials having a mesopores of smaller widths, this isotherm is common for mesoporous materials [30]. The entire pore volume was calculated by quantity of adsorbed nitrogen at  $p/p_0 = 0.990$  and found to be  $0.1393 \text{ cm}^3 \text{ g}^{-1}$ . **Fig. 3.9(b)** displays the distribution of pore size using the Barrett-Joyner-Halenda (BJH) method. The  $\text{La}_2\text{O}_3$  contains four types of dominant pores centered at 6, 10.49, 16 and 21.75 nm indicating  $\text{La}_2\text{O}_3$  has of mesoporous structure with average pore size 39.30 nm. The mesoporous structure facilitates excellent active sites to the diffusion of glucose at surface of  $\text{La}_2\text{O}_3$  electrode.

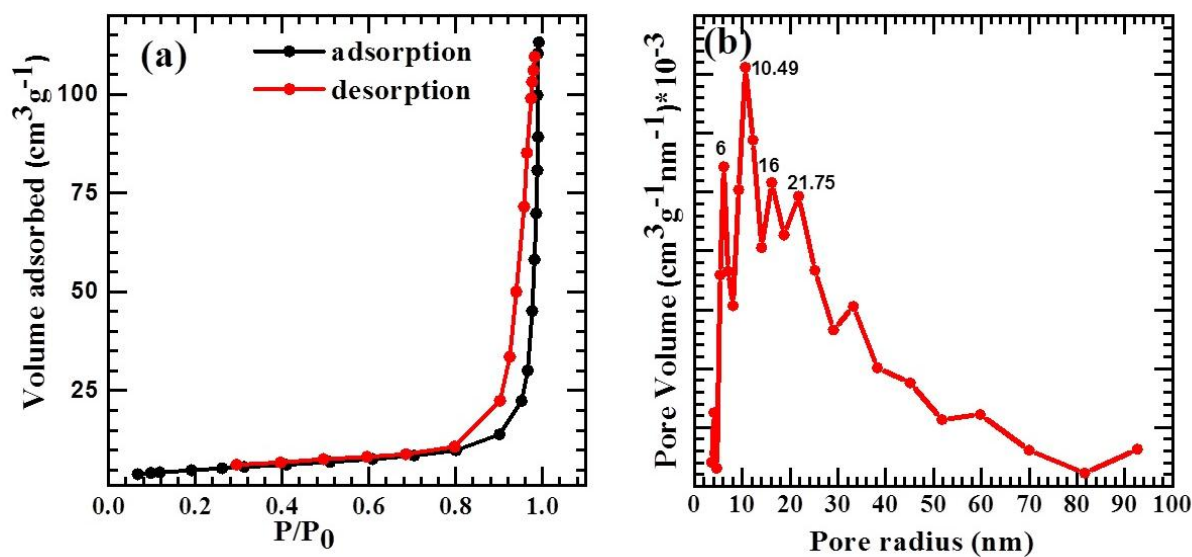


**Figure 3.9** (a, b) The  $\text{N}_2$  sorption isotherms of mesoporous  $\text{La}_2\text{O}_3$  sample

### 3.7 Enzymeless glucose detection:

In order to examine the electrochemical kinetic properties of  $\text{La}_2\text{O}_3$  film electrode, CV and  $i-t$  amperometry measurements were carried out. Typical CV curve of  $\text{La}_2\text{O}_3$  film electrode in 1 M KOH electrolyte at different scanning rates varied from 10 to  $100 \text{ mV s}^{-1}$  within the potential window of 0 to +0.5 V/SCE are displayed in **Fig. 3.10(a)**. All the CV curves display noticeable characteristic redox peaks that specify the oxidative behavior.

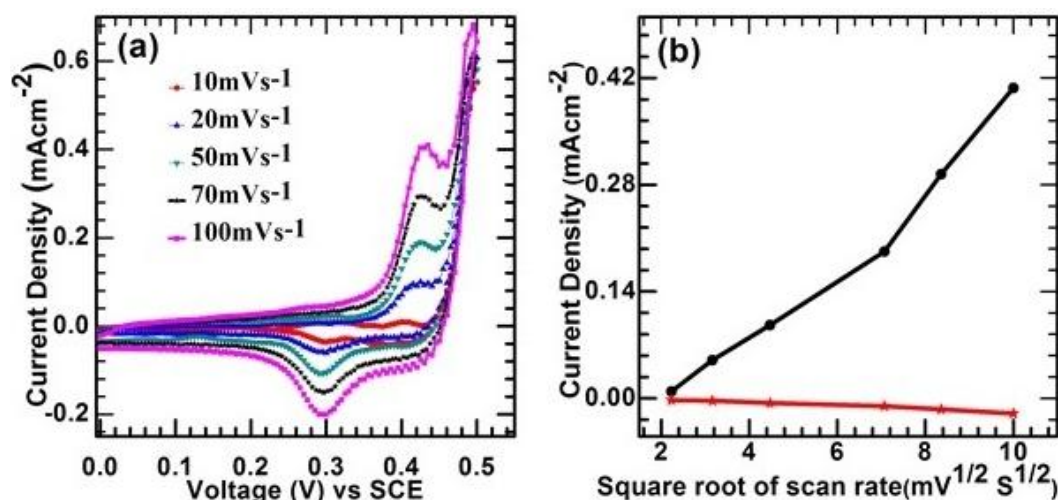


**Figure 3.10** (a) The CV curves at various scan rates of 10 to 100 mV s<sup>-1</sup> and (b) displays peak current as a function of square root of different scan rate ( $V^{1/2}$ )

The above CV curves reveal that the oxidation and reduction peaks for La<sub>2</sub>O<sub>3</sub> film electrode are at +0.43 and +0.29 V/SCE, respectively. The voltage values of these peaks become shifted toward more positive and negative side by increasing the scan rate. Cathodic peak current vs. the square root of scan rate ( $v^{1/2}$ ) shows the linear correlation with a slight increase in anodic current after 7.4 mV<sup>1/2</sup> (**Fig. 3.10(b)**).

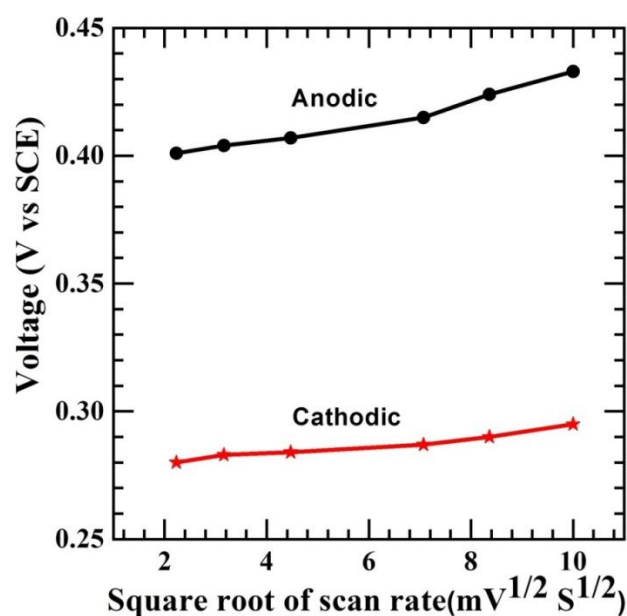


**Figure 3.11** Plots of anodic and cathodic peak voltages vs. square root of the different scan rates

A detailed CV study is shown in **Fig. 3.11**. Anodic current density rises from 0.007 to 0.407 mA cm<sup>-2</sup> with increased scan rate as of 5 to 100 mV s<sup>-1</sup>. During this time, anodic potential changes from +0.401 to +0.431 V/SCE. Also, change in cathodic potential from +0.280 to +0.295 V/SCE is observed with decrease in current density from -0.00233 to -0.020 mA cm<sup>-2</sup>, justifying a characteristic diffusion controlled ideal electrochemical progression [31].

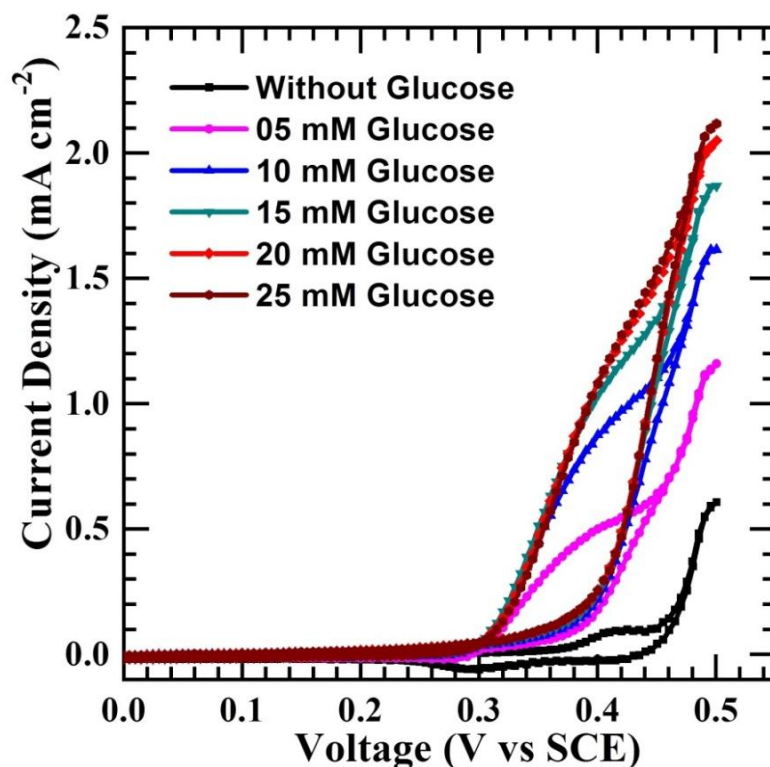
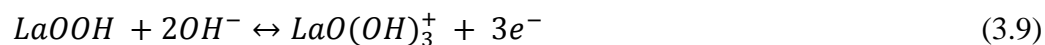


**Figure 3.12** The CV curves in absence and presence of different glucose concentrations in 1 M KOH solution at 20 mV s<sup>-1</sup>

The electrochemical performance of La<sub>2</sub>O<sub>3</sub> film electrodes towards glucose oxidation in an alkaline electrolyte was revealed by the *i-t* amperometric technique. **Fig. 3.12** displays CV curves of the La<sub>2</sub>O<sub>3</sub> film electrode in 1 M KOH solution at scan rate of 20 mV s<sup>-1</sup> presences and absence of different concentration of glucose (5 to 25 mM). The anodic peak current was proportional to glucose concentration, indicative of significant

catalytic activity of  $\text{La}_2\text{O}_3$  electrode for glucose oxidation through a cyclic mediation redox process. The reason behind that the oxidation peak potential moved to high potential might to be assigned a diffusion limitation of glucose at the surface of the electrode. Surges in current response with rising glucose concentration highlights that electrodeposited  $\text{La}_2\text{O}_3$  film electrode can be employed for electrocatalytic non-enzymatic glucose detection.

A possible reaction mechanism of electrocatalytic oxidation of glucose owing to being of  $\text{La(III)}$  ions are defined with the following reactions.



In the anodic scan,  $\text{La(III)}$  species present in the dissolved solution hydrolyse to form  $\text{LaO}(\text{OH})_3^+$  by the releasing electrons. Presence of glucose molecule, the unrestricted electron reacts with glucose molecule to convert it into the glucanolactone [24]. Since, oxidation of glucose and reduction of ion species, glucose molecule detected by the material.

The  $i$ - $t$  amperometric study of  $\text{La}_2\text{O}_3$  film electrode was performed at +0.43 V/SCE. different molar concentrations of glucose from 1.25 to 11.25 mM was inserted to 1 M KOH solution through a regular interval of 60 s, to make the staircase-like graph as depicted in **Fig. 3.13a**. Thus,  $\text{La}_2\text{O}_3$  film electrode tells a good electrocatalytic linear response near the glucose in the range between 1.25-11.25 mM. A easily electron transfer process through  $\text{La}_2\text{O}_3$  film electrode shows a well defined concentration dependence. Thus, it is one of the most important analytical factors: for  $i$ - $t$  amperometric glucose sensor is the quick response time as less than 1 second. **Fig. 3.13b** displays that within

the one second glucose oxidation takes place with successive addition of 1.25 mM glucose solution and 0.46 mA cm<sup>-2</sup> current increases is observed. Thus, successive addition of glucose (within one second) reveals steady state response due to rapid electron transport on the surface of electrode.

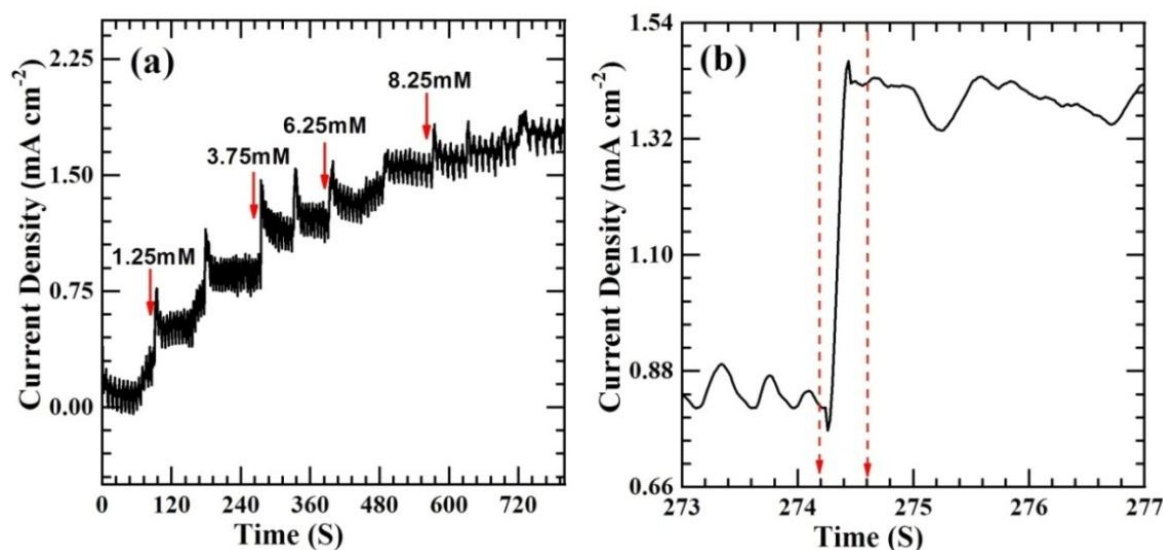


**Figure 3.13** (a) Response time obtained with increasing glucose concentration in steps of 1.25 mM at La<sub>2</sub>O<sub>3</sub> electrode and (b) detection time (less than 1 second).

**Fig.3.14** displays the relationship between the electrocatalytic current and different concentrations of glucose at La<sub>2</sub>O<sub>3</sub> film electrode. The current response was linear at low concentration between 1.25-3.75 mM with excellent sensitivity of 616  $\mu\text{A mM}^{-1} \text{cm}^{-2}$  and LOD of 0.27 mM as well as correlation coefficient of 0.9924 was obtained. Higher concentrations between 3.75-11.25 mM, the sensitivity were 263  $\mu\text{A mM}^{-1} \text{cm}^{-2}$  with correlation coefficient (R) 0.98. The correlation coefficient describes how one variable moves in relation to another. A correlation indicates that the two move in the same direction, with +1 correlation when they move in pair. Rising the glucose concentration, blocks mass transfer which affects the diffusion of fresh glucose molecules near electrode surface.

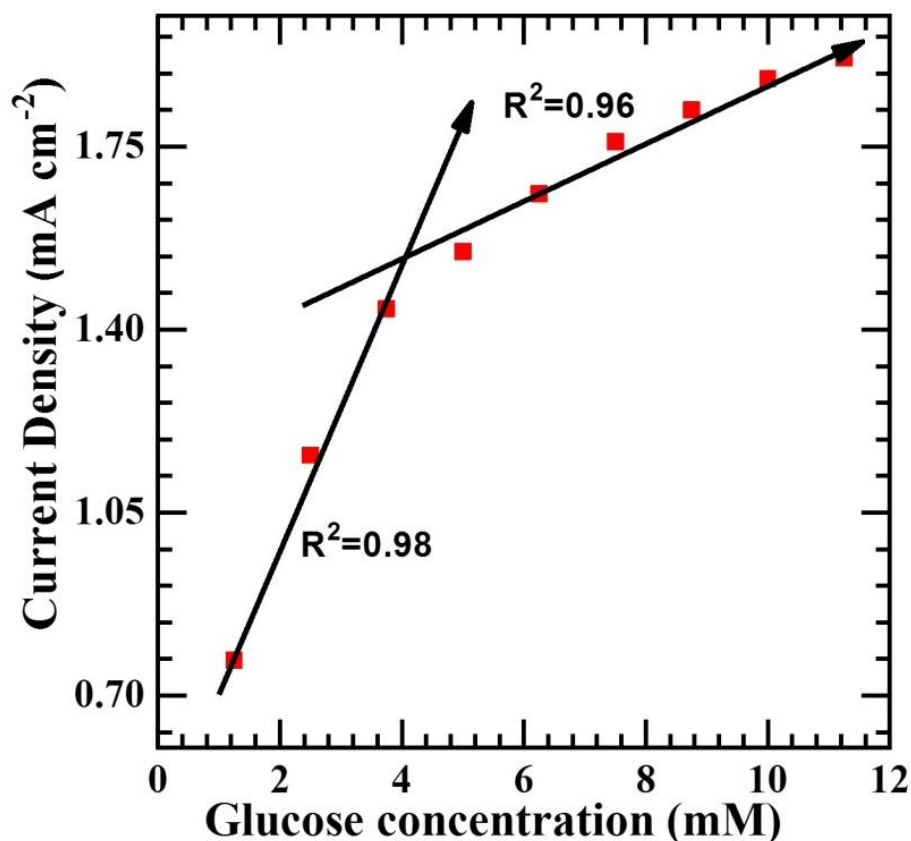


**Figure 3.14** Current response verses the glucose concentration at  $\text{La}_2\text{O}_3$  electrode with two different slopes

At higher concentration of glucose (>11.25 mM), the *i-t* amperometric curve reached its saturation point later current response is declined may be due to the adsorbed intermediates [32]. Finally, we concluded that; the vertically aligned  $\text{La}_2\text{O}_3$  nano-sheets help fast electron transfer and more electrocatalytic active sites owing to higher specific surface area to glucose oxidation.

### 3.8 Selectivity, reproducibility and stability:

The normal physiological glucose level in the human blood sample was about 3-8 mM. This was higher than those of lactose (Lac), fructose (Fru), and ascorbic acid (AA) (1mM). To calculate the sensitivity, the interference effect of Fru, lac, and AA with glucose was also studied in aqueous 1 M KOH solution at a potential of +0.43 V/SCE. **Fig. 3.15** displays glucose detection selectivity with Fru, Lac and AA at  $\text{La}_2\text{O}_3$  electrode.

The current response for Fru, Lac and AA was also significantly lower as compare to glucose. Thus, the electrodeposited  $\text{La}_2\text{O}_3$  film electrode can be employed for glucose detection in presence of other interferences.

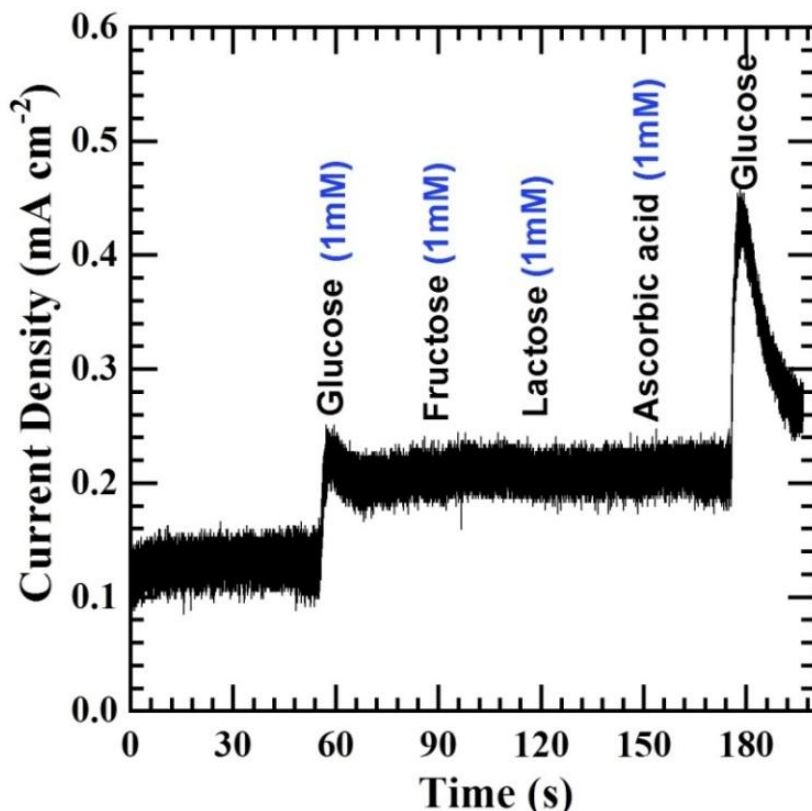


**Figure 3.15** Plot of the  $\text{La}_2\text{O}_3$  film electrode for successfully addition of glucose and interferences in aqueous 1 M KOH solution at +0.43 V/SCE

Lua et al. [33] prepared CuO derived from metal-organic framework (MOFW) for non-enzymatic glucose sensing application that indicates excellent selectivity performance. The response current density to 0.1 mM glucose concentration at potential +0.55V was observed with addition of other interference such as Fru, Lac, AA, DA, UA, NaCl. Felix et al. [34] synthesized novel CuO-N-doped graphene composite based electrode for the enzymeless glucose detection. CuO-N doped graphene electrode exhibits excellent selectivity performance towards glucose.

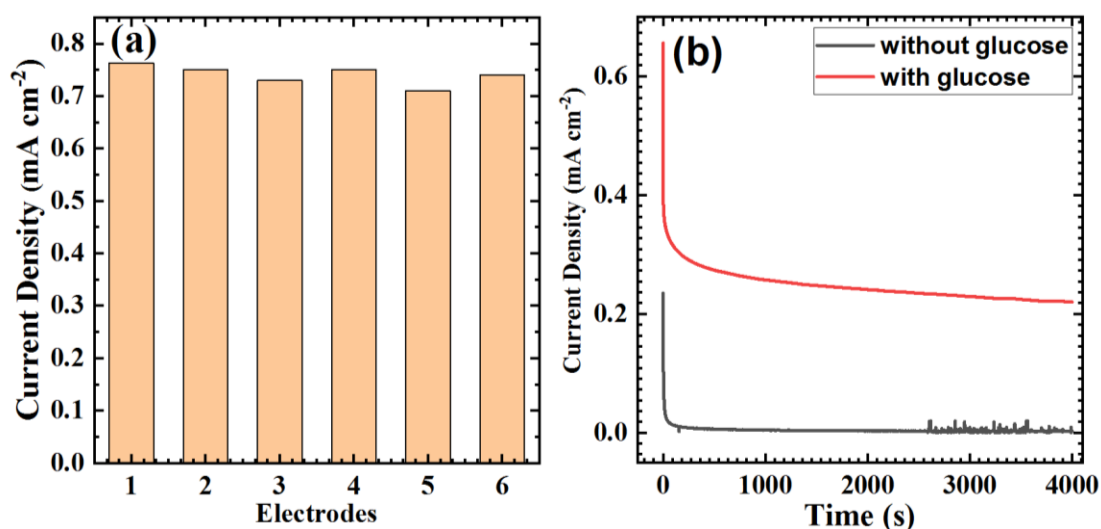


**Figure 3.16** (a) Bar graph of reproducibility and (b) stability graph in the presence of 1 mM glucose concentration of La<sub>2</sub>O<sub>3</sub> film electrode.

To examine the reproducibility of the La<sub>2</sub>O<sub>3</sub> film electrode, *i-t* amperometric response of six similar fabricated electrodes were tested at identical condition. A result of the experiments is shown in **Fig. 3.16(a)**. A satisfactory reproducibility with a relative standard deviation (RSD) of 2.5% was found that indicates the excellent reproducibility of La<sub>2</sub>O<sub>3</sub> film electrode. To evaluate the long term stability of the La<sub>2</sub>O<sub>3</sub> film electrode, *i-t* amperometric response was noted with and without 1 mM glucose concentration at potential of +0.43 V/SCE for 4000 s. After 1 mM glucose concentration, current response is more than that of without glucose concentration. The La<sub>2</sub>O<sub>3</sub> film electrode displays linear characteristics and noble stability with retaining 84.56% of current response is as shown in **Fig. 3.16(b)**.

### 3.9 Conclusions:

The La<sub>2</sub>O<sub>3</sub> film electrodes were studied employing the scalable and inexpensive cathodic ED method. The XRD peak pattern was displayed monoclinic phase with a crystalline size (16.55 nm). As deposited film electrode displayed vertically aligned nano sheets like structure. Further, the specific surface area of La<sub>2</sub>O<sub>3</sub> material (14.17 m<sup>2</sup> g<sup>-1</sup>)

with a meso-porous structure helped the diffusion of glucose molecule into  $\text{La}_2\text{O}_3$  film electrode that convert diffused glucose to oxidize into gluconolactone, an ideal process designed for the numerical analysis of glucose detection was observed. Also, the  $\text{La}_2\text{O}_3$  film electrode showed high sensitivity to glucose detection ( $616 \mu\text{A mM}^{-1} \text{cm}^2$ ) with LOD of 0.87 mM. The film electrode showed less quick response time. The  $\text{La}_2\text{O}_3$  film electrode can be used for the measurable detection of glucose molecule in the presence of other interferents. Later,  $\text{La}_2\text{O}_3$  film electrode can be used as a potential candidate in electrocatalytic non-enzymatic glucose sensing application.

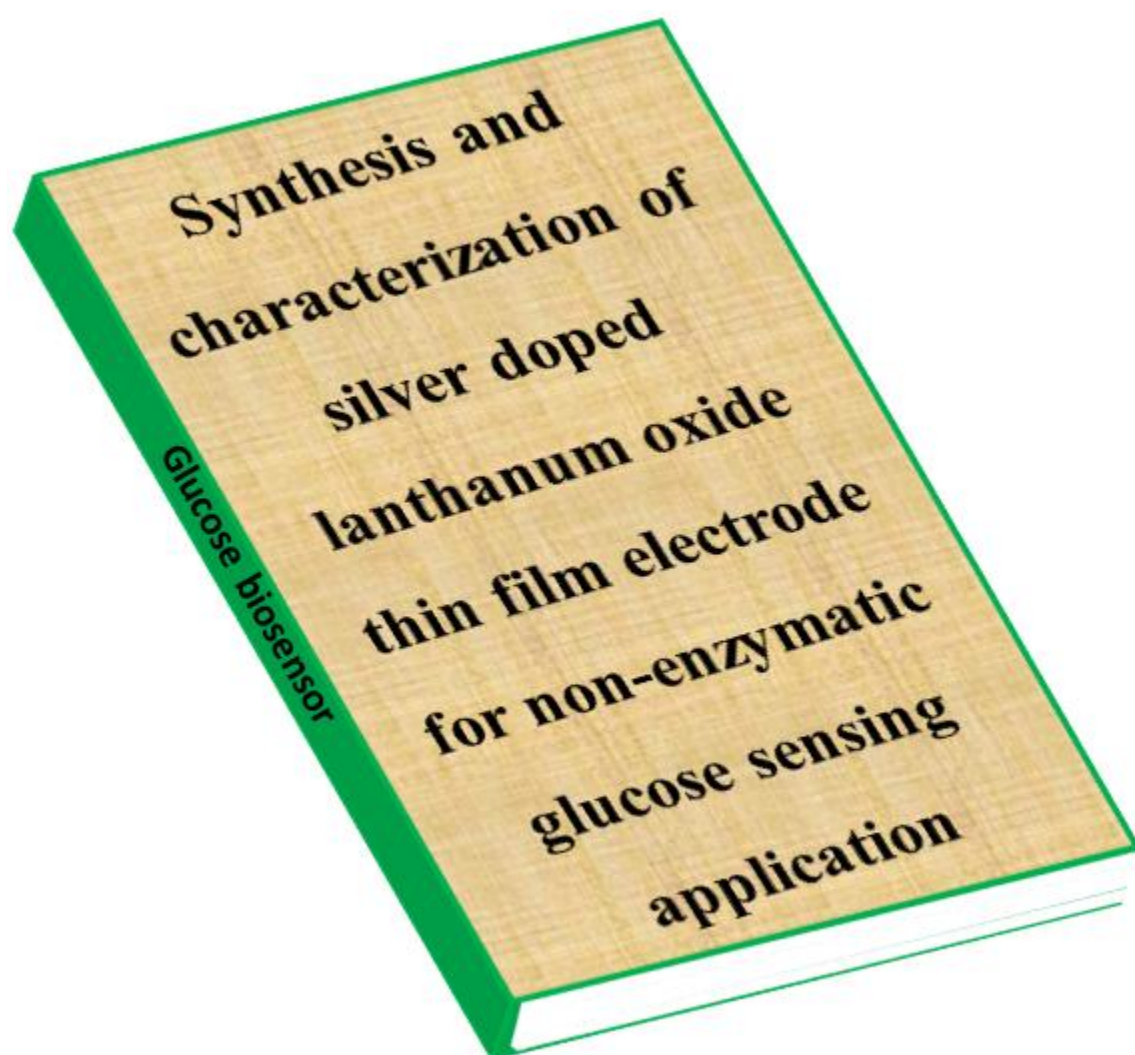
#### 3.10 References:

1. J. J. Xu, J. J. Feng, X. Zhong, H.-Y. Chen. *Electroanalysis*, (2008), DOI: 10.1002/elan.200704076.
2. L. C. Clark, C. Lyons, *Ann. N. Y. Acad. Sci.* (1962), DOI:10.1111/j.1749-6632.1962.tb13623.x.
3. Z. Zhuang, X. Su, H. Yuan, Q. Sun, D. Xiao, M. F. Choi, *Analyst*, (2008), DOI: 10.1039/B712970J.
4. W. Meng, Y. Wen, L. Dai, Z. He, L. Wang, *Actuators B Chem*, (2018), DOI: 10.1016/j.snb.2018.01.109.
5. A. A. Yadav, A. C. Lokhande, R. B. Pujari J. H. Kim, C. D. Lokhande, *J. Colloid Interface Sci*, (2016), DOI: 10.1016/j.jcis.2016.08.056.
6. C. Yang, H. Fan, S. Qiu, Y. Xi, Y. Fu, *Non-Cryst. Solids*, (2009), DOI: 10.1016/j.jnoncrysol.2008.09.029.
7. J. Liu, G. Wang, L. Lu, Y. Guo, L. Yang, *RSC Adv*, (2017), DOI: 10.1039/C7RA07521A.
8. J. J. Gooding, R. Wibowo, J. Q. Liu, W. R. Yang, D. Losic, S. Orbons, F. J. Mearns, J. G. Shapter, D. B. Hibbert, *J. Am. Chem. Soc*, (2003), DOI: 10.1021/ja035722f.
9. K. J. McKenzie, F. Marken, *Langmuir*, (2003), DOI: 10.1021/la0267903.
10. A. H. Liu, M. D. Wei, I. Honma, H. S. Zhou, *Anal. Chem*, (2005), DOI: 10.1021/ac051640t.

- 
11. T. Kong, Y. Chen, Y. Ye, K. Zhang, Z. Wang and X. Wang, *Sens. Actu. B*, (2009), DOI: 10.1016/j.snb.2009.01.002.
  12. M. Zhao, Z. Li, Z. Han, K. Wang, Y. Zhou, J. Huang and Z. Ye, *Biosens. Bioelectron.* (2013), DOI: 10.1016/j.bios.2013.05.017.
  13. L-k. Tsui and G. Zangari, *Electrodeposition and Surface Finishing*, 217-239. (2014), DOI: 10.1007/978-1-4939-0289-7\_4.
  14. H. Wang, X. Wang, X. Zhang, X. Qin, Z. Zhao, Z. Miao, N. Huang and Q. Chen, *Biosens. Bioelectron.* (2009), DOI: 10.1016/j.bios.2009.06.022.
  15. W. Jia, K. Wang, Z. Zhu, H. Song and X. Xia, *Langmuir*, (2007), DOI: 10.1021/la7020269.
  16. C. W. Hsu, G. J. Wang, *Biosens. Bioelectron.* (2014), DOI: 10.1016/j.bios.2014.01.023.
  17. Y. Liu, X. Feng, J. Shen, J.-J. Zhu and W. Hou, *J. Phys. Chem. B*, (2008), DOI: 10.1021/jp801938w.
  18. S. Palanisamy, S. Cheemalapati, S. M. Chen, *J. Electroanal Chem*, (2015), DOI: 10.1016/j.jelechem.2015. 11.017.
  19. H. Dhyani, M. A. Ali, M. K. Pandey, B. D. Malhotra, P. Sen, *J. Mater. Chem*, (2012), DOI: 10.1039/C2JM15914G.
  20. X. Meng, J. Wei, X. Ren, J. Ren, F. Tang, *Biosens. Bioelectron.* (2013), Doi:10.1016/j.bios.2013.03 .053.
  21. H. Yamada, T. Shimizu, A. Kurokawa, K. Ishii, E. Suzuki, *J. Electroche. Soc*, (2003), DOI: 10.1149/1.1585055.
  22. S. Y. No, D. Eom, C. S. Hwang, H. J. Kim, *J. App. Phy.* (2006), DOI: 10.1063/1.2218465.
  23. M. Nieminen, M. Putkonen, L. Niinistö, *Applied Sur. Sci.* (2001), DOI: 10.1016/s0169-4332(01)00149-0.
  24. A. A. Yadav, V. S. Kumbhar, S. J. Patil, N. R. Chodankar, C. D. Lokhande, *Ceram. Int.* (2016), DOI: 10.1016/j.ceramint.2015.09.098.
  25. Q. Mu, Y. Wang, *J. Alloy Compd*, (2011), DOI: 10.1016/j.jallcom.2010.09.041.
  26. Yan Wu, Yuejiao chen, Jun Zhou, *Mater. Lett*, (2013), DOI: 10.1016/j.matlet.2012.12.055.

27. A. Subasri, K. Balakrishnan, E. R. Nagarajan, V. Devadoss, A. Subramania, *Electrochim. Acta*, **(2018)**, DOI: 10.1016/j.electacta.2018.05.142.
28. J. G. Kang, Y. Kim, D. W. Cho, Y. Sohn, *Mater. Sci. in Semicond. Pro*, **(2015)**, DOI: 10.1016/j.mssp.2015.07.050.
29. U. Kolitsch, H. J. Seifert, F. Aldinger, *J. Solid State Chem*, **(1995)**, DOI: 10.1006/jssc.1995.1372.
30. F. Ambroz, T. J. Macdonald, V. Martis, I. P. Parkin, *Small*, **(2018)**, DOI: 10.1002/smtd.201800173.
31. X. Li, J. Yao, F. Liu, H. He, M. Zhou, N. Mao, P. Xiao, Y. Zhang., *Sens. Act. B. Chem.* **(2013)**, DOI: 10.1016/j.snb.2013.02.035.
32. S. premlatha, P. Sivasakti, G. N. K Ramesh Bapu, *RSC Adv.* **(2015)**, DOI: 10.1039/C5RA12316J.
33. Y. Luo, Q. Wang, J. Li, F. Xu, L. Sun, Y. Bu, Y. Zou, H.-B. Kraatz F. Rosei, Tunable hierarchical surfaces of CuO derived from metal–organic frameworks for non-enzymatic glucose sensing, *Inorg. Chem. Front.*, **(2020)**, DOI: 10.1039/D0QI00104J.
34. S. Felix, P. Kollu, S. K. Jeong, A. N. Grace, A novel CuO-N-doped graphene nanocomposite-based hybrid electrode for the electrochemical detection of glucose, *Appl. Phys. A.*, **(2017)**, DOI 10.1007/s00339-017-1217-6

# CHAPTER IV



## Index

Sr. No.	Details	Page No.
4.1	Introduction	95
4.2	Experimental process	97
4.2.1	Material synthesis	97
4.2.2	Structural and physical characterization	100
4.2.3	Electrochemical measurement	100
4.3	Results and discussion	101
4.3.1	<i>Thin film formation mechanism</i>	101
4.3.2	<i>XRD analysis</i>	101
4.3.3	<i>FE-SEM, EDX and elemental mapping analysis</i>	102
4.3.4	<i>BET analysis</i>	104
4.4	The effect of Ag doping in La <sub>2</sub> O <sub>3</sub> film electrode	105
4.5	Enzymeless glucose detection	107
4.6	Selectivity, stability and reproducibility	111
4.7	Conclusions	112
4.8	References	113

#### 4.1 Introduction:

During last few decades the environmental issues at the topmost level around the world causing health and energy related problems more adverse. The academics, scientists, and the industries are working together to address these issues consistently. Enormous efforts were dedicated in materials science to develop new materials and to find out applicability of the known materials in different forms for various purposes. The properties of the materials at the nano/microlevel such as crystal structure and optical and electrical properties have been utilized in many applications. Almost every appliance we use in the daily life has two dimensional (2D) materials. Health, energy conversion and storage devices intensively use 2D materials for sensors, charge storage, catalyst, etc [1].

Most of the peoples are suffering to diabetes disease which is growing worldwide leading to a variety of complications including chronic damage to the heart, eyes, kidneys, nerves, blood vessels, and other organs. The large increase in the diabetes patient still attracts much attention to glucose sensing and the periodic monitoring of glucose is essential for the diagnosis of diabetes [2-4]. Enzymatic sensors are commercialized owing to their sensitivity and selectivity due to higher electrocatalytic activity. These sensors suffer from elaborated enzyme immobilization process, stability, pH, and high cost of the enzyme [5, 6]. On the other side, electrochemical non-enzymatic sensors are also attracted enormously due to high sensitivity, good reproducibility, and low cost. Hence, there is a need to develop cost-effective, fast respondent and accurate non-enzymatic glucose sensors based on thin film.

Rare earth (RE) metal oxides have attractive prospects viz the optical, magnetic and high electrical conductivity due to the variation in the valence states. Mathulakshami et al. [7] synthesized lanthanum oxide nanoparticles from and rographis paniculata leaves

extract and used for antibacterial activity applications. No et al. [8] synthesized lanthanum oxide thin films using cyclic chemical vapor deposition and investigated electrical properties. Nieminen et al. [9] prepared lanthanum oxide thin film using atomic layer epitaxy on soda-lime glass substrate and studied its chemical stability in the ambient air [10, 11]. RE metal oxide with variety in the composition, texture and presence of 4f electron has attracted much attention in recent years [12].

The 2D materials like metals, metal oxide and alloy metals have been used for the fabrication of non-enzymatic glucose sensors [13, 14] and charge storage applications [15]. Nevertheless, these electrode materials have limitations as high cost, low sensitivity, easy loss of activity, and surface poisoning from the adsorbed intermediates. One of RE metal oxide,  $\text{La}_2\text{O}_3$  has attracted much interest owing to its stability, non-toxicity, and biocompatibility. A porous material have been developed using different methods such as electrospinning [16], acoustic controlled micro bubbles generation method [17], ED [18], and these methods leads to enhance sensing, catalysis and supercapacitive properties. On the other hand, silver may provide more opportunities for electron transfer due to its good electron conductivity [19]. The non-enzymatic electro-chemi-luminescence (ELC)  $\text{La}_2\text{TiO}_3 \text{ Ag}_{0.1}$  nanomaterial sensor exhibits excellent electrocatalytic properties such as high sensitivity, low detection limit, wide linear range and good selectivity [20]. Nickel nanoporous film electrode deposited on indium tin oxide plates by physical vapor deposition method and used for non-enzymatic glucose sensing application [21]. Silver nanoparticles have been used as conductive dopants in electrode materials for catalytic efficiency for reduction [22]. Ag doping with manganese oxide significantly enhance surface area, decrease resistive properties and improved capacitive behavior [23]. Lupan et al. [24] synthesized Ag doping with zinc oxide by ED method and enhanced

performance of nanosensor application. Demirci et al. [25] prepared Ag doping  $\text{TiO}_2$  by sol gel spin coating technique on Si substrate and used for photocatalytic application. Salazar et al. [26] synthesized silver nanoparticles with modified reduced graphene oxide nanoparticles by green synthesis method and used for  $\text{H}_2\text{O}_2$  sensing application. In this framework we believe that the Ag doping in La materials is a promising approach in the enhancement of the electrocatalytic activity for glucose detection. Presently yet there are no such reports for the silver composite lanthanum material. Silver has highest conductivity among noble metals.

In this chapter, a novel vertically grown nanoflakes of Ag- $\text{La}_2\text{O}_3$  is prepared using potentiostatic ED method and studied for its application for non-enzymatic glucose sensing. The basic structural, morphological and elemental composition properties were evaluated using XRD, XPS, FE-SEM, BET, and EDX.

## **4.2 Experimental Process:**

All chemical reagents viz, lanthanum nitrate hexahydrate, silver nitrate, potassium hydroxide, dextrose, fructose, lactose, ascorbic acid, and dopamine were purchased from Thomas Beaker and used without further purification.

### **4.2.1 Material synthesis:**

Synthesis of  $\text{La}_2\text{O}_3$  and Ag- $\text{La}_2\text{O}_3$  thin films were carried out using simple and facile ED method using three electrode system. Pt sheet, SCE and SS sheet were used as counter, reference, and working electrodes, respectively. The cathodic ED was carried out employing the CHI660E electrochemical workstation. Initially, SS substrate (305 grade) was mirror polished by grade 1000 polish paper, ultra-sonicated for 20 min and sequentially washed using acetone, and DD water. After cleaning, the substrate was dried in air and used for further deposition. Before deposition, we have taken LSV curve to

observe exact deposition potential within the potential window (0 to -1.2 V vs. SCE) as shown in **Fig 4.1**.

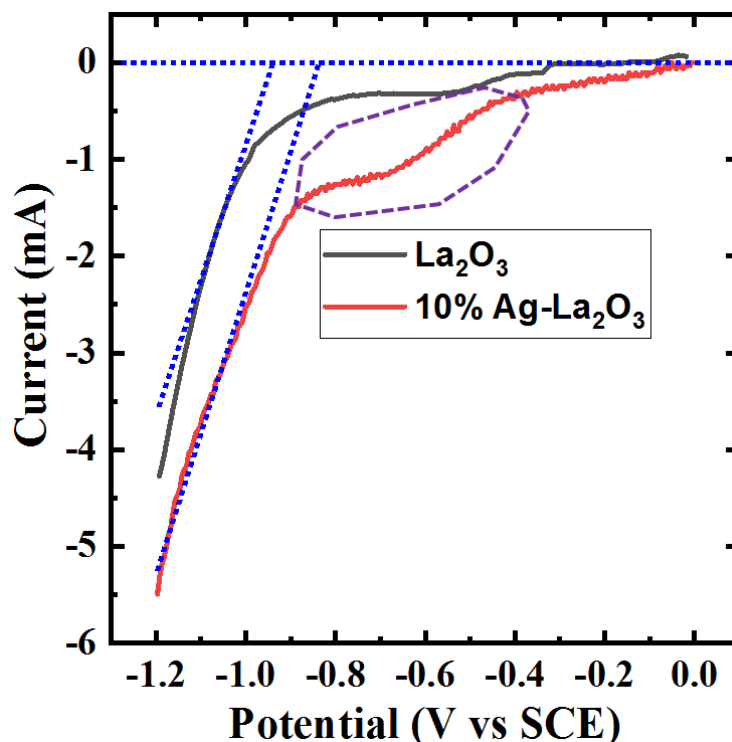


**Figure 4.1** LSV curves for precursor solution of lanthanum nitrate (black curve) and silver-lanthanum nitrate (red curve) at  $20 \text{ mV s}^{-1}$ .

The 10% Ag solution was added in the lanthanum solution followed by LSV curve. In this scan, the silver precursor solution does show increment in current at initial potential, but both lanthanum and silver precursor solution does not show increment in current at same potential. Then, increase negative potential the current increment start was observed and reaches up to -0.8 V vs. SCE. The reduction of solution starts due to nucleation process of silver. After that, the current increment start at -0.9 V vs. SCE was observed and reaches up to -1.1 V vs. SCE. Silver precursor solution has lower current response and lower negative potential compared to lanthanum precursor solution. So, the deposition was take place at different potential -0.6 and -1 V vs. SCE for silver and lanthanum respectively on the electrode surface. Firstly silver and after that lanthanum

was deposited on the surface of the electrode. For ED of  $\text{La}_2\text{O}_3$  film, 10 mM  $\text{La}(\text{NO}_3)_3$  was dissolved in 50 mL DD water and potential of -1.0 V vs. SCE was applied to working electrode. For typical synthesis of 1, 3, 5, and 10% Ag doped  $\text{La}_2\text{O}_3$  thin film, separately prepared 0.01 M  $\text{La}(\text{NO}_3)_2$  and 0.01 M  $\text{Ag}(\text{NO}_3)_3$  solutions were mixed together in various volumetric ratios as 0:50, 0.5:49.5, 1.5:48.5, 2.5:47.5 and 5:45 to obtain final solution of 50 mL.

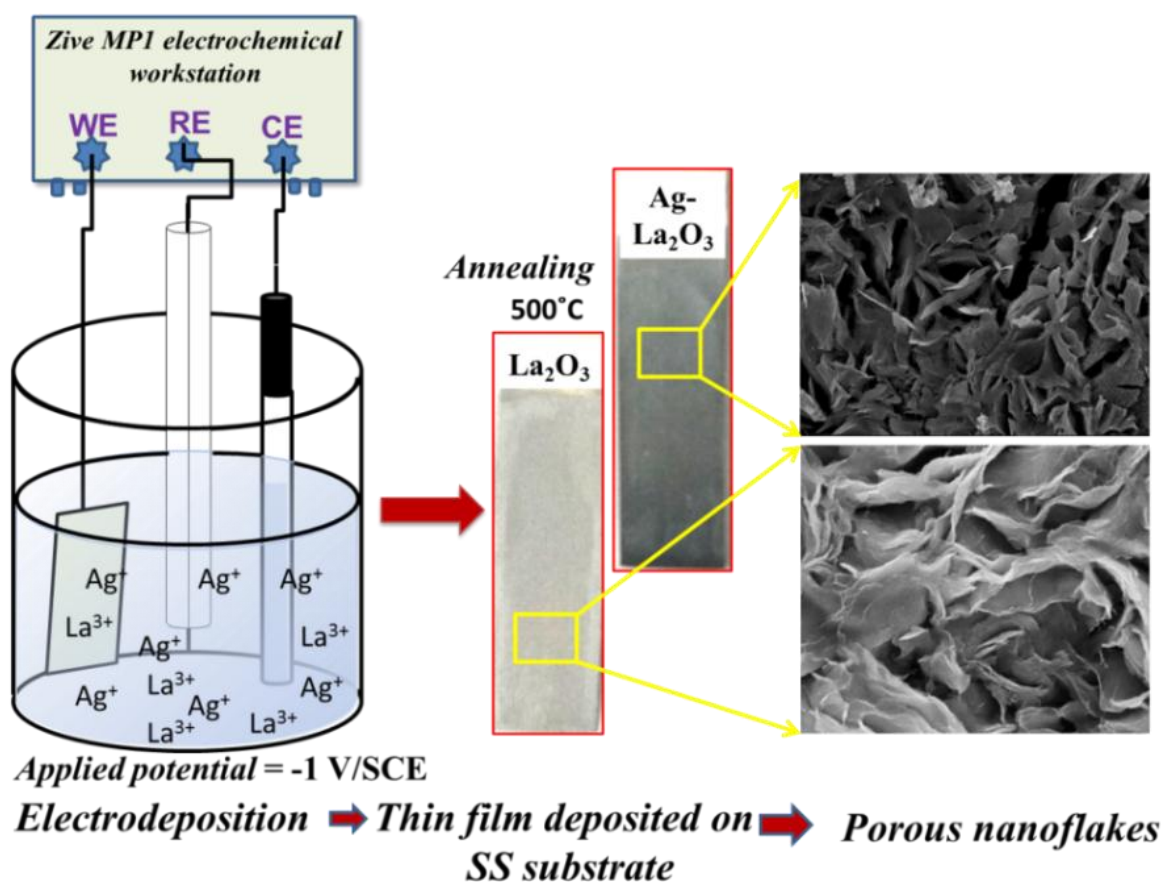


**Figure 4.2:** Schematic presentation of ED method of  $\text{La}_2\text{O}_3$  and  $\text{Ag-La}_2\text{O}_3$  thin films.

The deposition was executed for 1 h. Uniform and adherent thin films were deposited on SS substrate. The deposited films were annealed at 773K in air muffle furnace for 2 h and used for further characterization. The schematic illustration of the ED process, deposited films and morphology of  $\text{La}_2\text{O}_3$  and  $\text{Ag-La}_2\text{O}_3$  material is shown in **Fig. 4.2**.

#### 4.2.2 Structural and physical characterization:

The  $\text{La}_2\text{O}_3$  and Ag- $\text{La}_2\text{O}_3$  thin films were characterized by XRD. The XRD patterns were obtained using Rigaku miniflex-600 ( $\text{CuK}\alpha$ ,  $\lambda=1.5406\text{\AA}$  radiation). The surface morphology was studied with FE-SEM (ISM-7001F, and JEOL). Elemental analysis was carried out using EDX (X-max, Oxford instruments). Porosity of films was studied using BET (Belsorp II mini).

#### 4.2.3 Electrochemical Measurement:

All electrochemical characterizations were carried out using three electrode system on ZIVE MP1 multichannel electrochemical workstation with  $\text{La}_2\text{O}_3$  and Ag- $\text{La}_2\text{O}_3$  thin films as the working, Pt plate as a counter, and SCE as a reference electrodes. The glucose sensing performance of thin film electrode was investigated in freshly prepared 0.1 M aqueous NaOH electrolyte solution using CV, *i-t* amperometry techniques. The CV study was carried out in the potential window from 0 to +0.5 V vs. SCE for  $\text{La}_2\text{O}_3$  and Ag- $\text{La}_2\text{O}_3$  thin film electrodes. For glucose sensing, 40 mL of 0.1 M NaOH electrolyte was taken in the glass cell and then glucose solution of different molar concentrations (100  $\mu\text{M}$  to 2.8 mM) was pipetted into the electrolyte to observe the current response of the material. Similarly, for *i-t* experiment, 40 mL of 0.1 M NaOH electrolyte was kept stirring at a constant speed of 310 rpm and potential of +0.43 V vs. SCE was applied to the working electrode. The analytes of different molar concentrations were added to the rotating solution to observe the sensing response of the electrode. The interference study was executed by performing *i-t* experiment in the presence of different interfering species such as ascorbic acid, fructose, lactose, and dopamine.

The limit of detection (LOD) calculated from plot of current density vs. glucose concentration of the electrode by the equation;

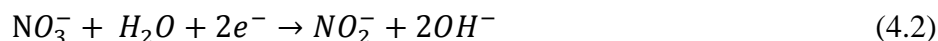
$$\text{Limit of detection } (\mu\text{M}) = \frac{3.3 \times SD}{y}, \quad (4.1)$$

where  $SD$  is standard deviation,  $y$  is the slop of calibration graph.

### 4.3 Results and Discussion:

#### 4.3.1 Thin film formation mechanism:

$\text{La}_2\text{O}_3$  and  $\text{Ag-La}_2\text{O}_3$  composite thin films were deposited on the SS substrate through a mechanism of base ( $\text{OH}^-$ ) electro-generation in nitrate solution. The possible cathodic reactions for  $\text{La}(\text{NO}_3)_3$  can be written in the following way.



The above reaction results in the local pH increase near the SS electrode surface. The increased  $\text{OH}^-$  ions concentration forms  $\text{La}(\text{OH})_3$  on the cathode surface as.



Moreover, to deposit  $\text{Ag-La}_2\text{O}_3$  film 5 mL 10 mM  $\text{AgNO}_3$  aqueous solution was added into  $\text{La}^{+3}$  precursor. Further, deposited films were annealed at 773K in air muffle furnace to form stoichiometric oxide.

#### 4.3.2 XRD analysis:

The XRD patterns of  $\text{La}_2\text{O}_3$  and  $\text{Ag-La}_2\text{O}_3$  nanocomposite thin films are shown in **Fig. 4.3**. The peaks in  $\text{La}_2\text{O}_3$  diffraction patterns at  $(2\theta)$  correspond (111), (401), (702), (611) and (703), planes of monoclinic  $\text{La}_2\text{O}_3$  and matches well with JCPDS card no. 22-0641. The high intensity XRD peaks confirms the crystalline nature of  $\text{La}_2\text{O}_3$  thin film. The XRD pattern of nanocomposite  $\text{Ag-La}_2\text{O}_3$  thin film show less intense peaks of lanthanum oxide. Lack of intense peak indicates nanocrystalline amorphous nature of  $\text{Ag-La}_2\text{O}_3$ . No significant difference appeared in the XRD patterns of  $\text{La}_2\text{O}_3$  and  $\text{Ag-La}_2\text{O}_3$  nanocomposite. The peaks marked by \* corresponds to SS substrate.

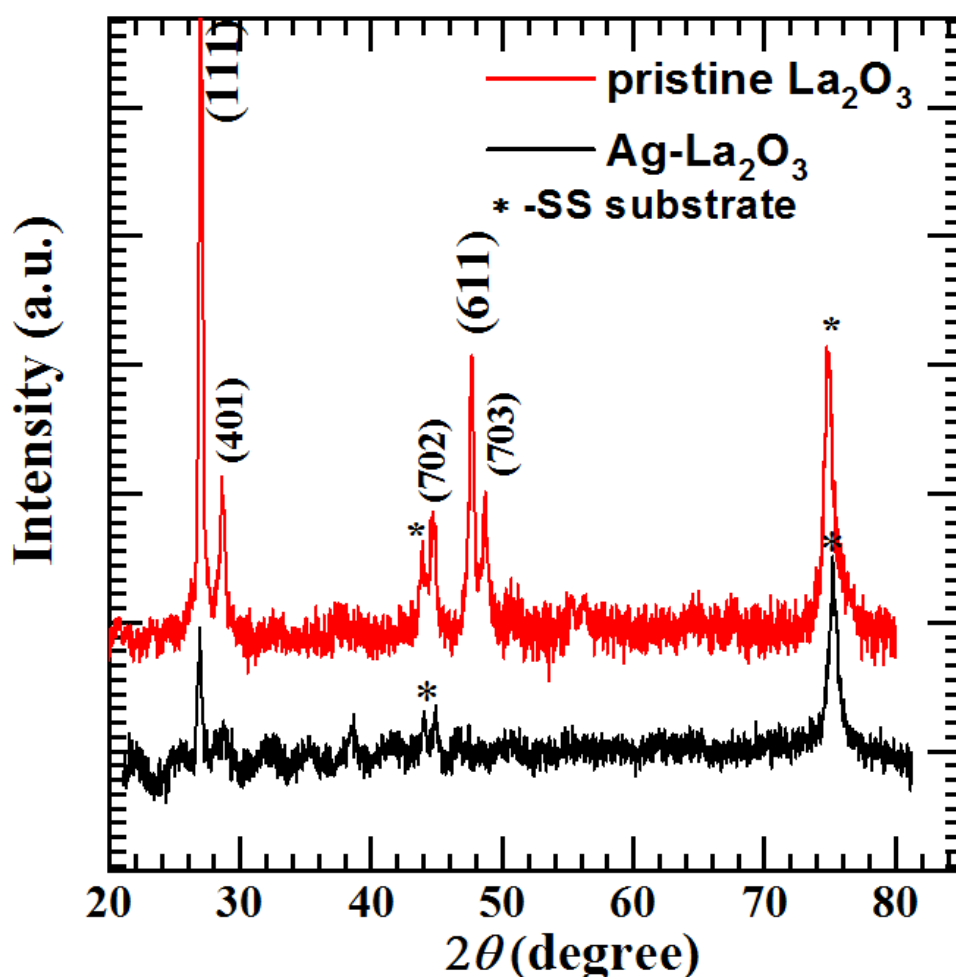


**Figure 4.3:** XRD patterns of  $\text{La}_2\text{O}_3$  and  $\text{Ag-La}_2\text{O}_3$  thin films

#### 4.3.3 FE-SEM, EDX and elemental mapping analysis:

The surface morphology of pristine  $\text{La}_2\text{O}_3$  and  $\text{Ag-La}_2\text{O}_3$  thin films are shown in **Fig. 4.4**. The surface of  $\text{La}_2\text{O}_3$  is composed of interconnected; vertically uneven nanoflakes. The average length of the nanoflakes is about  $1.4\ \mu\text{m}$  as shown in **Fig. 4.4a**. The topography of  $\text{Ag-La}_2\text{O}_3$  thin film is shown in **Fig. 4.4b**. The morphology with the composite of Ag, the average length to  $1.3\ \mu\text{m}$  and thickness of the nanoflakes between  $0.05$  to  $0.13\ \mu\text{m}$ . the average thickness of the nanoflakes appears to be decreased to  $0.1\ \mu\text{m}$ . The vertically nanoflakes creates path to the charge transfer through pores and decreases contact resistance of the electrode, efficiently [27].

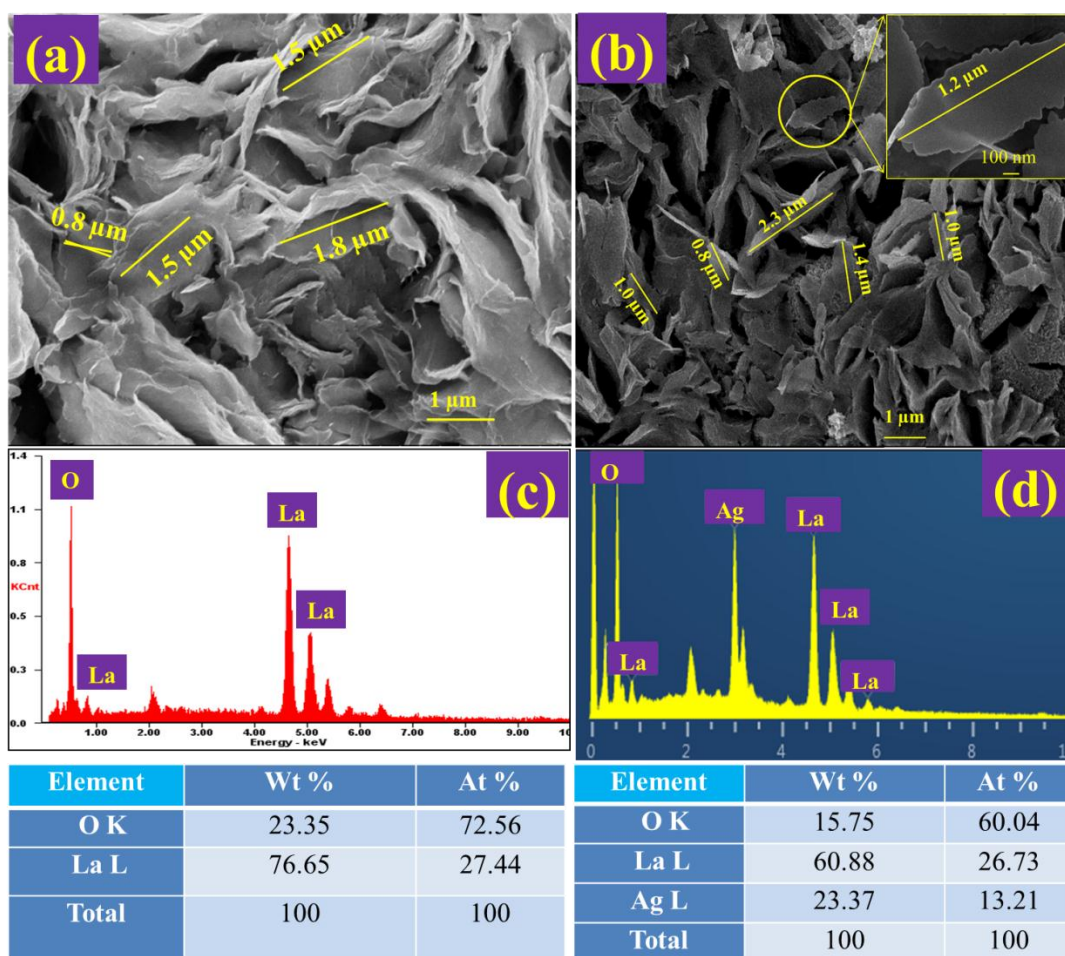


**Figure 4.4:** FE-SEM images of (a)  $\text{La}_2\text{O}_3$  at 15KX, (b)  $\text{Ag-La}_2\text{O}_3$  at 10KX magnification, (c) EDX spectrum of  $\text{La}_2\text{O}_3$ , (d) EDX spectrum of  $\text{Ag-La}_2\text{O}_3$  thin film electrode

The EDX plays most important role for material identification and composition. The EDX spectrum of  $\text{La}_2\text{O}_3$  thin film is shown in **Fig. 4.4c**. The atomic percentage of La and O in  $\text{La}_2\text{O}_3$  is 38.18 and 61.82 %, respectively nearly equal to ideal value of 40:60%. The EDX of  $\text{Ag-La}_2\text{O}_3$  composite thin film is presented in **Fig. 4.4d**. The atomic percentages of O, La, and Ag elements are 60.04, 26.74, and 13.22 %, respectively. The atomic ratio of La to Ag in the  $\text{Ag-La}_2\text{O}_3$  nanocomposite film is 1:0.5. The EDX confirmed the formation of  $\text{La}_2\text{O}_3$  and  $\text{Ag-La}_2\text{O}_3$  nanocomposite thin films using ED method. The elemental mapping of  $\text{Ag-La}_2\text{O}_3$  nanocomposite thin film is shown in **Fig.**

(4.5). It shows the uniform distribution of the silver, oxygen, and lanthanum; indicated with green, red, and blue colors, respectively.

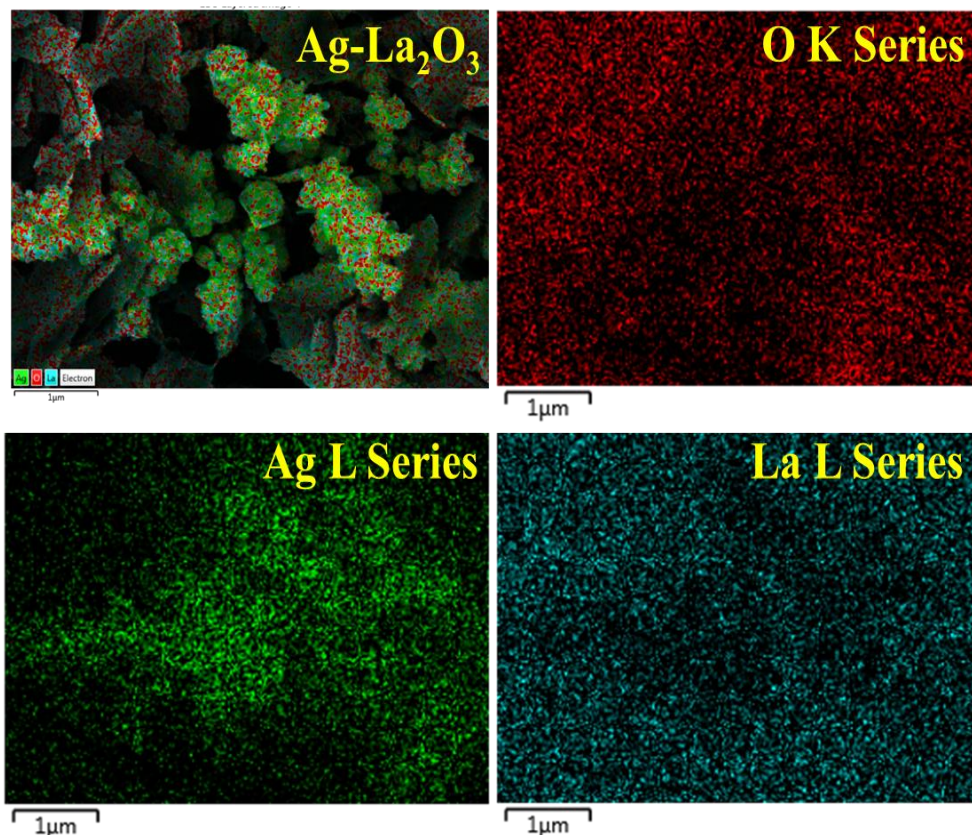


**Figure 4.5:** Elemental mapping image show the distribution of oxygen, lanthanum and silver

#### 4.3.4 BET analysis:

The specific surface area, pore volume and pore size distribution of La<sub>2</sub>O<sub>3</sub> and Ag-La<sub>2</sub>O<sub>3</sub> nanocomposite films were obtained using BET method by physical adsorption-desorption of N<sub>2</sub> gas at 77K. The pore volume and pore size distribution were calculated by BJH method. Typical isotherm curves of La<sub>2</sub>O<sub>3</sub> and Ag-La<sub>2</sub>O<sub>3</sub> nanocomposite are displayed in **Fig. 4.6a and b**. The isotherms observed for samples La<sub>2</sub>O<sub>3</sub> and Ag-La<sub>2</sub>O<sub>3</sub> are of the type-IV which confirms the mesoporous surface [28]. In addition, pore size distributions are shown in **Fig. 4.6c and d**. The specific surface area of La<sub>2</sub>O<sub>3</sub> and Ag-

$\text{La}_2\text{O}_3$  nanocomposite samples are  $14.17$  and  $22.45 \text{ m}^2 \text{ g}^{-1}$ , respectively. The average pore radius of  $\text{La}_2\text{O}_3$  and  $\text{Ag-La}_2\text{O}_3$  samples are  $39.26$  and  $19.97 \text{ nm}$ , respectively that predominantly indicate mesoporous nature of both the samples. Vertically grown  $\text{Ag-La}_2\text{O}_3$  nanoflakes improvise specific surface area due to decrease of pore radius; as a result,  $\text{Ag-La}_2\text{O}_3$  nanocomposite can avail more active sites for electrocatalysis and electrochemical reactions.

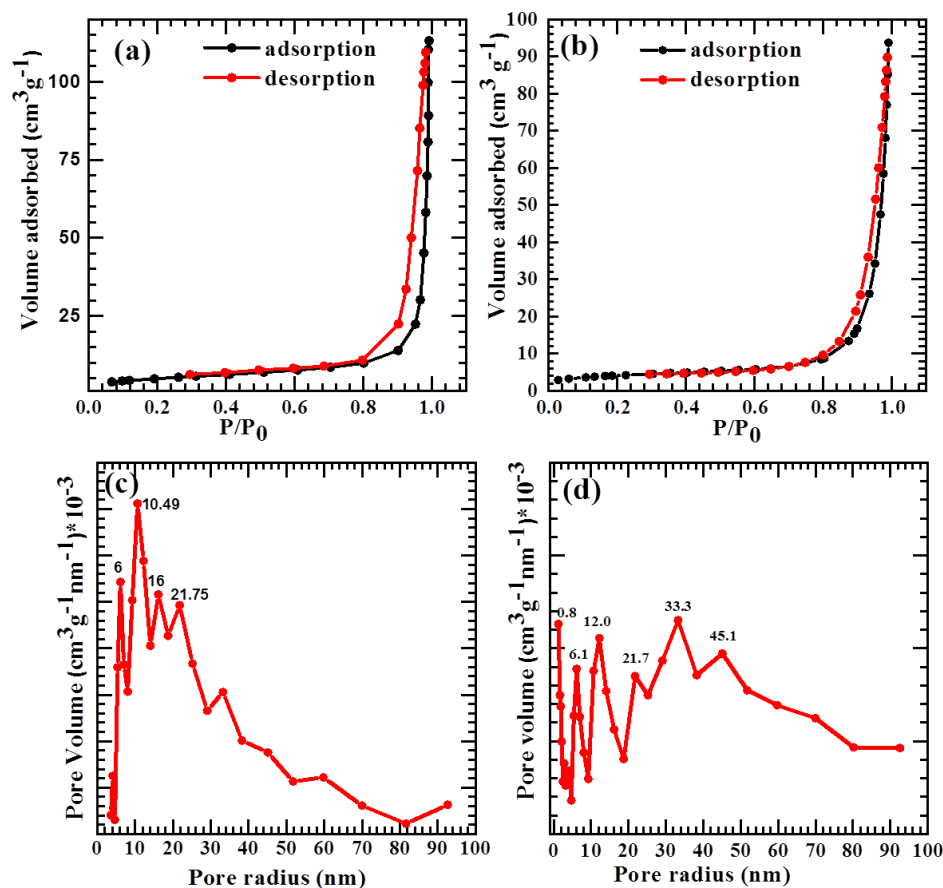


**Figure 4.6:** BET surface area analysis of (a)  $\text{La}_2\text{O}_3$ , (b)  $\text{Ag-La}_2\text{O}_3$  samples, the BJH pore size distribution plots of (c)  $\text{La}_2\text{O}_3$ , (d)  $\text{Ag-La}_2\text{O}_3$  samples

#### 4.4 The effect of Ag doping $\text{La}_2\text{O}_3$ thin film in electrochemical performance:

The CV study of  $\text{La}_2\text{O}_3$ , 1, 3, and 5%  $\text{Ag-La}_2\text{O}_3$  film electrodes was carried out in 0.1 M aqueous NaOH electrolyte. All electrodes were scanned at scan rates from 10 to  $100 \text{ mV s}^{-1}$  by varying applied potential between 0 to  $+0.5 \text{ V}$  vs. SCE as shown in **Fig**

**4.7(a-d).** It is visible that the current response of  $\text{La}_2\text{O}_3$  electrode is less than that of 1, 3, and 5% Ag- $\text{La}_2\text{O}_3$  electrode. In other side, 1, 3 and 5% Ag doping  $\text{La}_2\text{O}_3$  film does not show proper oxidation and reduction peaks as well the increment of current response.

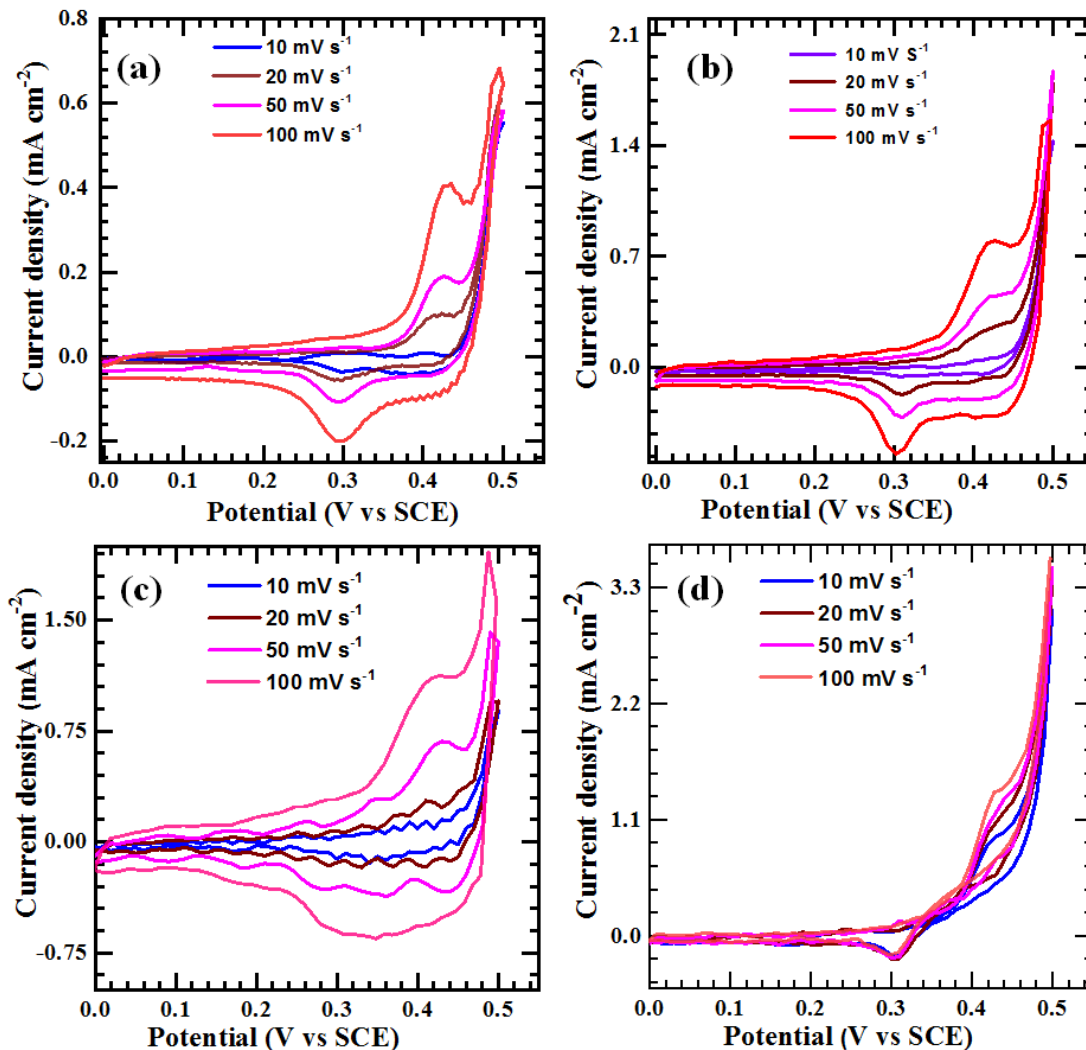


**Figure 4.7** CV curves of (a)  $\text{La}_2\text{O}_3$ , (b) 1%Ag-  $\text{La}_2\text{O}_3$ , (c) 3%Ag-  $\text{La}_2\text{O}_3$ , and (d) 5%Ag-  $\text{La}_2\text{O}_3$  film electrode at various scan rates from 10 to 100 mV s<sup>-1</sup> in 0.1M NaOH electrolyte.

Further, we have added 10% Ag solution in lanthanum precursor and deposition take place. Then, we have taken the CV curve at the same potential window and compared with  $\text{La}_2\text{O}_3$ , 1, 3 and 5% Ag doping  $\text{La}_2\text{O}_3$  film electrode. This reveals that 10% Ag doping  $\text{La}_2\text{O}_3$  improves electrochemical performance compared to other electrodes.

Therefore, 10% Ag-La<sub>2</sub>O<sub>3</sub> thin films electrode were selected for non-enzymatic glucose sensing application.

#### 4.5 Enzymeless glucose detection:

The CV study of La<sub>2</sub>O<sub>3</sub> and Ag-La<sub>2</sub>O<sub>3</sub> nanocomposite electrodes carried out in a potential range of 0 to +0.5 V vs SCE at scan rate of 50 mV s<sup>-1</sup> is depicted in **Fig. 4.8**. Ag-La<sub>2</sub>O<sub>3</sub> nanocomposite shows increased current density than that of pristine La<sub>2</sub>O<sub>3</sub>. The CV curves of both the electrodes contain visible redox peaks.

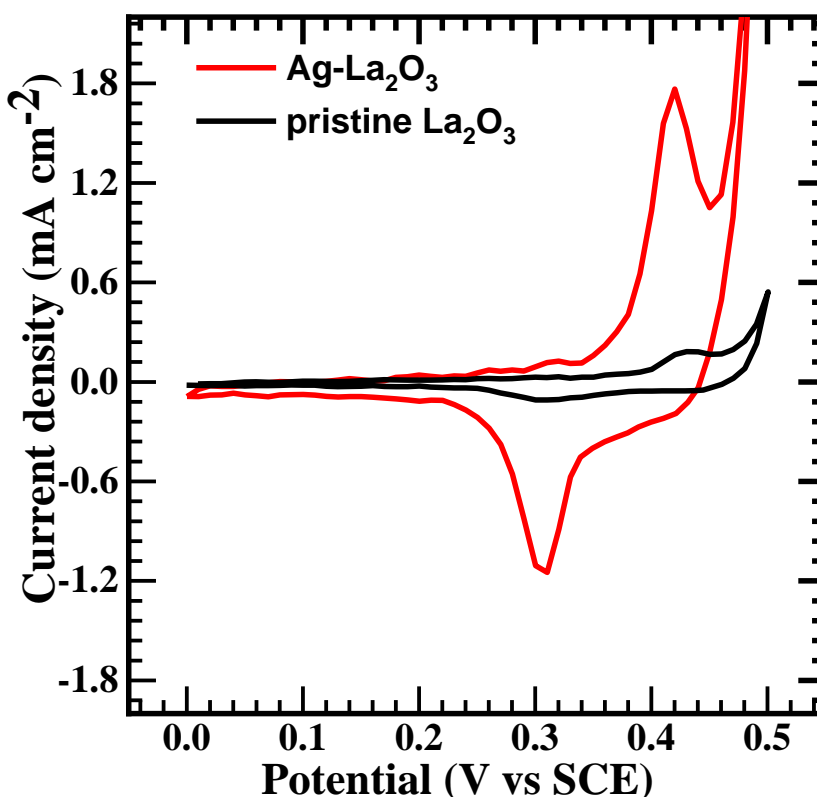


**Figure 4.8:** The CV curves of La<sub>2</sub>O<sub>3</sub> and Ag-La<sub>2</sub>O<sub>3</sub> at 50 mV s<sup>-1</sup> in 0.1 M NaOH electrolyte.

This reveals that Ag-La<sub>2</sub>O<sub>3</sub> electrode improves electrochemical response compared to pristine La<sub>2</sub>O<sub>3</sub> electrode. The CV curves of La<sub>2</sub>O<sub>3</sub> electrode at different scan rates (5-100 mV s<sup>-1</sup>) are shown in **Fig. 4.9**. This shows that current density much lower than that of Ag-La<sub>2</sub>O<sub>3</sub>.

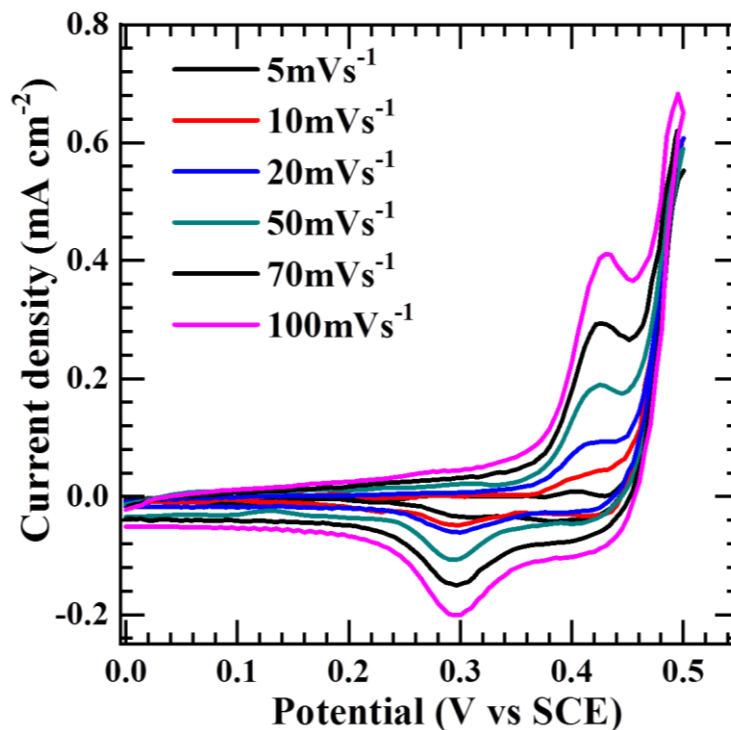
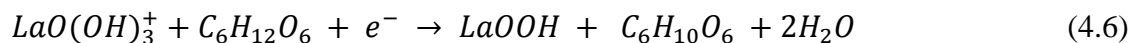
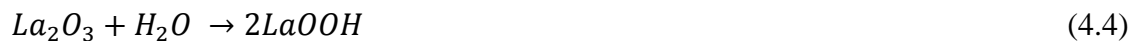


**Figure 4.9:** CV curves of  $\text{La}_2\text{O}_3$  electrode at different scan rates (5 to 100  $\text{mV s}^{-1}$ ) in 0.1 M NaOH solution.

The CV curves of Ag- $\text{La}_2\text{O}_3$  at various scan rates (10-100  $\text{mV s}^{-1}$ ) are shown in **Fig. 4.10a**. With the rise of scan rates oxidation peaks shift toward more positive side and reduction peaks toward the more negative side. No other electrochemical peaks are observed, which suggest that the presence of Ag element inside of the nanostructure has no individual electrochemistry in the oxidation and reduction of electrolyte. It has combined effect with  $\text{Ag}^+$  and  $\text{La}^{+3}$  ions towards oxidation of electrolyte. The possible electrocatalytic oxidation of glucose due to  $\text{La(III)}$  ions is described with the following reaction [18].



This phenomenon ascribed for glucose oxidation to gluconolactone, which is able to the conversion of La (V) to La (III). As it is well know that Ag element is excellent catalytic material due to their intrinsic unshared and unfilled “d” orbital electrons [19]. Therefore, the oxidation peak current of the Ag-La<sub>2</sub>O<sub>3</sub> material shows more enhanced current values than the oxidation peak current of pristine La<sub>2</sub>O<sub>3</sub>. The performance of glucose sensing activity with and without different glucose concentration (0.4 mM to 2 mM) in 0.1 M NaOH electrolyte is shown in **Fig. 4.10b**, and the electrocatalytic peaks at +0.43 V vs SCE were increased with increasing concentration of glucose in 0.1 M NaOH electrolyte.

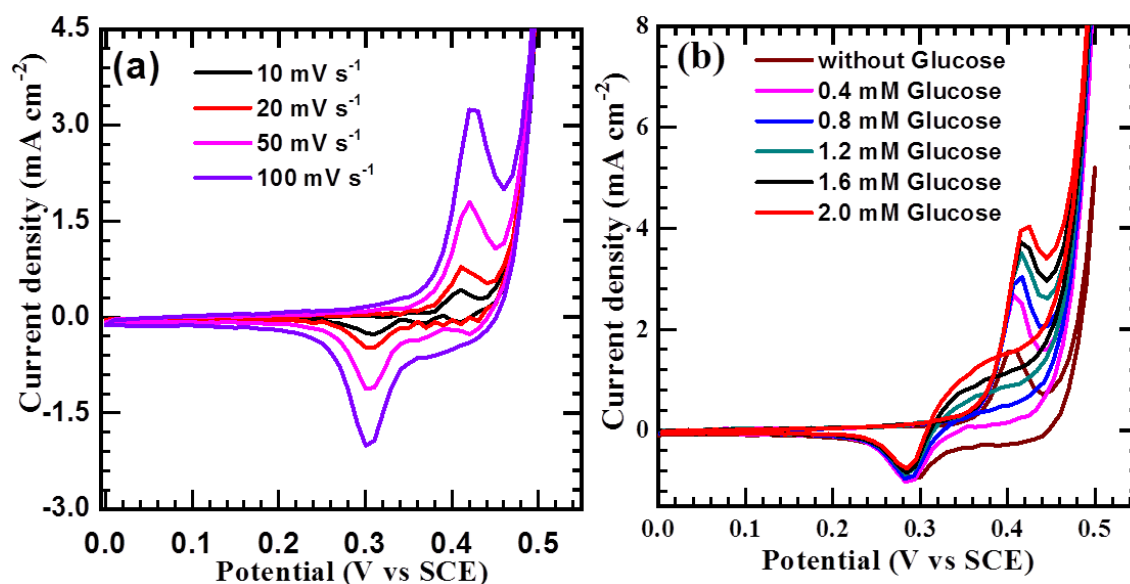


**Figure 4.10:** The CV curves of Ag-La<sub>2</sub>O<sub>3</sub> at (a) different scan rates (10-100 mV s<sup>-1</sup>) and (b) different glucose concentration at fixed scan rate of 50 mV s<sup>-1</sup>.

The *i-t* amperometric study of Ag-La<sub>2</sub>O<sub>3</sub> electrode was executed at +0.43 V vs SCE. The glucose solution of different molar concentrations from 100  $\mu$ M to 2.8 mM was injected into 0.1 M NaOH solution with a regular interval of 60 s, producing staircase-like graph as depicted in **Fig. 4.11a**. The Ag-La<sub>2</sub>O<sub>3</sub> electrode reveals a good electrocatalytic multi-linear response towards glucose in the ranges of 100  $\mu$ M to 600  $\mu$ M

and 600  $\mu\text{M}$  to 1.6 mM. These experimental results are shown in **Fig. 4.11b**, where the current response found to be linear in wide range of concentration from 100  $\mu\text{M}$  to 600  $\mu\text{M}$  with a high sensitivity of  $1677 \mu\text{A mM}^{-1} \text{cm}^{-2}$  and a correlation coefficient of 0.9910. Similarly, another linear behavior for high concentration of glucose ranged from 600  $\mu\text{M}$  to 1.6 mM with a sensitivity of  $1022 \mu\text{A mM}^{-1} \text{cm}^{-2}$  and a correlation coefficient of 0.9967 was measured. Additionally, limit of detection for lower as well as higher concentration of glucose was calculated to be 0.62  $\mu\text{M}$  and 1.09  $\mu\text{M}$  respectively using equation (1).

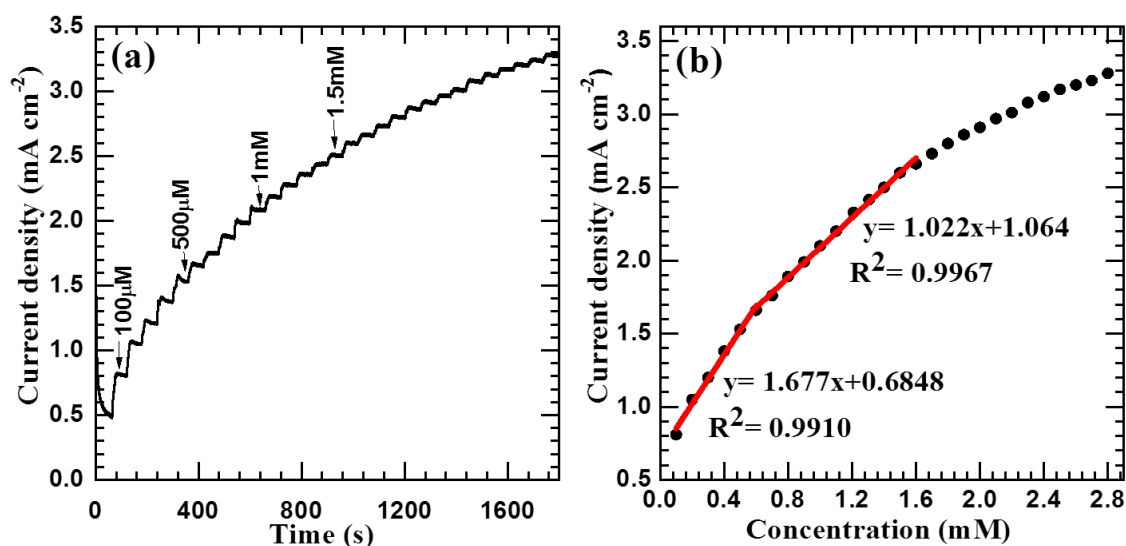


**Figure 4.11:** (a) Current versus time measurement at +0.43 V vs SCE with successive addition of 100  $\mu\text{M}$  of glucose in 60 s time intervals, (b) calibration graph of dependence on current with respect to glucose concentration.

The steady state response time of  $\sim 5\text{s}$  was observed for the course of addition of glucose which highlights very fast electron transfer on electrode surface. In particular, while increasing the glucose concentration, initially the anodic current density response increases but shows non-linearity above the concentration of 1.6 mM may be due to the limit generated from saturation of number of catalytic sites for oxidation [29]. The enhanced electrical conductivity, surface area and sensing performance are due to Ag

composite and vertically grown Ag-La<sub>2</sub>O<sub>3</sub> nanoflakes film electrode. As the thickness of shell layer in the nanoregion results with active surface area which can provide more reactive sites for redox reaction and electrocatalytic activity [30]. Therefore, it can be concluded that; vertically grown Ag-La<sub>2</sub>O<sub>3</sub> nanoflakes facilitate fast electron transfer and more electrochemical active sites due to higher specific surface area for glucose oxidation.

#### 4.6 Selectivity, stability and reproducibility:

In real samples, the oxidizable compounds such as ascorbic acid (AA), dopamine (DA) and other carbohydrates such as lactose (Lac), fructose (Fru), often interfere with the analysis of glucose. So, to investigate the selectivity of the sensor, the *i-t* amperometric responses toward the addition of 500  $\mu$ M glucose, ascorbic acid, fructose, lactose, and dopamine were examined in 0.1 M NaOH solution at a potential of +0.43 V. It is observed from **Fig. 4.12a**, that response current for AA, Fru, Lac, and DA are significantly lower than that of glucose. All the results demonstrated that, the selectivity of the sensor for glucose detection is satisfying. The above consequence indicates that Ag-La<sub>2</sub>O<sub>3</sub> electrode has a good selectivity for glucose during the detection. In an attempt to evaluate the long term stability of the electrode, the *i-t* amperometric response was recorded in 100  $\mu$ M glucose concentration (black line) and without glucose concentration (red line) at +0.43 V vs SCE for 3600 s and the result is shown in **Fig. 4.12b**. The graph clearly indicates that the Ag-La<sub>2</sub>O<sub>3</sub> electrode offers linear characteristics for glucose oxidation. To evaluate reproducibility and reliability of Ag-La<sub>2</sub>O<sub>3</sub> electrode, *i-t* amperometric response of six similar electrodes were carried out at identical conditions. Result of the experiment is shown in **Fig. 4.12c**. The relative standard deviation (RSD) of 4.3% was obtained indicating the excellent reproducibility of Ag-La<sub>2</sub>O<sub>3</sub> electrodes.

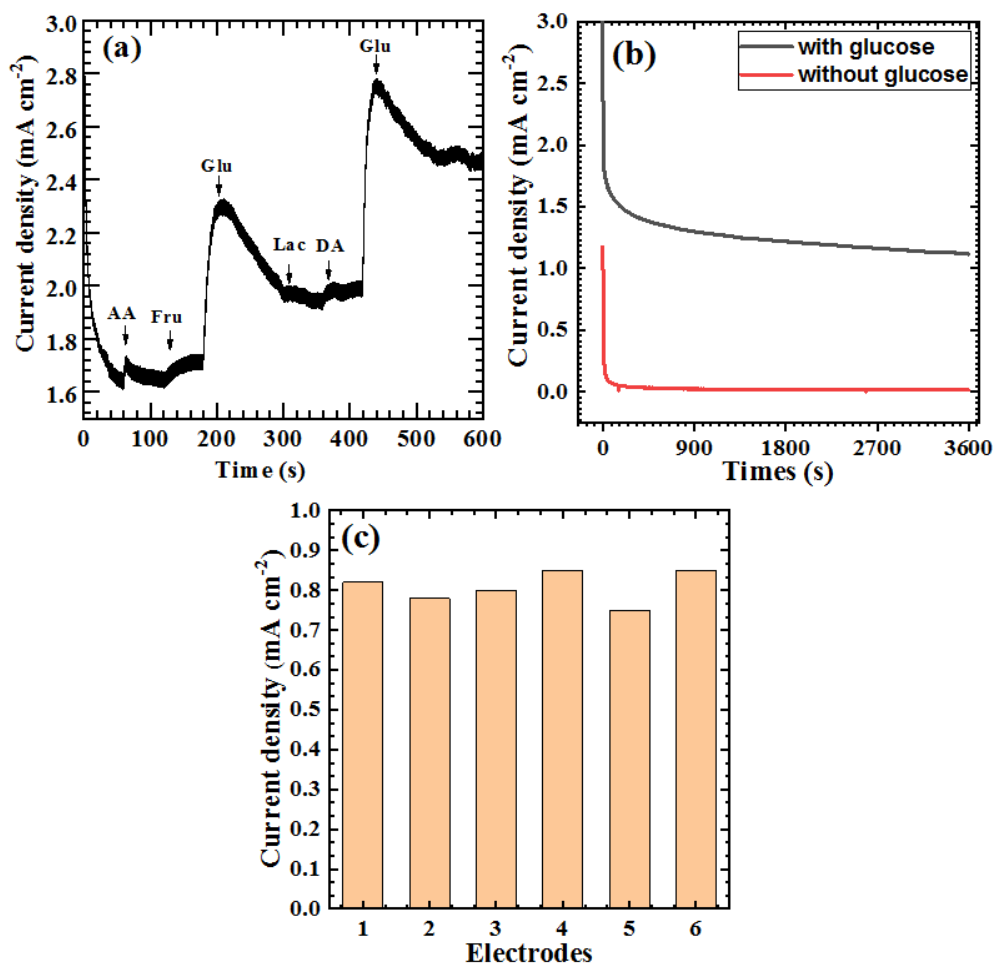


**Figure 4.12:** (a) *i-t* amperometric response of Ag-La<sub>2</sub>O<sub>3</sub> electrode for successive addition of glucose and interferences in 0.1 M NaOH at +0.43 V vs SCE, (b) stability graph in presence of 500 μM glucose concentrations in 0.1 M NaOH solution, and (c) reproducibility of Ag-La<sub>2</sub>O<sub>3</sub> electrodes in 100 μM glucose concentration.

#### 4.7 Conclusions:

In this study, we demonstrate that the Ag composition affects crystal structure of electrodeposited La<sub>2</sub>O<sub>3</sub> thin film and it becomes nanocrystalline amorphous nature but topography of the film remains similar. Along with physical properties, enhancement in electrocatalytic and electrochemical properties of the La<sub>2</sub>O<sub>3</sub> was observed after Ag composite. The electrocatalytic oxidation of glucose at the electrode was investigated and the supercapacitor properties were discussed. The sensing performance of Ag-La<sub>2</sub>O<sub>3</sub> film electrode at +0.43 V vs. SCE revealed a high sensitivity (1677 μA mM<sup>-1</sup> cm<sup>-2</sup>) and good

reproducibility in glucose determination in a wide linear range of 100  $\mu\text{M}$  to 2.8 mM with a LOD of 0.62  $\mu\text{M}$ . This result reveals that vertically grown Ag-La<sub>2</sub>O<sub>3</sub> film electrode is applicable for glucose sensing application.

#### 4.7 References:

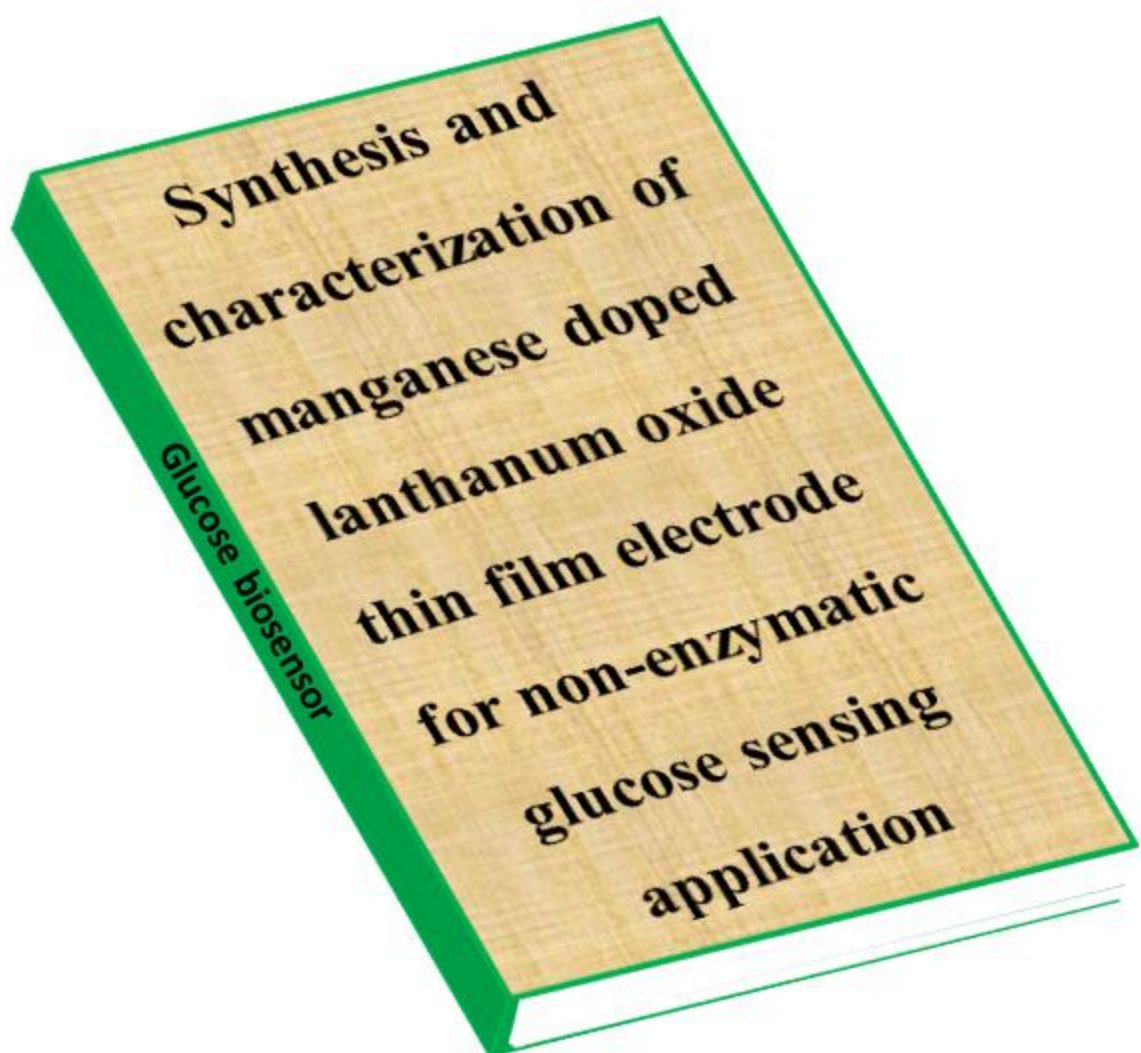
1. M. Saraf, K. Natarajan, S. Mobin, Robust nanocomposite of nitrogen-doped reduced graphene oxide and MnO<sub>2</sub> nanorods for high-performance supercapacitors and nonenzymatic peroxide sensors. *ACS Sustain. Chem. Eng.*, 6, (2018), 10489–10504. DOI: 10.1021/acssuschemeng.8b01845.
2. L. Cui, C. Li, Chun-yang Zhang. Advances in the integration of quantum dots with various nanomaterials for biomedical and environmental applications. *Analyst*, 143, (2018), 2469-2478. DOI: 10.1039/C8AN00222C.
3. M. A. Yassin, B. K. Shrestha, R. Ahmad, S. Shrestha, C. H. Park, Cheol Sang Kim. Exfoliated nanosheets of Co<sub>3</sub>O<sub>4</sub> webbed with polyaniline nanofibers: A novel composite electrode material for enzymeless glucose sensing application. *J. Ind. Eng. Chem.*, 73, (2019), 106-117. DOI: 10.1016/j.jiec.2019.01.011.
4. B. Li Zhang, Y. Yang, Z. Q. Zhao, X. D. Guo. A gold nanoparticles deposited polymer microneedle enzymatic biosensor for glucose sensing. *Electrochim. Acta.*, 358, (2020), 136917, DOI: 10.1016/j.electacta.2020.136917.
5. W. C. Lee, K. B. Kim, N. G. Gurudatt, K. K. Hussain, C. S. Choi, D. S. Park, Y. B. Shim. Comparison of enzymatic and non-enzymatic glucose sensors based on hierarchical Au-Ni alloy with conductive polymer. *Biosens. Bioelectron*, 130, (2019), 48-54, DOI: 10.1016/j.bios.2019.01.028.
6. S. Park, H. Boo, T. Dong Chung, Electrochemical non-enzymatic glucose sensors, *Anal. Chim. Acta*, 556, (2006), 46-57, DOI:10.1016/j.aca.2005.05.080.
7. V. Muthulakshmi, M. Balaji, M. Sundrarajan, Ionic liquid mediated morphologically improved lanthanum oxide nanoparticles by andrographis paniculata leaves extract and its biomedical applications. *J. of Rare Earths*. 38, (2020), 281-291, DOI:10.1016/j.jre.2019.06.006.

8. S. Y. No, D. Eom, C. S. Hwang, H. J. Kim, Properties of lanthanum oxide thin films deposited by cyclic chemical vapor deposition using tris (isopropyl-cyclopentadienyl) lanthanum precursor. *J. Appl. Phys.*, 100, **(2006)**, 024111, DOI: 10.1063/1.2218465.
9. M. Nieminen, M. Putkonen, L. Niinistö, Formation and stability of lanthanum oxide thin films deposited from  $\beta$ -diketonate precursor. *Appl. Surf. Sci.*, 174, **(2001)**, 155-166, DOI: 10.1016/S0169-4332(01)00149-0.
10. E. Katz, I. Willner, Integrated Nanoparticle-Biomolecule Hybrid Systems: Synthesis, Properties, and Applications. *Chem. Plus. Chem.*, 43, **(2004)**, 6042-6108, DOI:10.1002/anie.200400651.
11. N. A. Rakow, K. S. Suslick, A colorimetric sensor array for odour visualization. *Nature*, 406, **(2000)**, 710-713, DOI: 10.1038/35021028.
12. V. J. Mane, D. B. Malavekar, S. B. Ubale, R. N. Bulakhe, Insik In, C. D. Lokhande. Binder free lanthanum doped manganese oxide @ graphene oxide composite as high energy density electrode material for flexible symmetric solid state supercapacitor. *Electrochim Acta*, 335, **(2020)**, 135613, DOI:10.1016/j.electacta.2020.135613.
13. L. Jayasingha, C. Jayathilaka, R. Kumara, K. Ohara, M. Kaumal, S. Gunewardene, D. Dissanayake, S. Jayanetti, Nanoporous Cu<sub>2</sub>O nanotube/nanorod array electrodes for non-enzymatic glucose sensing with high sensitivity and very low detection limit. *Electrochim Acta*, 329, **(2020)**, 135177. DOI: 10.1016/j.electacta.2019.135177.
14. K. K. Naik, S. Kumar, C. S. Rout, Electrodeposited spinel NiCo<sub>2</sub>O<sub>4</sub> nanosheet arrays for glucose sensing application, *RSC Adv*, 5, **(2015)**, 74585-74591, DOI:10.1039/C5RA13833G.
15. D. B. Malavekar, V. C. Lokhande, V. J. Mane, S. B. Ubale, U. M. Patil, C. D. Lokhande, Enhanced energy density of flexible asymmetric solid state supercapacitor device fabricated with amorphous thin film electrode materials, *J. of Phys. Chem. Solids*, 141, **(2020)**, 109425, DOI: 10.1016/j.jpcs.2020.109425.
16. X. Wang, X. Hu, J. Huang, W. Zhang, W. Ji, Y. Hui, X. Yao, Electrospinning synthesis of porous carbon fiber supported Pt-SnO<sub>2</sub> anode catalyst for direct ethanol fuel cell, *solid state sci.*, 94, **(2019)**, 64-69, DOI: 10.1016/j.solidstatesciences.2019.05.018.

17. S. Jin, X. Wei, Z. Yu, J. Ren, Z. Meng, Z. Jiang, Acoustic-controlled bubble generation and fabrication of 3D polymer porous materials, *ACS Appl. Mater. Interfaces*, 12, **(2020)**, 22318-22326, DOI: 10.1021/acsami.0c02118.
18. S. B. Jadhav, U. M. Patil, R. N. Bulakhe, Insik In, C. D. Lokhande, P. N. Pawaskar, vertically aligned nanosheets of an electrodeposited lanthanum oxide electrode for non-enzymatic glucose sensing application, *J. Electron. Mate.* 50, **(2020)**, 675-685, DOI: 10.1007/s11664-020-08605-w.
19. K. K. Naik, A. Gangan, B. Chakraborty, C. S. Rout, Superior non-enzymatic glucose sensing properties of Ag-/Au-NiCo<sub>2</sub>O<sub>4</sub> nanosheets with insight from electronic structure simulations, *Analyst*, 143, **(2018)**, 571-579, DOI: 10.1039/C7AN01354J.
20. F-F. Jia, H. Zhong, W-G. Zhang, X-R. Li, G-Y. Wang, J. Song, Z-P. Cheng, J-Z. Yin, L-P. Guo, A novel nonenzymatic ECL glucose sensor based on perovskite LaTiO<sub>3</sub>-Ag<sub>0.1</sub> nanomaterials, *Sens. Actuators B*, 212, **(2015)**, 174-182, DOI: 10.1016/j.snb.2015.02.011.
21. P. Salazar, V. Rico, A. R. González-Elipé, Non-enzymatic glucose sensors based on nickel nanoporous thin films prepared by physical vapor deposition at oblique angles for beverage industry applications, *J. Electrochem. Soc.* 163, **(2016)**, B704-B709, DOI: 10.1149/2.1241614jes.
22. K. de O. Santos, W. C. Elias, A. M. Signori, F. C. Giacomelli, H. Yang, J. B. Domingos, Synthesis and catalytic properties of silver nanoparticle-linear polyethylene imine colloidal systems, *J. Phys. Chem. C*, 166, **(2012)**, 4594-4604, DOI:10.1021/jp2087169.
23. Y. Wang, I. Zhitomirsky, Cathodic electrodeposition of Ag-doped manganese dioxide films for electrodes of electrochemical supercapacitor, *Mater. Lett.*, 65, **(2011)**, 1759-1761, DOI:10.1016/j.matlet.2011.03.074.
24. O. Lupan, V. Cretu, V. Postica, M. Ahmadi, B. R. Cuenya, L. Chow, I. Tiginyanu, B. Viana, T. Pauporté, R. Adelung. Silver-doped zinc oxide single nanowire multifunctional nanosensor with a significant enhancement in response. *Sens. Actuators B*. 223, **(2016)**, 893-903, DOI: 10.1016/j.snb.2015.10.002.
25. S. Demirci, T. Dikici, M. Yurddaskal, S. Gultekin, M. Toparli, Erdal Celik, Synthesis and characterization of Ag doped TiO<sub>2</sub> heterojunction films and their photocatalytic

- performances, *Appl. Surf. Sci.*, **390**, (2016), 591–601, DOI: 10.1016/j.apsusc.2016.08.145.
26. P. Salazar, I. Fernandez, M. C. Rodriguez, A. H. Creus, J. Luis Gonzalez-Mora, One-step green synthesis of silver nanoparticle-modified reduced graphene oxide nanocomposite for H<sub>2</sub>O<sub>2</sub> sensing applications, *J. Electroanal. Chem.* **855**, (2019), 113638, DOI:10.1016/j.jelechem.2019.113638.
27. S. I. Mogal, V. G. Gandhi, M. Mishra, S. Tripathi, T. Shripathi, P. A. Joshi, D. O. Shah, Single-step synthesis of silver-doped titanium dioxide: influence of silver on structural, textural, and photocatalytic properties, *Ind. Eng. Chem. Res.* **53**, (2014), 5749-5758, DOI: 10.1021/ie404230q.
28. M. R. Sovizi, S. Mirzakhani, A chemiresistor sensor modified with lanthanum oxide nanoparticles as a highly sensitive and selective sensor for dimethylamine at room temperature, *New J. Chem.*, **44**, (2020), 4927-4934, DOI: 10.1039/C9NJ06329C.
29. J. Cui, J. Luo, B. Peng, X. Zhang, Y. Zhang, Y. Wang, Y. Qin, H. Zheng, X. Shu, Y. Wu, Synthesis of porous NiO/CeO<sub>2</sub> hybrid nanoflake arrays as a platform for electrochemical biosensing, *Nanoscale*, **8**, (2016), 770-774, DOI: 10.1039/C5NR05924K.

# CHAPTER V



## Index

Sr. No.	Details	Page No.
5.1	Introduction	117
5.2	Experimental details	119
	5.2.1 <i>Materials</i>	119
	5.2.2 <i>Synthesis of <math>\text{La}_2\text{O}_3</math> and Mn-<math>\text{La}_2\text{O}_3</math></i>	120
	5.2.3 <i>Structural and physical characterization</i>	122
	5.2.4 <i>Electrochemical measurement</i>	122
5.3	Results and discussion	123
	5.3.1 <i>XRD analysis</i>	123
	5.3.2 <i>FE-SEM and EDS analysis</i>	124
	5.3.3 <i>XPS analysis</i>	126
5.4	Enzymeless glucose detection	127
	5.4.1 <i>The CV study of <math>\text{La}_2\text{O}_3</math>, 1, 3, and 5% Mn-<math>\text{La}_2\text{O}_3</math> electrodes</i>	127
	5.4.2 <i>Electrocatalytic activity of 1% Mn-<math>\text{La}_2\text{O}_3</math> electrode towards glucose sensing</i>	129
	5.4.3 <i>Selectivity, reputability and reproducibility studies of 1% Mn-<math>\text{La}_2\text{O}_3</math> electrode</i>	134
5.5	Conclusions	135
5.6	References	136

### 5.1 Introduction:

Diabetes mellitus affects millions of peoples worldwide. The international diabetes federation (IDF) reported that diabetes is the leading cause of death for 5 million people in 2015 [1]. But it is an often underestimated as low risk diseases. Due to pandemic in last two year it gained intension of common people due to comorbidities. Till today, continuous monitoring of glucose molecule is the most important universal way to restrain the severe effects of diabetes on life. There are several methods are available for access of blood glucose level. The most prominent technique being come forward in the past few years is electrochemical oxidation of glucose due to its high sensitivity, easy detection of low glucose concentration in the sample, favorable response time, and cost-effectiveness [2, 3]. There are two categories of glucose sensors viz. enzymatic and non-enzymatic sensors. The enzymatic glucose sensor possesses high sensitivity and selectivity but suffers from some distinct disadvantages such as immobilization process of enzyme, poor long term stability, difficulty to maintain pH, humidity, and high storage cost. The non-enzymatic glucose sensors have advantages in terms of high sensitivity, long-term stability, low detection limit (LOD), and reusability. However, some drawbacks likes surface poisoning, temperature dependence, structural stability, and consistent decreasing sensitivity loss are observed for non-enzymatic glucose sensors. In that context, academics and researchers joined hands with industries to overcome some of these drawbacks.

The surface texture, electrical conductivity, temperature dependence, and electrochemical stability plays important role in non-enzymatic glucose detection. The tunable redox-activity of lanthanum and manganese can be used to enhance their electrochemical/electrocatalytic behavior. Furthermore, higher valence states and narrow

band gap may lead to improved electrical conductivity. Such transition metal-like properties of La based oxides make a significantly better electrocatalyst [4]. Metal oxide based materials can easily transfer electrons during the electrooxidation process as material changes the valence state. Apart from transition metal doping, the electrode materials can enhance electrocatalytic performance owing to multiple oxidation state as well as conducting elements [5].

Jadhav et al. [6] synthesized Ag-doped  $\text{La}_2\text{O}_3$  film electrode via ED method and used for enzymeless glucose detection and energy storage application. Jaffar et al. [7] synthesized bismuth (Bi) doped  $\text{La}_2\text{O}_3$  particle by sol- gel method and evaluated for optical properties. Doping of Bi ions enhanced the optical performance of  $\text{La}_2\text{O}_3$  material. Schucker et al. [8] prepared strontium (Sr) doped  $\text{La}_2\text{O}_3$  material and described elemental activity and selectivity of the Sr ion to provide more active sites that leads to increase catalytic properties. Jbeli et al. [9] synthesized Co doped  $\text{La}_2\text{O}_3$  film electrode via spray pyrolysis method and used for anti-bacterial and photocatalytic applications. As aforementioned, doping of metal ions can show internal changes such as crystal structure, morphology, electrochemical activity, and electrical conductivity. Yang et al. [10] synthesized reduced graphene oxide/ $\text{La}_2\text{O}_3$  material by hydrothermal reduction approach for highly stable innovative of rechargeable lithium-sulfur batteries. Considerable redoxactive mechanisms have been employed for the glucose electrooxidation process [11, 12]. Lanthanum and manganese based materials were used for catalytic and electrochemical applications. Shaterian et al. [13] synthesized  $\text{LaMnO}_3$  nanoparticles by sol-gel method for photocatalytic application. Mefford et al. [14] prepared  $\text{LaMnO}_3$  by reverse phase hydrolysis method and evaluated it for practical pseudocapacitors application. Ashok et al. [15] synthesized  $\text{LaMnO}_3$  nanoparticle using the salt-assisted

combustion method and tested for fuel cell and charge storage application. Mane et al. [16] synthesized lanthanum doped manganese oxide thin film electrode using SILAR method for energy storage application.

Previous reports are related to the facile ED methods such as potentiostatic, galvanostatic, CV, chrono-amperometric, and potential reversal ED methods [17]. Anuratha et al. [18] reported synthesis of  $\text{NiCo}_2\text{O}_4$  nanocomposite with hyper-branched flower-like morphology by the facile multipotential ED method. One step reversible ED method for synthesis of amorphous nickel cobalt sulfide on fluorine doped tin oxide reported by Jiang et al. [19] exhibited high-efficiency in dye sensitized solar cell application. The electrocatalytic activity of electrode material is affected not only by two or more structure, but also by its appearance such its morphology, grain boundaries, and porous structure. Extensive network-like structure, high porosity, and 3D mesoporous structure can provide huge electrocatalytic active sites which leads easy electron transfer rate and decrease in charge transfer resistance [20].

In this chapter, we have adopted facile multipotential ED method to prepare binder-free  $\text{La}_2\text{O}_3$  with Mn on SS substrate. The formation of Mn- $\text{La}_2\text{O}_3$  electrodes was confirmed by various characterization techniques like XRD, FE-SEM, EDX, and XPS. Furthermore, thin films were employed for non-enzymatic glucose detection using standard three electrode system. Glucose detection from real blood sample were evaluated using best performing thin film electrode

## 5.2 Experimental details:

### 5.2.1 Materials:

All reagents of analytical grade, e.g. lanthanum nitrate hexahydrate ( $\text{La}(\text{NO}_3)_3 \cdot 6\text{H}_2\text{O}$ ), manganese nitrate tetrahydrate ( $\text{Mn}(\text{NO}_3)_2 \cdot 4\text{H}_2\text{O}$ ), NaOH, glucose,

Fru, Lac, AA, and DA of analytical grade were purchased from Thomas Baker (India) and used as received.

### 5.2.2 Synthesis of $\text{La}_2\text{O}_3$ , and Mn- $\text{La}_2\text{O}_3$ :

Multipotential step ED technique was used to deposit pure  $\text{La}_2\text{O}_3$  and Mn-doped  $\text{La}_2\text{O}_3$  thin film. Deposition was carried out at room temperature. Doping concentration of Mn varies from 1 to 5 volume % (Vol%). A typical three electrode system composed of SS substrate, Pt sheet, and SCE were used in which SS is a working, Pt is a counter, and SCE as reference electrode. The cathodic and anodic ED was carried out employing the CHI660E electrochemical workstation. The detail explanation and deposition growth mechanism of  $\text{La}_2\text{O}_3$  thin film is given to the chapter no. III. For deposition of Mn doped  $\text{La}_2\text{O}_3$  thin films, separately prepared 0.01M manganese nitrate and 0.01 M lanthanum nitrate solutions were mixed together in volumetric ratios of 0:50, 0.5:49.5, 1.5:48.5, and 2.5:47.5, to obtain final solution of 50 mL. The modified multipotential step technique was carried out to deposit manganese at +0.8 V/SCE and lanthanum at -1 V/SCE potential. The deposition time for manganese was 30 s, and that for lanthanum was 60 s. the deposition curve for Mn and  $\text{La}_2\text{O}_3$  is shown in in **Fig. 5.1**.

After 30 cycles of deposition, uniform and adherent thin film was deposited on SS substrate. The thin films were annealed at temperature of 573 K in air atmosphere for 2 h and used for further characterizations.

The electrochemical reduction of aqueous nitrate solution equation was described by Sasaki et al. [21] and Therese et al. [22]. The reaction mechanism can be divided in to two groups; first reaction is related to the nitrate solution reduction and second related to the hydrogen evolution.





The above both reactions release  $OH^-$  ion and it lead to an increase pH of the solution close to the electrode. Therefore, metal ions present in the solution that can electrodeposited by anodic and cathodic applied potential to the electrode. Hydroxide/oxide material was deposited on the electrode surface and thicknesses of the coating can be easily varied from nano to micrometers.



The reaction of nitrate reduction was occurring at negative potential of -0.17 V/SCE then it was less than that of lanthanum deposition potential -1V/SCE. The different deposition potential for lanthanum and manganese was selected as -1 and 0.8 V/SCE respectively.

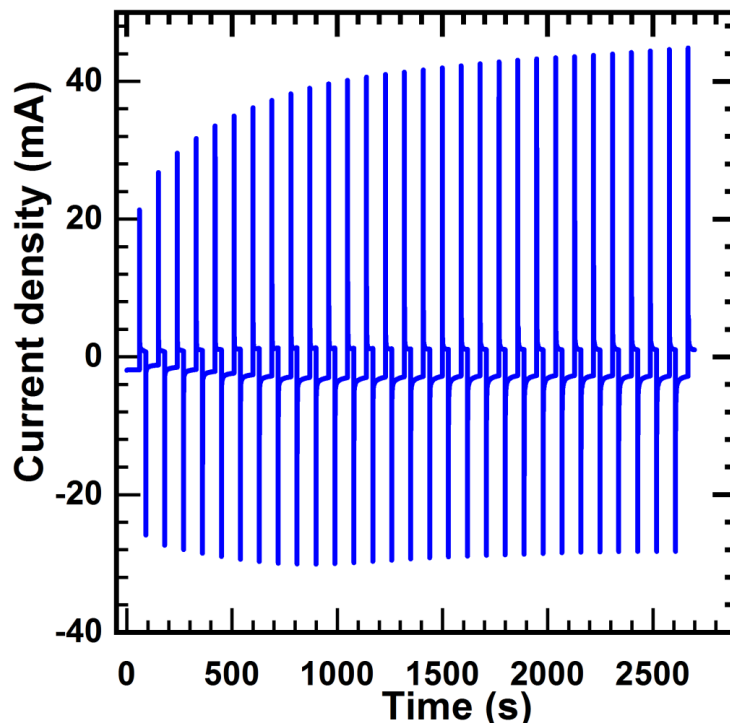


**Fig. 5.1:** Deposition curve of 1% Mn doped  $La_2O_3$  film electrode on SS substrate

Jadhav et al. [10] synthesized lanthanum oxide film electrode by cathodic ED method at -1 V/SCE and used for glucose sensing application. Jadhav et al. [23] prepared

manganese oxide by anodic ED method at 0.8 V/SCE and also used for glucose sensing application. Thus, nitrate reduction promising to control the pH increment, leading to formation of hydroxide precipitates. In that regards, we have selected simple multipotential ED technique for deposition of Mn-La<sub>2</sub>O<sub>3</sub> film electrode on SS substrate. This technique is employed for simultaneous anodic and cathodic metal ions deposition that can lead to form the doping, composite or hybrid materials.

### 5.2.3 Structural and physical characterization:

The details characterization techniques were explained in previous chapter III (Section-3.4)

### 5.2.4 Electrochemical measurement:

The non-enzymatic glucose sensing performance of film electrode was studied using CV and *i-t* amperometry techniques in freshly prepared 0.1 M aqueous NaOH solution. The CV experiments were carried out in the optimized potential window from 0 to +0.5 V/SCE. For glucose sensing, freshly prepared 40 ml of 0.1 M NaOH solution was taken in the glass cell and then glucose solution was injected into the electrolyte at different molar concentrations (50 to 950  $\mu$ M) to observe the current response of the electrode. Similarly, for *i-t* amperometry experiment, 40 ml of 0.1 M NaOH electrolyte was taken in the glass cell and kept stirring at a constant speed of 300 rpm and optimized potential +0.41 V/SCE were applied to the working electrode. The analytes were injected to the rotating solution at different molar concentrations to observe the sensing response of the materials at different potentials. The interference study was executed by performing *i-t* experiment in the presence of different interfering species such as AA, Fru, Lac, and DA. The LOD of analyte was calculated using the equation no. 4.1. Standard deviation of the analyte concentration calculated from current response of the

consecutive addition of glucose into the electrolyte and the sensitivity of the electrode was calculated by the slope of the calibration curve.

### 5.3 Results and discussion:

#### 5.3.1 XRD analysis:

The XRD patterns of  $\text{La}_2\text{O}_3$ , 1, 3, 5% Mn-doped  $\text{La}_2\text{O}_3$  thin films deposited on SS substrates are shown in **Fig. 5.2**. The diffraction peaks are associated with hexagonal and monoclinic crystal structures of  $\text{La}_2\text{O}_3$ . The diffraction peaks for planes (002), (110), and (200) correspond to hexagonal  $\text{La}_2\text{O}_3$  (JCPDS cards no 00-002-0688) and (301), (303), and (404) to monoclinic  $\text{La}_2\text{O}_3$  (JCPDS cards no 00-022-0641). The ionic radius of La ( $1.06\text{\AA}$ ) is higher than Mn ion due to substitutional doping of Mn ion in  $\text{La}_2\text{O}_3$  lattice interface. The high intensity peaks of  $\text{La}_2\text{O}_3$  were reduced by increasing Mn concentration due to disturbed crystal structure of  $\text{La}_2\text{O}_3$ .

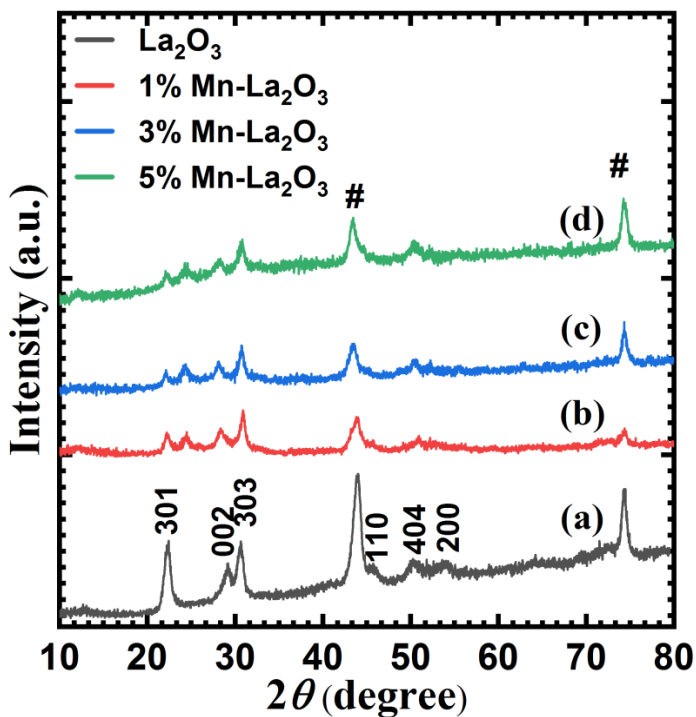


**Fig. 5.2** The XRD patterns of (a)  $\text{La}_2\text{O}_3$ , (b) 1% Mn-  $\text{La}_2\text{O}_3$ , (c) 3% Mn- $\text{La}_2\text{O}_3$ , and (d) 5% Mn- $\text{La}_2\text{O}_3$  thin films on SS substrate.

### 5.3.2 FE-SEM and EDX analysis:

The surface texture of electrodeposited thin films is shown in **Fig. 5.3**. The FE-SEM images of **(a, b)**  $\text{La}_2\text{O}_3$ , **(c, d)** 1% Mn- $\text{La}_2\text{O}_3$ , **(e, f)** 3% Mn- $\text{La}_2\text{O}_3$  and **(g, h)** 5% Mn- $\text{La}_2\text{O}_3$  films at different magnifications (10 kX and 70 kX) are shown in **Fig 5.3**. The above films were deposited under similar condition; surface pore texture of 1% Mn- $\text{La}_2\text{O}_3$  was more than other films that can help for to enhance the electrocatalytic performance. Vertically grown nanoflakes like network are randomly distributed over the SS substrate. After addition of Mn ions, no drastic changes observed in morphology and these nanoflakes formed the sheet-on-sheet porous network in all electrodes. Such flakes-like nanostructure leads to uneven surface of the electrode which enhances glucose sensing properties due to good surface to volume ratio and reduced contact resistance [26]. Even distribution of all the constituent elements indicates uniform composition of thin film.

The chemical composition of the deposited thin film was investigated by EDX analysis as shown in **Fig. 5.4**. The  $\text{La}_2\text{O}_3$  sample shows lanthanum, and oxygen elements, and confirms formation of  $\text{La}_2\text{O}_3$  as shown in **Fig. 5.4(a)**. The surface composition of 1% Mn- $\text{La}_2\text{O}_3$  thin film electrode was investigated. The presence of La, O, and Mn was confirmed. 1.45 atomic % of Mn was present in  $\text{La}_2\text{O}_3$  thin film as shown in **Fig. 5.4(b)**. The surface composition of 3% Mn- $\text{La}_2\text{O}_3$  electrode was investigated. 3.08 atomic % of Mn was present in  $\text{La}_2\text{O}_3$  thin film as shown in **Fig. 5.4(c)**. Similarly, the surface composition of 5% Mn- $\text{La}_2\text{O}_3$  electrode was investigated. 5.54 atomic % of Mn was present in  $\text{La}_2\text{O}_3$  thin film as shown in **Fig. 5.4(d)**.

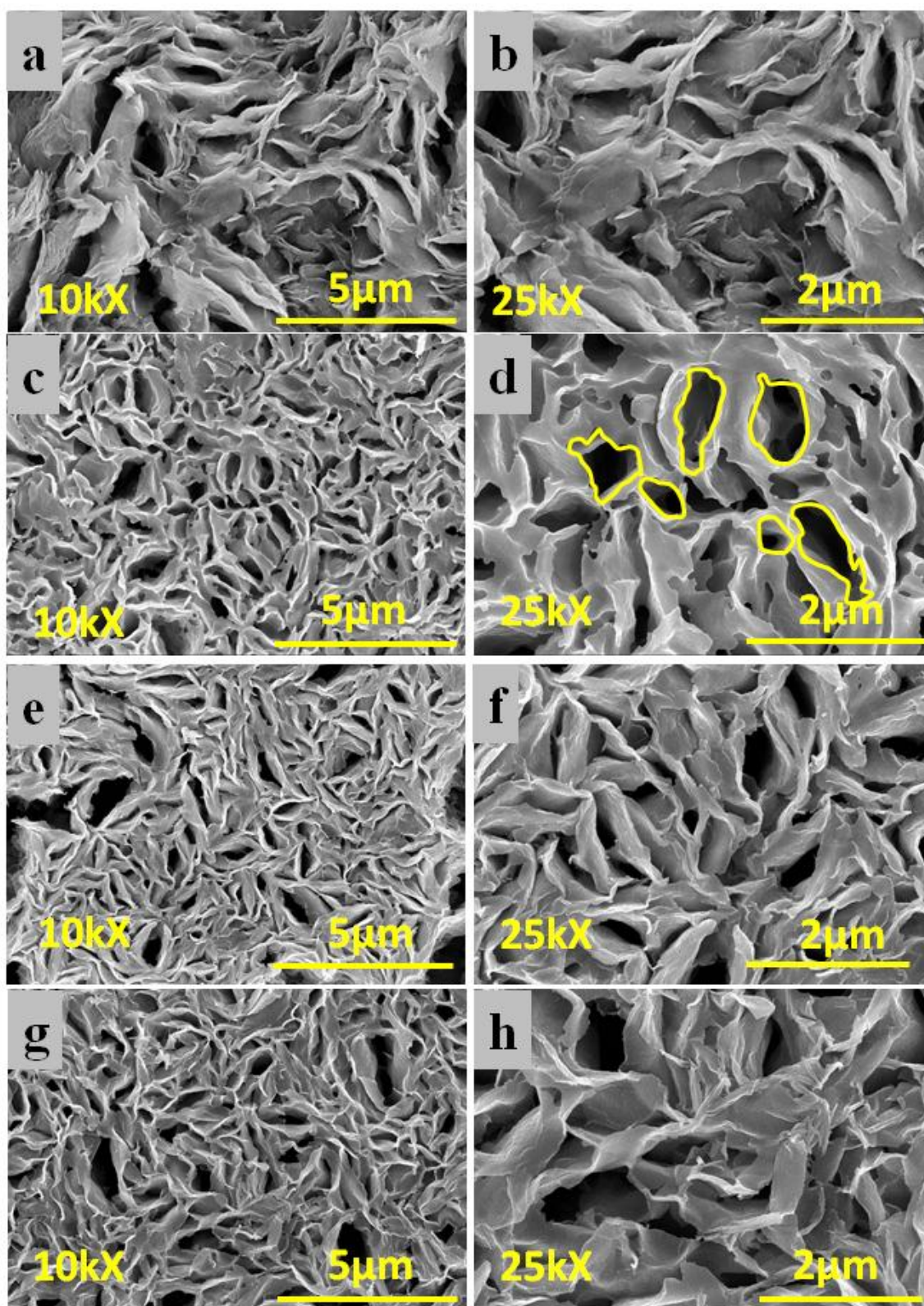


**Fig. 5.3** The FE-SEM images of (a, b)  $\text{La}_2\text{O}_3$ , (c, d) 1% Mn- $\text{La}_2\text{O}_3$  and (e, f) 3% Mn- $\text{La}_2\text{O}_3$  and (g, h) 5% Mn- $\text{La}_2\text{O}_3$  at different magnifications.

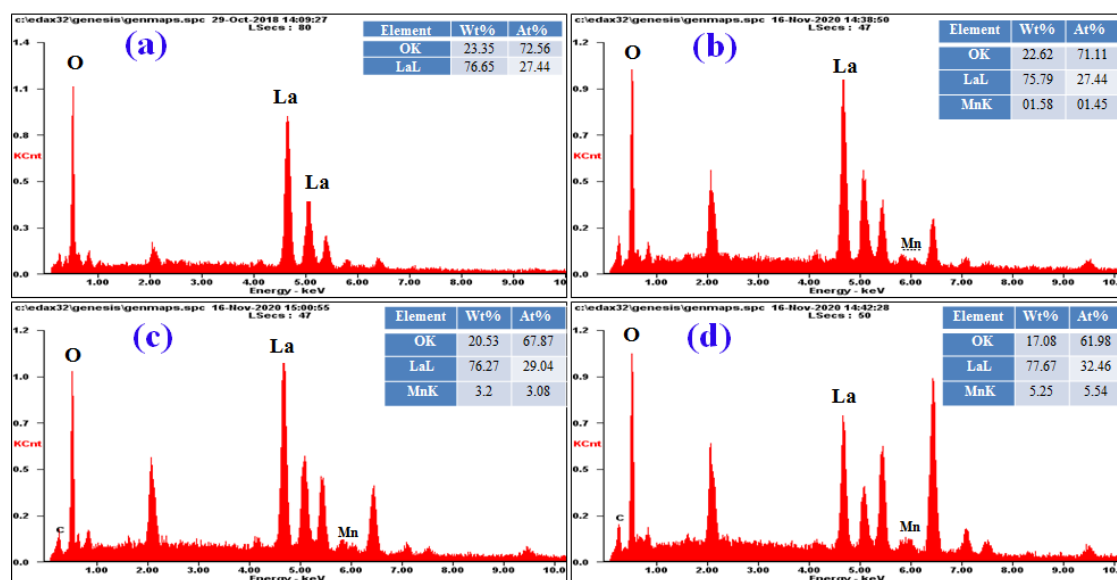


**Fig. 5.4** The EDX spectra of (a)  $\text{La}_2\text{O}_3$ , (b) 1, (c) 3 and (d) 5% Mn- $\text{La}_2\text{O}_3$  thin film electrodes

### 5.3.3 XPS analysis:

The XPS analysis of 1% Mn- $\text{La}_2\text{O}_3$  film electrode was carried out to understand the oxidation states of constituent elements. Wide range XPS spectrum displayed in **Fig. 5.5a** reveals an existence of oxygen, lanthanum and manganese elements in the film. The XPS spectrum of La3d is displayed in **Fig. 5.5b**. The spectrum is deconvoluted into two peaks at 838.69 and 855.54 eVs proportional to  $\text{La}3d_{5/2}$  and  $\text{La}3d_{3/2}$ , respectively. The energy separation of 16.85 eV between two peaks again confirms presence La in  $\text{La}3d_{5/2}$  and  $\text{La}3d_{3/2}$  states [27]. Very less amount of Mn ions (1.45 atomic %) cannot be detected in XPS. Hence peak from Mn is absent as shown in **Fig. 5.5c**. The typical high resolution oxygen spectrum is presented in **Fig. 5.5d**. The main O 1s peak is due to oxide La-O-La bond (529.9 eV), hydroxide C-OH bond (531.31 eV), and carboxyl (O-C=O) bond (532.97 eV). These outcomes are in agreement accompanied by XPS characteristics of  $\text{La}_2\text{O}_3$  presented by Maih et al. [28].

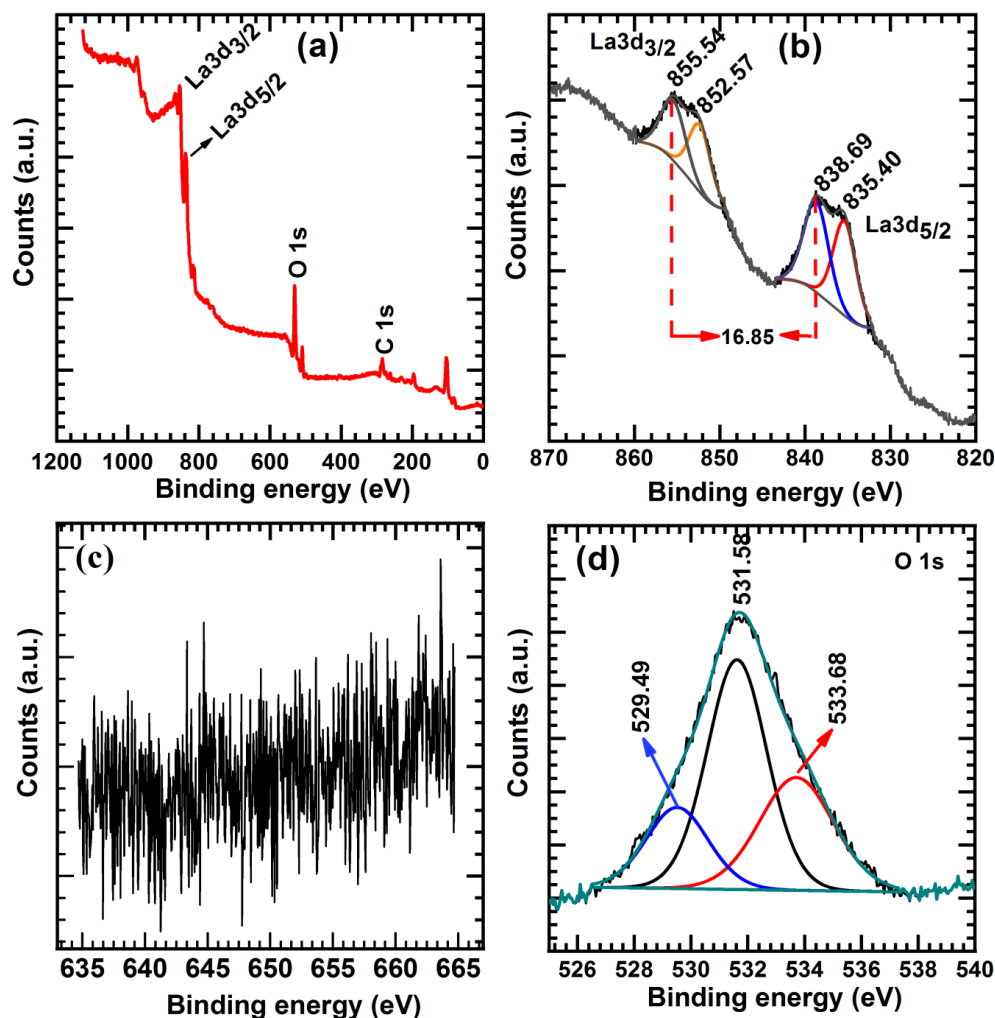


**Fig. 5.5** The XPS spectrum of 1% Mn-La<sub>2</sub>O<sub>3</sub> electrode, XPS spectrum of b) La3d, c) Mn, and d) O

#### 5.4 Enzymeless glucose detection:

##### 5.4.1 The CV study of La<sub>2</sub>O<sub>3</sub>, 1, 3, and 5% Mn-La<sub>2</sub>O<sub>3</sub> electrodes:

The CV study of La<sub>2</sub>O<sub>3</sub>, 1, 3, and 5% Mn-La<sub>2</sub>O<sub>3</sub> film electrodes was carried out in 0.1 M aqueous NaOH electrolyte. All electrodes were scanned at scan rates from 5 to 150 mV s<sup>-1</sup> by varying applied potential between 0 to +0.5 V/SCE as shown in **Fig 5.6a-d**. **Fig. 5.7** displays the CV curves within the potential window 0 to +0.5 V/SCE for La<sub>2</sub>O<sub>3</sub>, 1, 3, and 5% Mn-La<sub>2</sub>O<sub>3</sub> thin film electrodes at the scan rate of 50 mV s<sup>-1</sup>.

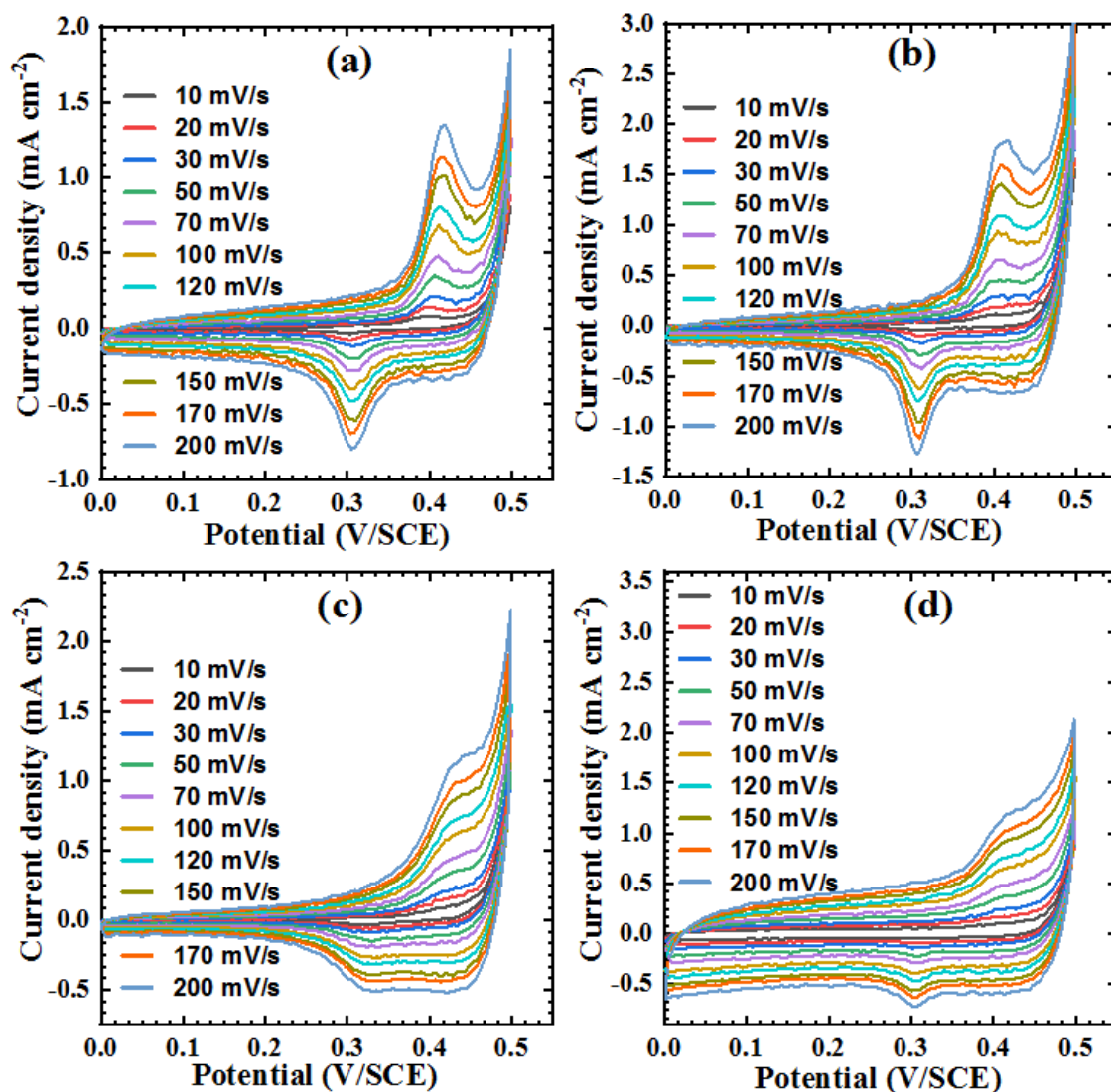


**Fig. 5.6:** CVs studies of a) La<sub>2</sub>O<sub>3</sub>, b) 1% Mn-La<sub>2</sub>O<sub>3</sub>, c) 3% Mn-La<sub>2</sub>O<sub>3</sub>, d) 5% Mn-La<sub>2</sub>O<sub>3</sub> film electrode at various scan rates (5 to 150 mV s<sup>-1</sup>) in 0.1 M NaOH solution.

It is visible that the current response of La<sub>2</sub>O<sub>3</sub> electrode is less than that of 1% Mn-La<sub>2</sub>O<sub>3</sub> electrode. Notably, 1% Mn-La<sub>2</sub>O<sub>3</sub> film electrode has the larger area enclosed by the CV curve as compared to other electrodes. This reveals that 1% Mn-La<sub>2</sub>O<sub>3</sub> improves electrochemical response compared to other electrodes. Therefore, 1% Mn-La<sub>2</sub>O<sub>3</sub> film was selected for electrocatalytic activity towards glucose.

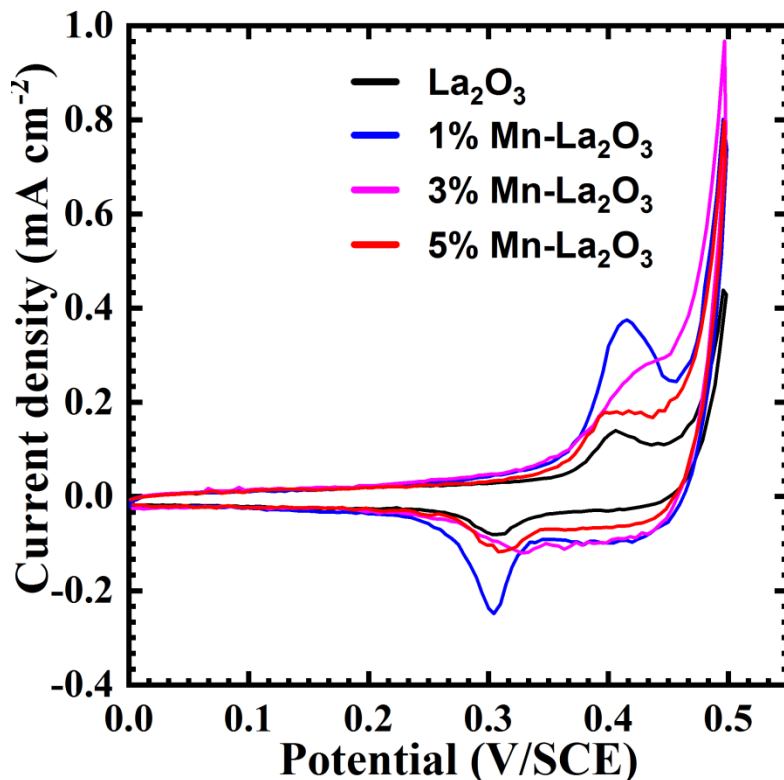


**Fig. 5.7:** The CV curves of  $\text{La}_2\text{O}_3$ , 1, 3, and 5%  $\text{Mn-La}_2\text{O}_3$  electrodes at the scan rate of  $50 \text{ mV s}^{-1}$

#### 5.4.2 Electrocatalytic activity of 1% $\text{Mn-La}_2\text{O}_3$ electrode towards glucose sensing:

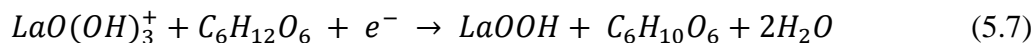
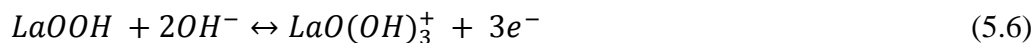
The CV study of 1%  $\text{Mn-La}_2\text{O}_3$  electrode was performed in the potential range of 0 to +0.5 V/SCE at the scan rates between 10 to  $200 \text{ mV s}^{-1}$  as showed in **Fig. 5.8a**. It is observed that, the current density increased with the increasing the potential scan rate. In that case, the area under the curve (1% Mn-doped  $\text{La}_2\text{O}_3$ ) represents the total area employed for the electrocatalytic process. In addition, **Fig. 5.8b** shows the plot of  $\log I_p$  vs.  $\log v$ . It can be explained using equation (5.4).

$$I_p = av^b \quad (5.4)$$

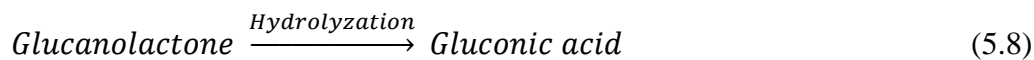
The value of  $b$  is determined from slope of  $\log I_p$  vs.  $\log v$ . In equation (5.4), ‘ $a$ ’ and ‘ $b$ ’ are the coefficients, if slope value of  $b$  is  $\sim 1$  then the maximum catalytic reactions occur on surface of the material due to the adsorption process. On the other hand, if slope

value of  $b$  is  $\sim 0.5$  then the maximum reaction mechanism is by diffusion controlled process. From the slope of graph, the value of  $b$  is 0.95 indicating maximum reaction occurred through a surface adsorption process. In that context, there is exact mechanism process for electro-oxidation of glucose on 1% Mn-La<sub>2</sub>O<sub>3</sub> electrode surface in alkaline medium. Also, deprotonation and isomerization of glucose molecule is the electro catalyzed through oxidative Mn and La ions in the electrode, resulting adsorption process and removal of glucose molecule in the bulk electrolyte trailed by the rebuilding of active sites during the negative scan [29, 30].

To determine the oxidation potential of glucose in the electrolyte, the CV curves were carried out at different glucose concentrations at the scan rate of 50 mV s<sup>-1</sup>. Current response of the electrode was increased with increasing the glucose concentration. Instead of separate electrocatalytic response from Mn<sup>2+</sup> and La<sup>3+</sup>, single oxidation and reduction peaks were observed (**Fig. 5.8c**). These observations suggest the existence of Mn elements inside the nanostructure of La<sub>2</sub>O<sub>3</sub> has shown combined electrochemistry. The possible reaction of a glucose molecule with Mn and La has been explained with the following reaction.



This phenomenon assigned for glucose oxidation to glucanolactone. Further glucanolactone converts into gluconic acid by hydrolyzing process [31]. The reaction mechanism for this process can be written as:



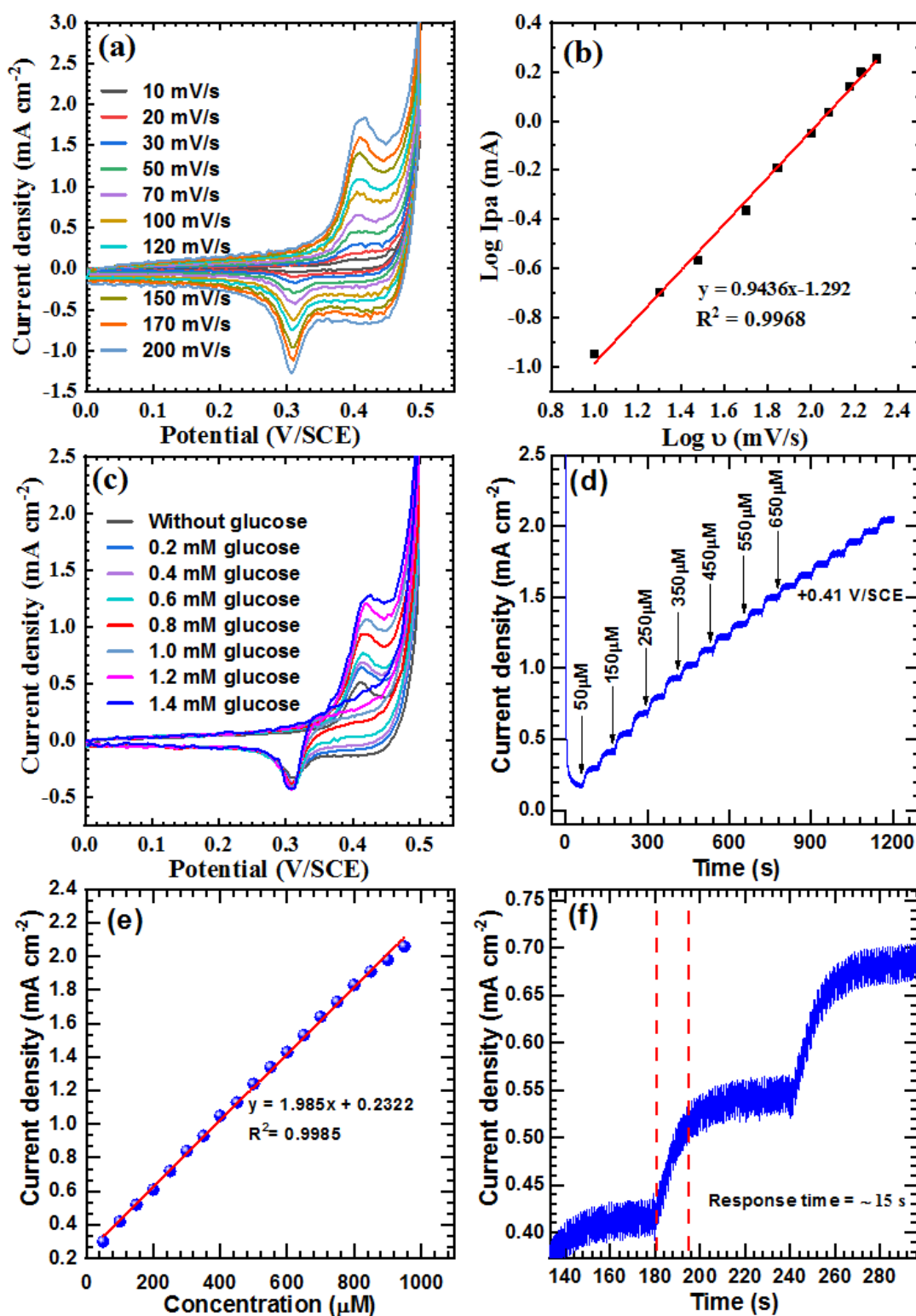


**Fig. 5.8** a) The CV curves of 1% Mn-La<sub>2</sub>O<sub>3</sub> at various scan rates (5 to 150 mV s<sup>-1</sup>), b) log I<sub>pa</sub> vs. log v (c) the CV curves in absence and presence of glucose at the fix scan rate of 50 mV s<sup>-1</sup>, d) current vs. time measurement at potential +0.41 V/SCE with successive

addition of 50  $\mu\text{M}$  of glucose in 60 s time intervals, e) calibration curve, and f) response time curve of 1% Mn-La<sub>2</sub>O<sub>3</sub> film electrode in 0.1 M NaOH electrolyte.

In addition to this, *i-t* amperometric (**Fig. 5.8d**) technique was employed to investigate catalytic response of the electrode after successive addition of glucose concentration in the range of 50 to 950  $\mu\text{M}$ . To achieving reliable and accurate steady state response. This study was performed at potential of +0.41 V/SCE on 0.1 M NaOH electrolyte under the constant stirring (310 rpm). The highly stable steady-state response is 96%. Rise in current response with increasing glucose concentration indicates that linear characteristics of electrode material towards glucose molecule.

The calibration curve for the 1% Mn-La<sub>2</sub>O<sub>3</sub> electrode is shown in **Fig.5.8e**. Linear fit of the calibration plot in the glucose concentration range of 50 to 950  $\mu\text{M}$  ( $R^2=0.9988$ ) yield that sensitivity of the glucose detection 1985  $\mu\text{A mM}^{-1} \text{ cm}^{-2}$  with LOD 32  $\mu\text{M}$ . wide linear response of 1% Mn-La<sub>2</sub>O<sub>3</sub> electrode is due to vertical sheet-like morphology which provide huge electroactive site for oxidation of glucose. The shorter response time of ~15 s was obtained for the electrode (**Fig. 5.8f**) due to combined effect of La<sup>3+</sup> and Mn<sup>2+</sup> ions.

1% Mn-La<sub>2</sub>O<sub>3</sub> electrode was investigated for long term stability as displayed in **Fig.5.9a**. The catalytic stability of the electrode was evaluated using various glucose concentrations ranging from between 0.1 to 2.0 mM for 1h. Linearity in the current response indicate negligible surface poisoning to deteriorate inefficiency in long term stability. Therefore, these films can be deemed as a promising material for enzyme-less glucose sensing application. To understand mechanism of electrocatalytic oxidation of glucose and to check the catalytic rate constant, the catalytic rate constant ( $K_{\text{cat}}$ ) was calculated using equation (5.9) [32].

$$\frac{I_{\text{cat}}}{I_L} = \pi^{\frac{1}{2}} * (K_{\text{cat}} * C * t)^{\frac{1}{2}} \quad 5.9$$

It is the slope of  $I_{\text{cat}}/I_L$  vs.  $t^{1/2}$  (**Fig. 5.9b**). The estimated  $K_{\text{cat}}$  value for 0.5, 1, 1.5, and 2 mM glucose concentration were 306, 1281, 1373 and 1936  $\text{cm}^3 \text{M}^{-1} \text{s}^{-1}$ , respectively. The exponential characteristic of the  $i$ - $t$  curve with increasing current density with the concentration of glucose appeared on the surface of the electrode due to the electrocatalytic properties of the material. **Fig. 5.9c** shows plot of  $K_{\text{cat}}$  vs. glucose concentrations. The value of  $K_{\text{cat}}$  is depends upon the amount of glucose concentrations, type and concentration of supporting electrolyte.

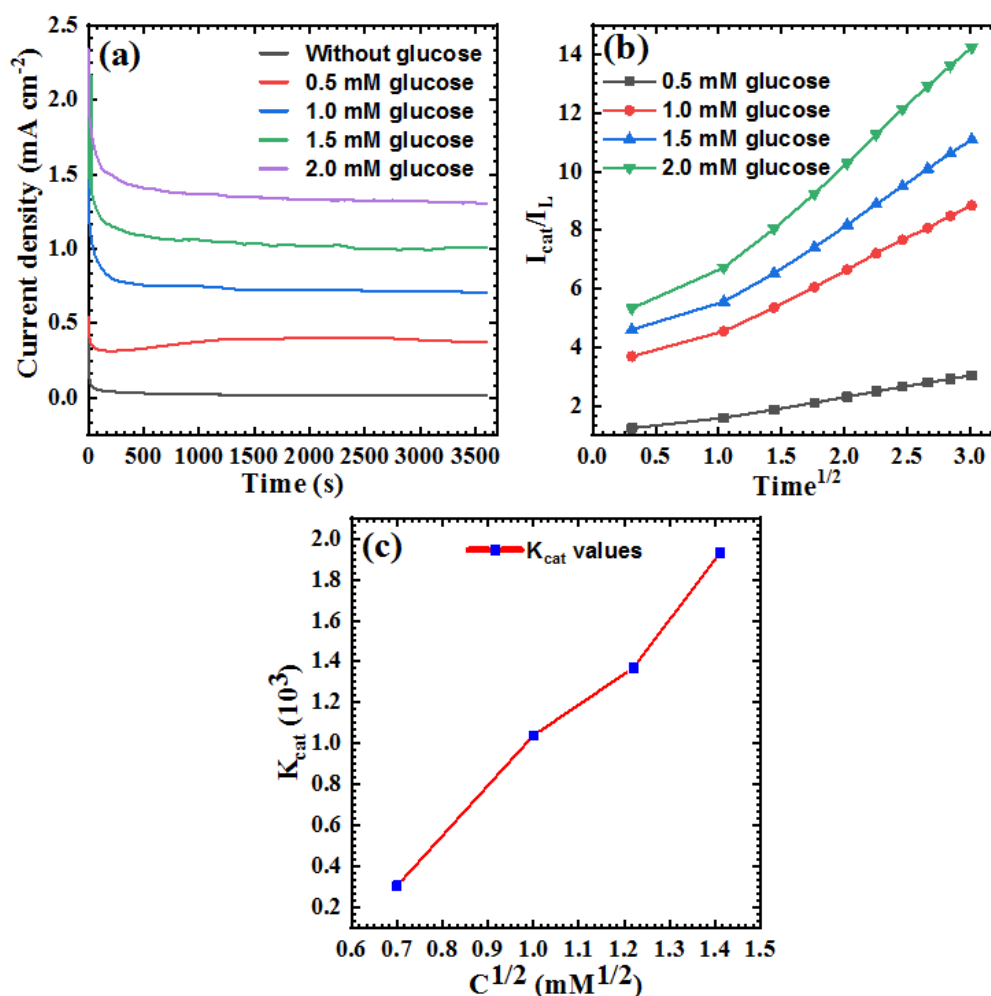


**Fig. 5.9** a)  $i$ - $t$  amperometric curve obtained at 1% Mn-La<sub>2</sub>O<sub>3</sub> film electrode in the presence of 0, 0.5, 1.0, 1.5, and 2.0 mM glucose concentrations, (b)  $I_{\text{cat}}/I_L$  vs.  $t^{1/2}$  plot obtained from  $i$ - $t$  amperometric data for 0.5, 1.0, 1.5, and 2.0 mM glucose concentrations, and (c) catalytic rate constant vs. concentration of glucose.

### 5.4.3 Selectivity, reputability and reproducibility studies of the 1% Mn-La<sub>2</sub>O<sub>3</sub> thin film electrodes:

The two important and stimulating aspects of the enzymeless glucose detection are to measure the glucose concentration from human blood serum sample and to enhance long term stability of the film electrode. Various components basically found in human serum sample that can be interfere with glucose sensing as they are strong oxidizing agents similar to glucose molecule. Such common interfering species like Fru, Lac, AA, and DA usually coexist with glucose in real samples. The selectivity was studied by adding 250  $\mu$ M of interfering species towards glucose under constant stirring. The 1% Mn-La<sub>2</sub>O<sub>3</sub> electrode reaches maximum steady state current within 15 s. Later, common interfere species of quantity 250  $\mu$ M were successively injected in solution. It showed insignificant amperometric responses for other interferent species (**Fig. 5.10a**). The result indicates good selectivity of 1% Mn-La<sub>2</sub>O<sub>3</sub> electrode for enzymeless glucose sensing application.

The long-term stability of 1% Mn-La<sub>2</sub>O<sub>3</sub> electrode over 36 days was observed with the addition of 50  $\mu$ M glucose. Current response was set to 100% on the first day and current responses were normalized to the same concentration for other days as shown in the **Fig. 5.10b**, indicates that the current response of the 1% Mn-La<sub>2</sub>O<sub>3</sub> electrodes were about 95% after 36 days suggesting that these electrodes exhibits good reliability for oxidation of glucose. Further, we prepared (1% Mn-La<sub>2</sub>O<sub>3</sub>) six electrodes at same condition and tested for glucose sensing as shown in **Fig. 5.10c**. To evaluate reproducibility of the electrodes was tested for glucose detection and corresponding relative standard deviation (RSD) of 2.6% indicates excellent reproducibility of the 1% Mn-La<sub>2</sub>O<sub>3</sub> electrode.

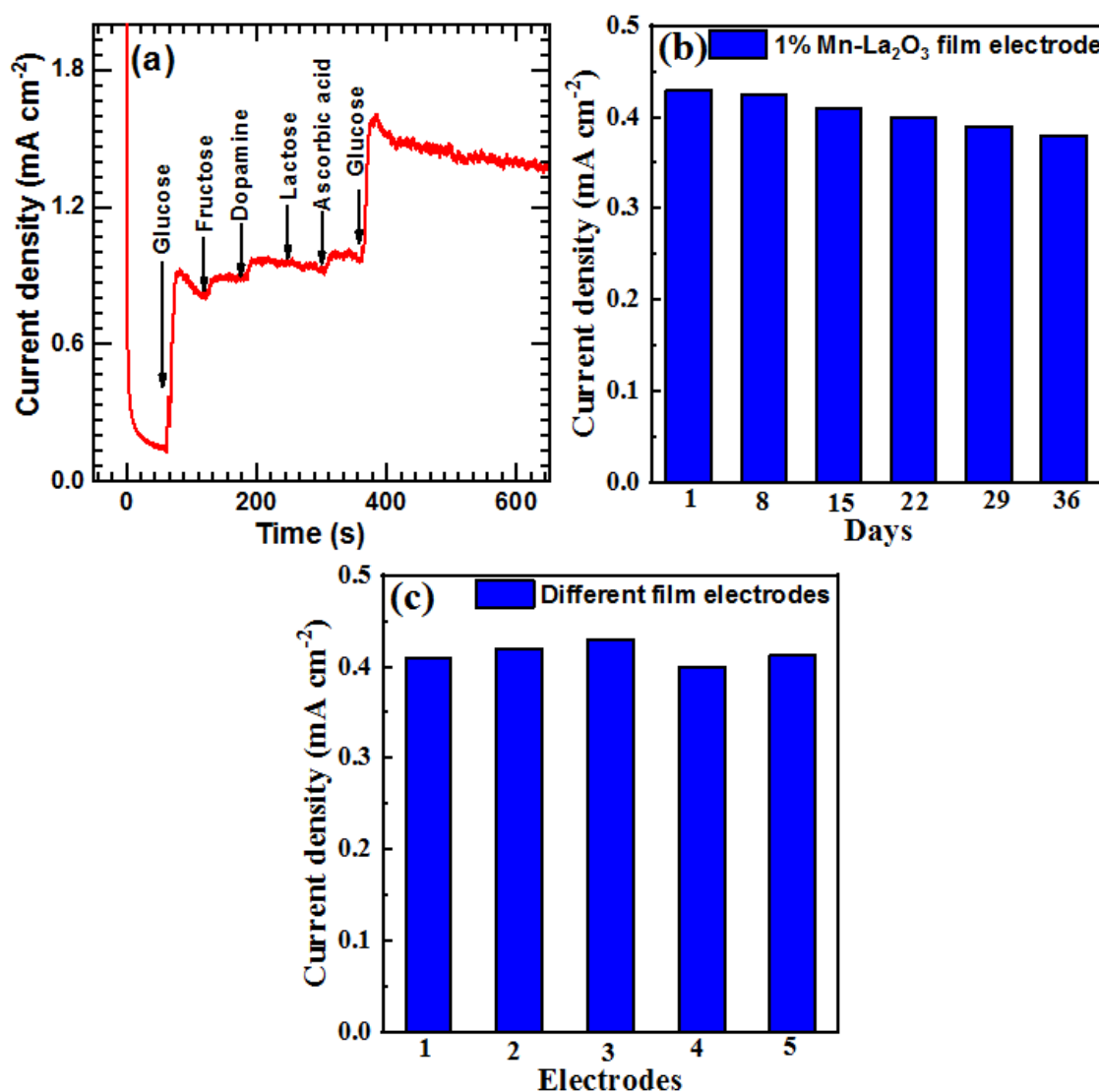


**Fig. 5.10** a) *i-t* amperometric response of 1% Mn-La<sub>2</sub>O<sub>3</sub> film electrode for successive addition of glucose and interferences, b) long term stability graph of during 36 days by adding 100  $\mu$ M glucose concentration, and c) current response at 5 different electrodes.

### 5.5 Conclusions:

We have successfully demonstrated a simple process for preparation of Mn-doped La<sub>2</sub>O<sub>3</sub> film electrodes on SS substrate using facile multipotential ED method. The multiple active sites available in 1% Mn-La<sub>2</sub>O<sub>3</sub> film lead to the enhanced electrocatalytic performance towards glucose oxidation. The catalyst showed high sensitivity of 1985  $\mu$ A

$\text{mM}^{-1} \text{cm}^{-2}$  with wide linear range of 50 to 950  $\mu\text{M}$  and LOD 32  $\mu\text{M}$ . Besides, this material shows excellent selectivity, stability and  $K_{\text{cat}}$  towards glucose oxidation. The vertically grown nanoflakes of 1% Mn- $\text{La}_2\text{O}_3$  film electrode showed remarkable catalytic resultsdetermination of glucose detection.

## 5.6 Reference:

- 1) M. Baghayeria, H. Veisi, M. Ghanei-Motlagh, Amperometric glucose biosensor based on immobilization of glucose oxidase on a magnetic glassy carbon electrode modified with a novel magnetic nanocomposite, *Sens. Actu. B: Chem.*, 249, (2017), 321-330, DOI: 10.1016/j.snb.2017.04.100.
- 2) N. Hui and J. Wang, *J. Electroanal Chem.*, 798, (2017), 9-16. DOI:10.1016/j.jelechem.2017.05.021.
- 3) J. Zhang, Y. Sun, X. Li, J. Xu, Fabrication of  $\text{NiCo}_2\text{O}_4$  nanobelt by a chemical co-precipitation method for non-enzymatic glucose electrochemical sensor application. *J. Alloys Compd*, 831, (2020) 154796, DOI: 10.1016/j.jallcom.2020.154796.
- 4) J. Zhou, L. Shi, Q. Liu, H. Zhang, X. Liu, F. Han, Z. Guo, X. Lu, J. Wang, Porous lanthanum-doped manganese oxide nanoparticles for enhanced sonodynamic cancer therapy, *part. part. syst. charact.*, 37, (2020), 1-6. DOI: 10.1002/ppsc.202000143.
- 5) N. R. Hosseini, N. M. Sammes, J. S. Chung, Manganese-doped lanthanum calcium titanate as an interconnect for flat-tubular solid oxide fuel cells, *J. Power Sources*, 245, 2014, 599-608.DOI:https://doi.org/10.1016/j.jpowsour.2013.07.010.
- 6) S. B. Jadhav, D. B. Malavekar, R. N. Bulakhe, U. M. Patil, I. In, C. D. Lokhande, P. N. Pawaskar, Dual-Functional electrodeposited vertically grown Ag- $\text{La}_2\text{O}_3$  nanoflakes for non-enzymatic glucose sensing and energy storage application. *Surf. Interfaces*, 23, (2021), 101018, DOI:10.1016/j.surfin.2021.101018.
- 7) B. M. Jaffar, H. C. Swart, H. A. A. Seed Ahmed, A. Yousif, R. E. Kroon, Stability of Bi doped  $\text{La}_2\text{O}_3$  powder phosphor and PMMA composites, *J. Phys. Chem. Solids*, 131, (2019), 156-163, DOI:10.1016/j.jpcs.2019.04.004.
- 8) R. C. Schucker, K. J. Derrickson, A. K. Ali, N. J. Caton, The Effect of Strontium Content on the Activity and Selectivity of Sr-Doped  $\text{La}_2\text{O}_3$  Catalysts in Oxidative

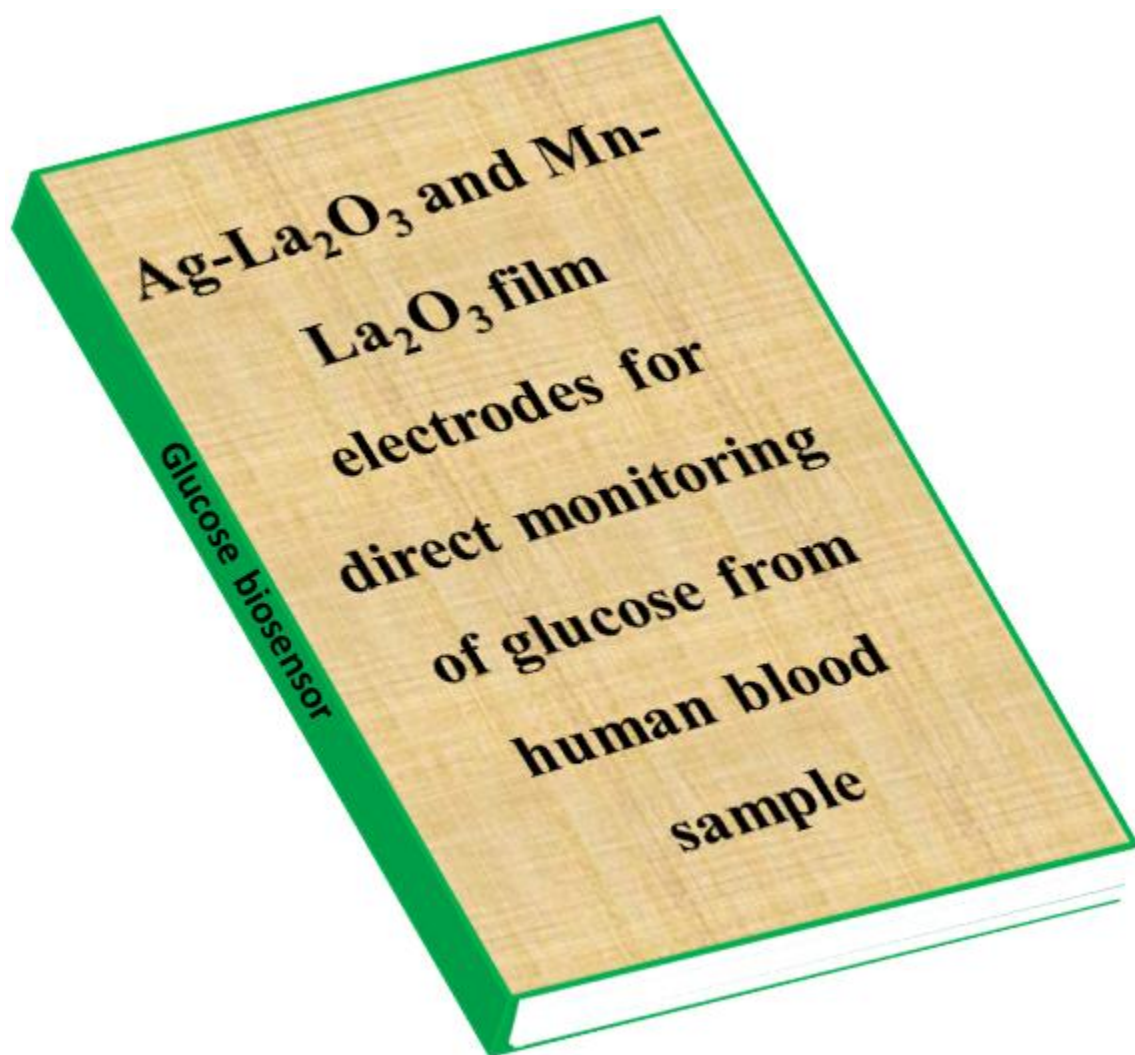
- Coupling of Methane, *Appl Catal a-gen*, 607, (2020), 117827, DOI: 10.1016/j.apcata.2020.117827.
- 9) R. Jbeli, M. Lahmar, C. Bilel, F. Saadallah, H. I. Ouzari, M. Bouaïcha, M. Amlouk, Structural and optical investigations on sprayed Co doped  $\text{La}_2\text{O}_3$  thin films along with photocatalytic and anti-bacterial applications, *Optik*, 242, (2021), 166837, DOI: 10.1016/j.ijleo.2021.166837.
- 10) Y. Yang, Y. Yu, G. Ma, J. Nan, H. Chen, Z. Zhang, W. Lin, High-performance lithium-sulfur batteries fabricated from a three-dimensional porous reduced graphene oxide/ $\text{La}_2\text{O}_3$  microboards/sulfur aerogel, *Ceram.*, 45, (2019), 9017-9024, DOI:10.1016/j.ceramint.2019.01.235.
- 11) K. Kumar Naik, A. Gangan, B. Chakraborty, S. K. Nayak, C. S. Rout, Enhanced nonenzymatic glucose-sensing properties of electrodeposited  $\text{NiCo}_2\text{O}_4$ -Pd nanosheets: experimental and DFT investigations, *ACS Appl. Mater. Interfaces*, 9, (2017), 23894-23903. DOI: 10.1021/acsami.7b02217.
- 12) S. B. Jadhav, U. M. Patil, R. N. Bulakhe, Insik In, C. D. Lokhande, P. N. Pawaskar, Vertically aligned nanosheets of an electrodeposited lanthanum oxide electrode for non-enzymatic glucose sensing application. *J. Electron Mater.*, 50, (2021), 675-685, DOI: 10.1007/s11664-020-08605-w.
- 13) M. Shaterian, M. Enhessari, D. Rabbani, M. Asghari, M. Salavati-Niasari, Synthesis, characterization and photocatalytic activity of  $\text{LaMnO}_3$  nanoparticles, *appl. Surf. Sci.*, 318, (2014), 213-217, DOI:10.1016/j.apsusc.2014.03.087.
- 14) J. Mefford, W. G. Hardin, S. Dai, K. P. Johnston, K. J. Stevenson, Anion charge storage through oxygen intercalation in  $\text{LaMnO}_3$  perovskite pseudocapacitor electrodes, *nature materials*, 13, (2014), 726-732, DOI: 10.1038/NMAT4000.
- 15) A. Ashok, A. Kumar, J. Ponraj, S. A. Mansour, F. Tarlochan, Enhancing the electrocatalytic properties of  $\text{LaMnO}_3$  by tuning surface oxygen deficiency through salt assisted combustion synthesis, *Catal.*, (2020), DOI: 10.1016/j.cattod.2020.05.065.
- 16) V. J. Mane, D. B. Malavekar, S. B. Ubale, R. N. Bulakhe, Insik In, C. D. Lokhande. Binder free lanthanum doped manganese oxide@graphene oxide composite as high energy density electrode material for flexible symmetric solid state supercapacitor. *Electrochim. Acta*, 335, (2020), 135613, DOI: 10.1016/j.electacta.2020.135613.

- 17) R. Manivannan, S. N. Victoria, Preparation of chalcogenide thin films using electrodeposition method for solar cell applications - A review, *J. Sol. Energy*, 173, (2018), 1144-1157, DOI:10.1016/j.solener.2018.08.057.
- 18) K. S. Anuratha, S. Mohan, S. K. Panda, Pulse reverse electrodeposited  $\text{NiCo}_2\text{S}_4$  nanostructures as efficient counter electrodes for dye-sensitized solar cells, *New j. chem.*, 40, (2016), 1785-1791. DOI: 10.1039/C5NJ02565F.
- 19) Q. S. Jiang, W. Cheng, W. Li, Z. Yang, Y. Zhang, R. Ji, X. Yang, Y. Ju, Y. Yu, One-step electrodeposition of amorphous nickel cobalt sulfides on FTO for high-efficiency dye-sensitized solar cells, *Mater. Res. Bull.*, 114, (2019), 10-17. DOI: 10.1016/j.materresbull.2019.01.025.
- 20) I. Shackery, U. Patil, A. Pezeshki, N. M. Shinde, S. Im, S. C. Jun, Enhanced Non-enzymatic amperometric sensing of glucose using  $\text{Co}(\text{OH})_2$  nanorods deposited on a three dimensional graphene network as an electrode material, *Microchem. Acta*. 183, (2016), 2473-2479. DOI: 10.1007/s00604-016-1890-8.
- 21) T. Sasaki, Y. Matsumoto, J. Hombo, Y. Ogawa. A new preparation method of  $\text{LaMnO}_3$  perovskite using electrochemical oxidation, *J. Sol. State Chem.* (1991), 91, 61-70. DOI: 10.1016/0022-4596(91)90058-P.
- 22) G. H. A. Therese and P. V. Kamath. Electrochemical Synthesis of  $\text{LaMnO}_3$  Coatings on Conducting Substrates, *Chem. Mater.*, 10, (1998), 3364-3367, DOI: 10.1021/cm980046f.
- 23) S. B. Jadhav, D. B. Malavekar, S. B. Kale, S. R. Sabale, U. M. Patil, C. D. Lokhande, P. N. Pawaskar, Reliable glucose sensing properties of electrodeposited vertically aligned manganese oxide thin film electrode, *Appl. Phys. A.*, 127, 391 (2021). DOI:10.1007/s00339-021-04544-3.
- 24) K. N. Patel, M. P. Deshpande, K. Chauhan, P. Rajput, V. P. Gujarati, S. Pandya, V. Sathe, S. H. Chaki. Effect of Mn doping concentration on structural, vibrational and magnetic properties of  $\text{NiO}$  nanoparticles, *Adv Powder Technol*, 29, (2018), 2394-2403. DOI:10.1016/j.appt.2018.06.018.
- 25) P. Mallicka, Chandana Rath, A. Rath, A. Banerjee, N. C. Mishra, Antiferro to superparamagnetic transition on Mn doping in  $\text{NiO}$ , *Solid State Commun.*, 150, (2010), 1342-1345, DOI:10.1016/j.ssc.2010.05.003.

- 
- 26) J. Wei, B. Liang, Q. Cao, C. Mo, Y. Zheng, X. Ye, Vertically aligned PANI nanorod arrays grown on graphene oxide nanosheets for a high-performance  $\text{NH}_3$  gas sensor, *RSC Adv*, 7, (2017), 33510-33520, DOI: 10.1039/C7RA04636G.
- 27) J. Zhang, Z. Zhang, Y. Jiao, H. Yang, Y. Li, J. Zhang, P. Gao, The graphene/lanthanum oxide nanocomposites as electrode materials of supercapacitor, *J. power sources*, 419, (2019), 99-105, DOI: 10.1016/j.jpowsour.2019.02.059.
- 28) M. Miah, S. Bhattacharya, D. Dinda, S. K. Saha, Temperature dependent supercapacitive performance in  $\text{La}_2\text{O}_3$  nano sheet decorated reduce graphene oxide, *Electrochem. Acta*, 260, (2018), 449-458, DOI: 10.1016/j.electacta.2017.12.098.
- 29) D. B. Malavekar, V. C. Lokhande, V. J. Mane, S. B. Ubale, U. M. Patil, C. D. Lokhande, Enhanced energy density of flexible asymmetric solid state supercapacitor device fabricated with amorphous thin film electrode materials, *J Phys Chem Solids*, 141, (2020), 109425, DOI:10.1016/j.jpcs.2020.109425.
- 30) N. Padmanathan, H. Shao, K. M. Razeeb, Multifunctional nickel phosphate nano/micro flakes 3D electrode for ,electrochemical energy storage, non-enzymatic glucose and sweat pH sensors, *ACS Appl. Mater. Interfaces*, (2018), 10, 8599-8610, DOI:10.1021/acsami.7b17187.
- 31) L. Zhang, Y. Ding, R. Li, C. Ye, G. Zhao, Y. Wang, Ni-based metal-organic framework derived Ni@C nanosheets on Ni foam substrate as a supersensitive non-enzymatic glucose sensor, *J. Mater. Chem. B.*, 5, (2017), 5549-5555, DOI: 10.1039/c7tb01363a.
- 32) P. Kanyong, S. Rawlinson, J. Davis, Fabrication and electrochemical characterization of polydopamineredox polymer modified screen-printed carbon electrode for the detection of guanine, *Sens. Actu. B: Chem.*, 233, (2016) 528-534, DOI:10.1016/j.snb.2016.04.099.



# CHAPTER VI



## Index

Sr. No.	Details	Page No.
6.1	Introduction	141
6.2	Experimental	142
6.3	Real sample analysis	142
6.4	Conclusions	146
6.5	References	147

## 6.1 Introduction:

Glucose is a principle energy source even for the brain and human body and called simple monosaccharide sugar. Carbohydrates present in the foods are all ultimately broken do to glucose in the body [1]. If any person is looking to manage his blood glucose level, then it becomes more important to compare his intake of both sugar and carbohydrate. Low blood glucose level leads to hunger, anxiety, and confusion. In other side, high blood glucose can lead to increased fatigue, thirst, and blurred vision. Diabetes is generally called a chronic disease that can be destructive to human health, social, and economic consequences. In the human body, D-glucose is important for its role in metabolic homeostasis; it takes action as stimulate in living systems and also maintains functioning of the human body properly when consumed or by the way of formation other essential saccharides by biosynthesis technique [2]. When stimulate by human cells, glucose can be broken down (glycolysis) to yield energy and it is converted into other metabolites such as metabolic intermediates to form cellulose and starch over all by biosynthesis to function properly. In human beings, apart from existing in free form, glucose molecules covalently link to the lipids (glycolipids) and proteins (glycoproteins) and also with another biological molecule as glycol-conjugates, which have crucial role in structure components of cell membranes and are mostly involved in the structure of intercellular recognition [3, 4]. Non-enzymatic glucose sensing with nanostructured Ag-La<sub>2</sub>O<sub>3</sub> film electrode have a longer lifetime than enzymatic glucose sensing electrodes as they do not contain biological component. To improve the efficiency, durability and reusable capacity of the glucose diagnosing electrodes by reducing its complications and alleviate its symptoms all through appropriate medications while monitoring glucose of the blood sample, to deal with decisions to control glucose [5]. Here, with above aim

said, we have attempted to develop Ag-La<sub>2</sub>O<sub>3</sub> and Mn-La<sub>2</sub>O<sub>3</sub> thin film electrode for glucose sensing. Ag-La<sub>2</sub>O<sub>3</sub> and Mn-La<sub>2</sub>O<sub>3</sub> thin film electrodes were successfully used to determine glucose detection of the real human blood sample.

### 6.2 Experimental:

Detailed preparation, characterization and glucose sensing of Ag-La<sub>2</sub>O<sub>3</sub> and Mn-La<sub>2</sub>O<sub>3</sub> thin film electrodes are presented in chapter IV and chapter V respectively.

The human blood samples were collected from D Y Patil Hospital and Research Centre, Kolhapur. These samples were stored in the blood bulb tube containing sodium fluoride. Sodium fluoride stabilizes the whole blood glucose molecule, and is widely used as a preservative for glucose in blood samples. Blood samples were taken in the range of 60 to 300 mg/dl and used within 30 min for the detection of glucose.

### 6.3 Real sample analysis:

Glucose sensing experiments using human blood samples have been carried out using VersaSTAT electrochemical workstation that provides more reliable detailed *i-t* amperometry data. Six different human blood samples were collected randomly from the blood bank in Kolhapur and glucose level was checked from the commercial glucometer. We have taken blood samples from diabetes patient with glucose levels ranging from 90-300 mg/dL. Both sets of units (mg/dL and mmol/L) are used to measure the blood sugar levels and also both give a measurement of the concentration of glucose in the blood samples, albeit in faintly different ways. mmol/L unit gives the molarity that is the number of glucose molecules of a substance within a specified volume within 1 litre. mg/dL unit gives the concentration by the weight to volume ratio, in this case milligrams per decilitre. The unit of mmol/L is mostly common used measurement in UK, and mg/dL is largely used in USA and in other European countries.

Essential experimental requirements are glass cells, three-electrode systems with reference, counter and working electrodes, hand gloves, micropipette, and magnetic stirrers.

The Ag-La<sub>2</sub>O<sub>3</sub> and Mn-La<sub>2</sub>O<sub>3</sub> film electrodes were employed to monitor the glucose level present in the human blood samples.

Detail experimental procedure is given below:

- 1) The human blood samples (2 mL) collected from blood bank (D Y Patil Hospital and research centre Kolhapur with institutional ethical permission).
- 2) These samples were stored in regular fridge machine and temperature was maintained at 4°C.
- 3) *i-t* amperometry technique was selected during the detection of glucose present in human blood sample.
- 4) Three electrode system was connected to the counter, reference and working electrodes.
- 5) 50  $\mu$ L of blood samples was added in 40 mL of 0.1 M NaOH electrolyte and current responses of Ag-La<sub>2</sub>O<sub>3</sub> and Mn-La<sub>2</sub>O<sub>3</sub> electrode at +0.43 and +0.41 V/SCE, respectively were recorded
- 6) Glucose sensing experiment was carried out from whole blood at oxidation potentials of Ag-La<sub>2</sub>O<sub>3</sub> and Mn-La<sub>2</sub>O<sub>3</sub> film electrodes with constant stirring (310 rpm).
- 7) The *i-t* amperometric experiment was performed without blood in supporting electrolyte.
- 8) Then, *i-t* amperometric experiment was performed with blood measure the actual current of the glucose during oxidation.

- 9) After experiment, the difference in current response with and without blood was calibrated and compared with commercial glucometer.

The above experimental procedure was carried out for both electrodes in whole human blood samples. Figs. 6.1A, B, C, D, E, and F show  $i-t$  curves of both electrodes with and without blood sample, as a result both electrodes exhibiting different current responses. The difference in current response was measured in terms of current density and calibrated for further analysis.

Lower as well as higher glucose concentrations, Ag-La<sub>2</sub>O<sub>3</sub> and Mn-La<sub>2</sub>O<sub>3</sub> film electrodes showed similar magnitude of current response for the human blood samples. With 50  $\mu$ L blood sample in the supporting electrolyte, only glucose molecules was dissociated and also that the converted into the gluconolactone because of the oxidation of glucose molecules and reduction of ions, glucose molecules was detection by the electrode materials. The redox of lanthanum and glucose molecule from the human samples occurs simultaneously in the working potential. The rate of oxidation of lanthanum ions presents on the film electrode surface determines the rate of detection of glucose. However, the detection of glucose molecules is a intrinsic electrochemical properties of the material and the rate of detection of glucose molecules present in the human samples can be enhanced by engineering of surface morphology, designing of composite material, electrolyte and conducting substrate.

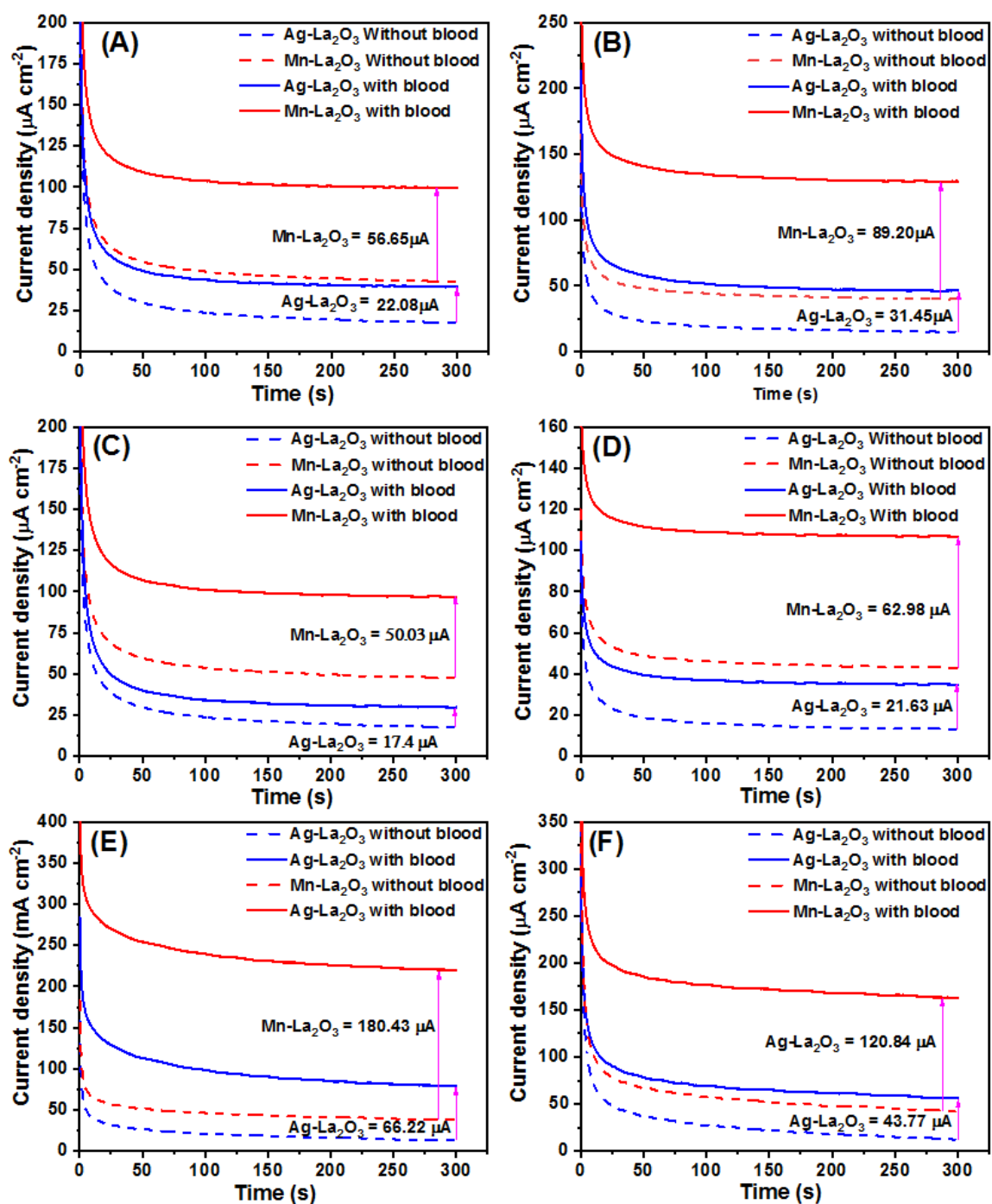


**Figure 6.1** The *i-t* amperometry plots of with and without blood samples. A, B, C, D, E, and F are the different human blood samples tested in 0.1M NaOH electrolyte.

From above results, we concluded that the different human blood samples are a very well distinguished by the sensor. The Ag-La<sub>2</sub>O<sub>3</sub> and Mn-La<sub>2</sub>O<sub>3</sub> film electrodes displayed efficient glucose sensing with good recovery. Statistical data is presented here

to analysis of glucose concentration along with current response to compare with prepared electrodes and commercial glucometer as shown in **table number 6.1**. The statistical data was taken from above *i-t* amperometric graphs.

**Table 6.1:** The statistical data of successive addition of pure glucose and human samples

Sr. No.	samples	Glucometer readings (mg/dl)	Ag-La <sub>2</sub> O <sub>3</sub> electrode					
			Observed current (μA)	(mg/dl)/ μA	Mean	calculated readings (mg/dl)	Recovery (%)	
1	A	74	22.08	3.35	3.58	79	106	
2	B	115	31.45	3.65		112	97	
3	C	65	17.4	3.73		62	95	
4	D	80	21.63	3.69		77	96	
5	E	234	66.22	3.53		237	101	
6	F	156	43.77	3.56		156	100	
			Mn-La <sub>2</sub> O <sub>3</sub> electrode					
1	A	74	56.65	1.30	1.29	73	98	
2	B	115	89.20	1.28		115	100	
3	C	65	50.03	1.29		64	98	
4	D	80	62.98	1.27		81	101	
5	E	234	180.43	1.29		233	99	
6	F	156	120.84	1.29		156	100	

The analytical results, recovery of six samples examined by Ag-La<sub>2</sub>O<sub>3</sub> and Mn-La<sub>2</sub>O<sub>3</sub> electrodes in the range of 106 to 95 % and 101 to 98 %, respectively, were presented above table. The non-enzymatic glucose sensors based on Mn-La<sub>2</sub>O<sub>3</sub> electrodes have shown highest sensitivity and efficient sensing performance with good recovery for glucose oxidation than Ag-La<sub>2</sub>O<sub>3</sub> electrode.

#### 6.4 Conclusions:

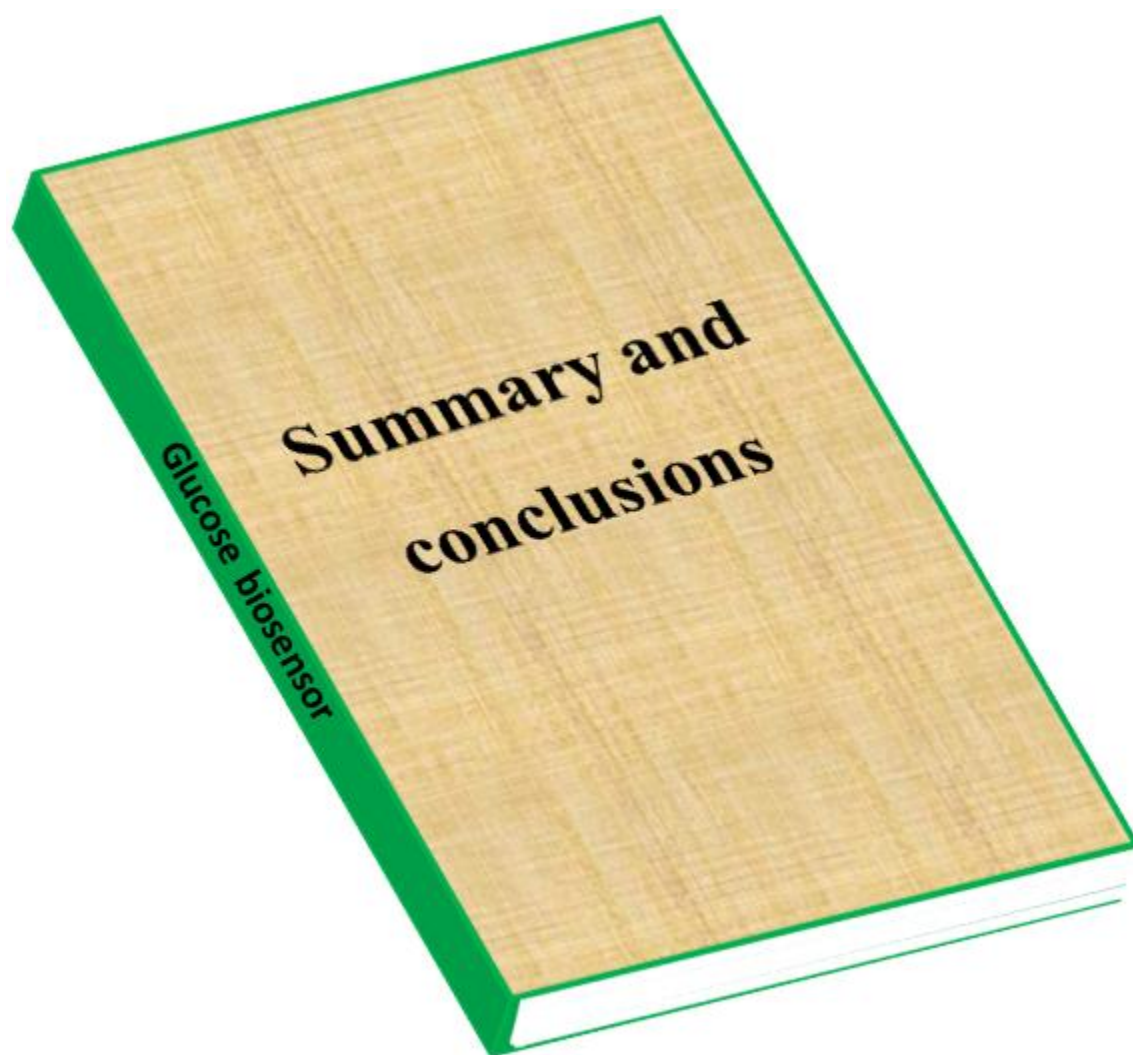
In this present work, synthesized Ag-La<sub>2</sub>O<sub>3</sub> and Mn-La<sub>2</sub>O<sub>3</sub> were investigated for glucose detection present in the human blood sample for the first time. The surface texture of the electrode is highly active in basic media. It is also proved that, the glucose present in the real blood sample measured using *i-t* amperometric technique and obtained

data accuracy is comparable with the data provided by commercial glucometer. These results emphasize the possibility of innovative development of commercial glucose sensor by using Ag-  $\text{La}_2\text{O}_3$  and Mn- $\text{La}_2\text{O}_3$  electrodes at reduced cost with renewable surface. In addition, Ag-  $\text{La}_2\text{O}_3$  and Mn- $\text{La}_2\text{O}_3$  electrodes work as the backbone in enhancing sensing performance. The fabrication method is simple, cheaper and easily constructed using inexpensive protocols and chemicals and can be produced in large quantity.

### 6.5 References:

- 1) E. W. Nery, M. Kundys, P. S. Jelen, M. J. Niedziolka, Electrochemical glucose sensing -is there still room for improvement?, *Anal. Chem*, 88, 2016, 11271-11282 DOI: 10.1021/acs.analchem.6b03151.
- 2) E. Sehit and Z. Altintas, Significance of nanomaterials in electrochemical glucose sensors: An updated review (2016-2020), *Biosens. Bioelectron*, 159, 2020, 112165, DOI:10.1016/j.bios.2020.112165.
- 3) Brown WH, Foote CS. *Organic Chemistry*. 2<sup>nd</sup> ed. Fort Worth: Sanders College Publishing; 1998.
- 4) H. -C and Wang, A. -R. Lee, Recent developments in blood glucose sensors, *J Food Drug Anal*, 23, 2015, 191-200, DOI: 10.1016/j.jfda.2014.12.001.
- 5) S. A. Zaidi and J. H. Shin, Recent developments in nanostructure based electrochemical glucose sensors, *Talanta*, 149, 2016, 30-42. DOI:10.1016/j.talanta.2015.11.033.

# CHAPTER VII





**Summary and conclusion of the Research Work:**

In the present scenario, the numbers of diabetic patients are constantly increasing worldwide. This disease is harmful for human body that damages some body parts revealing to require regular monitoring for which glucose oxidase based sensor strips are being used. The increase monitoring cost is very high. In order to reduce this cost, the new development of non-enzymatic glucose sensors with reusable, highly sensitive and selective properties are being essential. The many researchers and scientist in the field of science technology and industry is now focused on non-enzymatic glucose sensing devices which develops it a rising star in the high sensitivity and stability.

The extensively developed with restricted nature of the present one time usable glucose sensors strips have drawbacks in their usage. This demands synthesis of easily portable, flexible and reusable miniature sized glucose sensing strips. With this focus, we aimed to synthesis reusable, easily portable, non-enzymatic, low cost and environmentally stable glucose sensing strips. The flexible nature of enzymeless strips eliminates the problem that arises due to the bulky nature of enzymatic glucose sensing strips. Hence, the important aspect in synthesizing the flexible enzymeless glucose sensing strips needs improvement in sensitivity, wide linear range, quick response time, LOD and performance without affecting its other electrochemical features. These crucial requirements of non-enzymatic electrochemical glucose sensor requires development of competent electrode material with highly stable and good conductivity, that can enhance easily electron transfer rate in the electrochemical reaction process with long term durability. Along with electrode material properties, the alkaline electrolyte has the considerable effective role in between the working and counter electrode surface that leads to better enzymeless electrochemical glucose sensing performance.

The aim of the present perceptive research work is to synthesis  $\text{La}_2\text{O}_3$  thin films using simple electrodeposition method. Then, the synthesized  $\text{Ag-La}_2\text{O}_3$  thin films to enhance the properties of the pristine  $\text{La}_2\text{O}_3$  film electrode material by facile electrodeposition method on conducting (stainless steel) substrate. This is followed by the synthesis of  $\text{Mn-La}_2\text{O}_3$  thin films to upraise the pristine  $\text{La}_2\text{O}_3$  electrode material by the newly developed multipotential electrodeposition method. Synthesized well adherent, good quality and binder-free thin films will be characterized by various physico-chemical methods. The best performing thin film electrodes from the above mentioned ones then were used for the analysis of glucose present in real human blood sample in freshly prepared 0.1 M NaOH electrolyte. The present thesis work is systematically described in six chapters.

**Chapter I:** In this chapter, we have discussed with the general introduction to chronological improvement in glucose sensors families and then followed by the need of improvement in enzymeless glucose sensor electrode material in the recent research. Present developments and working principle of glucose sensors, also the glucose sensing properties based on sensitivity and selectivity are discussed. It is seen that, the enzymeless electrochemical glucose sensing performance can be achieved by synthesizing innovative active electrode materials with peculiar electrochemical glucose sensing properties. The desired electrochemical glucose sensing properties of the material are successfully discussed in detail. Furthermore, chapter consists a literature survey of transition metal oxides based composites and doping materials used for enzymeless glucose sensing application. Finally the scope and purpose of dissertation is described.

**Chapter II:** This chapter begins with the basic introduction of thin film electrode with deep discussion of their properties. Simple electrodeposition method with their different

types of deposition techniques and deposition mechanism is discussed. As well theoretical background of electrodeposition method with various preparative parameters and their advantages are briefly explained. The working principles of characterization techniques used for thin film analysis such as XRD for structural analysis, FE-SEM for surface morphological study and EDS for elemental mapping and XPS for elemental analysis are given in this chapter. Also, the electrochemical technique used for the electrochemical performance evaluation of electrode material such as CV, and *i-t* amperometry study with their features are discussed in detail.

**Chapter III:** This chapter deals with basic introduction, synthesis, characterization and non-enzymatic electrochemical performance evaluation of electrodeposited  $\text{La}_2\text{O}_3$  thin films. This chapter explains synthesis of  $\text{La}_2\text{O}_3$  thin films by electrodeposition method. The highly conducting and stable SS substrate in acid/base solution was selected for the deposition. The  $\text{La}_2\text{O}_3$  was directly grown on SS substrate by electrodeposition method. The deposited  $\text{La}_2\text{O}_3$  thin films were characterized by various characterization techniques. The XRD analysis confirms deposition of  $\text{La}_2\text{O}_3$  material with monoclinic phase in thin film form. The lanthanum and oxygen elements were detected and successfully confirmed by XPS study. The lanthanum and oxygen molar content influences the morphology of thin film form in nanosheets like structure and EDS analysis confirms expected molar ratio of lanthanum and oxygen in the samples.

Three electrode system was used for the enzymeless glucose sensing performance evaluation. The glucose sensing electrochemical performance evaluation of electrodeposited  $\text{La}_2\text{O}_3$  thin films was studied. The current response was linear at low concentration from 1.25 to 3.75 mM with high sensitivity of  $616 \mu\text{A mM}^{-1} \text{cm}^{-2}$  and a low detection limit (LOD) of 0.27 mM with correlation coefficient of 0.9924 was obtained.

Fabrication of this binder free electrode was simple and has the characteristic features of faster response time (less than 1 second), highly stable, reusable, better sensitive and excellent selective for enzymeless glucose sensing in alkaline media. Observed linear range was 1.2 mM to 11.25 mM (converted into dynamic range 21.6 to 202.5 mg/dl), which was the diagnostic range required for screening the hypo and hyperglycemic glucose level without enzyme. The good non-enzymatic electrochemical glucose sensing results concluded that, nanosheets-like structure of  $\text{La}_2\text{O}_3$  thin film offers a large number of channels for easy ion penetration and charge transportation.

**Chapter IV:** This chapter deals with study of synthesis, characterization and non-enzymatic electrochemical performance evaluation of electrodeposited Ag- $\text{La}_2\text{O}_3$  thin film electrodes. The electrodeposited Ag- $\text{La}_2\text{O}_3$  thin films were used for non-enzymatic glucose sensing study. The XRD, BET, XPS, FE-SEM, EDS and elemental mapping analysis were used for confirmation of prepared material. Nanocrystalline nature of Ag- $\text{La}_2\text{O}_3$  thin film electrode was observed in XRD analysis. The vertically aligned nanoflakes like morphology and expected elemental composition were observed from FE-SEM and EDX study respectively. The silver ions enhance the active surface area which influences sensitivity increment. The non-enzymatic glucose sensing electrochemical performance evolution of electrodeposited Ag- $\text{La}_2\text{O}_3$  film electrode was detected in 0.1 M NaOH electrolyte. The high sensitivity value of 1677 and 1022  $\mu\text{A mM}^{-1} \text{ cm}^{-2}$  by silver doped lanthanum oxide film electrode with multi linear response towards glucose in the range of 100  $\mu\text{M}$  to 600  $\mu\text{M}$  and 600  $\mu\text{M}$  to 1.6 mM was exhibited respectively. The enhanced electrical conductivity, surface area and improved sensing performance are due to Ag composite and vertically grown Ag- $\text{La}_2\text{O}_3$  nanoflakes form film electrode. As the thickness of shell layer in the nanoregion results with active

surface area which can provide more reactive sites for redox reaction and electrocatalytic activity.

**Chapter V:** This chapter deals with the study of non-enzymatic glucose sensing application of Mn-La<sub>2</sub>O<sub>3</sub> film electrode synthesized by multipotential electrodeposition method for different variation of manganese concentration. XRD, FE-SEM, EDX and XPS analysis of Mn-La<sub>2</sub>O<sub>3</sub> film electrode was discussed in detail. Mn-La<sub>2</sub>O<sub>3</sub> film electrode exhibited range of glucose concentration detection in between 50 to 950  $\mu$ M ( $R^2=0.9476$ ) and glucose sensitivity detection was about 1985  $\mu$ A mM<sup>-1</sup> cm<sup>-2</sup> with a LOD 32  $\mu$ M. Manganese ions in the La<sub>2</sub>O<sub>3</sub> electrode material promotes to enhance better electrocatalytic performance and also as manganese element is one of the most promising nanomaterial due to its unique combination of multi valence property leads to most essential characteristics such as thermal stability and good electrical conductivity.

**Chapter VI:** This chapter deals with study of glucose detection from present in the human sample by using simple *i-t* amperometric technique. We have taken six human blood samples from various persons. These samples were collected from D Y Patil Hospital and Research Centre, Kolhapur. The percentage of glucose present in the human blood samples was measured by commercial glucometers in the unit of mg/dl. Also, the measurement of glucose from human sample was carried out by addition of 50  $\mu$ L of whole blood in 40 mL of 0.1M NaOH electrolyte for comparison. These statistical results emphasizes the possibility of innovative development of commercial glucose sensor by using Ag-La<sub>2</sub>O<sub>3</sub> and Mn-La<sub>2</sub>O<sub>3</sub> film electrodes. In that regards Mn-La<sub>2</sub>O<sub>3</sub> electrode exhibits high sensitivity with nearly equal glucose concentration from human blood sample than Ag-La<sub>2</sub>O<sub>3</sub> electrode. Therefore, the electrodeposited Mn-La<sub>2</sub>O<sub>3</sub> film

electrode can be used for strip fabrication process. Metal oxide based thin film electrodes was compared with our electrodes and summarized in **Table 7.1**.

**Table 7.1** Metal oxide based electrodes for non-enzymatic glucose sensing application

Film electrodes	Sensitivity ( $\mu\text{AmM}^{-1}\text{cm}^{-2}$ )	Linear range (mM)	LOD ( $\mu\text{M}$ )	potential (+V)	Ref.
Ni/ZnO	824.34	0.001 -8.1	0.28	0.50	1
NiO/Pt	668.2	0.05-5.66	0.2	0.6	2
CoO/r-GOPE	1210	0.040 - 4	1.4	0.45	3
NiCo <sub>2</sub> O <sub>4</sub>	387.1	0.01 - 21	1	0.45	4
Cu <sub>x</sub> O/Cu	1210	0.01 - 7	10	0.6	5
CuO <sub>x</sub> -CoO <sub>x</sub>	507	0.005 -0.570	0.5	0.5	6
NiO	1323	0.0025-1.10	0.32	0.6	7
IrO <sub>2</sub> @NiO	1439.4	0.005-2.5	0.31	0.35	8
NiO/CeO <sub>2</sub>	154.4	0.001-2.9	1.0	0.6	9
ZnCo <sub>2</sub> O <sub>4</sub>	436.1	0.01-0.55	5	0.55	10
Mn <sub>2</sub> O <sub>3</sub> /NiCo <sub>2</sub> O <sub>4</sub>	956	0.01-0.15	35	0.7	11
<b>La<sub>2</sub>O<sub>3</sub></b>	<b>616</b>	<b>1.25-11.25</b>	<b>270</b>	<b>0.43</b>	This work
<b>Ag-La<sub>2</sub>O<sub>3</sub></b>	<b>1677</b>	<b>0.1-1.6</b>	<b>0.62</b>	<b>0.43</b>	
<b>Mn-La<sub>2</sub>O<sub>3</sub></b>	<b>1985</b>	<b>0.05-0.95</b>	<b>32</b>	<b>0.41</b>	

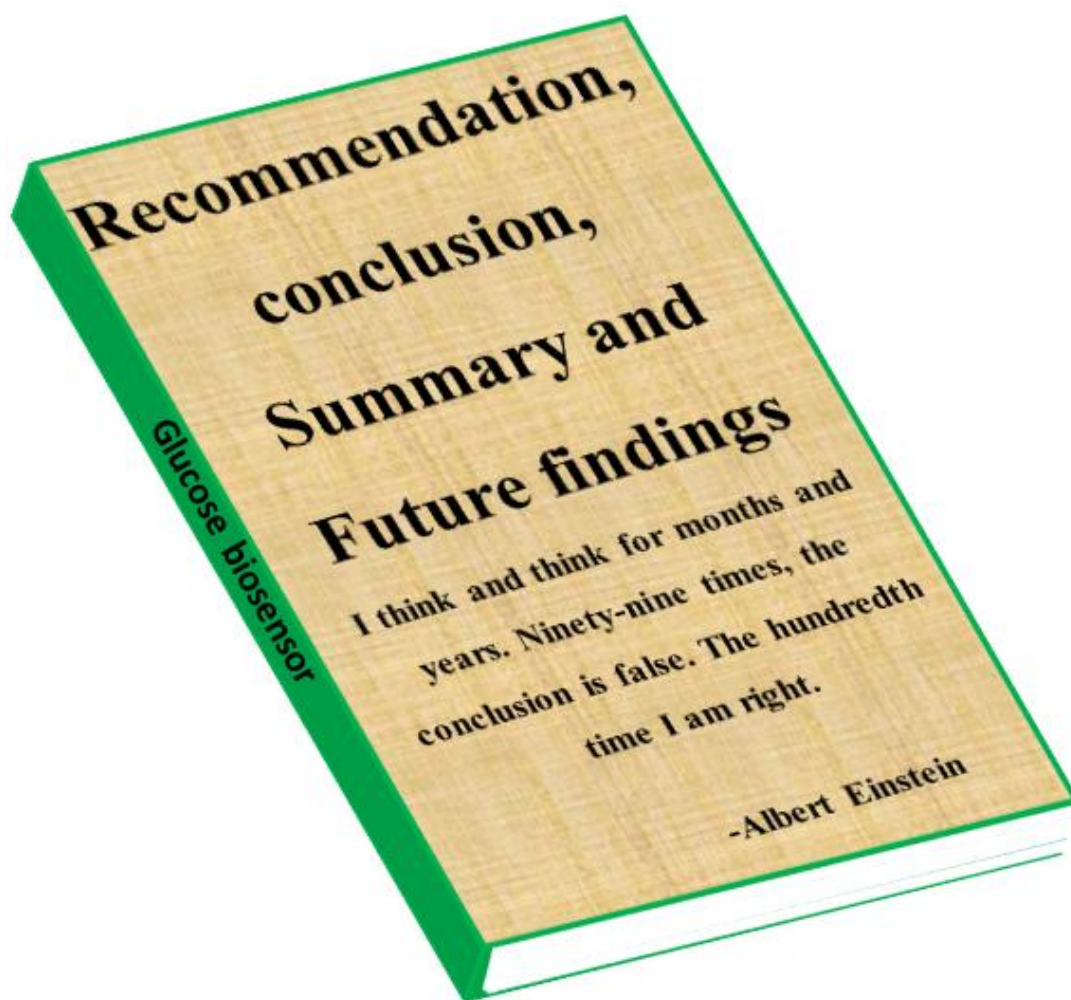
### References:

1. Y. Yang, Y. Wang, X. Bao, H. Li, Electrochemical deposition of Ni nanoparticles decorated ZnO hexagonal prisms as an effective platform for non-enzymatic detection of glucose, J. Electroanal. Chem., 775, (2016), 163-170.
2. Li, M.; Bo, X.; Mu, Z.; Zhang, Y.; Guo, L., Electrodeposition of nickel oxide and platinum nanoparticles on electrochemically reduced graphene oxide film as a nonenzymatic glucose sensor. Sens. Actuators B: Chem., 192, (2014), 261-268.
3. H. Heidari, and E. Habibi, Amperometric enzyme-free glucose sensor based on the use of a reduced graphene oxide paste electrode modified with electrodeposited cobalt oxide nanoparticles, Microchim. Acta, 183, (2016), 2259-2266.

4. W. Li, H. Qi, B. Wang, Q. Wang, S. Wei, X. Zhang, Y. Wang, L. Zhang, X. Cui, Ultrathin  $\text{NiCo}_2\text{O}_4$  nanowalls supported on a 3d nanoporous gold coated needle for non-enzymatic amperometric sensing of glucose, *Microchim. Acta*, 185, (2018), 1-9.
5. H. Fan, W. Weng, C. Lee, C. Liao, Electrochemical cycling-induced spiky  $\text{Cu}_x\text{O}/\text{Cu}$  nanowire array for glucose sensing, *ACS Omega*, 4, (2019), 12222-12229.
6. S. Li, L. Hou, Bai-Qing. Yuan, M. Chang, Y. Ma, J. Du, Enzyme-free glucose sensor using a glassy carbon electrode modified with reduced graphene oxide decorated with mixed copper and cobalt oxides, *Microchim. Acta.*, 183, (2016), 1813-1821.
7. G. He, L. Tian, Y. Cai, S. Wu, Y. Su, H. Yan, W. Pu, J. Zhang, L. Li, Sensitive nonenzymatic electrochemical glucose detection based on hollow porous  $\text{NiO}$ , *Nanoscale Res. Lett.* 13, (2018), 1-10.
8. J. Wang, L. Xu, Y. Lu, K. Sheng, W. Liu, C. Chen, Y. Li, B. Dong, H. Song, Engineered  $\text{IrO}_2@\text{NiO}$  core-shell nanowires for sensitive nonenzymatic detection of trace glucose in saliva, *Anal. Chem.* 88, (2016), 12346-12353.
9. J. Cui, J. Luo, B. Peng, X. Zhang, Y. Zhang, Y. Wang, Y. Qin, H. Zheng, X. Shu, Y. Wu, Synthesis of porous  $\text{NiO}/\text{CeO}_2$  hybrid nanoflake arrays as platform for electrochemical biosensing, *Nanoscale*, 8, (2016), 770-774.
10. D. Zhang, Z. Wang, J. Li, C. Hu, X. Zhang, B. Jiang, Z. Cao, J. Zhang, R. Zhang, MOF-derived  $\text{ZnCo}_2\text{O}_4$  porous micro-rice with enhanced electro-catalytic activity for the oxygen evolution reaction and glucose oxidation, *RSC Adv.* 10, (2020), 9063-9069.
11. A. J. C. Mary, S. S. Shalini, R. Balamurugan, M. P. Harikrishnan, A. C. Bose, Supercapacitor and non-enzymatic biosensor application of the  $\text{Mn}_2\text{O}_3/\text{NiCo}_2\text{O}_4$  composite material, *New J. Chem.* 2020, 1-20.

***“SYNTHESIS, CHARACTERIZATION AND GLUCOSE SENSING OF  
ELECTRODEPOSITED LANTHANUM OXIDE THIN FILMS DOPED WITH  
SILVER AND MANGANESE”***

**CHAPTER VIII**  
**80-Recommendation**



## Index

<b>Sr. No.</b>	<b>Details</b>	<b>Page No.</b>
8.1	Recommendations	157
8.2	Conclusion of the research work	157
8.3	Summary	161
8.4	Future findings	162

### **7.1 Recommendations:**

Based on the findings and conclusion of the synthesis, characterization and glucose sensing performance of non-enzymatic glucose sensors, there are several recommendations to be proposed. The ultimate target of this research work was to prepare  $\text{La}_2\text{O}_3$ ,  $\text{Ag-La}_2\text{O}_3$  and  $\text{Mn-La}_2\text{O}_3$  materials deposited on SS substrate by electrodeposition method for glucose sensing application. The main achievement of the present research work is that, the prepared lanthanum based film electrodes showed efficient glucose sensing performance present in human blood samples with long term stability. In this investigation, we have calibrated and compared our results with the commercial glucometer. Overall,  $\text{Ag-La}_2\text{O}_3$  and  $\text{Mn-La}_2\text{O}_3$  film electrodes showed excellent non-enzymatic glucose sensing performance present in the human blood samples.

Finally, it is recommended that, due to the simplicity, efficiency, and industrial viability of the technique. The  $\text{Mn-La}_2\text{O}_3$  film electrode can consider for the production of glucose testing strips.

### **7.2 Conclusion of the Research Work:**

In the present scenario, the numbers of diabetic patients are constantly increasing worldwide. This disease is harmful for human body that damages some body parts revealing to require regular monitoring for which glucose oxidase based sensor strips are being used. The monitoring cost is very high. In order to reduce this cost, the new development of non-enzymatic glucose sensors with reusable, highly sensitive and selective properties are being essential. The many researchers and scientists in the field of

science technology and industry have focused on non-enzymatic glucose sensing devices with high sensitivity and stability.

The extensively developed with restricted nature of the present one time usable glucose sensors strips have drawbacks in their usage. This demands synthesis of easily portable, flexible and reusable miniature sized glucose sensing strips. With this focus, we aimed to synthesis reusable, easily portable, non-enzymatic, low cost and environmentally stable glucose sensing strips. The enzymeless strips eliminate the problem that arises due to the bulky nature of enzymatic glucose sensing strips. Hence, the important aspect in synthesizing the enzymeless glucose sensing strips needs improvement in sensitivity, wide linear range, quick response time, LOD and performance without affecting its other electrochemical features. These crucial requirements of non-enzymatic electrochemical glucose sensor requires development of competent electrode material with highly stable and good conductivity, that can enhance electron transfer rate in the electrochemical reaction process with long term durability. Along with electrode material properties, the alkaline electrolyte has the considerable effective role in between the working and counter electrode surface that leads to better enzymeless electrochemical glucose sensing performance.

The aim of the present perceptive research work is to synthesis  $\text{La}_2\text{O}_3$  based thin films using simple electrodeposition method. This is followed by the synthesis of Ag- $\text{La}_2\text{O}_3$  and Mn- $\text{La}_2\text{O}_3$  thin films to upraise the performance of pristine  $\text{La}_2\text{O}_3$  electrode material by the newly developed multipotential electrodeposition method. Synthesized well adherent, good quality and binder-free thin films were characterized by various physico-chemical methods. The best performing thin film electrodes from the above

mentioned ones then were used for the analysis of glucose present in real human blood sample in freshly prepared 0.1 M NaOH electrolyte. This work is presented in thesis.

The basic introduction of thin film electrode and electrodeposition method with their different types of deposition techniques and deposition mechanism are discussed. As well theoretical background of electrodeposition method with various preparative parameters and their advantages are briefly explained. The characterization techniques used for thin film analysis such as XRD for structural analysis, FE-SEM for surface morphological study and EDS for elemental mapping and XPS for elemental analysis are discussed. Also, the electrochemical technique such as CV and *i-t* amperometry used for the electrochemical glucose sensing performance of electrode materials

This work explains synthesis of  $\text{La}_2\text{O}_3$  thin films by electrodeposition method. The highly conducting and stable SS substrate in acid/base solution was selected for the deposition. The  $\text{La}_2\text{O}_3$  was directly grown on SS substrate by electrodeposition method. The deposited  $\text{La}_2\text{O}_3$  thin films were characterized by various characterization techniques. The XRD analysis confirmed deposition of  $\text{La}_2\text{O}_3$  material with monoclinic phase in thin film form. The lanthanum and oxygen elements were detected. The lanthanum and oxygen molar content influences the morphology of thin film form in nanosheets-like structure and EDS analysis confirms expected molar ratio of lanthanum and oxygen in the samples.

Three electrode system was used for the enzymeless glucose sensing performance evaluation. The glucose sensing electrochemical performance evaluation of electrodeposited  $\text{La}_2\text{O}_3$  thin films was studied. The current response was linear at low concentration from 1.25 to 3.75 mM with high sensitivity of  $616 \mu\text{A mM}^{-1} \text{cm}^{-2}$  and a low

detection limit (LOD) of 0.27 mM with correlation coefficient of 0.9924 was obtained. Fabrication of this binder free electrode is simple and has the characteristic features of faster response time (less than 1 second), highly stable, reusable, better sensitive and excellent selective for enzymeless glucose sensing in alkaline media. Observed linear range was 1.2 mM to 11.25 mM (converted into dynamic range 21.6 to 202.5 mg/dl), which is the diagnostic range required for screening the hypo and hyperglycemic glucose level without enzyme. The good non-enzymatic electrochemical glucose sensing results concluded that, nanosheets-like structure of  $\text{La}_2\text{O}_3$  thin film offers a large number of channels for easy ion penetration and charge transportation.

The study of characterization and non-enzymatic electrochemical performance evaluation of electrodeposited Ag- $\text{La}_2\text{O}_3$  thin film electrodes was carried out. The Ag- $\text{La}_2\text{O}_3$  thin films are used for non-enzymatic glucose sensing study. Nanocrystalline nature of Ag- $\text{La}_2\text{O}_3$  thin film electrode is observed in XRD analysis. The vertically aligned nanoflakes like morphology and expected elemental composition are observed from FE-SEM and EDX study respectively. The silver ions enhance the active surface area which influences sensitivity increment. The non-enzymatic glucose sensing electrochemical performance evolution of electrodeposited Ag- $\text{La}_2\text{O}_3$  film electrode was detected in 0.1 M NaOH electrolyte. The high sensitivity value of 1677 and 1022  $\mu\text{A mM}^{-1} \text{cm}^{-2}$  by silver doped lanthanum oxide film electrode with multi linear response towards glucose in the range of 100  $\mu\text{M}$  to 600  $\mu\text{M}$  and 600  $\mu\text{M}$  to 1.6 mM was exhibited respectively. The enhanced electrical conductivity, surface area and improved sensing performance are due to Ag composite and vertically grown Ag- $\text{La}_2\text{O}_3$  nanoflakes form film electrode. As the thickness of shell layer in the nanoregion results with active

surface area which can provide more reactive sites for redox reaction and electrocatalytic activity.

Further for non-enzymatic glucose sensing application, Mn-La<sub>2</sub>O<sub>3</sub> film electrodes were synthesized by multipotential electrodeposition method. Mn-La<sub>2</sub>O<sub>3</sub> film electrode exhibits range of glucose concentration detection in between 50 to 950  $\mu$ M ( $R^2=0.9476$ ) and glucose sensitivity detection is about 1985  $\mu$ A mM<sup>-1</sup> cm<sup>-2</sup> with a LOD 32  $\mu$ M. Manganese ions in the La<sub>2</sub>O<sub>3</sub> electrode material promotes to enhance better electrocatalytic performance and also as manganese element is one of the most promising nanomaterial due to its unique combination of multi valence property leads to most essential characteristics such as thermal stability and good electrical conductivity.

The study of glucose detection from present in the human blood sample was carried out using simple *i-t* amperometric technique. We have taken six human blood samples from various persons from D. Y. Patil Hospital and Research Centre Kolhapur. The percentage of glucose present in human blood samples was measured by commercial glucometers in the unit of mg/dl. Also, the measurement of glucose from human blood sample was carried out by addition of 50  $\mu$ L of whole blood in 40 mL of 0.1 M NaOH electrolyte for comparison. These statistical results emphasizes the possibility of innovative development of commercial glucose sensor by using Ag-La<sub>2</sub>O<sub>3</sub> and Mn-La<sub>2</sub>O<sub>3</sub> film electrodes. In that regards Mn-La<sub>2</sub>O<sub>3</sub> electrode exhibits high sensitivity with nearly equal glucose concentration from human blood sample than Ag-La<sub>2</sub>O<sub>3</sub> electrode. Therefore, the electrodeposited Mn-La<sub>2</sub>O<sub>3</sub> film electrode can be used for strip fabrication process.

### 7.3 Summary

- 1) The uniform deposition of  $\text{La}_2\text{O}_3$ ,  $\text{Ag-La}_2\text{O}_3$  and  $\text{Mn-La}_2\text{O}_3$  on the stainless steel substrate was achieved by electrodeposition method.
- 2)  $\text{Ag-La}_2\text{O}_3$  and  $\text{Mn-La}_2\text{O}_3$  film electrodes exhibited excellent non-enzymatic glucose sensing performance present in the human blood samples.
- 3) The non-enzymatic glucose sensors based on  $\text{Mn-La}_2\text{O}_3$  electrodes have shown more sensitivity and efficient sensing performance with good recovery for glucose oxidation than  $\text{Ag-La}_2\text{O}_3$  electrode.

### 7.4 Future Findings:

In this study, the synthesized non-enzymatic glucose sensing electrode electrochemical performance evolution was carried out in alkaline medium such as sodium hydroxide and potassium hydroxide. However, they are highly basic with fairly high pH value compared to pH of physiological content. Hence in further studies, it is planned to perform glucose sensing application at physiological pH with synthesized nanomaterial. The synthesized  $\text{La}_2\text{O}_3$ ,  $\text{Ag-La}_2\text{O}_3$  and  $\text{Mn-La}_2\text{O}_3$  sensing electrodes were exhibited glucose detection performance in the range of 50  $\mu\text{M}$  to 11.25 mM (0.9 to 202.5 mg/dl). However, it is insufficient to detect whether the diabetic patient is in hypo or hyperglycemic glucose level. Thus in our further studies it is planned to synthesis better metal oxide electrode material with electrocatalytic properties that may lead to enhance sensitivity with wide linear range of glucose detection performance.